Università degli Studi di Palermo (Palermo, Italy)
Dipartimento di Scienze della Terra e del Mare (DISTEM)

National and Kapodistrian University of Athens (Athens, Greece)
Department of Geology and Geoenvironment

Istituto Nazionale di Geofisica e Vulcanologia (sez. Palermo, Italy)

Co-supervision PhD in Geochemistry
DOTTORATO DI RICERCA IN SCIENZE DELLA TERRA – GEOCHIMICA XXX° CICLO (GEO/08)
DOCTORATE OF PHILOSOPHY IN APPLIED AND ENVIRONMENTAL GEOLOGY

Geochemistry of Gas Manifestations in Greece

PhD thesis by:
Kyriaki Daskalopoulou

IL COORDINATORE
Aiuppa Alessandro

SUPERVISORS
Parello Francesco **Kyriakopoulos Konstantinos**

CO-SUPERVISORS
D'Alessandro Walter

CICLO XXX
January 2015 – December 2017

Università degli Studi di Palermo (Palermo, Italy)
Dipartimento di Scienze della Terra e del Mare (DISTEM)

National and Kapodistrian University of Athens (Athens, Greece)
Department of Geology and Geoenvironment

Istituto Nazionale di Geofisica e Vulcanologia (sez. Palermo, Italy)

Co-supervision PhD in Geochemistry
DOTTORATO DI RICERCA IN SCIENZE DELLA TERRA – GEOCHIMICA XXX° CICLO (GEO/08)
DOCTORATE OF PHILOSOPHY IN APPLIED AND ENVIRONMENTAL GEOLOGY

Geochemistry of Gas Manifestations in Greece

PhD thesis by:
Kyriaki Daskalopoulou

IL COORDINATORE
Aiuppa Alessandro

SUPERVISORS

Parello Francesco

Kyriakopoulos Konstantinos

CO-SUPERVISORS
D'Alessandro Walter

CICLO XXX
January 2015 – December 2017

Στους γονείς μου Κώστα και Έφη, που με δίδαξαν να μάχομαι και να μην τα παρατάω…

Στον Νίκο, τον «μικρό πρίγκηπα» που με έμαθε να ονειρεύομαι και να πετάω….

Acknowledgments

During the three years of my thesis, many people contributed to this achievement, each one with his way. There is no doubt that my supervisors, Prof. Francesco Parello and Prof. Konstantinos Kyriakopoulos, stood by me all along this research. Always available for any discussion, scientific or not, each of their advice was always illuminating. It is impossible to count the hours we worked together. For these reasons I would like to greatly thank them. Nevertheless, I was lucky enough to have Dr. Walter D'Alessandro as a co-supervisor. Our collaboration counts more than four years, since the time when I was a master student in the Department of Geology and Geoenvironment at the National and Kapodistrian University of Athens. For all these years Dr. Walter D'Alessandro has been a mentor and a friend and I am really grateful to him for his continuous presence and support.

Since the beginning of my PhD course, I had the pleasure to collaborate with Dr. Sergio Calabrese, a brilliant researcher of Università degli Studi di Palermo, who provided me with the opportunity to join a multidisciplinary team, and made me "discover" and "travel" in the magic world of Geochemistry and Volcanology. Also, I would like to thank Prof. Franco Tassi for the fruitful discussions regarding the evolution of this project and his helpful advices during these years. My collegue, Manfredi Longo, who helped me with the expansion of the database. Furthermore, I kindly acknowledge Francesco Capecchiacci (GC laboratory, UniFi), Mauro Martelli and Francesco Salerno (GC laboratory INGV-Pa), Ygor Oliveri and Aldo Sollami (MS laboratory INGV-Pa), Andrea Rizzo and Mariano Tantillo (Noble Gas laboratory INGV-Pa) for their kind and valuable support in the analyses. Among them, I am indebted with Dr. Markos Xenakis and Dr. Konstantinos Athanasoulis of the IGME for their precious information about the location of many interesting sites all around the Hellenic territory. I am also grateful for the insightful comments of Andri Stefansson and an anonymous referee and of the editor Hailiang Dong that helped me significantly improve the part of hydrocarbons. I am also indebted to David Hilton, who managed as editor the first round of review of the same manuscript. I was deeply touched by the notice of his death. Also, I kindly acknowledge Prof. Orlando Vaselli and Prof. Carlo Cardellini for their suggestions in the final revision of my thesis.

Nevertheless, none of these would have happened without the moral and psychological support of my parents Kostas and Efi Daskalopoulos, who were always there to help me stand on my feet and go forward. Although he is not longer with us, I would like to thank my brother Nikos

Daskalopoulos, who taught me how to fly and I am sure that he would have been very proud for his little sister. Also, I am grateful to my friends Despoina Zoura, Silvia Milazzo, Luciana Randazzo and Stefano Dell'Aria who showed great patience and gave priceless moral and psychological support during these three years despite my paranoias and stress.

Last but not least, the Ministero dell'Istruzione, dell'Università e della Ricerca (MIUR) of Italy is greatly acknowledged for providing me the economic support through the 3-year scholarship, which was essential for accomplishing this task, and of course the Università degli Studi di Palermo and the Istituto Nazionale di Geofisica e Vulcanologia- Palermo are especially thanked for giving me the opportunity to carry out this thesis.

INDEX

FIGURE INDEX

TABLE INDEX

ABSTRACT

In the period from 2004 to 2017, more than 350 samples of free and dissolved gases were collected along the whole Hellenic area. Some literature data have also been taken into consideration. For a better comprehension of this study, Greece was subdivided in four geologic units (External [EH], Internal [IH] Hellenides, Hellenic Hinterland [HH] and active Volcanic Arc [VA]) and based on that division, I investigate the possible relationship of the main geochemical composition of the gases with the different geological and geodynamical settings of the sampling sites. Samples have been analysed for their chemical (O_2, N_2, CH_4, CO_2, He, Ne, Ar, H_2, H_2S and C_2-C_6 hydrocarbons) and isotope (R/R_A, $\delta^{13}C$-CO_2, $\delta^{13}C$-CH_4 and $\delta^{2}H$-CH_4) composition. The concentrations range from 0.10 to 3370 μmol/mol for He, 600 to 995,000 μmol/mol for N_2, 0.60 to 915,000 μmol/mol for CH_4 and 17 to 1,000,000 μmol/mol for CO_2, whereas the isotope values range from 0.01 to 7.10 for R/R_A, -29.91 to +6.00 vs. V-PDB for $\delta^{13}C$-CO_2, -79.8 to +45.0‰ vs. V-PDB for $\delta^{13}C$-CH_4 and -311 to +301‰ vs. V-SMOW for $\delta^{2}H$-CH_4. Considering the R/R_A and $^4He/^{20}Ne$ ratios the atmospheric, mantle and crustal contributions for He have been calculated. The highest mantle contribution (up to 90%) is found in the VA, whereas the lowest in continental Greece (0-20%). Atmospheric contribution is mostly negligible. Taking into consideration the geographical distribution of the gases, it is evident that the R/R_A increases in areas characterised by: i) thin crust; ii) elevated heat flow values; iii) recent (Pleistocene-Quaternary) volcanic activity; and iv) deep routed extensional or transtensional regional faults. The highest values are therefore found along VA and the lowest in EH. Furthermore, based on the $CO_2/^3He$ and $\delta^{13}C$-CO_2 values, the contribution of Sediment, Mantle and Limestone end-members for CO_2 was determined. The majority of the collected samples present a prevailing limestone C component and only few samples have a prevailing mantle C component. However, with the present data, it is not possible to distinguish CO_2 deriving from crustal and slab-related limestones. Additionally, due to the complex geodynamic history, the mantle C isotope composition could be affected by subduction-related metasomatism and, similarly to the nearby Italian area, the C isotope composition could be more positive. In this case, the mantle contribution is probably underestimated. Some samples display very low $CO_2/^3He$ and $\delta^{13}CO_2$ values due to the CO_2 loss caused either by dissolution of CO_2 in shallow groundwater or by the calcite precipitation that is taking place in most of the thermal springs. On the other hand, the $CH_4/(C_2H_6+C_3H_8)$ ratios (from 1.5 to 93,200) coupled with CH_4 isotopic features, suggest the

light alkanes derive from a different primary source and are sometimes affected by secondary processes. An almost exclusive biotic, mainly microbial, origin of CH_4 can be attributed to EH gases. Cold gases at IH have mainly a thermogenic origin, although some gases connected to continental serpentinization may have an abiogenic origin. Methane in gases bubbling in thermal waters of IH, HH and VA and fumarolic gases of the VA seem to have a prevailing abiogenic origin, although their chemical and isotopic characteristics may have been produced by secondary oxidation of thermogenic CH_4. Finally, in some of the sampled gases, the isotopic values are extremely positive ($\delta^{13}C$-CH_4 up to +45.0‰ vs. V-PDB and $\delta^{2}H$-CH_4 up to +301‰ vs. V-SMOW) most probably caused by microbial oxidation.

RIASSUNTO

Nel periodo compreso dal 2004 al 2017, più di 350 campioni di gas liberi e disciolti sono stati raccolti su tutto il territorio ellenico. Sono stati presi in considerazione anche alcuni dati di letteratura. Per meglio indagare le possibili relazioni tra la geochimica dei gas e la conformazione geologica e geodinamica delle aree di campionamento l'area di studio è stata suddivisa in quattro unità geologiche principali (Ellenidi esterne [EH] ed interne [IH], Hinterland ellenico [HH] e arco vulcanico [VA]). I campioni raccolti sono stati analizzati per la loro composizione chimica (O_2, N_2, CH_4, CO_2, He, Ne, Ar, H_2, H_2S ed idrocarburi C_2-C_6) ed isotopica (R/R_A, $\delta^{13}C$-CO_2, $\delta^{13}C$-CH_4 e $\delta^{2}H$-CH_4). Le concentrazioni vanno da 0.10 to 3370 μmol/mol per He, da 600 a 995,000 μmol/mol per N_2, da 0.60 a 915,000 μmol/mol per CH_4 e da 17 a 1,000,000 μmol/mol per CO_2, mentre i valori isotopici vanno da 0.01 a 7.10 per R/R_A, da -29.9 a +6.0 ‰ vs. V-PDB per $\delta^{13}C$-CO_2, da -79.8 a +45.0‰ vs. V-PDB per $\delta^{13}C$-CH_4 e da -311 a +301‰ vs. V-SMOW per $\delta^{2}H$-CH_4. Per l'elio sono stati calcolati i contributi di atmosfera, crosta e mantello tenendo in considerazione i rapporti R/R_A e $^4He/^{20}Ne$. Icontributi più alti del mantello (fino al 90%) sono stati trovati in VA ed i più bassi nella Grecia continentale (0-20%). Il contributo atmosferico è generalmente basso. Osservando la distribuzione geografica delle manifestazioni gassose è evidente che i valori di R/R_A sono più elevati in aree caratterizzate da: i) crosta sottile; ii) valori di flusso di calore più elevati; iii) presenza di attività vulcanica recente (Plio-Quaternaria); e iv) faglie regionali profonde distensive o transtensive. A causa di ciò i valori più elevati sono stati misurati in campioni di VA ed i più bassi in quelli di EH. Inoltre, in base ai valori di $CO_2/^3He$ e $\delta^{13}C$-CO_2, sono stati calcolati i contributi dei sedimenti organici, carbonati e mantello per la CO_2 emessa. La quasi totalità dei campioni presenta per la CO_2 una componente derivante dai carbonati e solo in pochi prevale la componente mantellica. Questi dati non consentono però di distinguere il contributo dei carbonati della placca in subduzione da quelli della crosta soprastante. Inoltre, a causa della complessa storia geodinamica dell'area, la CO_2 mantellica potrebbe essere affetta da metasomatismo indotto da fluidi rilasciati durante la subduzione e, similmente alla vicina area italiana, potrebbe avere una composizione isotopica più positiva. In tale caso il contributo della CO_2 mantellica sarebbe sottostimato. Alcuni campioni mostrano valori di $CO_2/^3He$ e $\delta^{13}CO_2$ molto bassi dovuti a perdita di CO_2 legati alla sua dissoluzione in acqua oppure alla precipitazione di carbonati nei sistemi idrotermali. L'ampio intervallo di valori del rapporto $CH_4/(C_2H_6+C_3H_8)$ (da 1.5 a 93,200) e della composizione

isotopica del CH_4 suggeriscono che gli alcani leggeri abbiamo diverse sorgenti e siano talvolta affetti da importanti processi secondari.Un'origine esclusivamente biogenica, prevalentemente microbica, può essere attribuita al CH_4 dei gas di EH. Il metano nei gas campionati nelle manifestazioni fredde di IH hanno una origine prevalentemente termogenica escludendo quello delle manifestazioni connesse a serpentinizzazione in ambiente continentale che invece hanno una probabile origine abiogenica. Il metano dei gas gorgoglianti in acque termali di IH, HH e VA e i gas fumarolici di VA sembrano avere una prevalente origine abiogenica anche se le loro caratteristiche chimiche ed isotopiche possono derivare pure da ossidazione secondaria di CH_4 termogenico. Infine, in alcuni dei gas campionati, la composizione isotopica misurata raggiunge valori estremamente elevati ($\delta^{13}C$-CH_4 fino a +45.0‰ vs. V-PDB e $\delta^{2}H$-CH_4 fino a +301‰ vs. V-SMOW) molto probabilmente causati da ossidazione microbiologica.

ΠΕΡΙΛΗΨΗ

Κατά την περίοδο 2004 με 2017, συλλέχθηκαν περισσότερα από 350 δείγματα ελεύθερων και διαλελυμένων αερίων στην Ελλάδα. Μαζί με αυτά συνυπολογίστηκαν και βιβλιογραφικά δεδομένα. Για καλύτερη κατανόηση της μελέτης, η χώρα διαιρέθηκε σε τέσσερις γεωλογικές ενότητες (Εξωτερικές [EH] και Εσωτερικές [IH] Ελληνίδες, Ελληνική Ενδοχώρα [HH] και ενεργό ηφαιστειακό τόξο [VA]) και με βάση τον συγκεκριμένο διαχωρισμό ερευνήθηκε η πιθανή σχέση της κύριας γεωχημικής σύστασης των αερίων με τα διάφορα γεωλογικά και γεωδυναμικά καθεστώτα των περιοχών δειγματοληψίας. Τα δείγματα αναλύθηκαν για την χημική (O_2, N_2, CH_4, CO_2, He, Ne, Ar, H_2, H_2S και C_2-C_6 υδρογονάνθρακες) και ισοτοπική τους (R/R_A, $\delta^{13}C$-CO_2, $\delta^{13}C$-CH_4 and $\delta^{2}H$-CH_4) σύσταση. Οι συγκεντρώσεις κυμαίνονταν από 0.10 έως 3370 μmol/mol για το He, 600 έως 995,000 μmol/mol για το N_2, 0.60 έως 915,000 μmol/mol για το CH_4 και 17 έως 1,000,000 μmol/mol για το CO_2, ενώ οι ισοτοπικές τους τιμές από 0.01 έως 7.10 R/R_A, -29.91 έως +6.00 vs. V-PDB για το $\delta^{13}C$-CO_2, -79.8 έως +45.0‰ vs. V-PDB για το $\delta^{13}C$-CH_4 και -311 έως +301‰ vs. V-SMOW για το $\delta^{2}H$-CH_4. Λαμβάνοντας υπ'όψιν τις τιμές των R/R_A και $^4He/^{20}Ne$, υπολογίστηκε η συνεισφορά της ατμόσφαιρας, του μανδύα και του φλοιού για το He. Η μεγαλύτερη μανδυακή συνεισφορά (έως και 90%) βρέθηκε στο VA, ενώ η χαμηλότερη (0-20%) στο EH. Η συνεισφορά της ατμόσφαιρας ήταν σχετικά αμελητέα. Σύμφωνα με την γεωγραφική κατανομή των αερίων, είναι εμφανές πως το R/R_A αυξάνεται σε περιοχές που χαρακτηρίζονται από: i) λεπτό φλοιό; ii) αυξημένες τιμές ροής θερμότητας; iii) πρόσφατη (Πλειστόκενο-Τεταρτογενής) ηφαιστειακή δραστηριότητα; και iv) τοπικά εκτατικά ή διασταλτικά ρήγματα. Οι υψηλότερες τιμές βρέθηκαν κατά μήκος του VA και οι χαμηλότερες στις EH. Επιπλέον, με βάση τις τιμές των $CO_2/^3He$ και $\delta^{13}C$-CO_2, υπολογίστηκε η συνεισφορά των Ιζηματογενών, Μανδυακών και Ασβεστολιθικών end-members του CO_2. Οι πλειοψηφία των δειγμάτων παρουσίασε μία κυρίως ασβεστολιθική σύσταση για τον C, ενώ μόνο λίγα δείγματα έδειξαν μανδυακή σύσταση. Παρ'όλα αυτά, με τα υπάρχοντα δεδομένα, είναι αδύνατος ο διαχωρισμός του CO_2 που προέρχεται από τους ασβεστολίθους του φλοιού και από εκείνους της υπό βύθισης πλάκας. Επί προσθέτως, λόγω της σύνθετης γεωδυναμικής ιστορίας, η ισοτοπική σύσταση του μανδυακού C θα μπορούσε να είναι επηρεασμένη από μετασωμάτωση συσχετιζόμενη με την βύθιση της πλάκας, όπως συμβαίνει και στην γειτνιακή περιοχή της Ιταλίας, κάνοντας την ισοτοπική του σύσταση πιο θετική. Σε τέτοια περίπτωση, η συνεισφορά του μανδύα θεωρείται ότι έχει υποτιμηθεί. Κάποια δείγματα παραθέτουν πολύ χαμηλες τιμές

$CO_2/^3He$ και $\delta^{13}CO_2$ λόγω απώλειας του CO_2, η οποία έχει προκληθεί είτε από διάλυση του CO_2 σε υπόγεια νερά μικρού βάθους είτε από την καθίζηση του ασβεστίτη που λαμβάνει μέρος στε ορισμένες θερμές πηγές. Από την άλλη μεριά, οι τιμές του $CH_4/(C_2H_6+C_3H_8)$ (από 1.5 έως 93,200) σε συνδιασμό με τα ισοτοπικά χαρακτηριστικά του CH_4, συνιστούν πως οι ελαφριές αλκάνες προέρχονται από διαφορετική αρχική πηγή και αρκετές φορές επηρεάζονται από δευτερογενή διαδικασίες. Στα αέρια των ΕΗ παρατηρείται μια σχετικά αποκλειστική βιοτική, κυρίως μικροβιακή, προέλευση για το CH_4. Τα αέρια των ψυχρών πηγών των ΙΗ έχουν κυρίως θερμογενή προέλευση, αν και κάποια από αυτά συνδέονται με ηπειρωτικές σερπεντινιώσεις και μοιάζει να έχουν αβιοτική προέλευση. Το CH_4 στις θερμές πηγές των ΙΗ, HH and VA και στα φουμαρολικά αέρια του VA φαίνεται να είναι κυρίως αβιοτικό, αν και τα χημικά και ισοτοπικά χαρακτηριστικά του μοιάζει να έχουν επηρεαστεί από δευτερογενή οξείδωση του CH_4 θερμογενούς προέλευσης. Τέλος, κάποια από τα δείγματα παρουσιάζουν αρκετά θετικές ισοτοπικές τιμές ($\delta^{13}C$-CH_4 έως +45.0‰ vs. V-PDB και δ^2H-CH_4 έως +301‰ vs. V-SMOW) πιθανότατα λόγω οξείδωσής τους από μικρόβια.

Introduction

The composition of gases released from geothermal systems depends on deep-seated processes, so that detailed studies on the geothermal gases can help to understand the tectonic and geological settings of the studied areas (Giggenbach, 1992; 1996; Lee et al., 2005). Gases exist ubiquitously in natural waters sometimes exsolving as a separate phase. Isotope geochemistry of the gas is one of the major techniques for tracing the origins of gases. Noble gases derived from the deep earth can provide important information about their crust or mantle origin because these gases hardly react with other materials during migration. Helium is a sensitive tracer for both fluid migration and gas origins. $^{3}He/^{4}He$ ratios in Earth's materials have a range from about 10^{-9} to 10^{-5}. Gases of different origins have different isotope compositions (Ozima & Podosek, 1983; Du, 1994, Xu et al., 1998). The He isotope composition is generally expressed as R/R_A, a multiple of the present-day atmospheric $^{3}He/^{4}He$ ratio (R/R_A), which is 1.38×10^{-6} (Anderson, 1998b). Most of the R/R_A ratio in the gases emitted at the Earth's surface can be explained in terms of mixing among three end-members: atmosphere (1 R/R_A), crust (0.01 R/R_A) and upper mantle (8 R/R_A) (Mamyrin and Tolstikhin, 1984; Du, 1998). The characteristics of the gases derived from various tectonic regions are geochemically different (Lupton, 1983). Helium isotope ratios are directly correlated with heat flow because the latter is mainly derived from the crust and mantle (Du et al. 1998; 2006; Ozima & Podosek, 1983). Consequently, heat flow has a close relationship with tectonics related to both active faults and geothermal anomalies and for that reason the majority of the earthquake epicenters occur in geothermal zones worldwide (Du et al., 1998; 2006). Furthermore, the heat flow has a strict connection with the ascent of magmas. This process transfers mass and heat from the planet's interior towards its surface by melting (Douce, 2011).

The carbon content of undegassed mid-oceanic ridge basalts (MORB) and of the upper mantle has been an ongoing debate for several decades (Marty and Jambon, 1987, Javoy & Pineau, 1991, Saal et al., 2002, Cartigny et al., 2008, Dasgupta, et al., 2013). Carbon is a volatile element that plays a key role in major geodynamical processes such as mantle melting and volcanic degassing. The amount of carbon present in the mantle affects the onset of deep melting, the geophysical properties of the mantle, as well as long-term climate change when CO_2 is released into the atmosphere (Dasgupta, et al., 2013). Because of its very low solubility (Dixon and Stolper, 1995) magmatic degassing depletes carbon in the melt during ascent and eruption, which

prevents direct measurements of the original carbon content of most basaltic melts formed in equilibrium with the mantle source.

There is a substantial relationship among the variations of He and C isotope compositions, temperatures of the springs and tectonics. The hot springs are surface manifestations of thermal fluids in the lithosphere and the thermal spring provide us with information about deep earth. As already proposed by Du (2006) and Miller (1999), anatectic fluids play an important role in earthquake generation by reducing friction between the fault blocks and transporting upper mantle energy with geochemical anomalies that occur before, during and after earthquakes (Rikitake, 1982).

Furthermore, based on the environmental impact of the C gases, geogenic emissions of carbon greenhouse gases (mainly CO_2 and CH_4) have a significant impact on the global carbon budget (Kvenvolden, 1993; Klusman and Jakel, 1998; Mörner and Etiope, 2002). Notwithstanding, a reliable estimation of the effective amount discharged from natural manifestations is still a challenge (Milkov, 2000 and references therein; Etiope et al., 2009).

Methane, the most abundant organic gas compound in Earth's atmosphere, has a potential global warming 28 times higher than that of CO_2 on a 100-year time horizon (Ciais et al. 2013; Etiope, 2015). In a natural environment, the production of CH_4 involves organic matter either as an active (microbial production) or as a passive agent (thermogenic degradation) (Schoell, 1980; 1988; Whiticar, 1999). Microbial activity by Archaea occurring during the diagenesis of sediments at relatively low temperatures (up to 122°C – Takai et al., 2008) predominantly produces methane, subordinately ethane and, likely, trace amounts of propane (Formolo, 2010). On the other hand, thermogenic methane is produced at higher temperatures (>150°C – Quingley and MacKenzie, 1988) by the thermal cracking of organic matter (catagenesis) or oil. Thermogenic gases can be either independent from oil reservoirs or associated with them, having variable amounts of ethane, propane, butane, and condensate (C_{5+} higher hydrocarbons).

Abiogenic processes able to synthesize CH_4 from inorganic molecules at high temperatures, have been also hypothesized to occur in natural environments (Etiope and Sherwood Lollar, 2013). Among others, reduction of graphite (Holloway, 1984) or, thermal decomposition of siderite (McCollom, 2013) has been proposed. However the main abiotic process is considered to be the reduction of gaseous CO or CO_2 (Berndt et al., 1996; Horita and Berndt, 1999; Foustoukos and

Seyfried, 2004). The reduction process occurs mainly through the so-called Fischer-Tropsch-type reactions, which are the Fischer-Tropsch reaction (sensu stricto)

$$(2n+1)\ H_2 + nCO \rightarrow C_nH_{2n+2} + nH_2O \qquad (1)$$

that allows also the production of minor amounts of light hydrocarbons and the Sabatier reaction:

$$4H_2 + CO_2 \rightarrow CH_4 + 2H_2O \qquad (2).$$

Both reactions have high activation energies but in the presence of catalysts, such as native transition metals like Fe, Co, Cr or Ni in natural systems, these reactions occur also in the 100-300°C range (McCollom, 2013), while recently Etiope and Ionescu (2015) suggested that CH_4 can be effectively produced in the temperature range 20-90°C in the presence of Ru catalyst within chromite-rich serpentinized rocks.

The Hellenic territory has an intense geodynamic activity, giving rise to (i) the highest seismicity of whole Europe (Burton et al., 2004), (ii) the presence of an active volcanic arc (Pe-Piper and Piper, 2002) and many areas of anomalous high geothermal gradient (Fytikas and Kolios, 1979), and (iii) the widespread occurrence of cold and thermal springs (D'Alessandro and Kyriakopoulos, 2013). Until now only scarse data on chemical and isotope composition of these gas manifestations have been published. Furthermore these data are either limited to single volcanic /geothermal systems (Marini and Fiebig, 2005; D' Alessandro et al., 2008; Dotsika et al., 2009; Tassi et al., 2013; Rizzo et al., 2016) or if considering geographically wider areas, they refer only to their chemical (Minissale et al., 1989; 1997) or to their noble gas isotope (Shimizu et al., 2005) composition. Aim of this project is to present an improved catalogue of gas manifestations located along the Hellenic territory by studying both the chemical and isotope composition of the gases and attempt to reveal possible relationships with the geodynamic situation and the processes that are affecting them. Furthermore, to constrain the origin of CH_4 and the post-genetic modifications that could affect the sampled gases along the Hellenic area.

1. Study Area

1.1. Geodynamic and Geotectonic setting

The African plate subducts underneath the Eurasian along the Hellenic Arc at a rate of about 10 mm/yr, while the Aegean Sea represents an extensional basin with opening rates in the order of 35-40 mm/yr (McClusky et al., 2000). The plate interactions and the associated crustal deformation taking place in the region, make the Hellenic area one of the most seismically active and rapidly deforming areas worldwide (e.g., Tsokas and Hansen, 1997; Taymaz et al., 2007; Le Pichon et al. 2001). The Hellenic Arc is bounded at its northwestern and eastern ends by two major transform faults, known as the Cephalonia (right lateral) and the Rhodes (left lateral) transform faults (Yolsal et al. 2009). The subduction is accompanied by a prominent shallow seismicity with low-angle thrust faults along the Hellenic arc, and normal faults in the back arc Aegean area (Ambraseys 2000; Papazachos et al. 2006).

The dynamic interaction between the Mediterranean and the Aegean lithospheric plates results in the generation of shallow earthquakes in the broad Aegean Sea area and of intermediate focal depth earthquakes in the South Aegean Sea. Besides, the intermediate depth seismicity may be of particular relevance for a better understanding of the volcanism in island arc structures since there is evidence that the two phenomena are geodynamically related (e.g., Papadopoulos 1991). One of the most important properties of the intermediate depth seismicity is the pattern of irregular geographic distribution of seismic intensities, which was described by a number of authors (e.g., see Ambraseys 2001, for recent results and a short review). According to the configuration of the subduction structure of the Hellenic Trench, the relation between the total deformation and the seismic energy release, could be biased because it seems to be seismically deformed. This generates a non-homogenous pattern of the seismic energy release, which is correlated with the total amount of deformation. Generally, the high seismic conductivity is generated towards the Mediterranean Sea (in the subducting lithosphere), whereas the other component of low seismic conductivity is generated towards the direction of the Central and North Aegean Sea, which is in the back-arc domain (Mantovani et al. 2001a).

Tectonic evolution of the Hellenic Arc is dominated by the effects of the northward subduction of the African under the Eurasian plate (Figure 1). The thinner oceanic lithosphere is currently subducting under Crete and is causing extension of the continental crust and volcanism in the overlying Aegean extensional province. Furthermore, differential displacements of several

microplates (Aegean, Anatolian, and Apulian plates) are making the overall active tectonic setting very complicated (Grigoriadis et al., 2016; Figure 1).

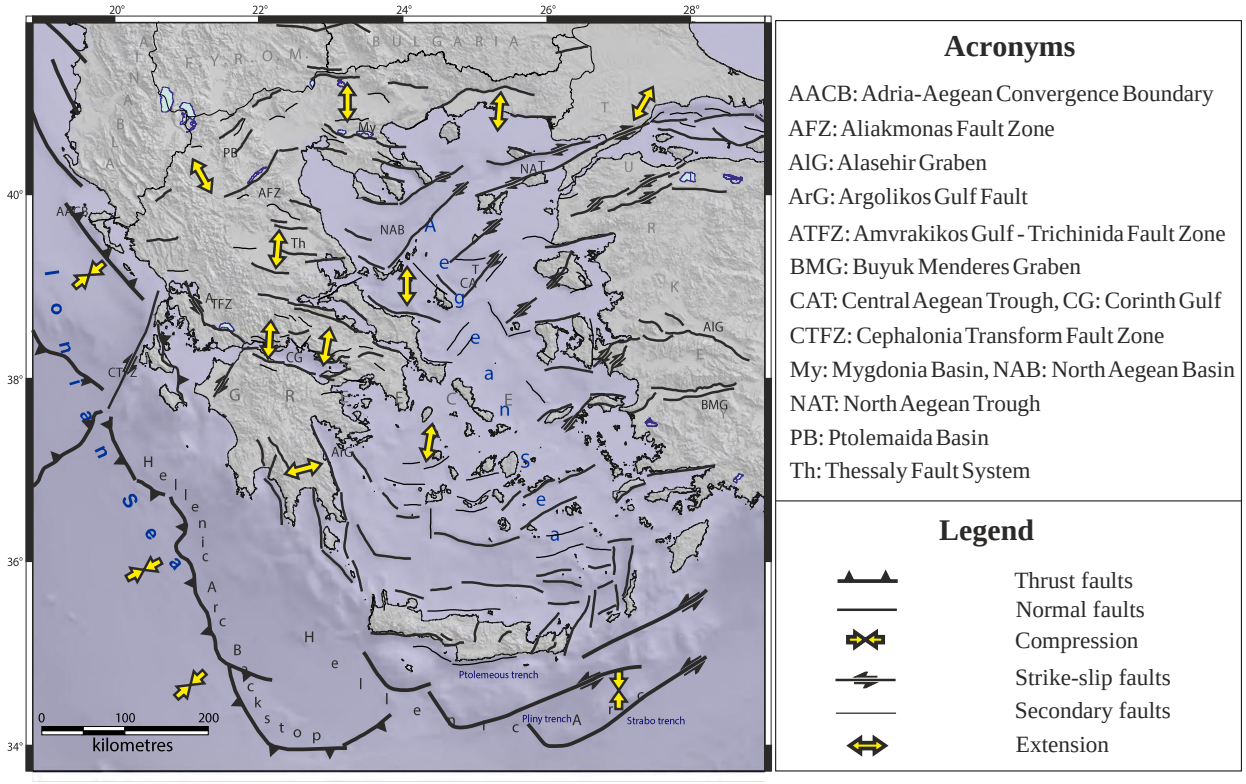

Figure 1: Map of the major tectonic structures and the current horizontal stress field main axes. Fault lines derive from the CSSs upper edge of GreDaSS (2014).

Schematically, the present-day shape, topography and bathymetry of the region are the result of three main relief-forming geotectonic processes, which were or still are active within the last 10-15 million years:

- the Middle - to Late Miocene post-orogenic extension and exhumation of the alpine mountain belts;
- the migration of the North Anatolian Fault (NAF) westwards into the north Aegean Sea in Late Miocene - Early Pliocene and the westward motion of the Anatolian continental block;
- the northward subduction of the eastern Mediterranean crust below the Aegean microplate and the resulted stretching of the latter in a north-northeast - south-southwest direction.

The onset of the westward movement of the Anatolian block along the NAF has resulted in the reorganisation of the strain in the Aegean microplate. This movement, along with the ongoing collision between the Aegean and the Adriatic microplates in the Ionian region north of the

Cephalonia Transform Fault (CTF), forced the Aegean microplate to stretch southwards (Dewey and Sengör, 1979; Jackson & McKenzie, 1988). Multidisciplinary studies during the last decades have shown that the Aegean microplate undergoes significant extensional deformation in a northnortheast - south-southwest direction. It has been estimated that the island of Crete, the leading edge of the overriding Aegean microplate, is moving south-southwestwards over the subducting eastern Mediterranean crust with a velocity of about 40 mm/yr in respect of the stable Eurasian Continent (Jackson et al., 1994; Le Pichon & Angelier, 1979). Note that the region north of the North Aegean Trough (NAT) is being considered as part of stable Eurasia. Thus, deformation of the Aegean microplate is mainly focused between the NAT to the north and the East Mediterranean Ridge to the south. The kinematic situation of the Aegean is characterised by a gradual increase of deformation velocities with respect to Europe, from 10 mm/yr in the NAT up to 35-40 mm/yr in the Southern Hellenic Arc (Le Pichon & Angelier, 1979; Jackson & McKenzie, 1988).

1.2. Geological regime

The palaeogeographic, environmental and structural evolution of Greece, allows us to divide the region into several isopic or structural zones (Figure 2). Mountrakis (1985; 2010) described these zones supporting the theory of gradual rifting of various continental fragments from the Gondwana at the beginning of Mesozoic, their independent motion towards Eurasia that create a new oceanic crust to the rear, and their final collision with the Eurasia at the end of the Mesozoic. The structural zones are (from west to east):

i) The External Hellenides: a part of the Apulian microplate, which corresponds to a neritic continental sea depositional environment. It consists of the Parnassos, Gavrovo-Tripolis, Ionian and Paxos zones. A palaeogeographic difference of the Ionian zone is that, during the Middle-Upper Jurassic, it stood for an intracontinental basin with pelagic sediments. According to Doutsos et al. (2006), three major rift structures occurred during Mesozoic within the eastern margin of the Apulian continent that were reactivated in the Tertiary by forming intracontinental thrusts.

ii) The Internal Hellenides: the Circum-Rhodope zone represents the continental slope of the Hellenic Hinterland towards the ocean that was ending up in a trough where the subduction of the Tethys was taking place. The general Alpidic lithostratigraphic succession includes

volcanoclastic deposits, sea deposits ending up in deep-sea sediments westwards, and flysch. The Vardar zone corresponds to the ocean of Tethys characterised by the presence of deep-sea sediments and the obducted ophiolites. The Pelagonian zone is envisaged as a fragment of the Cimmerian microcontinent and mainly consists of neritic sediments. The most characteristic lithological unit of the Subpelagonian zone is the obducted ophiolites. This zone is considered as the continental slope of the Cimmerian continent towards the ocean, whose sedimentary remnants form the Pindos zone. Both zones consist of sea deposits showing a progressively deepening sea towards the west. The Attico-Cycladic zone, similar to the Pelagonian, is envisaged as a continental fragment having undergone neritic sedimentation.

iii) The Hellenic Hinterland: the Rhodope and Serbomacedonian Massifs represent an old continental crust affected by Alpidic metamorphism. Both zones mainly consist of crystalline rocks bearing few neritic deposits and also document Late Eocene–Early Oligocene granitoid intrusions (Figure 2).

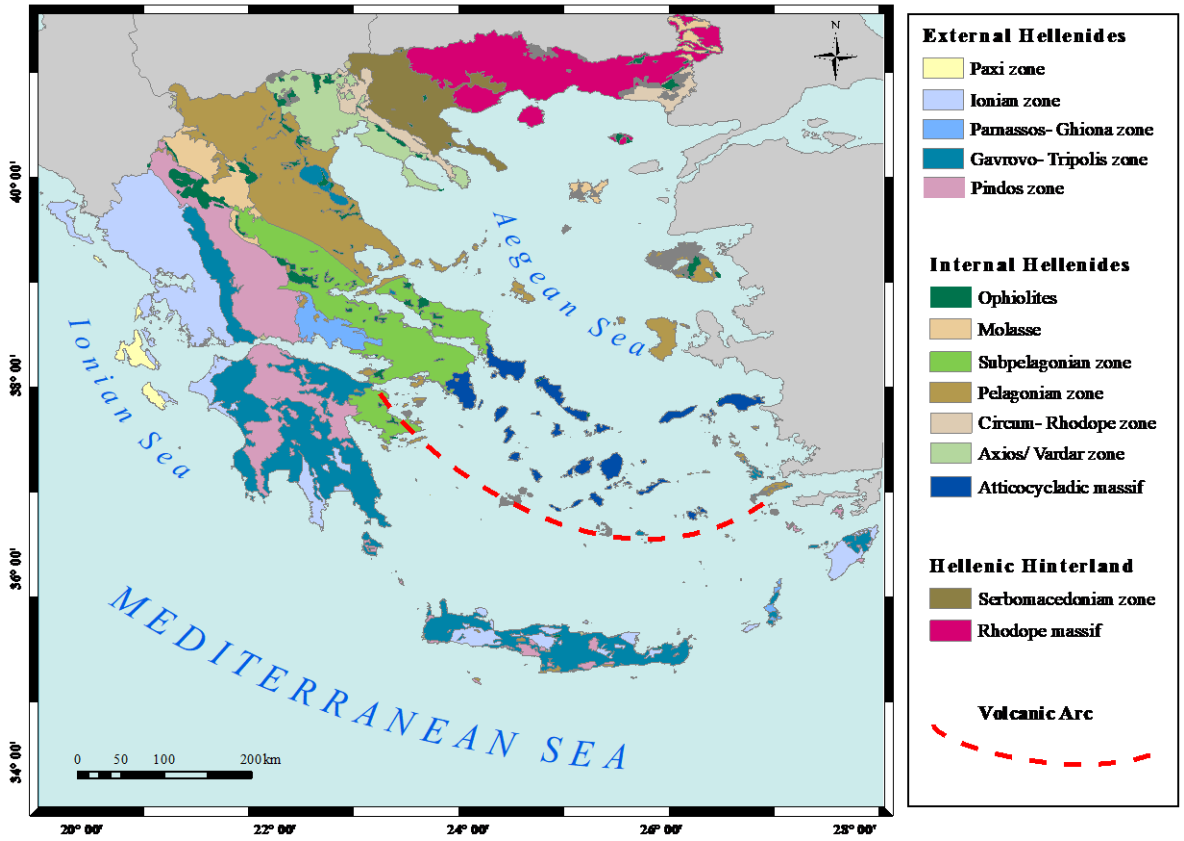

Figure 2: Structural zones of the Hellenides after Mountrakis (1986)

All three groups of zones have undergone various tectonic phases that affected them diversely during geological time. The Alpidic orogenetic phase documents two compressional stages (Mountrakis, 2010). The first one took place during the Late Jurassic and Cretaceous with the Meso-Tethys subduction, while the second one occurred during the Paleogene (Eocene-Oligocene- Miocene) with the final continental collision of the Apulia microplate with the Eurasia. According to the same author, the stacking of the nappes and the thickening of the crust, are attributed to the second Alpidic stage. Indeed, the broader Pindos Mountain chain documents a thick cover of successively repeated carbonate sedimentary layers.

1.3. Geothermal fields

Geology along with volcanism and tectonics contributed to the existence of many thermal and cold manifestations (Figure 3, Figure 4). In particular, the geologically recent volcanism of Greece and the high terrestrial heat flow have resulted in the development of a large number of geothermal fields varying from low to high enthalpy. After more than 30 years of extensive exploration activities (geological mapping, geochemical investigations, and geophysical and thermal gradient surveys), as well as drilling of a large number of shallow wells, and a few deeper ones, the significant geothermal potential of the country has been confirmed and new areas of geothermal interest have been identified (Andritsos et al., 2013; 2015). The bulk of exploration activities were carried out by the Institute of Geological and Mineral Exploration (IGME).

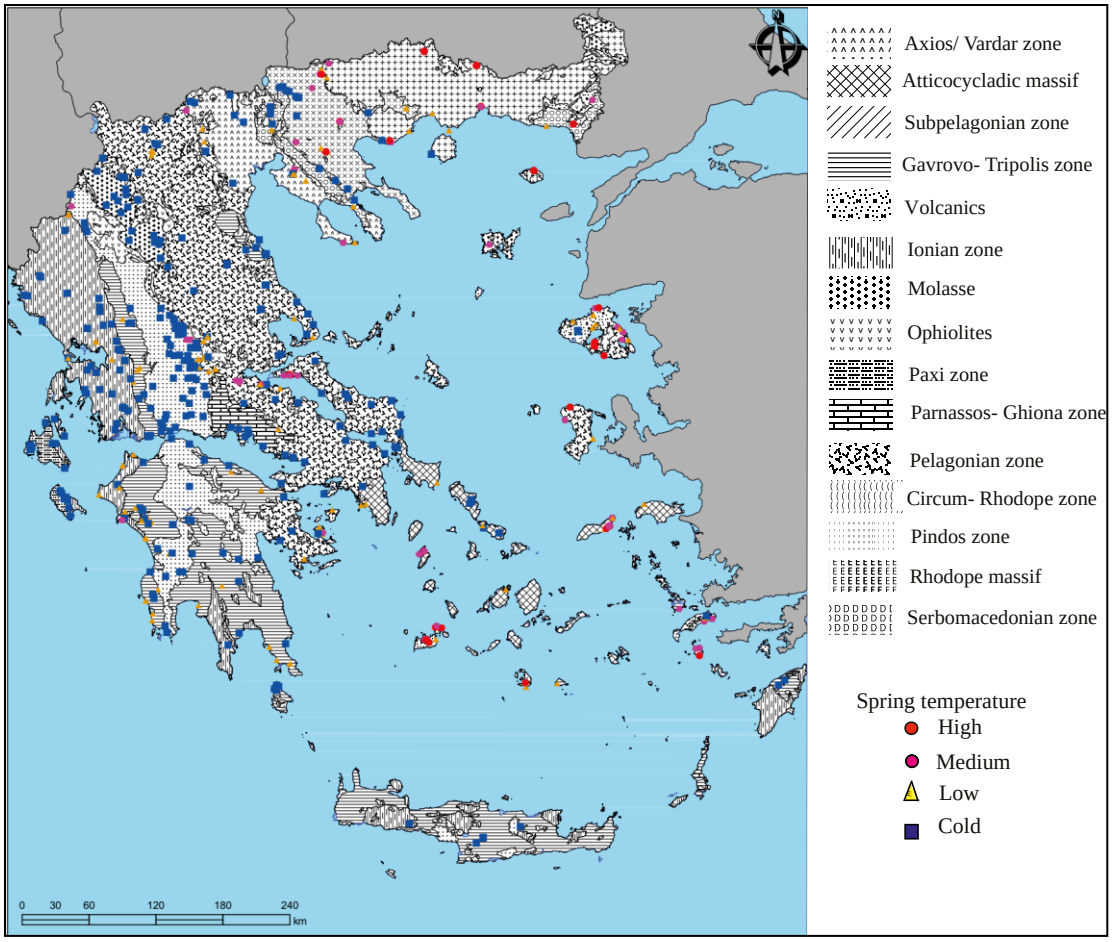

Figure 3: Map of geotectonic zones and thermal springs (Athanasoulis et al., 2009)

The most important geothermal fields are found in the back-arc regions, the South Aegean Active Volcanic Arc (SAAVA) and western Greece. The back-arc regions include the Tertiary sedimentary basins of Strymonas, Nestos and Evros deltas in northern Greece. These regions are low to medium enthalpy back-arc geothermal fields with extensional tectonics, which presumably also results in crust thinning (Figure 4 b). This type of tectonics trigger the formation of faults, which favor the quick rise of thermal fluids justifying the increased heat flow observed at these regions (Fytikas and Kolios, 1979; Figure 4 a). An additional cause for the increase of heat flow is the existence of felsic plutonism, e.g. Chrysochorafa, Eraklias, and Aggistro in the Prefecture of Serres and of N. Erasmios- Maggana in the Prefecture of Xanthi.

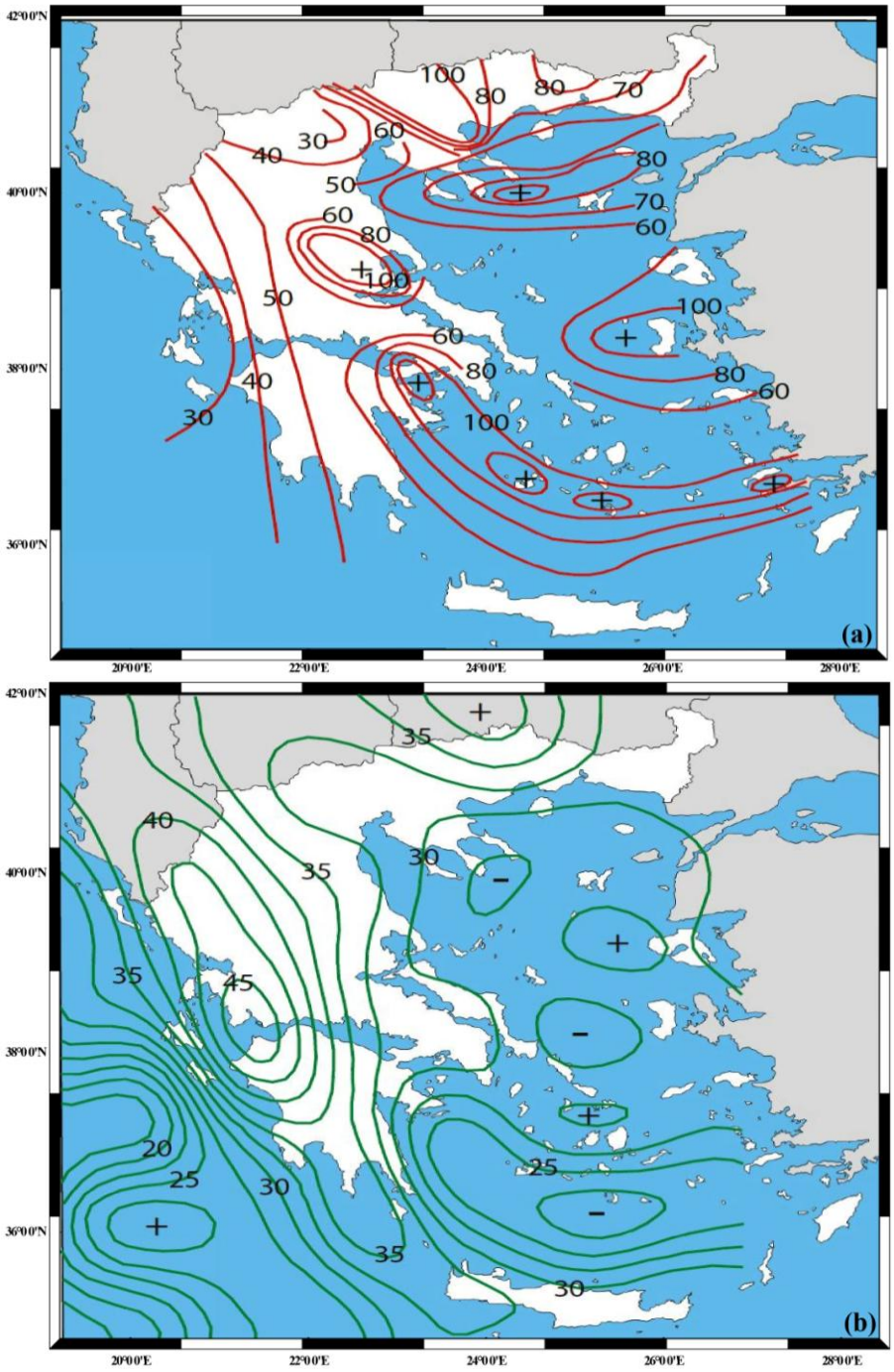

Figure 4: a) Heat flow map of Greece by Fytikas and Kolios (1979). The heat flow values are presented in mWm^{-2}; b) The new Moho depth model (km) from deep seismic imaging data as proposed by Grigoriadis et al., 2016.

The regions of north Euboea and Sperchios river drainage basins also belong to the back-arc geothermal fields with higher heat flow rates than the previous group (Figure 4 a). This is mostly due to the effect of the NAF in northern Turkey, which extends through the NE Aegean Sea (between Samothraki and Limnos) and ends up in the Sperchios basin (central Greece). East Aegean Sea islands, Samothraki, Limnos, Lesvos, Chios, and Ikaria also belong to the back-arc regions and their increased heat flow is due to active tectonics (Jackson & McKenzie, 1988). The activity of large faults (Figure 1) is also responsible for the increased heat flow of Lagadas and Volvi fields.

The increased heat flow along the SAAVA is a result of the presence of magma at relatively low depths. These are high-enthalpy regions and are more or less consistent with the theory of the normative geothermal system (Goguel, 1953). The high-enthalpy fields of Milos and Nisyros islands were studied in the early 1970s (Fytikas, 1988; Fytikas et al, 1995; Chiotis et al, 1990). In those two high enthalpy geothermal fields, seven deep wells were drilled and the highest measured temperatures were of 320 ºC and 350 ºC respectively. The proven potential of the well-explored high-enthalpy fields of these Islands for power generation purposes is estimated to exceed 250 MW_e. The heat flow in western Greece is substantially lower with the geothermal fields of Amarantos, Kavassila, Sykies Artas, Antirio, Kyllini, Kaiafas, and Vromoneri formed under a normal geothermal grade of 30^o C/km (Figure 4 a).

At present, geothermal energy exploitation in Greece is connected to the use of thermal and mineral water. It is estimated that 1% of the energy that derives from the exploitation of the geothermal fields is used for domestic heating, 7% in fish farms, 21% is used in healing facilities, 30% is consumed in greenhouses, and 41% in geothermal heat pumps (Hatziyannis, 2011). The total installed thermal capacity in Greece is estimated to exceed 130MW_t (Arvanitis, 2011).

1.4. Heat flow and Crustal Thickness using the new Moho model, an overview

According to the heat flow map as proposed by Fytikas and Kolios, (1979- Figure 4 a), low heat flow values are observed along the Hellenic subduction zone (IH) and in the western part (EH) of mainland Greece (up to 60 $mW \times m^{-2}$), whereas high heat flow values are concentrated along the active volcanic arc (VA), in the central Aegean Sea (around the island of Chios; IH) and along the NAT (IH, HH). In the SAAVA, high heat flow values range between 80 and 120 $mW \times m^{-2}$, whereas on the other 2 referred above regions, they arrive up to 100 $mW \times m^{-2}$. Relatively high heat flow values are observed in central and eastern Macedonia (HH) and in the area between the north eastern part of central Greece (IH) and the southern margin of the Thessaly basin (IH) (from 40 up to 100 $mW \times m^{-2}$ and from 50 up to 114 $mW \times m^{-2}$ respectively).

Tsokas et al. (1998) found that the Curie point depth on the island of Crete (EH) is 26 km whilst, Stampolidis and Tsokas (2002) estimated that the depth in the geographical regions of Macedonia (IH, HH) and Thrace (HH) range from 11.2 to 17.3 km (Figure 4 b). According to Sachpazi et al. (2007) the Moho depth along the strike of the Hellenides mountain belt (IH) has an elevated value (up to 50km), whereas towards the Aegean Sea and in particular in the island of Euboea (IH), the depth is decreased (Figure 4 b). More specifically, in the southern and in a large part of the central Aegean Sea the crust has a thickness of approximately 20–22 km (Karagianni et al., 2005), whereas the remaining exhibits a crustal thickness of less than 28–30 km. In western Greece, the crustal thickness is of 40–46 km. The remaining part of continental Greece is characterised by a mean crustal thickness of 35 km (Karagianni et al., 2007). All the results mentioned above and after the interpretation of Papadakis at al. (2016), suggest that the central Aegean region is characterised by a thin, deformed crust and high heat flow values, whereas the western part of continental Greece is characterised by a thick crust and low heat flow values (Figure 4).

2. Materials and Methods

The gas samples used for the present study have been selected from a database of 568 samples collected by researchers of the Istituto Nazionale di Geofisica e Vulcanologia – sezione di Palermo in collaboration with the National and Kapodistrian University of Athens, Dept. of Geology and Geoenvironment in the period from December 2003 to October 2017 from almost all the known gas manifestations of Greece. Samples were analysed in the Gas Chromatography, Mass Spectrometry and Noble Gas laboratories of the Istituto Nazionale di Geofisica e Vulcanologia of Palermo and in the Gas Chromatography laboratory of the University of Florence. Aim of the analyses was to determine the chemical and isotope compositions of the gases. 253 samples were collected in 11 campaigns from October 2014 to October 2017 with my personal involvement. Some of the gas manifestations were repeatedly sampled and in this case it was decided to consider no more than 3 samples for each site. Selection of the samples was made giving precedence to those with the largest number of analysed parameters, the least affected by atmospheric contamination and the most recent. This resulted in 343 samples, 165 of which collected from October 2014 to October 2017. To these 9 samples taken from literature were added, totalling 352 samples, whose composition will be discussed in the present thesis. Names, sampling date, coordinates chemical and isotope results of all these sampling sites can be found in Table 1, Table 2 ,Table 4, Table 5, Table 6, Table 7, Table 8 of the appendix.

2.1. Sampling methods

2.1.1. Free gases

Free gases were sampled by the method proposed by Caprai (2005). Before sampling a bubbling gas, the site of greatest gas flow was determined. When such flow was believed to be sufficient to displace the air present in the sample holder, the funnel was inverted and appropriately ballasted, and then placed over the manifestation (often completely immersed in the water). The funnel was then connected to the gas sample holder by means of a silicone rubber tube, and the gas made flow through the sample holder for as long as was necessary to flush it out thoroughly (the volume of gas made to flow must be at least 5 times that of the holder). The flow of gas was controlled through a rubber tube connected to the sample holder's exit valve, which was immersed in a liquid that enables the bubbling of the outflowing gas to be checked visually. In the event that the flow was insufficient for proper flushing, one possibility was to fill the sample

holder with water and wait for the gas bubbles to displace the water while trying to help the gas rise by gently shaking the system and/or pinching and releasing the rubber tube.

In the case of fumarolic gases, the best site to perform such sampling was determined of the basis of the flow rate and/or the maximum temperature found in the zone in question. Temperature measurements were performed with a thermocouple. On field, a titanium pipe was introduced into the fissure.

Soil gases were sampled inserting a 50 cm long 3 mm ID Teflon tube in the soil. The sample was collected slowly sucking with a syringe connected through three-way valve to a sample holder.

Gases for light hydrocarbon gas analysis were collected in 12 ml Exetainer® vials. Gases for major gas analysis and for $\delta^{13}C\text{-}CO_2$, $\delta^{13}C\text{-}CH_4$ and $\delta^{2}H\text{-}CH_4$were collected either in 12 ml Exetainer® vials or in borosilicate glass flasks equipped with two vacuum stopcocks. The latter were used for He isotope analyses. The number of collected aliquots depended on the gas flux and on sampler availability. In the best case 2 vacuum stopcocks-equipped glass flasks and 4 Exetainer® vials were collected. In very few cases only 1 or 2 vials could be collected but in majority of cases 1 vacuum stopcocks-equipped glass flask and 4 Exetainer® vials were collected.

2.1.2. Dissolved gasses

Dissolved gas samples were analysed with the "*headspace technique*" following the method of Capasso and Inguaggiato (1998) for the chemical composition and Inguaggiato and Rizzo (2004) for isotope analysis. This method is based on the partitioning equilibrium of gases between liquid and gas phase. It is possible to derive the initial concentrations of the dissolved gases in the liquid phase from concentrations in the gas phase, using the partitioning coefficients of the different species.

The sampling apparatus consisted of a glass flask of known volume, that was sealed by gastight rubber/ teflon plugs. The flask had to be totally filled with the water sample to be analysed and sealed, taking care not to include air bubbles. On field, along with at least 3 vials of 150 ml for the analyses of the chemical composition of the gases and the He isotope composition, was also taken 1 vial of 50 ml for the analysis of $\delta^{13}C$-TDIC. At sampling sites were CH_4 concentrations were known or suspected to be high enough, 2 additional vials of 200 ml were collected in order to be analysed for $\delta^{13}C\text{-}CH_4$ and $\delta^{2}H\text{-}CH_4$. To avoid possible losses of gas (particularly He),

bottles were kept upside down until the analysis. In the laboratory a host gas had to be injected into the flask drawing out the equivalent water volume through a needle, thus leaving the apparatus at atmospheric pressure. The host gas used depends on the type of analysis (high purity Ar for chemical analysis and for isotope analysis of CH_4 and high purity N_2 for the isotope analysis of He).

Since dissolved gas phases in natural samples can be at conditions of undersaturation or supersaturation, before extraction, it was necessary to restore atmospheric pressure inside the flask. This was obtained by adding or removing a few ml of water connecting the flask upside down to a tube filled with water open to the atmosphere. After restoring the sample to standard conditions (25^o C, 1 atm) and shaking it for 5 min, a portion of gas was drawn for gas chromatography analysis. Two plastic syringes with stopcocks were used for the extraction of the gas. Some water was injected into the flask with a syringe and the equivalent gas volume was drawn by the second syringe and then analysed.

2.2. Analytic methods in the laboratory

In the laboratory, gas samples were analysed for He, H_2, H_2S, O_2, N_2, CH_4 and CO_2 by gas-chromatography (Perkin Elmer Clarus500 equipped with a double Carboxen 1000 columns, TCD-FID detectors) using Ar as the gas carrier. Ar was analysed with a Perkin Elmer XL gas-chromatograph with MSieve 5A column, TCD detector having He as carrier. Analytical uncertainties were ± 5%. Hydrocarbon analyses were performed with a Shimadzu 14a gas-chromatograph equipped with a Flame Ionization Detector (FID) using He as the carrier gas. The analytical error was ≤5%. To allow rapid comparison,dissolved gases have been recalculated as free gas phase in equilibrium with the sampled water. These, expressed in µmol/mol,have been obtained from the partial pressure values taking into account the solubility coefficients of each gas species at laboratory temperature.

Carbon isotope composition of CO_2 was determined by using a Thermo Delta Plus XP, coupled with a Thermo TRACE Gas Chromatograph (GC) and a Thermo GC/C III interface. The TRACE GC is equipped with a Poraplot Q (25 m x 0.32 mm) column and uses He (5.6) as carrier gas at a constant flow of 0.9 cc/min. Undesired gas species, such as N_2, O_2, and CH_4, are vented to atmosphere by means of back-flush of He and a Sige valve.

The $^{13}C/^{12}C$ ratios are reported as $\delta^{13}C_{CO2}$ values with respect to the V-PDB standard. Carbon isotope ratios were determined by comparing three in-house standards ($\delta^{13}C$ ranging from +0.3±0.1‰ to -28.5±0.3‰ vs V-PDB calibrated by using of a CO_2 standard (RM8564) with known isotopic composition ($\delta^{13}C$ = -10.45±0.04‰ vs V-PDB) and two international standards (NBS 18 and NBS 19). External precision, computed as1σ (standard deviation) on ten measurements of the same sample, is 0.1‰.

Isotope compositions of CH_4 were measured using a Thermo TRACE GC interfaced to a Delta Plus XP gas source mass spectrometer and equipped with a Thermo GC/C III and with GC/TC peripherals for Carbon and Hydrogen respectively.

The gas chromatograph was equipped with an Rt-Q Plot column (Restek 30 m × 0.32mmi.d.) and the oven was held at a constant temperature (50 °C for carbon and 40 °C for Hydrogen). The flow rate of carrier gas (He of 5.6 grade) was held at a constant flux of 0.8 cc min^{-1}. A split/splitless injector with a split ratio from 10:1 to 80:1 was used for sample introduction, except for diluted samples (CH_4 concentration lower than 10 mmol/mol) when direct on-column injection was performed.

The inlet system, better described in Grassa et al. (2010), consists of a stainless steel loop with a known volume (50 µl), connected to a two-position six-port Valco® valve. Before the introduction of the sample, a vacuum of 10^{-2} mbar measured with an EBRO pressure gauge is ensured by a rotary vane pump. Once CH_4 was separated from the gas mixture, it was quantitatively converted to CO_2 by passing through a combustion oven (T=940 °C) for $^{13}C/^{12}C$ ratios analysis or to H_2 by passing it through a reactor set at a temperature of 1440 °C for $^{2}H/^{1}H$ ratios analysis. Each sample analysis took about 500 s.

The $^{13}C/^{12}C$ ratios are reported as $\delta^{13}C$-CH_4 values values with respect to the V-PDB standard and$^{2}H/^{1}H$ ratios are reported here as $\delta^{2}H$-CH_4values with respect to the V-SMOW standard.Carbon isotope ratios were determined by comparing an in-house standard ($\delta^{13}C$= -49.5±0.2‰) calibrated by using of four CH_4 standards (Isometric Instruments) with known isotopic composition ($\delta^{13}C$ ranging from −23.9±0.3‰ to -66.5±0.3‰ vs V-PDB).

Hydrogen isotope ratios were determined comparing an in-house standard ($\delta^{13}C$= -200±2.0‰) with a CH_4 standard with known isotopic composition ($\delta^{2}H$= -186.1±3.0 ‰ vs V-SMOW).

External reproducibility, estimated as 1σ (standard deviation) on ten measurements of the samesample, is 0.2‰ and 2.0‰ for carbon and hydrogen isotopes respectively.

Isotope analyses of CO_2-dominated gases having CH_4 concentrations <1000 µmol/mol were carried out in the gas samples collected using pre-evacuated 60 mL glass flasks filled with 20 mL of a 4 N NaOH solution (Giggenbach and Gougel, 1989).

The abundance and isotope composition of He, and the $^4He/^{20}Ne$ ratios, were determined by separately admitting He and Ne into a split flight tube mass spectrometer (Helix SFT). Helium isotope compositions are given as R/R_A, where R is the ($^3He/^4He$) ratio of the sample and R_A is the atmospheric ($^3He/^4He$) ratio ($R_A=1.386\times10^{-6}$). The analytical technique is described more in detail in Paonita et al. (2012). The analytical errors were generally <1%.

3. Results

3.1. Chemical composition of the gases

In the period from 2004 to 2017, more than 352 samples of free and dissolved gases were collected along the whole Hellenic area (Figure 5, Table 1, Table 2). Basing on the spatial distribution of the gas discharges and their type of emission, the whole dataset was subdivided into 4 main geological domains, as follows: 1) External Hellenides (EH) –25 samples; 2) Internal Hellenides (IH) - 160 samples; 3) Hellenic Hinterland (HH) - 43 samples; 4) Volcanic Arc (VA) - 124 samples. The chemical composition of the dry gas fraction (CO_2, H_2S, CH_4, N_2, O_2, Ar, He and H_2) of the 352 gas samples analysed in the present study is reported in Table 4 (found in the appendix), whereas the 9 literature data were taken from Rigakis et al., 2001, Etiope, 2009, Etiope et al., 2009; 2013a; 2013b, D'Alessandro et al., 2008; 2014; 2017; Rizzo et al., 2016. A part of this dataset was extracted and chemical analysis for light hydrocarbons was performed (Table 5). Furthermore, all data were compared with the end-member values of AIR, Air Saturated Water (ASW), Air Saturated Sea Water (ASSW) after Kipfer et al. (2002), MORB after Javoy and Pineau (1991), Sub-Continental Lithospheric Mantle (SCLM) after Bräuer et al. (2008; 2013) and Kolumbo volcano after Rizzo et al. (2016) (Table 3).

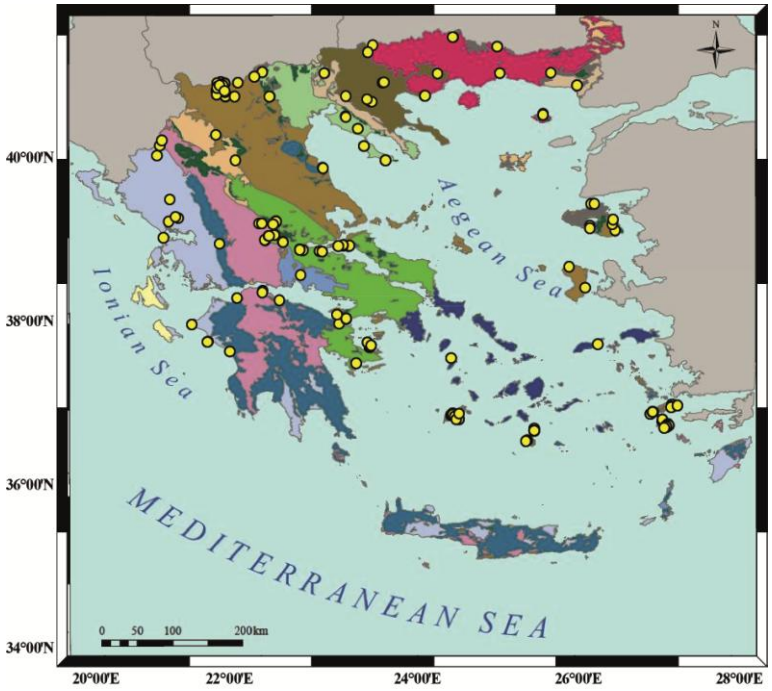

Figure 5: Geological map with the sampling sites

The dominating gas was either CO_2 (from 17 to 1,000,000 µmol/mol) or N_2 (from 600 to 995,000µmol/mol) or CH_4 (from < 0.5 to 915,000 µmol/mol) (Figure 6 a, b). O_2 and Ar showed concentrations up to 459,000 and 13,700 µmol/mol respectively). H_2S was either below detection limit or showing concentrations -generally lower than 10,000 µmol/mol except for the fumaroles of Nisyros, where the concentrations reached up to 192,000 µmol/mol (Fiebig et al., 2013). He concentrations were up to 3370 µmol/mol (Figure 6 c).

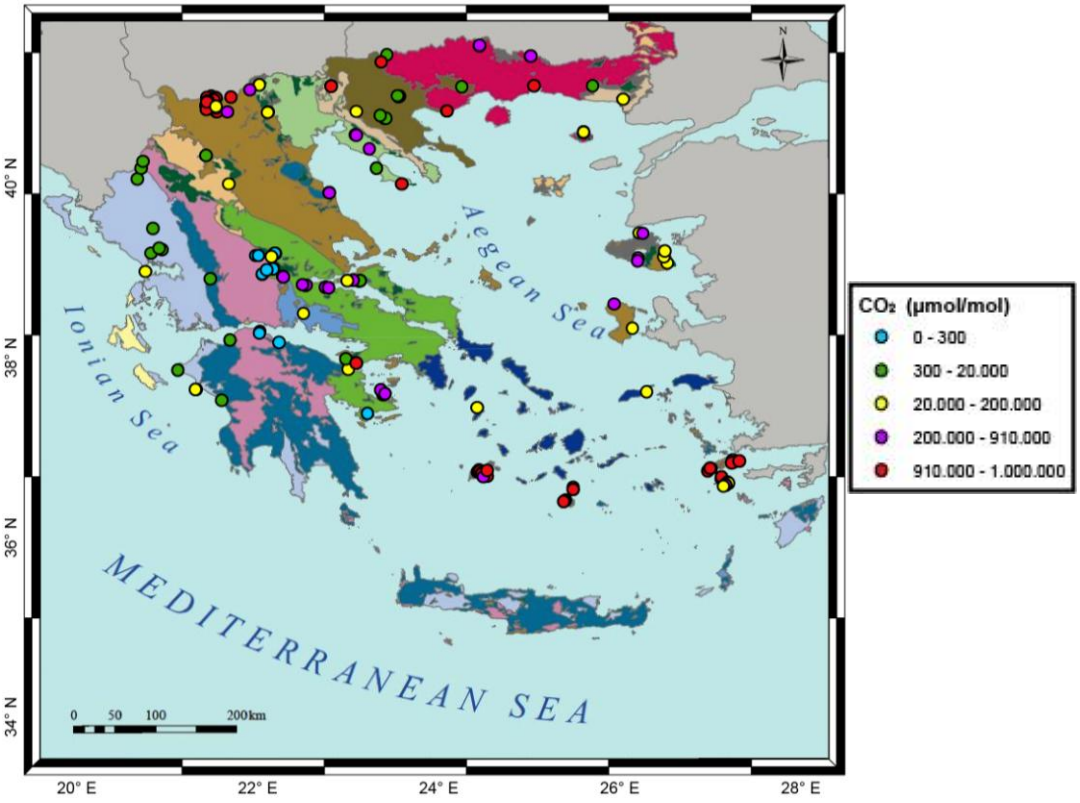

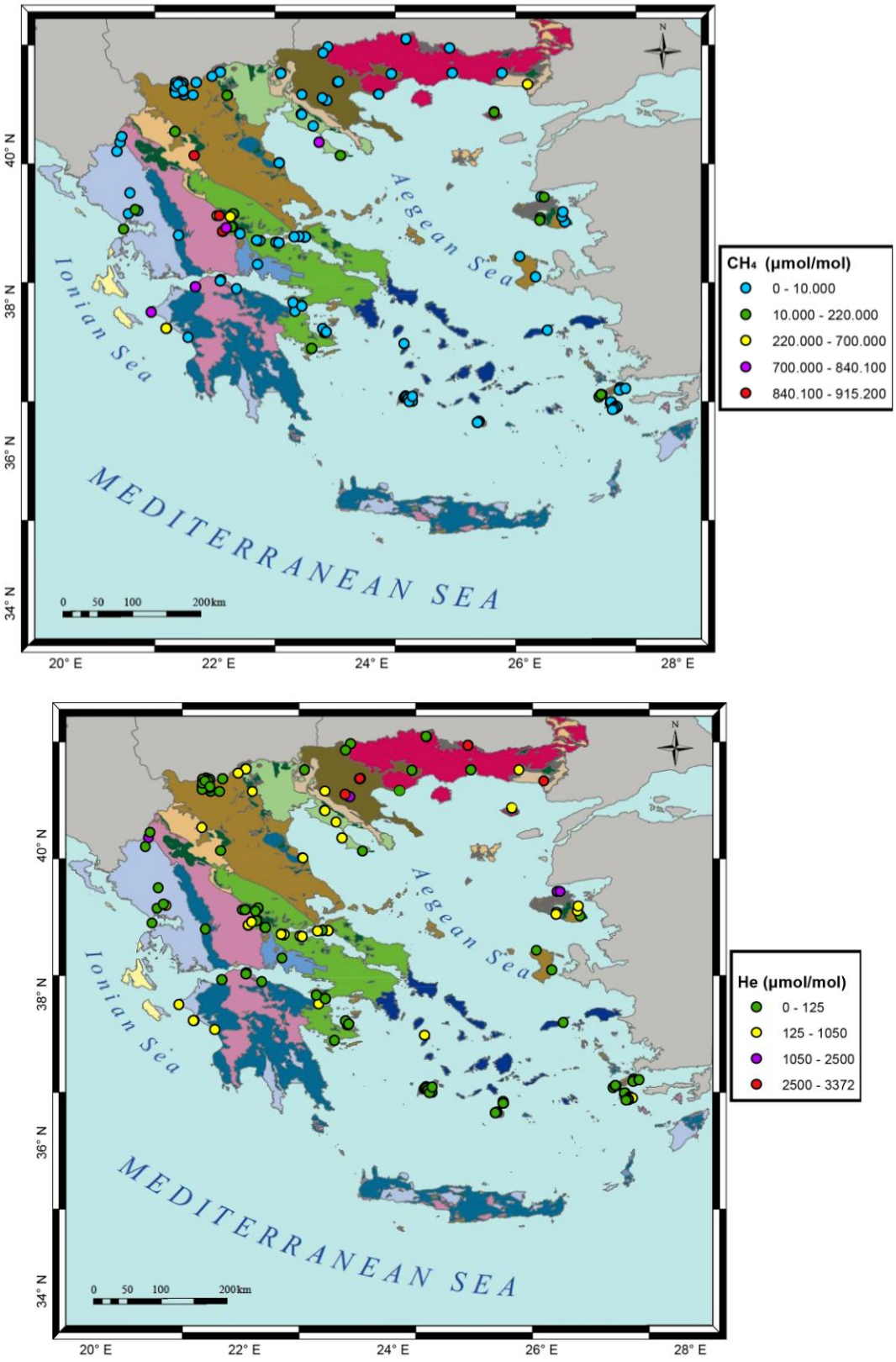

Figure 6: Geological map of Greece presenting the a) CO_2 b) the CH_4 and c) He concentrations. Classes were determined by the slopes of the probability plots.

From the database used for the light hydrocarbon study, gases from EH show the highest concentrations of CH_4, having a median of 721,200 μmol/mol (from 85,000 to 925,000 μmol/mol). In IH, they present a median of 2600 μmol/mol, with values ranging from <0.5 up to 880,000 μmol/mol, whereas the lowest concentrations are found in HH with a median of 545 μmol/mol (from 23 up to 879 μmol/mol). Finally, those collected in VA present a median of 1460 μmol/mol (from 5 up to 117,000 μmol/mol) (Table 5).

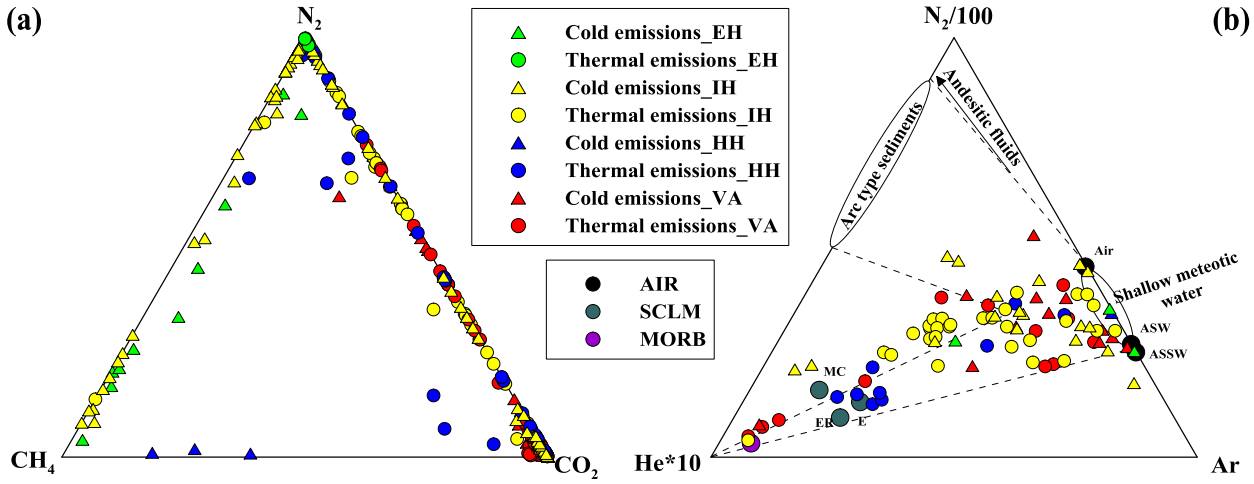

Figure 7: Chemical composition of the collected gases. a) CH_4-N_2-CO_2 ternary diagram and b) He-N_2-Ar ternary diagram. On the diagram are also plotted the typical values of AIR, ASW, ASSW after Kipfer et al. (2002), MORB after Javoy and Pineau (1991) and SCLM after Bräuer et al. (2008; 2013). Symbol colours refer to the geographical distribution of the samples while shape refers to the type of the emission (cold or thermal).

In the CO_2-CH_4-N_2 ternary diagram (Figure 7 a), samples collected in the EH show N_2 (thermal emissions) and CH_4-N_2 dominated gases (cold emissions) with relative low contents of CO_2 (from 145 up to 83,400 μmol/mol). Gases collected from the manifestations of IH are rich in CO_2-N_2 in their majority, whereas those collected from the cold manifestations of Subpelagonian and Vardar- Axios zones (23, 27, 28,107, 111-114 etc) are CH_4 dominated. In the thermal discharges of HH, CO_2-N_2 are the most abundant gas species, whilst in those of the cold emissions CH_4 is prevailing with small enrichments in CO_2 (from 3,680 up to 988,000 μmol/mol). Samples collected from both cold and thermal emissions of the VA are having CO_2 as the dominant gas species; however, they are also presenting enrichments, at points strong (samples no. 237, 239, 255, 299, 344, 345) in N_2 (from 415,000 up to 989,000 μmol/mol).

The N_2/Ar ratio can be used to distinguish the relative contributions to a gas mixture from air, air-saturated waters, and fluids deriving from interactions within subducting and crustal rocks/sediments and mantle gases (e.g. Snyder et al. 2001, 2003). The He-N_2-Ar ternary diagram (Giggenbach, 1996) (Figure 7 b) suggests important mixing processes between deep crustal or mantle gases and also gases originating in the upper crust or atmosphere. N_2 and CH_4-N_2 rich gases of EH and some of the CO_2-N_2 dominated cold emissions of IH (39, 44, 76, 88, 96, 117) plot close to the Air and ASW points, indicating that the atmospheric component for these gases prevails. Some of the samples from VA and the thermal emissions of IH (CO_2 and CO_2-N_2 dominated gases) fall on the theoretical line that connects ASW with a He-rich source, presenting a relatively low contribution of crustal N_2 (Giggenbach, 1996). Samples of HH rich in CO_2-N_2 and some of the emissions that occur in IH, characterised by a N_2-CO_2 composition, show atmospheric N_2 mixed with non-atmospheric N_2.

3.2. Isotope composition of the gases

The δ^{13}C-CO_2 values ranged from -29.9 to +6.0‰ although most of them are comprised in a narrower range from -6.4 to +0.8‰ (Table 6). Samples from EH have negative values, from -29.5 to -5.1‰. Gases collected from IH are presenting a wide range starting from the lowest value of δ^{13}C-CO_2 (from -29.9‰ to +0.3‰), whereas those of HH, reach the highest value (-16.3 to +6.0 ‰). Samples of VA range from -4.0 to 1.3 ‰, apart from the sample no. 255 whose δ^{13}C-CO_2 value was -20.1‰.

The isotope ratio of He range from 0.02 to 6.71 R/R_A; (Table 6, Figure 8). CO_2 dominated gases from VA show high values for the isotope ratio that ranges from 0.18 to 6.71 R/R_A, whereas the CO_2-N_2 thermal discharges of HH show values from 0.03 to 1.18 R/R_A. In the cold emissions of the same area, in which CH_4 is the dominant gas species, values range from 0.3 to 1.69 R/R_A. IH present isotope ratios that range from 0.02 to 1.30 R/R_A, however, in the CH_4-rich cold manifestations of the Subpelagonian and Vardar-Axios zones show values in the range 0.06-1.36 R/R_A. Finally, EH values present a range of 0.04 to 1.19 R/R_A, with the rich in CH_4-N_2 emissions showing a higher range in the isotope ratio of He with respect to the N_2 ones (from 0.04 to 1.19 R/R_A and from 0.08 to 0.46 R/R_A respectively).

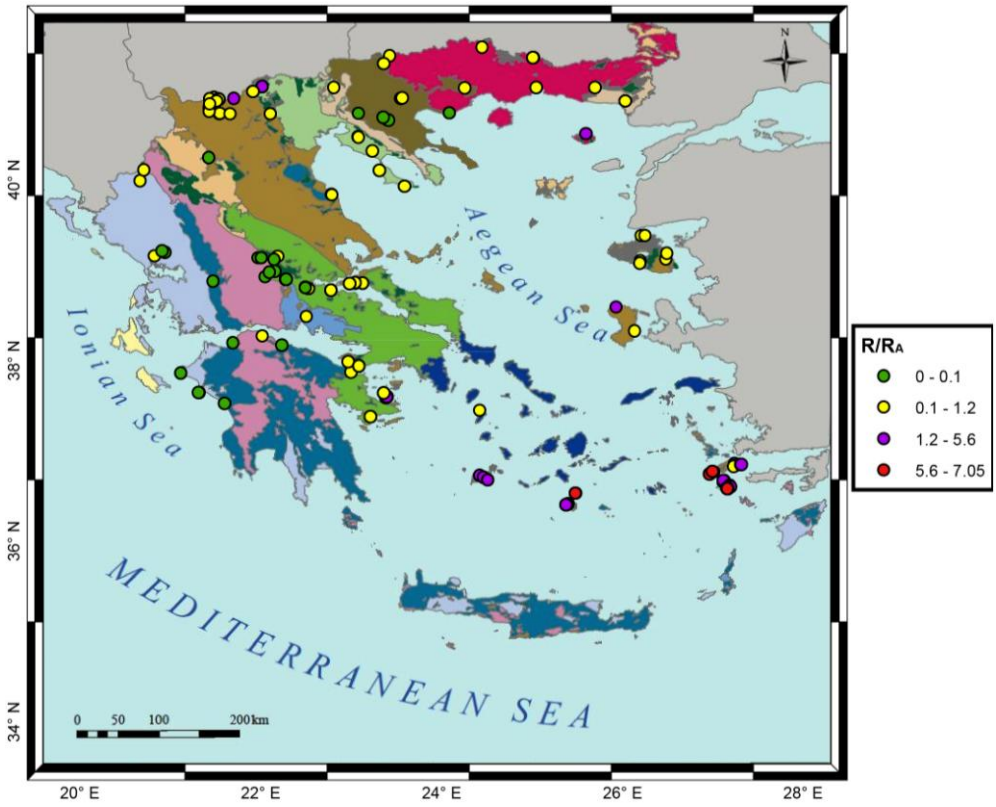

Figure 8: Geological map of Greece presenting R/R_A values. Classes were determined by the slopes of the probability plots.

For the description of the isotope values of CH_4 for both $\delta^{13}C$ and $\delta^{2}H$ the extracted dataset was used (Table 7). The $\delta^{13}C$ and $\delta^{2}H$ values of CH_4 range from -79.8 to +45.0 ‰ for $\delta^{13}C$-CH_4 and from -311 to +301 ‰ for $\delta^{2}H$-CH_4, respectively. Gases from EH have $\delta^{13}C$-CH_4 and $\delta^{2}H$-CH_4 values ranging from -79.8 to -31.3 ‰ and from -248 to -62 ‰, respectively. In IH, the values of $\delta^{13}C$ range from -64 up to +45 ‰, whereas $\delta^{2}H$ shows a wide range of values (from -311 to +301 ‰). The $\delta^{13}C$-CH_4 values of HH gases range from -34 up to +1 ‰, whereas their $\delta^{2}H$ values, apart from sample no.75 (-174 ‰), were not measured due to their extremely low concentrations. The gases from VA show $\delta^{13}C$-CH_4 values ranging from -38 up to +2 ‰ and $\delta^{2}H$ values from -135 to +36 ‰.

4. Discussion

4.1. Gas Components

Nitrogen, one of the main components found in the gas samples, shows generally decreasing concentrations from EH and IH to HH (Figure 9 a). Gases from the VA display generally even lower contents (Figure 9 a). As seen in the He-N_2-Ar ternary diagram (Figure 7 b), N_2 mostly originates from the atmosphere through the meteoric recharge or through diffusion in the shallowest soil layers. From the same diagram a contribution from crustal sources or from the subducting slab is apparent for some of the samples. At the moment only few N-isotope values of N_2 have been published (Grassa et al., 2010) indicating sometimes significant (up to 60 %) sedimentary contribution.

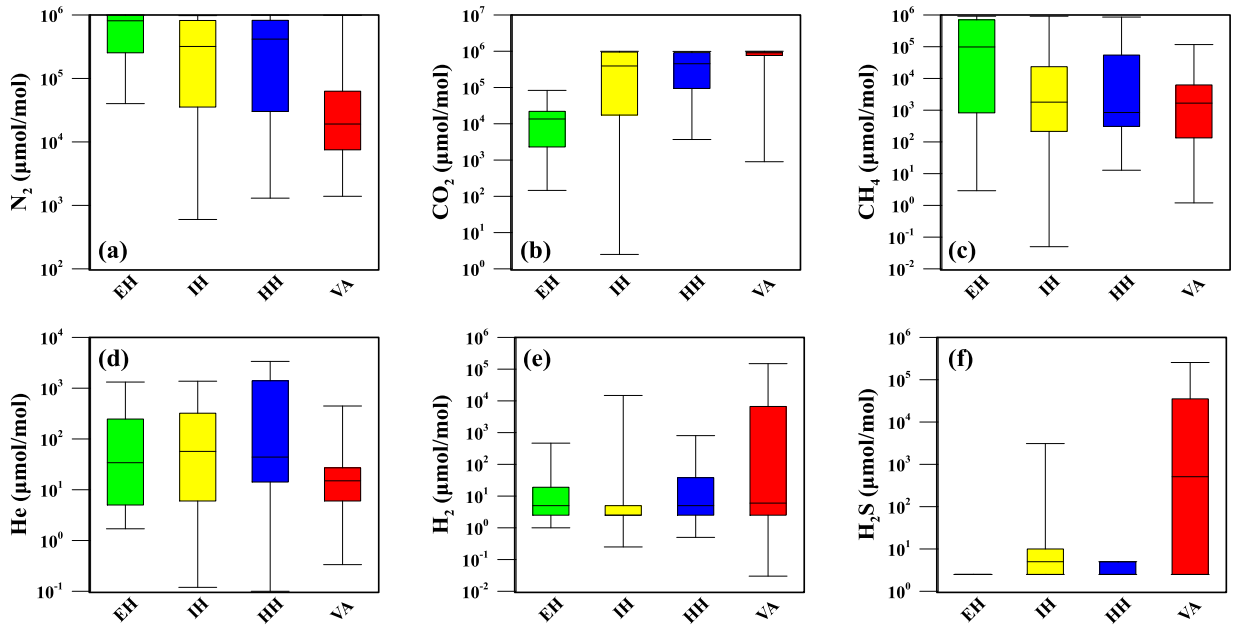

Figure 9: Box and whiskers plot in which the total range of concentrations (in µmol/mol) of a) N_2; b) CO_2; c) CH_4; d) He; e) H_2 and f) H_2S are presented for each region.

Carbon dioxide and He present the same increasing pattern in all the regions from west to east (Figure 9 b, d). However, in VA, they show an opposite pattern. On the other hand, CH_4 shows elevated concentrations in EH with respect to the other regions (Figure 9 c). All three gases along with the processes that are affecting them are going to be discussed in detail on the following Paragraphs.

The occurrence of relatively high concentrations of H_2 (up to 14,800 μmol/mol - Table 4, Figure 9 e) in gases from the volcanic systems of the SAAVA is most likely related to water-rock interactions at elevated temperatures. It is well known that Fe(II)-bearing minerals react with water at temperatures >300 °C generating H_2 (e.g., Giggenbach, 1987; Seewald, 2001). Most of the samples collected at IH and HH have H_2 below detection limit (Table 4). Concentrations of H_2 up to 50 μmol/mol are found in the EH gases and are related to the hydrocarbon reservoirs of the area.

Hydrogen sulfide in fumarolic gases from active volcanoes is likely produced by thermochemical reduction of magmatic SO_2 occurring within the hydrothermal reservoirs (Giggenbach, 1987, Allard et al, 1991; Oppenheimer, et al., 2014), and, therefore, shows the highest concentrations along the VA (Figure 9 f), where most of the geothermal systems evidence an input of magmatic gases (Marini and Fiebig, 2005; Rizzo et al., 2015). On the other hand, sedimentary sources of H_2S consist of i) alteration of sulfide minerals (Giggenbach, 1980; Chiodini, 1994), ii) microbial activity, and iii) thermochemical sulfate reduction (Machel et al., 1995; Worden and Smalley, 1996). The H_2S concentrations in the gas discharges of EH are below detection limit with few exceptions, likely because this compound has a relatively high solubility in water, thus whatever its origin, it may be partially or totally dissolved and oxidized in cold shallow aquifers present along the uprising gas pathways (Minissale, 2004). Most gases from IH and HH show also H_2S concentrations below detection limit, except samples 131, 132, 135, 136, 142, 144, 172-174, where concentrations up to 3.100 μmol/mol have been measured (Table 4). It is worth noting that these samples were collected in Vardar-Axios and Subpelagonian zone and in particular in the areas of Sperchios basin and Kassandra peninsula, which correspond to maxima on the heat flow map (Figure 4), suggesting the occurrence of medium enthalpy geothermal systems (Fytikas and Kolios, 1979).

4.2. Origin and sources of He and CO_2 in the gas manifestations of Greece

Carbon dioxide is the carrier phase for mantle-derived fluids. The combination of C and He isotope ratios is a useful tool to evaluate the origin of fluids. The He isotope ratios are used to distinguish between crustal and upper mantle-derived components. In order to evaluate the effects of geological processes, the CO_2-He data are plotted on a CO_2-^{3}He-^{4}He ternary diagram (Figure 10). Furthermore, the typical values of Air, ASW, ASSW (Kipfer et al., 2002), MORB (Javoy and Pineau, 1991), SCLM (Bräuer et al., 2008; 2013) and Kolumbo volcano (Rizzo et al., 2016) are also plotted for comparison (Table 3). The latter has recently been hypothesized to be the MORB-like end-member, at least of the south Aegean area (Rizzo et al., 2016). In the diagram are also plotted the binary mixing trajectories between MORB-type mantle fluids (R/R_A=8, $CO_2/^3He=2\times10^9$) and various crustal volatile end-members as well as the general trends expected from addition and/ or loss of a particular volatile phase. As can be seen from the plot (Figure 10), some of the samples (54, 55, 57, 63-66, 71, 72, 81, 96, 103, 116, 135, 142, 174 of IH; 196-198, 204, 205, 207, 219, 220 of HH) represent products of variable amounts of mixing between mantle-derived and crustal volatiles. It is also worth noting that samples no. 62, 67, 69, 70, 74-76, 87, 88, 91, 114, 136 (IH) and no.187, 191, 192 (HH) plot at or close to the CO_2 apex having exceptionally high $CO_2/^3$He ratios (Figure 10 b). On the other hand, all samples collected in EH and the majority of the remaining samples of IH and HH plot on the base of the diagram presenting extremely low $CO_2/^3$He ratios. Samples collected in VA plot close to the MORB and SCLM points, except from samples no. 253, 256-258, 277, 278, 286, 287, 341, 344 and 345 that present high $CO_2/^3$He ratios and samples 346-348, 350-352 that present low R/R_A ratios (Figure 10 b). Furthermore, from Figure 10 b is also noticeable that samples 237, 238, 254, 255 and 335 present $CO_2/^3$He ratios lower than the MORB and SCLM.

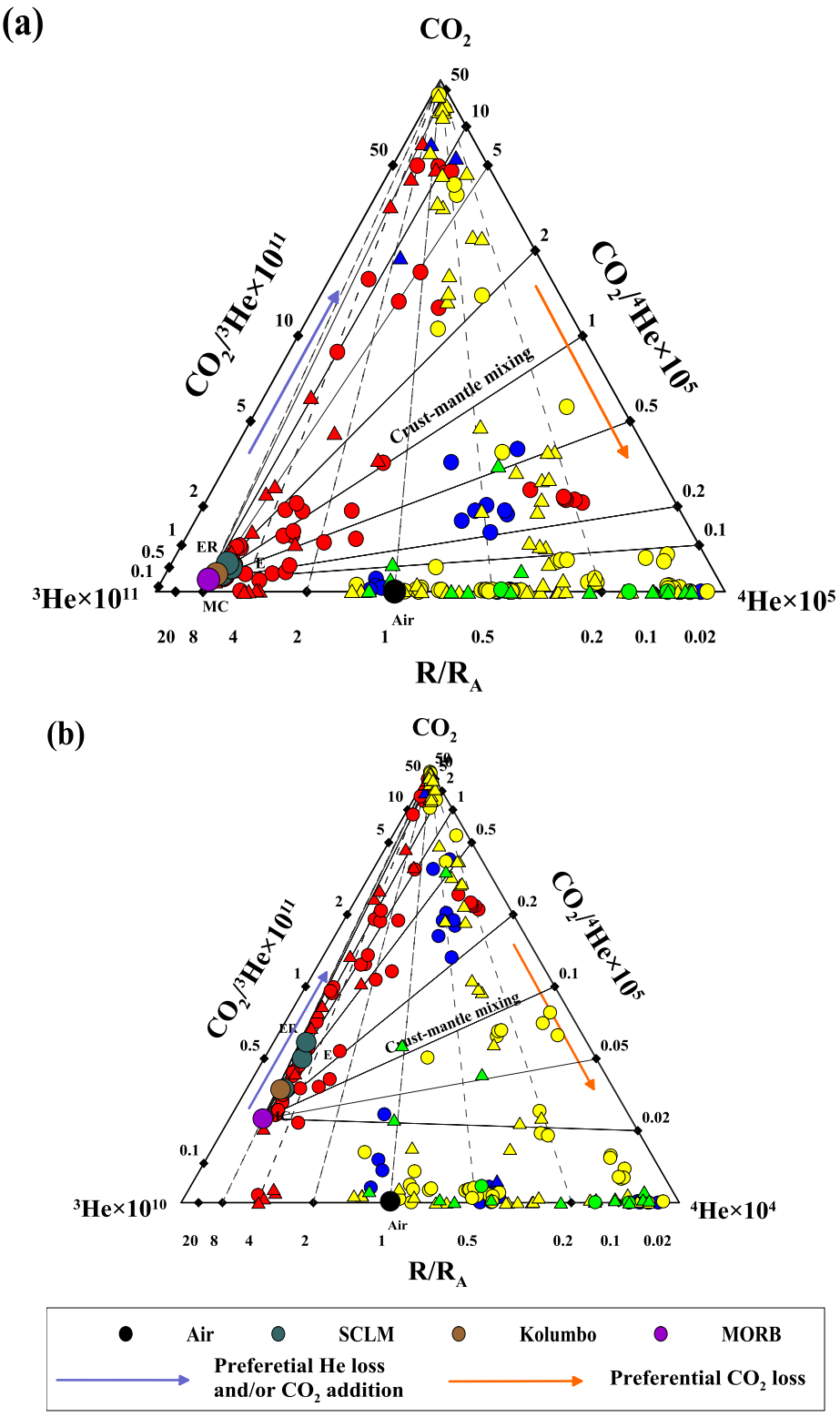

Figure 10: a) CO_2-^{3}He-^{4}He ternary diagram, b) CO_2-^{3}He-^{4}He ternary diagram with CO_2 multiplied per 10 times. Values of Air, ASW, ASSW, MORB, SCLM and Kolumbo volcano are also plotted in the diagram. Symbols as in Figure 7.

Hydrothermal degassing seems to be a plausible mechanism to explain the high $CO_2/^3He$ ratios, as He, being less soluble than CO_2 in aqueous phase, is preferentially lost into the first formed gas phase leading to an increase in the $CO_2/^3He$ ratio of the residual phase. An alternative possibility is the addition of pure CO_2 into geothermal fluids (e.g. directly from carbonate lithologies without accompanying He), which would also result in an increase in the $CO_2/^3He$ ratios (Arnorsson, 1995; Figure 11). On the contrary, samples that plot along the base of the diagram are consistent with preferential CO_2 loss, probably associated with calcite precipitation, which is a widespread phenomenon in most geothermal springs as evidenced by the travertine deposition around the hot springs and/ or calcite scaling in drilling wells. Another possible explanation about these samples is the dissolution of CO_2 in water (Reid et al., 1987). As known, the solubility of CO_2 in water decreases as the temperature increases and from both Figure 10 a and b, it is noticeable that the majority of the samples plotted along the base of the diagram are samples found in cold manifestations. However, the dissolution can be also caused by the fact that some bubbling gases at thermal springs show very low gas/water ratios (i.e. less intensely bubbling) and as a result they present lower $CO_2/^3He$ ratios with a noticeable CO_2 loss.

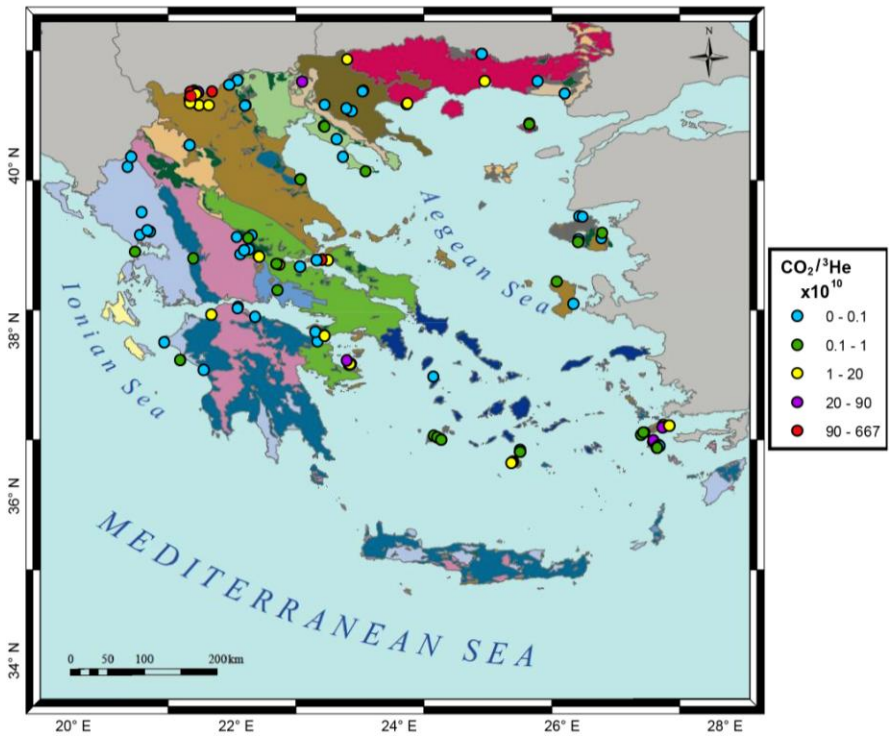

Figure 11: Geological map of Greece with the $CO_2/^3He$ ratios.

The distribution of R/R_A ratios versus the $^4He/^{20}Ne$ ratios is shown in Figure 12, where binary mixing curves display the trends drawn by mixtures of the atmosphere with different mantle and crustal sources (Sano and Wakita, 1985). Conformingly, the presence of N_2 and O_2 (Table 4) in the sampled gases of some cold manifestations of EH (1, 2, 17) and IH (19, 87, 124, 130) is possibly due to atmospheric contamination that occurred either because of intense bubbling (stripping dissolved air) of surface water bodies or mixing of shallow air-saturated ground waters (ASW) with waters of deeper provenance. The major part of the samples collected in VA display high mantle contribution (up to 80% considering a MORB-type source), whereas the majority of those collected in EH and some of IH (5, 7, 8, 12, 14, 114, 126, 174 etc) and HH (200, 202, 204, 208, 209) present the highest crustal contribution (from 85 to 99%). Remaining samples of IH and HH present a mixed mantle- crustal component with a mantle contribution comprised between 2 to10 % and 3 to 15 % respectively. Additionally, samples collected at Sousaki, Methana and some of the samples of Kos (VA) present also intermediate R/R_A ratio and consequently a mixed mantle- crustal origin for He with a mantle component of 2 to 20 %.

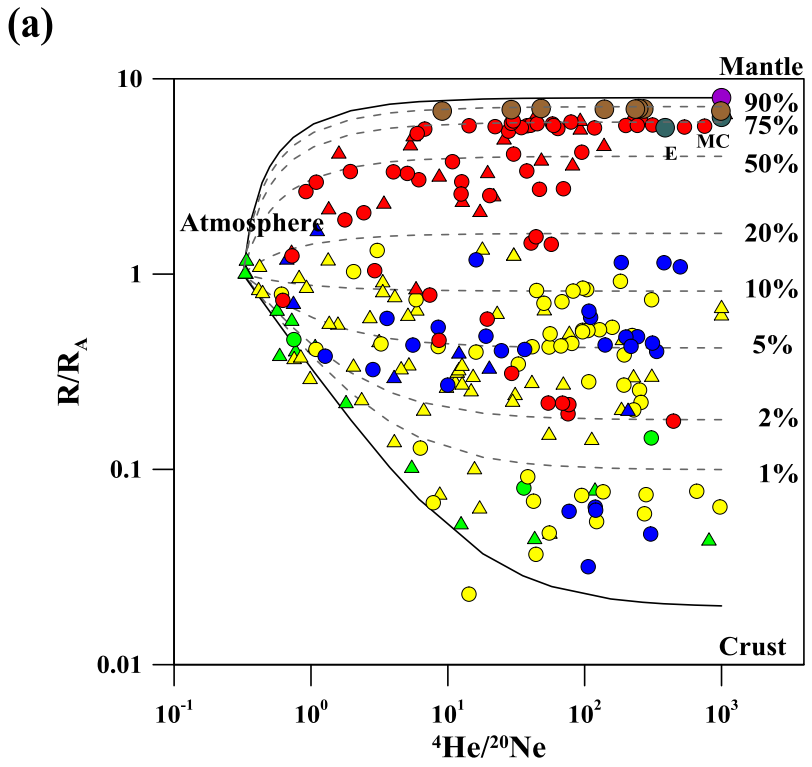

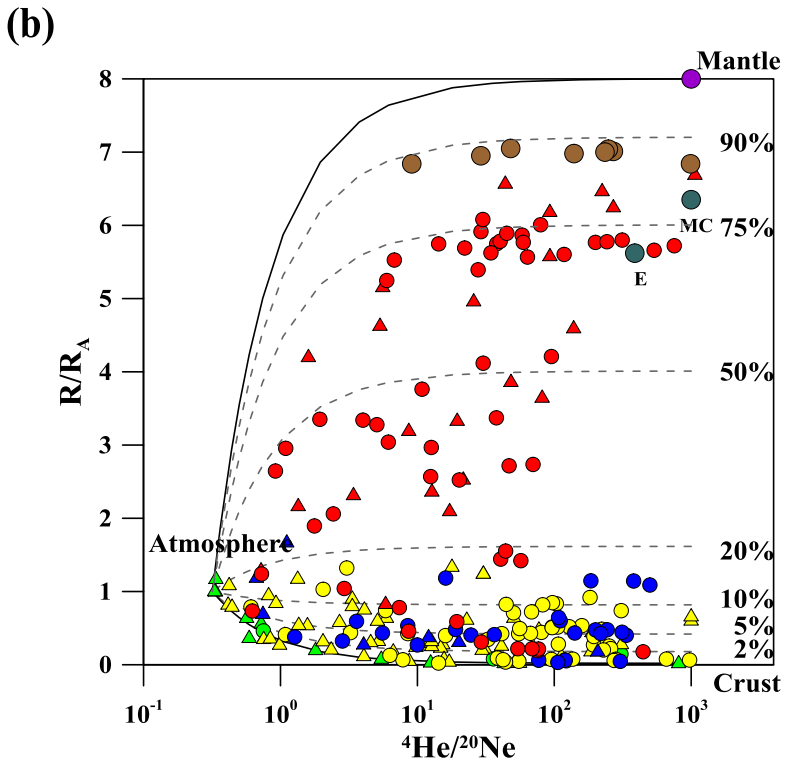

Figure 12: Binary plot of R/R_A vs. $^4He/^{20}Ne$ of the Hellenic gas emissions with a) YY' axis having a logarithmic scale; b) YY' axis having a linear scale. The mixing lines between Atmosphere and Mantle and between Atmosphere and Crust are also plotted. Dashed lines represent mixing between atmosphere and end-members with different percentages of mantle contribution. Symbols as Figure 7.

As said above, on the same plot, apart from the samples collected along the Hellenic territory, the literature data of the central European SCLM from Massif Central, Eger rift and Eifel after Bräuer et al. (2008; 2013) and of Kolumbo volcano after Rizzo et al. (2016) were plotted for comparison. It is noticeable that Kolumbo presents the highest R/R_A values (6.84 to 7.05 R/RA), followed by gases of Kos-Nisyros complex with values that range from 5.69 up to 6.71 R/R_A, which are, at least partially, higher than those of the central European SCLM (5.62 to 6.35 R/R_A). These data values and their schematical presentation on Figure 12 b support the hypothesis, at least for the south Aegean area, of a different mantle end-member in Greece with respect to SCLM. Such end-member falls within the MORB-Type mantle (8±1 R/R_A– Graham, 2002) and is represented by the gases released from Kolumbo volcano (Rizzo et al., 2016). In general, subduction zones exhibit a $^3He/^4He$ ratio slightly lower than that observed at the MOR, with a range in R/R_A of ~2-11, and a mean of ~6 (Lupton, 1983). The constancy of this ratio

across different regions indicates uniform proportions of recycled down-going slab and primary mantle material involved in the generation of subduction zone volcanics.

Additionally, Figure 13 shows the contribution of atmospheric, radiogenic and magmatic He. For the construction of this diagram, the percentage of magmatic He in the samples under investigation was estimated using the measured $^{3}He/^{4}He$ and $^{4}He/^{20}Ne$ ratios (calculation that includes atmospheric components, so for this reason the uncorrected $^{3}He/^{4}He$ ratio was used, Sano and Wakita, 1985), and the selected end-members. MORB was used as volcanic end-member ($8R_A$) and 0.318 as representative for $^{4}He/^{20}Ne$ ratio for Air (Holocher et al., 2002) (Figure 13). Furthermore, it shows the mixing between the atmospheric and radiogenic He in samples of EH, IH and HH (Figure 13 b) with a negligible presence of magmatic He (EH) and proportions between ~0 and 16.8 % for IH and between ~0 and 17.2 % for HH (Figure 13 a). The great majority of samples collected in VA show mixing between the radiogenic and magmatic He with a small contribution of the atmospheric end-member noticeable in the samples no. 235, 257, 259, 281, 284, 286, 287, 336, 339.

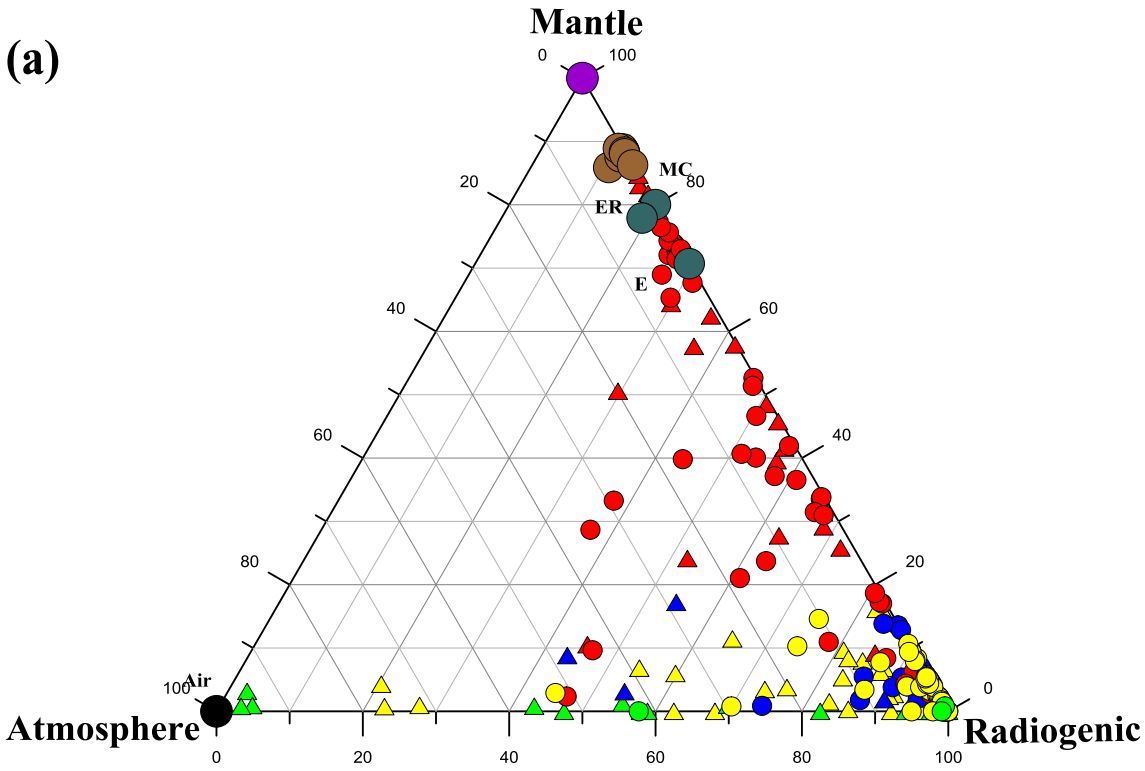

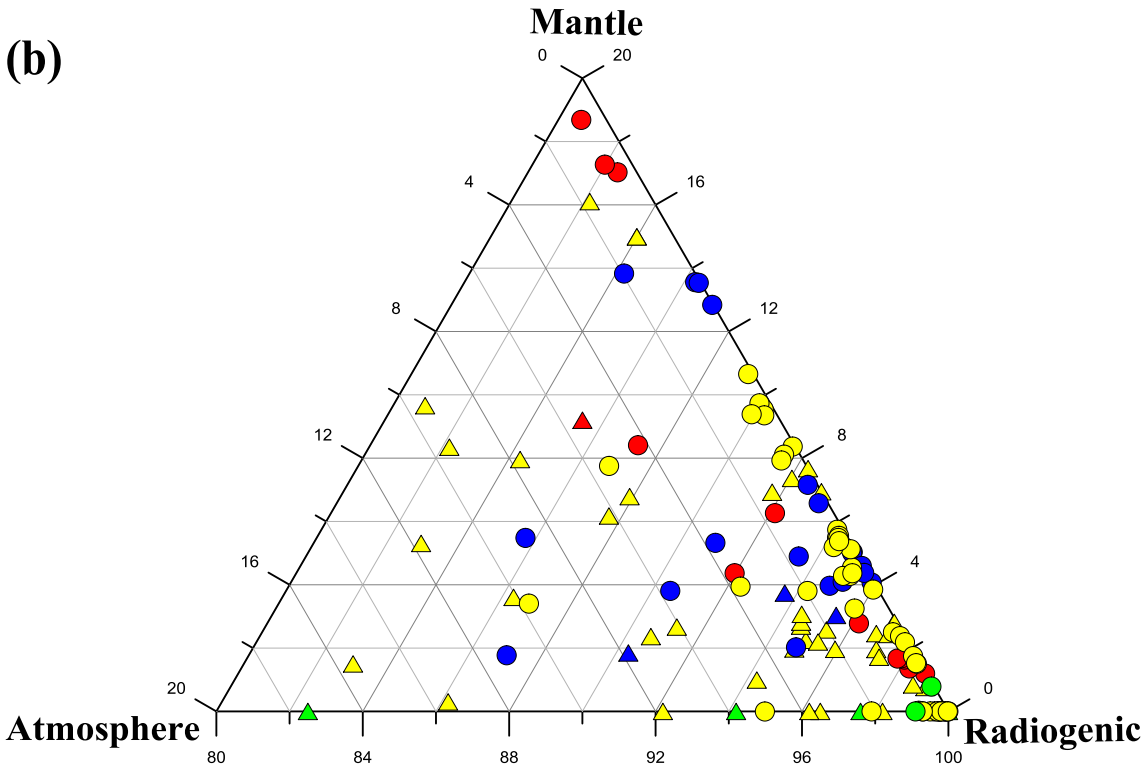

Figure 13: a) Ternary plot showing the atmospheric, radiogenic and mantle He contribution; b) Ternary plot showing the atmospheric, radiogenic and mantle He contribution focused on percentages above 80% for the radiogenic end member. Symbols as in Figure 7.

Helium isotope ratios are directly correlated with heat flow because heat flow is mainly derived from the crust and mantle (Du et al. 1998; 2006; Ozima & Podosek, 1983). As is commonly known, most of the heat production in the Earth is generated by the radioactive decay of the U and Th chain that produces ^{4}He atoms. However, several known geothermal areas of the world (i.e. Yellowstone - Morgan et al., 1977; The Geysers – Thomas, 1986; Larderello-Travale – Bellani et al., 2015) show heat flow anomalies positively related to the presence of ^{3}He enriched fluids in the upper continental crust, indicating a direct mass and heat input from the mantle, feeding the hydrothermal fluid circulation in the upper crust and the growth of strong thermal anomalies at the surface. The anomalous heat is generated by the presence of a crustal thinning. For a better comprehension of the argument, the R/R_A values of the collected gasses were plotted in maps of heat flow (Fytikas and Kolios, 1979- Figure 14 a) and crustal thickness (Grigoriadis et al., 2016- Figure 14 b).

R/R_A seems to have an increasing pattern from EH to HH, reaching its highest values in VA (Figure 14). In EH and in the subduction zone of IH, the heat flow values arrive up to 60 $mW \times m^{-2}$, whereas the crustal thickness has its maximum values in EH (40–46 km) and decreases versus IH presenting low crustal R/R_A values that arrive up to 0.32 and 1.04 respectively. However, in some cases (samples no. 91, 108-110, 127 of IH), the heat flow reaches values above 80 $mW \times m^{-2}$ and the R/R_A values arrive up to 1.37. In HH, there is an elevated heat flow (from 70 to 100 $mW \times m^{-2}$) with a crust of ~35 km and medium R/R_A values (from 0.03 up to 1.97 R/R_A). On the other hand, VA presents high mantle R/R_A values (up to 7.05 R/R_A) with an extremely elevated heat flow (more than 100 $mW \times m^{-2}$) and the thinnest crust (less than 30 km).

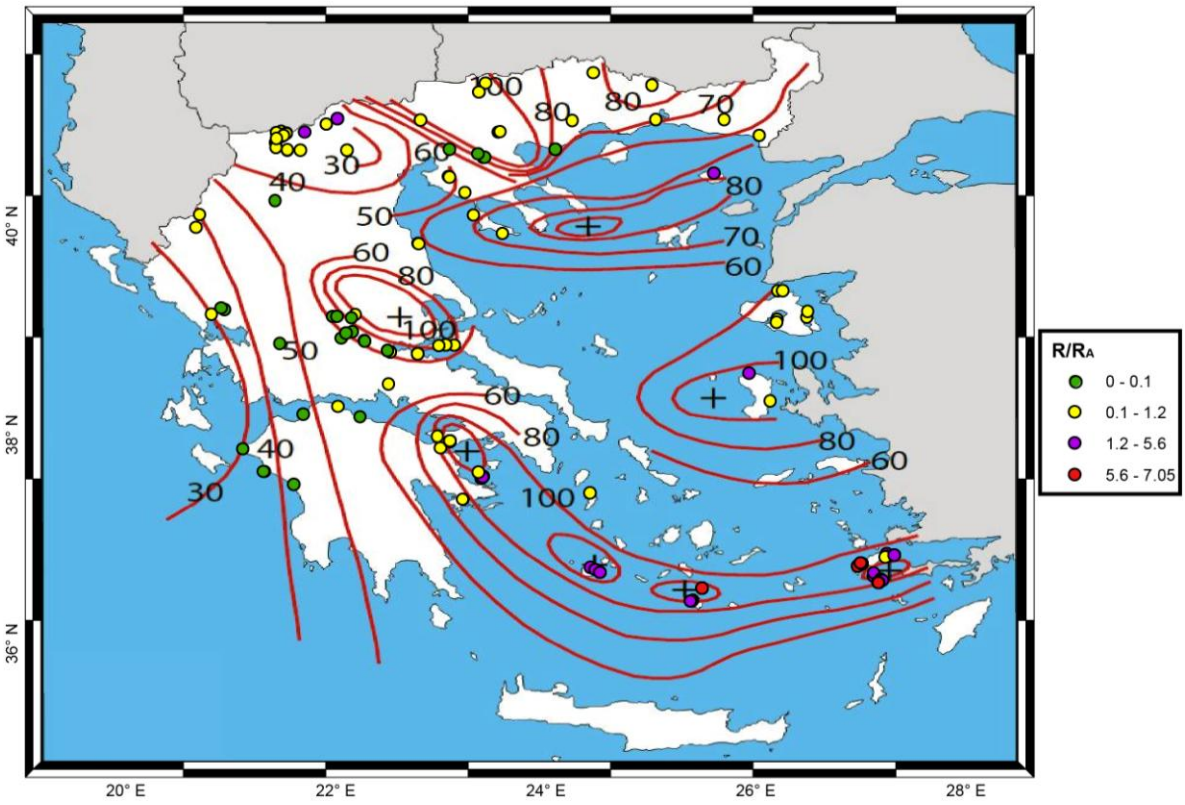

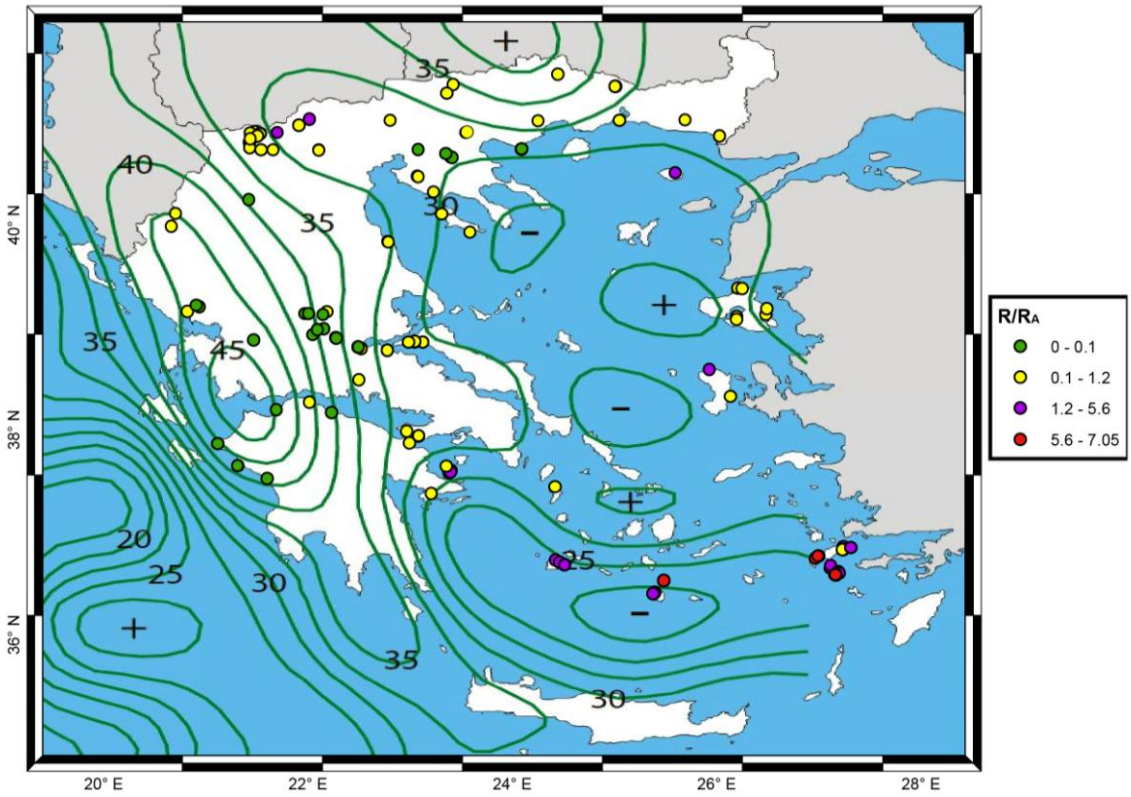

Figure 14: a) Heat flow, b) Crustal thickness map of R/R_A. Classes were determined by the slopes of the probability plots.

Due to the fact that the interpretation of $\delta^{13}C$ values alone does not allow a clear identification of the origin of CO_2, the $CO_2/^3He$ ratios are often consulted for this purpose. Mantle $CO_2/^3He$ ratio measured in MORB shows a small range, from 1.0×10^9 to 1.0×10^{10} (Burnard, et al. 2002; Marty and Jambon 1987; Trull, et al. 1993; Marty and Zimmermann, 1999), compared with the range observed in natural gases. Any natural CO_2 sample that plots above this MORB range irrespective of CO_2 content can only be attributed to a CO_2 source containing minimal ^3He, providing an unambiguous identification of a crustal CO_2 source. Samples within or below the MORB range contain a magmatic component but have been subjected to possible CO_2 loss or dilution (by addition of other gas species such as CH_4 or N_2). Careful study of both the $\delta^{13}C$-CO_2 isotopes and $CO_2/^3He$ ratios can distinguish between these processes and allow CO_2 origins to be determined (Ballentine, et al. 2001; 2002; Sherwood Lollar, et al. 1997; Sherwood Lollar, et al. 1994).

Figure 15 compares the $CO_2/^3He$ ratio and $\delta^{13}C$-CO_2 values of the gases collected along the Hellenic territory to those typical of Sediment, Limestone, and Mantle-derived CO_2 (Sano and

Marty, 1995). Generally, the $CO_2/^3He$ ratio for samples from volcanic arcs shows a large degree of variation and can be significantly greater than that observed at the MORB, with $(CO_2/^3He)_{ARC}$ ranging over 5 orders of magnitude from 3 $x10^8$ to greater than 6 $x10^{13}$. This reflects variable inputs from different CO_2 sources in arc systems, where CO_2 is derived from degassing of subducted slab and magma and additional crustal CO_2 inputs (e.g. Varekamp et al., 1992, Plank and Langmuir, 1993; Sano & Marty, 1995; Sano and Williams, 1996). The subducting slab carries C-rich material (limestones, slab carbonates and organic matter) into the magma generation zone, where thermal alteration produces CO_2 (decarbonation of limestone and thermal cracking of organic matter). Furthermore, CO_2 may also be added by the incorporation of volatiles from the overlying crust and sediments through which the magma then erupts. In Figure 15 this pattern is noticeable for samples collected in the VA that plot along the mixing line between mantle and limestone end-members, as well as a great part of the samples collected in IH and the thermal emissions of HH. This pattern further excludes important contributions from organic sediments to the fluids deriving from the descending slab, even though a small contribution from organic sediments can be detected in the CH_4-dominated gases of continental Greece (EH, HH) deriving probably from crustal sources.

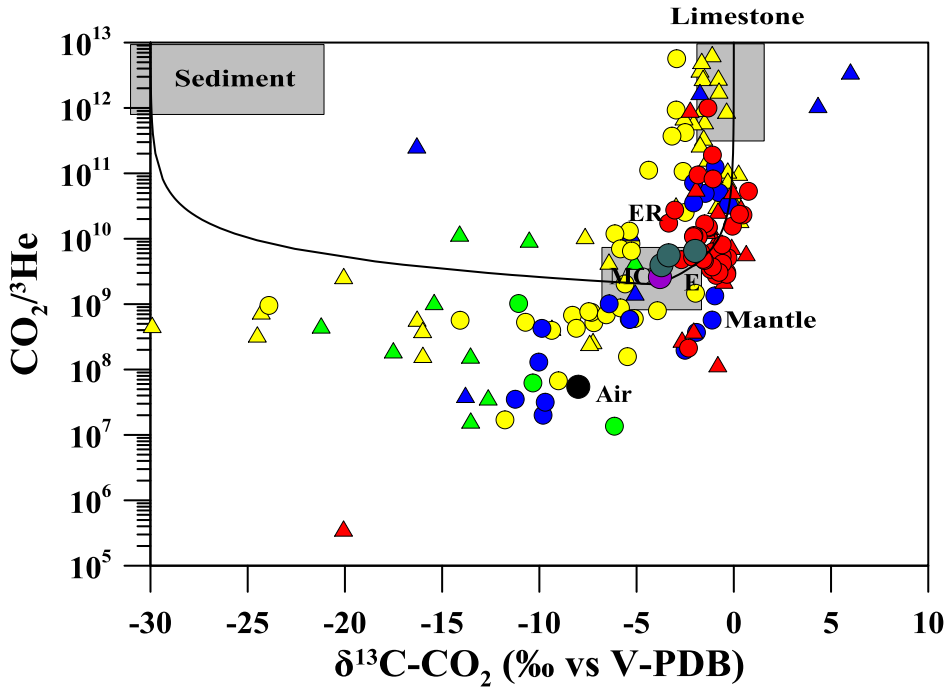

Figure 15: Binary plot of $CO_2/^3He$ vs. $\delta^{13}C\text{-}CO_2$. The composition for Sediments, MORB- like Mantle and Limestones end-members are: $\delta^{13}C\text{-}CO_2$ = -30 ‰, -5 ‰ and 0 ‰ and $CO_2/^3He$ = 1×10^{13}, 2×10^9 and 1×10^{13}, respectively (Sano and Marty, 1995). Symbols as in Figure 7.

Additionally, in Figure 16 the CO_2 dominated samples that are plotted above the MORB range, independently from their CO_2 concentration, contain very low ^3He concentrations indicating a crustal source for CO_2. The presence of significant quantities of magmatic ^3He for the samples (thermal emissions of VA and samples no. 213-215, 247, 248, 250, 251) plotted within and below the MORB range, points to a mantle origin for CO_2 (Gilfillan, et al. 2008).

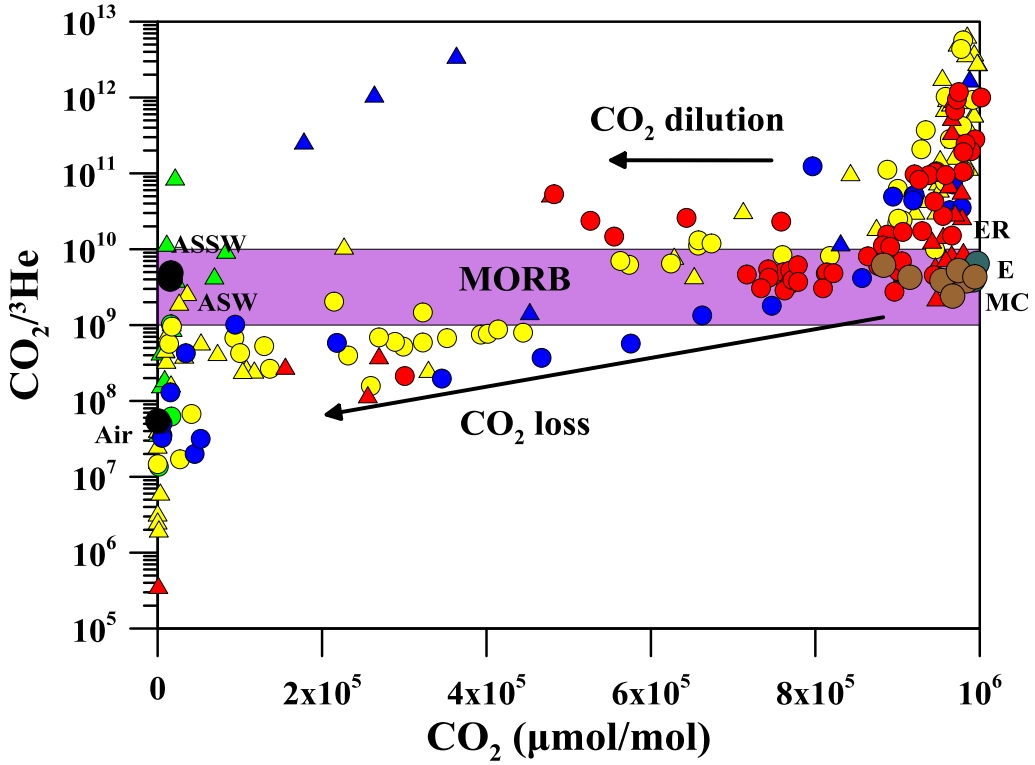

Figure 16: a) Binary plot of $CO_2/^3He$ ratio vs. CO_2 concentration of the investigated samples. The MORB $CO_2/^3He$ range is based on the data of Marty and Zimmermann (1999). Symbols as in Figure 7.

In both Figure 15 and Figure 16, samples collected in the thermal emissions of IH and HH and in the cold emissions of EH present $CO_2/^3He$ ratios within or lower than those of the MORB range indicating a possible CO_2 loss. This relative CO_2 loss could be due to interaction with shallow aquifers, as a result of CO_2's higher solubility in aquatic environments with respect to He (Figure 15, Figure 16). Moreover, CO_2 loss may also be produced by calcite deposition at relatively high pH (Stefánsson et al., 2016; 2017). This process involves deprotonation of CO_2 (aq) to HCO_3^- and CO_3^{-2} and formation of calcite, resulting in a decrease of the $\delta^{13}C$ values of the residual CO_2. It should be noted that most thermal water samples are oversaturated in carbonate minerals and

travertine depositions were recognized at some thermal areas (Kanellopoulos, 2012; Winkel et al., 2013; Kanellopoulos et al., 2017). Another possible process is the CO_2 dilution from CH_4 or N_2, the prevailing gas species in those areas, without a noticeable change in the $CO_2/^3He$ ratio. Three end-members are considered in their formulation, including MORB gases, marine limestone and organic carbon-rich marine sediment, which, respectively, represent the three vertices of Figure 17. The results show that the C from along the Hellenic territory is dominated by a limestone carbon source. In particular samples collected form IH and HH present percentages between ~90 and ~100 %, samples of VA present a wider range from ~40 to ~100 % and EH present lower percentages (~60 to ~80%) but always plot in the field of Limestone carbon source. The two other members seem to have a negligible percentage on the samples. However, samples no. 119, 186, 214, 301 seem to have a prevailing mantle C component, whereas samples no. 16, 190 present a mixed limestone- organic/ sedimentary carbon source. Unfortunately, this methodology does not allow discrimination between subducted carbonate bearing sediments and contributions from assimilated crust.

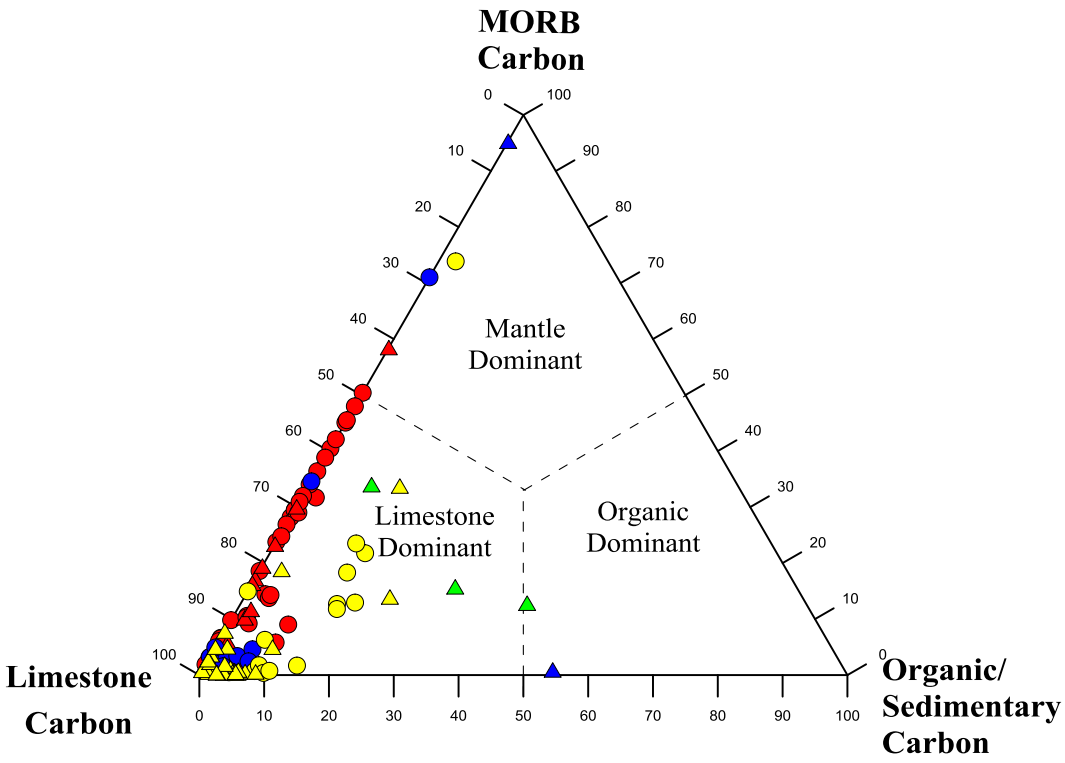

Figure 17: Carbon source contributions to the Hellenic discharges, plotted in terms of three end-member components (marine limestone, marine sediment and MORB-type mantle gas). Symbols as in Figure 7.

As also seen in Figure 9 b, CO_2 presents an increasing pattern from EH to HH, reaching its highest values in VA. From Figure 18, it is noticed that the highest CO_2 values are generally concentrated in areas with enhanced geothermal flow and thin crust. More specifically, in EH and in the subduction zone of IH, the heat flow values arrive up to 60 $mW \times m^{-2}$, whereas the crustal thickness has its maximum values in EH (40–46 km) and decreases versus IH presenting low CO_2 concentrations (Table 4). However, in some cases (samples no. 151, 154-159 of IH), the heat flow reaches values above than 80 $mW \times m^{-2}$ and the CO_2 concentrations arrive up to 830,800 μmol/mol. In HH, there is an elevated heat flow (from 70 until 100 $mW \times m^{-2}$) with a crust of ~35 km and relatively high CO_2 concentrations (median of 469,500 μmol/mol). Samples collected in VA present the highest CO_2 concentrations (up to 1,000,000 μmol/mol) with an extremely enhanced heat flow (more than 100 $mW \times m^{-2}$) and the thinnest crust (below 30 km).

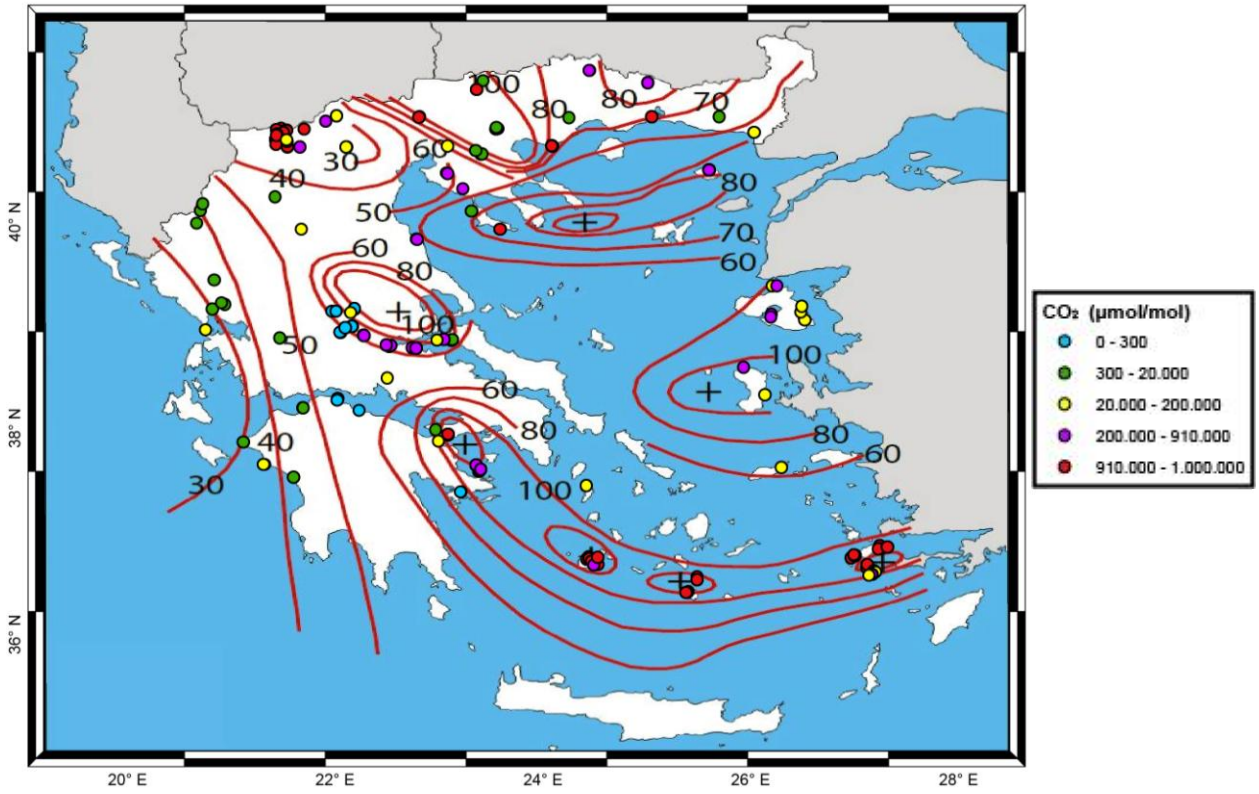

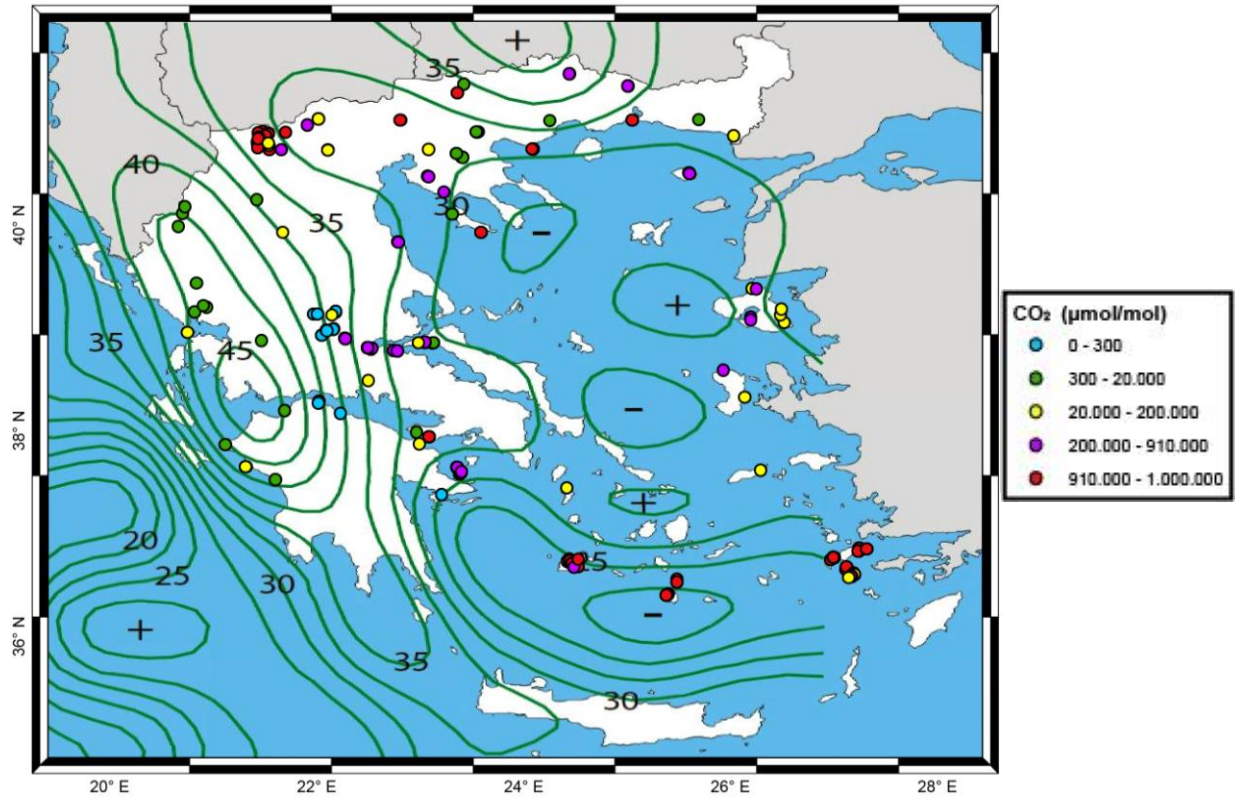

Figure 18: a) Heat flow, b) Crustal thickness map of CO_2. Classes were determined by the slopes of the probability plots.

As seen above (Figure 14), heat flow and R/R_A show a positive correlation in the majority of the cases, whereas crustal thickness and R/R_A a negative one. The same pattern seems to be followed also by heat flow and CO_2 and by crustal thickness and CO_2 (Figure 18).

As shown in Figure 19, samples with $CO_2/^3He$ ratios $>10^{10}$ are characterised by He concentrations clearly lower than in the gas phase of popping rock vesicles (Javoy and Pineau, 1991), which can be assumed as the end-member of mantle-derived origin. The negative correlation between $CO_2/^3He$ ratios and He concentrations in the gases indicates a preferential removal of He by degassing during migration. Elemental fractionation between He and CO_2 occurs because He is more efficiently degassed than CO_2 due to the high solubility of CO_2 in water, whereas He has the lowest solubility of all gas components. During interaction of the uprising gases with groundwater, the gas/water ratio significantly affects the magnitude of the fractionation effect. As said before, there are various mechanisms by which crustal CO_2 ($CO_2/^3He>10^{10}$) can be added to these systems (Bradshaw et al., 2004; Cathles & Schoell, 2007), but there is no plausible mechanism that enables crustal CO_2 to be variably added to these

systems, while preserving a correlation of $CO_2/^3He$ with the noble gases derived from formation water. Neglecting small amounts of ^3He dissolution back into the formation water (Gilfillan et al., 2008), changes in $CO_2/^3He$ must therefore be due to CO_2 loss in the subsurface by an amount directly proportional to the amount of formation water that has been degassed. CO_2 is soluble and reactive. The most probable mechanisms of subsurface CO_2 fluid phase removal are dissolution and/or mineral trapping (Bradshaw et al., 2004; Baines & Worden, 2004).

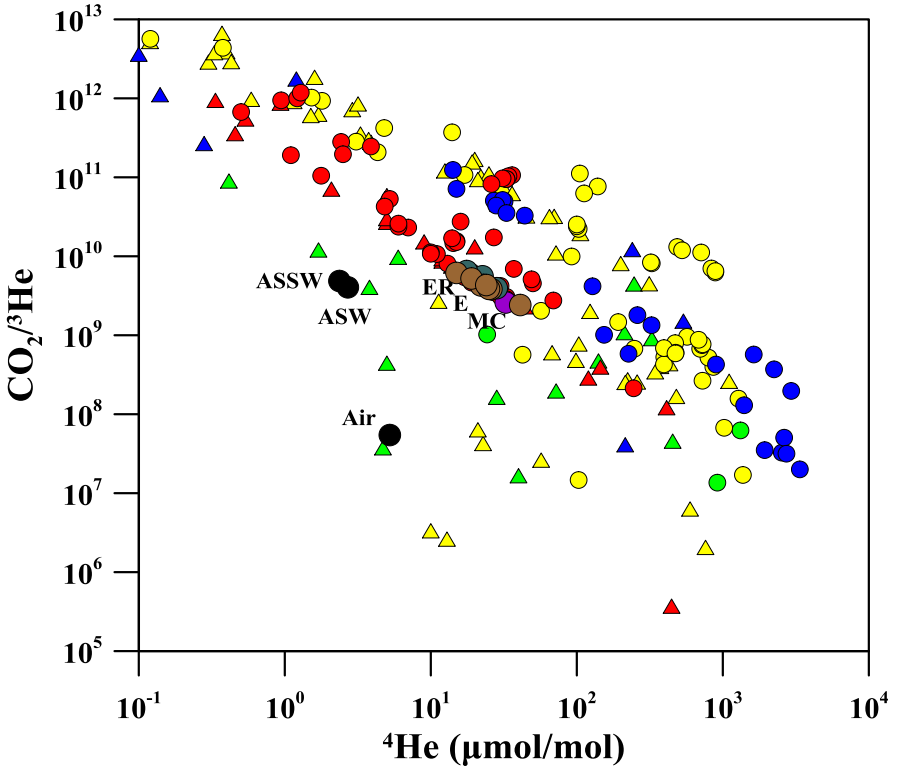

Figure 19: Diagram showing correlation of $CO_2/^3He$ ratios and He concentrations. Symbols as in Figure 7.

Additional support to the assumption of the elemental fractionation occurring during degassing due to different solubilities in water is given by the correlations between $CO_2/^3He$ vs $^4He/^{40}Ar$ and $^4He/^{20}Ne$ that are presented in Figure 20. The solubility difference between He and Ne in water is small, whereas that of Ar is higher than that of He but very small compared with that of CO_2. In Figure 20 a, 3 groups can be recognized. The 1st one has a $^4He/^{40}Ar$ ratio relatively stable, which seems to be independent from CO_2 loss. The 2nd shows values close to the Air end-members, which as it is also shown in Figure 20 b is caused by air contamination of the samples. The 3rd one seems to have a negative correlation between $CO_2/^3He$ ratios and $^4He/^{40}Ar$. This

might have to do with either a preferential loss of radiogenic He or a production of ^{40}Ar after the decay of an isotope of potassium (^{40}K) in rich in K materials such as micas, clay minerals, tephra and evaporates.

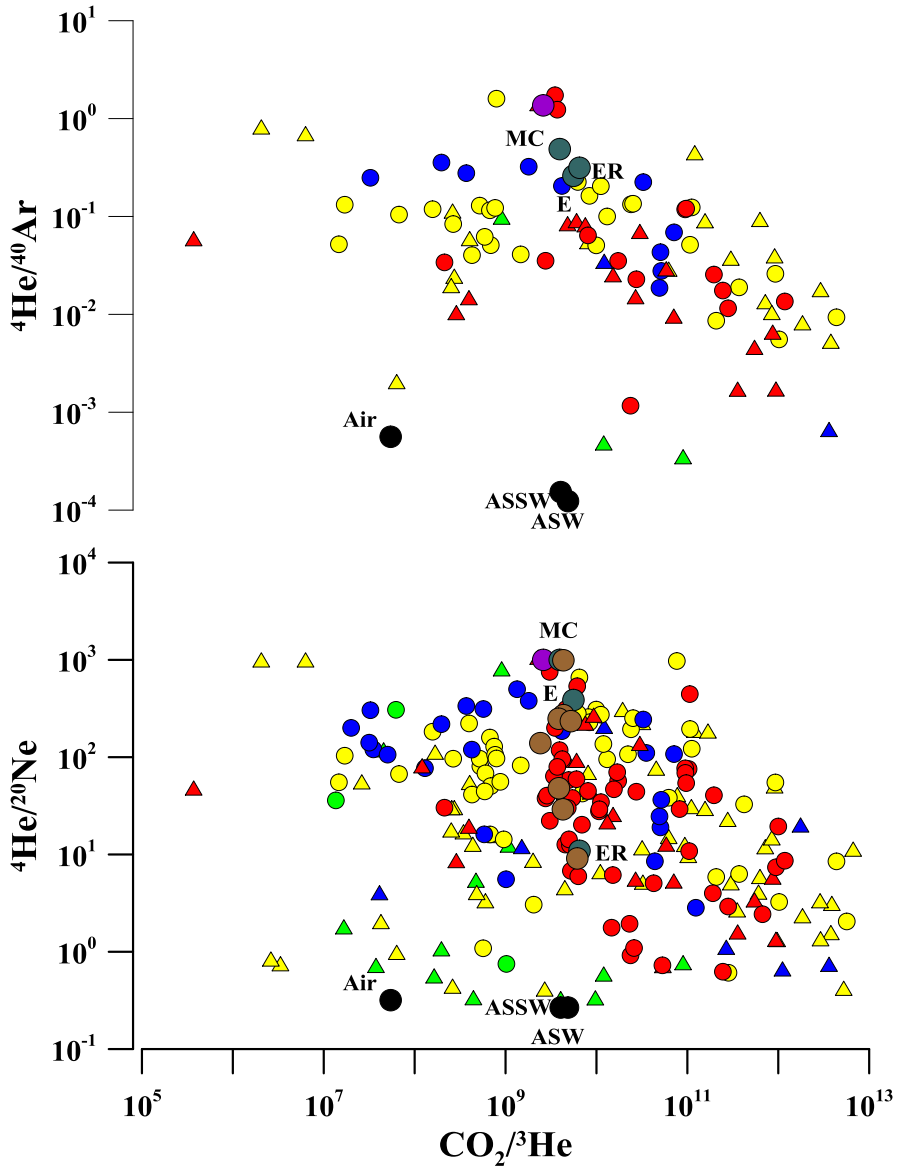

Figure 20: $CO_2/^3He$ vs a) $^4He/^{40}Ar$ and b) $^4He/^{20}Ne$, respectively. Symbols as in Figure 7.

Figure 21 shows a direct correlation between the amount of CO_2 and its carbon isotopic composition. Samples collected in HH seem to have a positive correlation, whereas those of EH present the lowest range of values for both chemical and isotopic composition and no correlation. In some samples, the high isotopic values ((-4.72) to 2.0‰) are in the range proposed for carbon

of different sources ($\delta^{13}C$ of marine carbonates $\delta^{13}C$~(-3) to 2‰ (Hoefs, 2009); magmatic carbon, including MORB and volcanic gases $\delta^{13}C$ ~(-7.2) to (-2)‰, Giggenbach et al., 1991; Sano and Marty, 1995). The great majority of thermal manifestations of IH and samples of VA dissolved CO_2 content of about 100,000 μmol/mol and are affected by intense gas separation with gas bubbling, visible on the field. Not surprisingly, the carbon isotope fractionation in C fixation is also temperature dependent (Figure 21). However, this observation also reflects a kinetic effect: there is generally less dissolved CO_2 available in warm waters because of the decreasing solubility at higher temperature. As a result, a larger fraction of the CO_2 is utilized and there is consequently less fractionation (Hoefs, 2003).

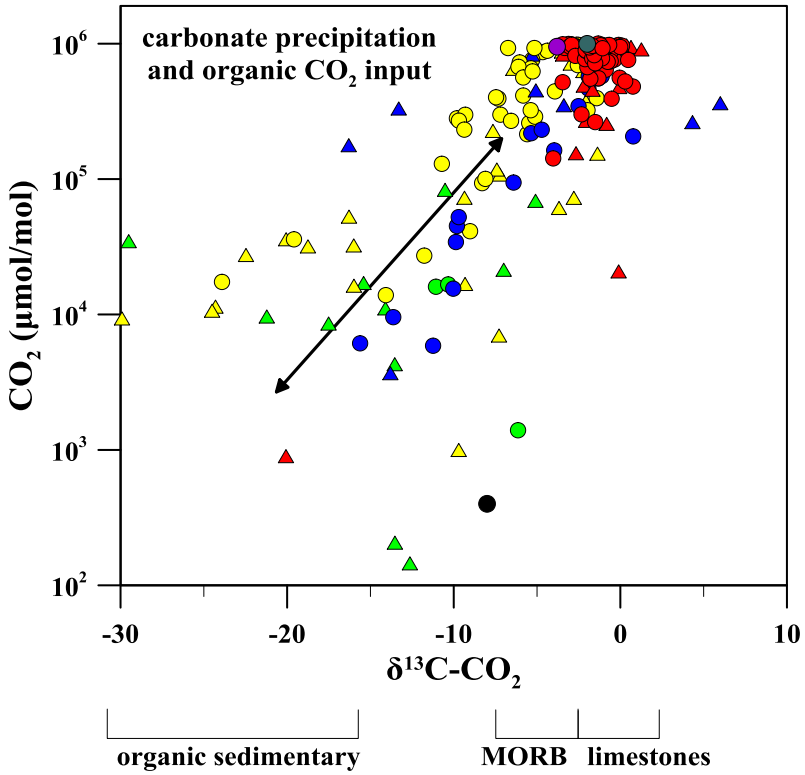

Figure 21: CO_2 vs. $\delta^{13}C$-CO_2. The trend denotes the fractionation with quantitative loss of CO_2 and the occurrence of further fractionation processes. Symbols as in Figure 7.

4.3. Helium isotope values and CO_2 concentrations related to Geodynamics and Volcanism

As already said, the Hellenic area is one of the most seismically active and rapidly deforming areas worldwide (e.g., Tsokas and Hansen, 1997; Taymaz et al., 2007; Le Pichon et al. 2001), strictly associated with the plate interactions and crustal deformation taking place in the region. In the Aegean Sea, the seismicity is mostly superficial, whereas the high geothermic gradient is probably responsible for the seismic disappearance of the slab underneath the basin. The opening of the Aegean-western Anatolian rift can kinematically be interpreted as a fast southwestward advancement of Greece over Africa (Figure 22 a). The rift generated a mantle uplift to compensate the lithospheric thinning and as a result, the underlying slab itself had been involved and folded by the mantle uprise beneath the rift (Figure 22 b). The stretching between Greece and Anatolia, and the differential velocity of convergence with the underlying slabs should have generated a sort of "horizontal windows" both in the hangingwall and in the footwall of the subduction, allowing melting of mantle, and generating the OIB magmatism after regular subduction/ collision evolution.

No relative motion occurs between the central and eastern Mediterranean, since both sides belong to the same African plate. However, the plate is subducting both below Greece and Cyprus, but at different velocities, or in another reference frame, the hangingwall plate is overriding at different velocities. Furthernore, Turkey is relatively moving apart from Greece toward the northeast in the absolute reference frame, and not converging. This extension may or may not be coeval with compression elsewhere, and the related normal faults and shear zones should flat out in the decollement planes at base of the lithosphere.

The Hellenic arc and the related Mediterranean Ridge (the accretionary prism, e.g., Camerlenghi et al., 1995) have a low dip foreland monocline (almost flat; Clément et al., 2000), deep metamorphic rocks involved in the orogen, and higher structural and a morphologic elevation. Moreover, the slab is regularly low dip and shallow. Due to the low dip of the Hellenic slab, in the Aegean Sea, the hangingwall has not enough space for a thick asthenospheric wedge. The hangingwall and footwall lithospheres are almost stacked one on top of the other, with thin (if any) sandwiched asthenosphere in between. Therefore the Aegean Sea represents a different type of extension associated to a subduction zone, where the hangingwall plate overrode the slab at different velocities, implying internal deformation (type 6 of extension) Figure 22.

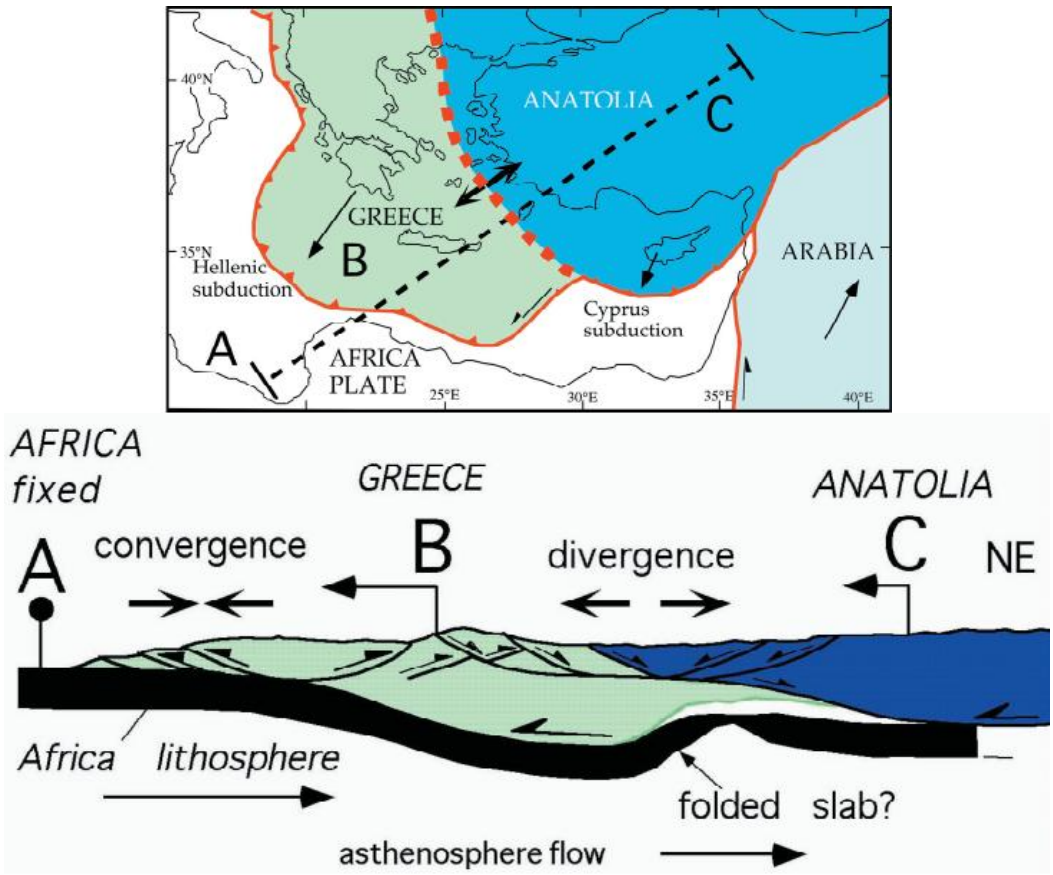

Figure 22: a) Map of the extension between Greece and Anatolia. On the map, Africa, Greece and Anatolia are designed and specified with symbols A, B and C.; b) cross-section cartoon showing that B is overriding A faster than C, generating extension between B and C (Doglioni et al., 2002).

Considering the "east-northeastward" mantle flow indicated by the hot spot reference frame (Ricard et al., 1991), the origin of backarc basins due to E-NE-directed subduction should not be due to lithospheric disappearance as found in west-directed subduction zones. It could rather be related to differential drag of the lithosphere in the hangingwall of the subduction (Figure 22), due to different viscosity contrasts generated by lateral heterogeneities that control the amount of decoupling at the interface between lithosphere and asthenosphere. The system is composed by three plates (A-B-C, Figure 22), in contrast with back-arc basins due to W-directed subductions where the backarc may develop with two converging plates or even within one single plate.

In Paragraph 4.2, a possible connection among heat flow, crustal thickness, He isotope composition and CO_2 concentrations was proposed. However, taking into consideration the relative maps (Figure 14, Figure 18), it is noticeable that this correlation pattern doesn't always work. Polyak and Tolstikhin (1985) established that the presence of mantle He in continental

settings correlates well with tectonic and magmatic activity, whilst O'Nions and Oxburgh (1988) and Marty et al., (1992) proved that the mantle He input occurs in areas of active or recent extension, often associated with young volcanism. Additionally, Bredehoeft and Ingebritsen (1990); Chiodini et al. (2004) and Miller et al., (2004), highlighted the important role of CO_2 in increasing pore pressure during fluid flow through highly permeable fault zones which, in turn, may trigger earthquakes. Based on the above, R/R_A values and CO_2 concentrations of the gases under investigation were plotted in tectonic maps in order to find possible connections with the geodynamic regime (Figure 24). Also, they were correlated with the map of Pe-Piper and Piper (2006 - Figure 23), which presents the relationship of the Pliocene-Quaternary volcanism to tectonic setting.

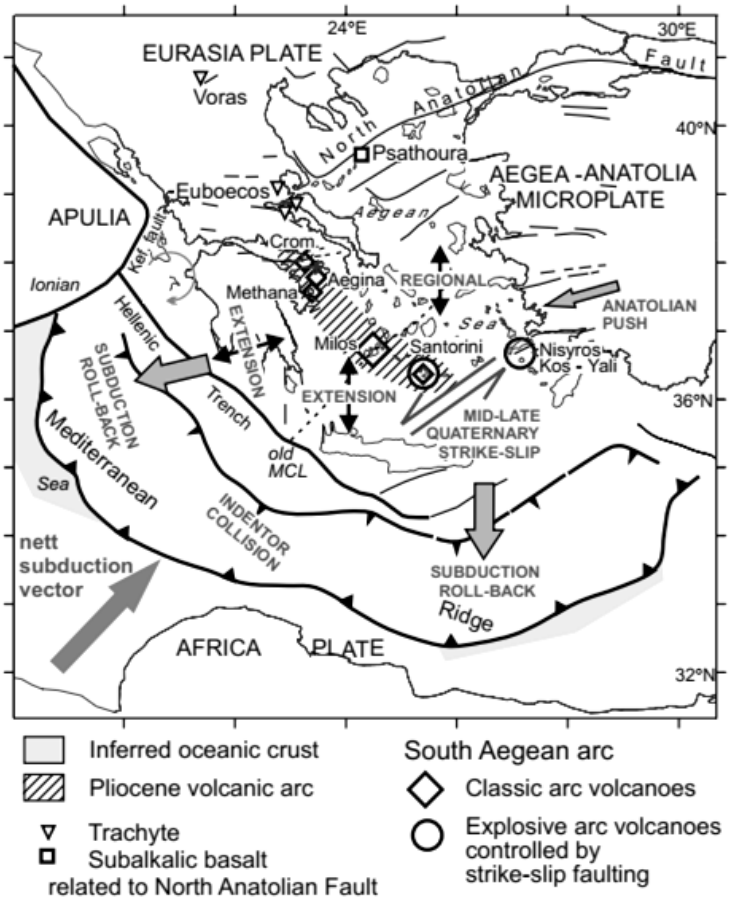

Figure 23: Modern tectonics of the Aegean region showing the relationship of Pliocene/Quaternary volcanism to faulting and subduction.

Four cases of particular interest were identified, which are analytically described below:

a) HH: The tectonic situation of this area is mainly controlled by the Strymon Fault System (SFS), which is ~200 km long and ~40 km wide and extends from southwest Bulgaria to the North Aegean Sea (e.g. Strymonikos Gulf). The SFS strikes NW-SE, defining a complex system of topographic lows, within which the Strymon (Struma) River flows. It comprises numerous individual smaller fault systems, each of which being about 80 km long and up to 5 km wide (Zagorcev, 1992a, 1992b). South of the Greek-Bulgarian border, the SFS traverses northern Greece for about 80 km before it extends offshore into the Strymonikos Gulf, where it may connect with the NAT, a feature formed in response to the prolongation of the NAF into the north Aegean Sea (Armijo et al., 1999; Taymaz et al., 1991). At its northern end, this segment of the SFS abuts against the E-W trending Belasitsa–Kerkini Fault System (BKFS) (Tranos et al., 2008). During the Mesozoic, this fault has formed the two alpine tectonic units of HH (Bornovas and Rondogianni, 1983). Along with the active extensional tectonics, the Strymon basin is characterised by enhanced heat flow favored by the Tertiary granitoids of Vrondou and Pangeon. The general geological settings are favorable for the formation of geothermal field, as: a) the existence of conglomerates and breccias on the top of the basement and as interbedded strata; b) the presence of an impermeable cap consisting of Neogene, clayey and marly sediments; and c) the water circulation intro the permeable sediments and the fractured crystalline, rocks supply continually the reservoir (Arvanitis, 2003). The elevated concentrations of CO_2 in HH occur due to the deep faults that provide a permeable pathway along which CO_2 can migrate to the atmosphere earth's surface (Wang and Jaffe, 2004 - Figure 24 b). Another possible reason is the thermo-metamorphic alteration of carbonates (Stephens and Hering, 2002) that results in the production of large volumes of CO_2. The U- and Th-rich minerals (i.e. zircon, apatite etc - Wüthrich, 2009) of the granitoids contribute to the low R/R_A values of this area. As already known, the decay of U and Th produces ^4He (Figure 9 c) and for this reason gases of HH are depleted in R/R_A. As also seen in Figure 13, samples of this region are found in the radiogenic part of the ternary diagram highlighting the depletion in the He isotope values (Figure 24 a).

b) "First phase" volcanic arc (Florina, Euboea, Chios): As proposed by Fytikas et al. (1984) and Vougioukalakis et al (2004), the Plio-Quaternary volcanic activity is not confined to the SAAVA, but its main bulk activity is identified in the north, in the Mount Voras area (Fytikas

et al., 1984). The geographical distribution of the volcanism of the "first phase" is unlikely to reflect a typical volcanic arc. However, a number of sites seem to have been associated both with Pliocene and Plio-Quaternary volcanism, for example, Patmos, Kos (Fytikas et al., 1984), possibly Chios (Besenecher and Pichler, 1974) and north Euboea (Katsikatsos et al., 1980; Fytikas et al., 1984). This volcanic activity left its trace in the areas referred above, not only by its relatively high heat flow values but also by the high CO_2 concentrations. However, Florina, apart from being located in Mount Voras, is flanked on the west side by a normal fault zone and metamorphic rocks intruded by granites, and on the east side by crystalline limestones, schists and gneisses. Moving eastward in the basin, sedimentary cover thins and changes from coarse clastics to sequences of sand, silt, clay, and lignite. This geological regime creates the perfect conditions for the creation of the vertically stacked reservoirs of >99.5 % CO_2. These are located in limestone basement and overlying sandstone units, with the top of the upper reservoir located at only 300 m depth (Beaubien et al., 2004). Sandstone reservoirs are capped by clayey sediments. CO_2 leakage at the surface in the Florina basin occurs as CO_2-rich springs throughout the area and, where basement limestones are exposed, as surface gas seeps (Beaubien et al., 2004). Furthermore, in Euboea there is a great deposition of travertines in the thermal springs.

c) Grecian Shear Zone (GSZ - Samothraki, Kassandra's peninsula North Euboea and Sperchios basin): The NAF is one of the largest currently active strike-slip faults in the world, forming the most prominent part of a medium-size strike-slip-dominated belt of deformation (Ketin, 1948; Şengör, 1979a) in northern Turkey. It extends from the Gulf of Saros in the northern Aegean Sea to the town of Karlıova in Eastern Turkey for 1200 km, paralleling roughly the southern Black Sea shores and keeping a fairly regular distance of some 100 km to the coast, connecting the Aegean taphrogen (Taymaz et al. 1991, Özeren 2002, Yilmaz et al. 2002) with the East Anatolian high plateau (Şaroğlu 1985, Koçyiğit et al. 2001, Şengör et al. 2003). The dextral shear associated with the NAF continues across the northern Aegean, crosses northern and central mainland Greece as a broad shear zone (termed the Grecian Shear Zone by Şengör, 1979a), and eventually links up with the Hellenic subduction zone (McKenzie and Jackson 1983, Le Pichon et al. 1993). Within this larger tectonic scheme, north-west Anatolia experiences deformation from both the extensional and right-lateral strike-slip systems. The presence of mantle He in regions of active compression not associated with

magmatism is less common and more difficult to reconcile with fluid (He) transfer between mantle and shallow crust. Regions of compression/strike-slip faulting such as NAF, San Andreas Fault (SAF) and the Dead Sea Transform (DST), are often associated with crust thickness or with heat flow anomalies which might indicate recent underplating by mantle melts. Thus, it is difficult to understand how the mantle underlying the fault liberates He (and presumably other volatiles), or how the released volatiles traverse several kms of ductile lower crust. Nevertheless, ≥50 % of the He along some sections of the SAF, of the Niigata–Kobe tectonic zone and of the NAF is derived from the mantle (Gulec and Hilton, 2006; Gulec et al., 2002; Kennedy et al., 1997; Mutlu et al., 2008; Umeda et al., 2008). For this reason the R/R_A values of the areas found in the GSZ are expected to be enriched in mantle He (Table 6). The increased CO_2 concentrations are also explained by the tectonic setting of GSZ and in some cases by the Quaternary Volcanic activity (Figure 24, Table 4).

d) Corinth Rift: The Corinth graben is 100 km long and 40 km wide that characterises an area of rapid subsidence that separates central Greece from Peloponnese. According to Poulimenos et al., (1989), Doutsos and Piper (1990) and Poulimenos (1993), WNW – trend listric faults are the major faults that influence the basin evolution, forming asymmetric grabens. Due to the major faults that deep northwards, several tilted blocks dipping southwards were formed and a wedge-shaped terrigenous clastic sequence accumulated during tilting. Along with major faults, minor deep southwards faults tend to reduce the structural relief. The synchronous activity of major and minor faults influenced the basin configuration and the depositional environments. As a result, several small sub- basins were formed at the southern margins of the Corinth graben (Poulimenos, 1993; Zelilidis & Kontopoulos, 1996; IGME, 1969, 1970, 1973, 1975). Furthermore, being one of the most seismically active zones in Europe, it is characterised by rapid present-day extension (10–15 mm/yr, Briole et al., 2000) and footwall uplift (>1 mm/yr - McNeill and Collier, 2004). Notwithstanding this strong extensional tectonic pattern, no mantle fluids can be recognized in the area. Gases collected are generally dominated by CH_4 and N_2 and the associated He shows always R/R_A values typical to pure crustal origin. This was previously highlighted by Pik and Marty (2009), who concluded that, due to the absence of mantle He, the fault system is not connected in depth, with zones in which mantle He can be trapped or that reaches the lower crust allowing the uprise of mantle fluids. However, in the western part of the graben system (Saronikos gulf)

where it meets the SAAVA, the Quaternary volcanic activity of Sousaki and Methana allowed CO_2-rich fluids to reach the surface.

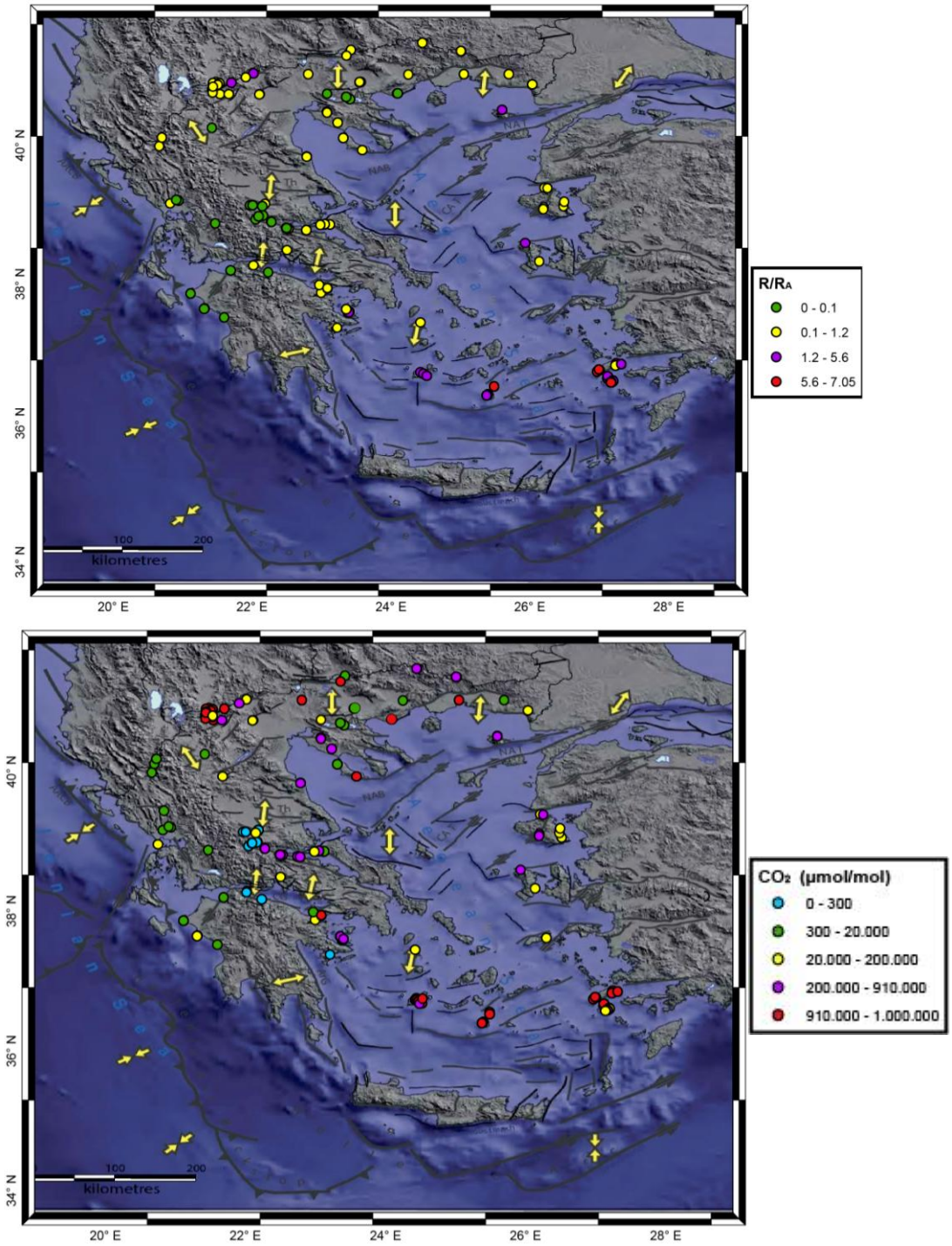

Figure 24: Tectonic map of Greece presenting a) He isotope values and b) CO_2 concentrations. Classes were determined by the slopes of the probability plots.

4.4. Light Hydrocarbons

4.4.1. An overview in the classification of hydrocarbons

Taran and Giggenbach (2003) highlighted that for the description of hydrothermal hydrocarbon production, two main mechanisms can be hypothesized. The first one deals with the biotic origin of methane, whereas the second one with its abiotic origin.

Gunter (1978), based on numerous observations, proposed that the nature and distribution of hydrocarbon species in hydrothermal vapours is more consistent with the thermal degradation of kerogen rather than inorganic production, a conclusion also supported by other researchers (e.g., Welhan, 1988; Darling, 1998; Mango, 2000; Taran and Giggenbach, 2003). More specifically, as indicated by Hunt (1996), biotic methane is produced either by microbial or thermogenic processes.

The second approach has to do with the formation of abiotic (or abiogenic) methane by chemical reactions that do not require the presence of organic matter. These reactions include magmatic processes and gas-water-rock reactions (for example Fischer Tropsch type reactions (Fischer and Tropsch, 1923; 1926)) occurring over a wide range of temperatures (Etiope and Sherwood Lollar 2013). These processes refer to the formation of organic compounds from a gaseous mixture of CO and H_2 in high temperature and pressure surface-catalysed process, involving sequential reduction and polymerization of single-carbon units (McCollom and Seewald, 2007; McCollom, 2013; Konn, 2015), see Reaction (1). From this process, it is noticeable that trace amounts of abiotic hydrocarbons can occur in volcanic and geothermal fluids. Moreover, considerable amounts of methane, reaching concentrations of 80–90 vol.%, have also been discovered in an increasing number of sites in Precambrian crystalline shields, in serpentinized ultramafic rocks along mid-ocean ridges and in land-based ophiolites, peridotite massifs, and igneous intrusions (Etiope and Sherwood Lollar 2013).

Considering these mechanisms, generally, although not exclusively, the origin of CH_4 can be investigated using the classification diagrams proposed by Bernard and Schoell (Bernard et al., 1978; Schoell, 1980; 1988; Etiope and Schoell, 2014, Figure 27). Bernard et al. (1978) introduced correlation between $CH_4/(C_2H_6+C_3H_8)$ concentration ratios and the $\delta^{13}C$-CH_4 ratios to qualitatively distinguish CH_4 derived from microbial and thermogenic sources. Furthermore, other researchers (Whiticar et al., 1986; Schoell, 1988; Burke et al., 1988a; 1988b; Whiticar, 1999; Hornibrook et al., 1997; Chanton et al., 2005) hypothesized that the production of CH_4 is

associated with inverse or antipathetic shifts in δ^2H and $\delta^{13}C$ of CH_4, in which fermentation of acetate will result in CH_4 enriched in ^{13}C and depleted in ^2H, something relative to CH_4 produced via the CO_2 reduction pathway. In those diagrams (Figure 27), thermogenic CH_4 has been reported to exhibit $\delta^{13}C$-CH_4 values ranging from -50 to -30‰ and δ^2H-CH_4 values <-150‰ (e.g., Schoell, 1980; Whiticar, 1999; Bradley and Summons, 2010). Microbial CH_4 usually has $\delta^{13}C$-CH_4 values <-50‰ (e.g. Whiticar, 1999; McCollom and Seewald, 2007) and can be produced either by i) methyl-type fermentation or by ii) carbonate reduction (^{13}C-depleted and ^2H-enriched CH_4 with respect to the methyl-type fermentation) (Whiticar et al., 1986; Whiticar, 1999). CO_2-reduction and acetate fermentation pathways may be distinguished also on the basis of the carbon isotope fractionation factor (α_C) between coexisting CO_2 and CH_4 (Whiticar et al. 1986)

$$\alpha_C = (\delta^{13}C\text{-}CO_2 + 1000) / (\delta^{13}C\text{-}CH_4 + 1000) \qquad (3)$$

The isotope fractionation of the carbon dioxide reduction is generally between α_C = 1.055 and 1.09, in contrast to acetate- type fermentation which is usually between α_C = 1.04 and 1.055.

Gases produced by the decay of organic matter at T>150°C (thermogenic gases) are commonly characterised by $CH_4/(C_2H_6+C_3H_8)$ concentration ratios (known as the "Bernard parameter") <100, with the exception of coal gases (Whiticar, 1999) and shale gases (Tilley & Muehlenbachs, 2013). Higher ratios (>1000) are expected when hydrocarbon production derives exclusively from microbial activity (Whiticar and Suess, 1990; Jenden et al., 1993). However, many processes can play a fundamental role for its origin, such as isotopic fractionation by diffusion (Prinzhofer and Battani, 2003), secondary methanogenesis and anaerobic biodegradation (Dimitrakopoulos and Muehlebnacts, 1987; Pallasser, 2000; Etiope et al., 2009). Methanotrophic bacteria, for instance, may oxidize biogenic CH_4, causing a shift toward less negative isotopic values of the residual gas (Coleman et al., 1981).

CH_4 of abiogenic origin, e.g. discharged from high-temperature hydrothermal fluids venting from sediment-free ultramafic systems, is thought to be characterised by δ^2H-CH_4 values higher than -150‰ (Welhan and Craig, 1983; Proskurowski et al., 2006; 2008; McCollom and Seewald, 2007; Bradley and Summons, 2010). Similarly, the $\delta^{13}C$-CH_4 values of CH_4 produced from water-rock reactions, such as hydration of ultramafic rocks, may vary in a wide range because it depends on the inorganic carbon source and the magnitude carbon isotope fractionation.

Another possible source of abiogenic CH_4 is the serpentinization process of ultramafic rocks within ophiolitic sequences. Such processes produce significant quantities of H_2 even at temperatures below 100°C (Miller et al., 2017) mainly through the following reactions:

$$2(Mg, Fe)_2SiO_4 + 3H_2O \rightarrow (Mg,Fe)_3Si_2O_5(OH)_4 + (Mg,Fe)(OH)_2 \quad (4)$$

olivine — serpentine — brucite

$$Fe_3Si_2O_5(OH)_4 + H_2O \rightarrow Fe_3O_4 + 2SiO_2 + H_2 \quad (5)$$

serpentine (greenalite) — magnetite — silica

The produced H_2 in turn may be transformed in CH_4 reacting with carbon oxides (CO, CO_2 or simple organic acids). Such reactions can be mediated either microbially or inorganically (Fischer-Tropsch type reactions – Etiope and Sherwood-Lollar, 2013). The latter are favoured at high temperatures but experiments show that they can proceed even at ambient temperature in the presence of a suitable catalyst (Etiope and Ionescu, 2015). Apart from significant H_2 and CH_4 gas production, the serpentinization processes lead to the formation of hyperalkline groundwaters (Barnes and O'Neil, 1969; Bruni et al., 2002).

Besides few exceptions (Hinrichs et al., 2006), Bernard and Schoell diagrams (Bernard et al., 1978; Schoell, 1980; 1988; Etiope and Schoell, 2014, Figure 27) work fairly well for the classification of CH_4 from thermogenic and microbial sources, however they are of limited use considering the identification of abiogenic CH_4. The reason is that there seems to be a considerable overlap of fields characteristic for thermogenic CH_4, thermogenic CH_4 affected by secondary oxidation and "abiogenic" CH_4. Furthermore, some studies evidenced that in carbon limited conditions the Carbon isotopic composition of CH_4deriving from microbial activity could reach values as high as those generally attributed to abiogenic origin (Kietäväinen & Purmako, 2015).

Recently, new proxies such as clumped isotopes, capable of determining the isotopologues of CH_4 molecules (Stolper et al., 2014; Wang et al., 2015), have been developed. Potential applications of this method include determination of CH_4 formation temperature (CH_4 thermometry), and detection of kinetic isotope fractionation, both of which might be used in separating biotic from abiotic CH_4 (Stolper et al., 2014; Wang et al., 2015). More applications are expected when this method comes more widely attainable.

4.4.2. Origin of hydrocarbon compounds in Greece

Taking into consideration the geo-lithological division of the study areas and the dominant gas species, it is noticeable that the manifestations found on the western part of Greece display higher CH_4 concentrations with respect to those found in the eastern part where CO_2 is the prevailing gas species (Figure 25). In particular, EH are characterised by widespread and thick sedimentary formations mainly originating from the erosion of elder rocks from IH and HH. This geological/petrological regime makes the stratigraphic sequences of EH richer in solid organic substances, as also supported by the hydrocarbon deposits occurring in this area (Palacas et al., 1986). On the other hand, IH and HH are characterised by more "mature" formations (Cavazza et al., 2004), mainly intrusive and metamorphic, and by significant erosion causing a substantial reduction of the crustal thickness before the post-orogenic extension. These formations contain much less organic matter than EH. Therefore, as also seen in Figure 27 a and b, the occurrence of biogenic CH_4 in these areas is likely related to the presence of a post-orogenic sedimentary cover.

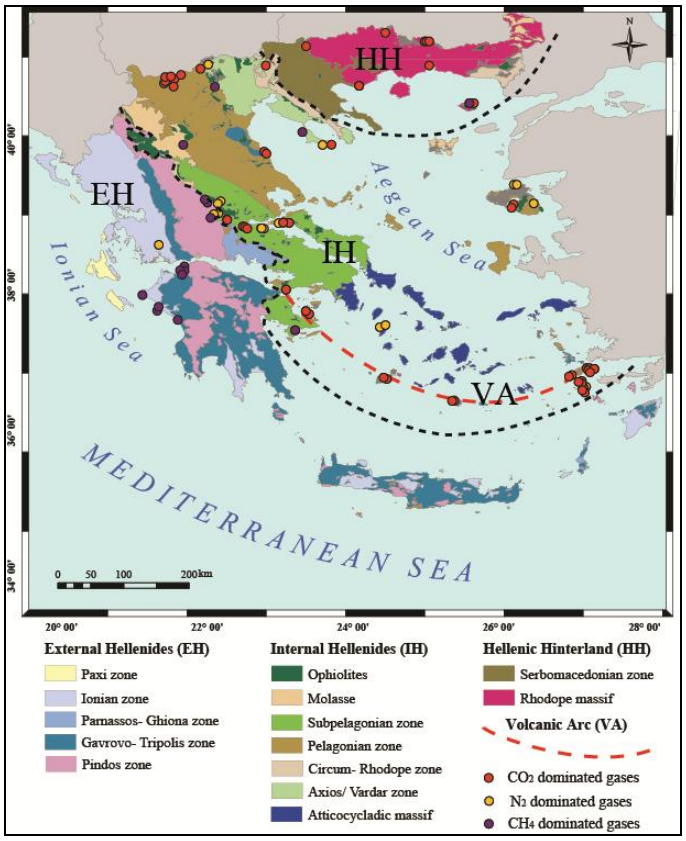

Figure 25: Geological map of Greece with the prevailing gas species

The most used parameters to discriminate the genetic processes of CH_4 are the C- and H-isotopic compositions of CH_4 (Schoell, 1980; Etiope and Schoell, 2014) and the $CH_4/(C_2H_6+C_3H_8)$ ratio (Bernard et al., 1978). Of course, it should be considered that secondary processes (e.g. mixing, inorganic or microbially-driven oxidation) affecting CH_4 and light hydrocarbons might change the chemical and isotopic composition of these compounds masking, at least partially, their primary origin (Coleman et al., 1981; Kiyosu and Imaizumi, 1996; Kinnaman et al., 2007). High $CH_4/(C_2H_6+C_3H_8)$ concentration ratios (> 1000) are generally limited to the "microbial" samples of EH and to many samples from IH, as well as for some samples of VA (Gyali and Kos islands) (Figure 27 a, Table 5, Table 8). For the remaining samples, the ratio shows lower values, indicating either a preferential loss of CH_4 due to microbial oxidation or the production of significant quantities of low-molecular-weight hydrocarbons through thermal degradation of organic matter. More specifically, in both Bernard and modified Schoell diagrams (Figure 27), the CH_4-dominated gases from EH plot in the biogenic fields. In particular, samples of the Gavrovo-Tripolis zone have a clear microbial origin with low $\delta^{13}C$ but relatively high $\delta^{2}H$ values of CH_4 that point to a microbial carbonate reduction, whereas those from the Ionian zone seem to be of thermogenic origin (Figure 27). Some gas samples from the Ionian and of Pindos zones (EH) are intermediate between the thermogenic and microbially derived group, (Figure 27 b). Such mixing pattern is also confirmed by the $CH_4/(C_2H_6+C_3H_8)$ ratio measured in gases collected in petroleum exploration wells of the Katakolo hydrocarbon field (NW Peloponnesus), which decreases from pure microbial-type values (1000 – 12,500) at shallower levels down to low values (3.27 – 24.4) at deeper levels (2000 – 2500m depth) where temperatures for thermogenic gas generation are reached (Kamberis et al., 2000).

Samples ascribable to a microbial origin on the basis of their $\delta^{13}C$ and $\delta^{2}H$ values of CH_4 display α_C values (Figure 26) compatible with the CO_2-reduction origin at least for the samples in which both $\delta^{13}C$-CO_2 and $\delta^{13}C$-CH_4 are available (samples 1, 13,25, 50 and 82- Table 7).

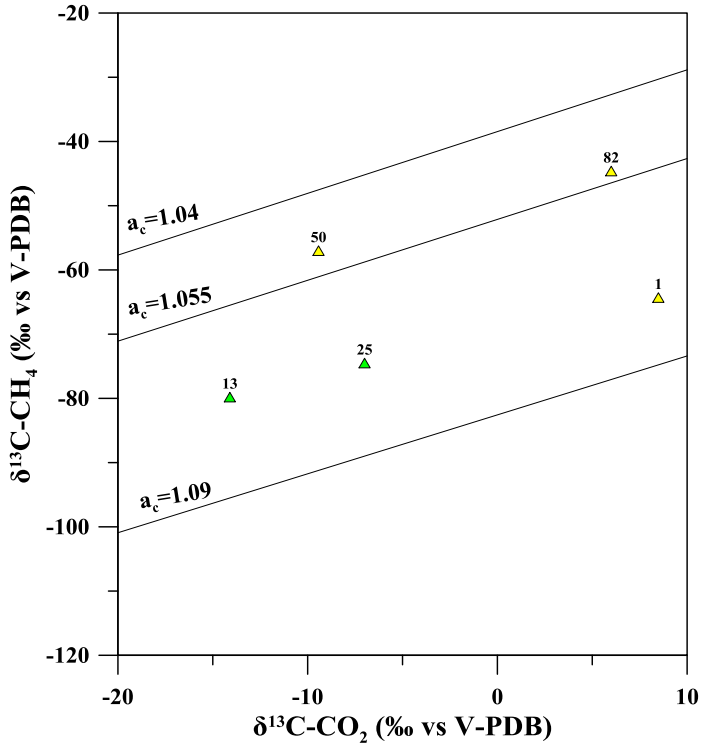

Figure 26: $\delta^{13}C–CO_2$ vs. $\delta^{13}C–CH_4$.Carbon isotope fractionation factor (α_C) is based on the Whiticar et al. (1986) functions. Symbols as in Figure 7.

Furthermore, some of the N_2-CO_2 dominated samples collected from the thermal emissions that occur in the Subpelagonian and Vardar/Axios zones (IH) plot in the field characteristic for abiogenic hydrocarbons emitted from volcanic-geothermal systems after McCollom and Seewald (2007; Figure 27 a). At the same time, also the CO_2-rich thermal manifestations from HH (Rhodope massif) and IH (Pelagonian and Subpelagonian zones) are found in a another field proposed by Sherwood Lollar et al. (2006) to be characteristic for an abiogenic origin, releasing gases mainly related to hydrothermal systems within the crystalline or metamorphic rocks of the Precambrian shield (Anders et al., 2006; Reischmann and Kostopoulos, 2007) (Figure 27 a). In both cases, a contribution from a biogenic source cannot be excluded due to the closeness to the thermogenic field. In the latter case however, the samples are found in low to medium enthalpy back-arc geothermal fields in an area characterised by extensional tectonics, which presumably also results in crust thinning (Fytikas and Kolios, 1979). CO_2 dominated thermal gases from the VA show chemical and isotopic characteristics that are apparently consistent with an abiogenic origin for CH_4 ($\delta^{13}C$-CH_4 values around -20‰,and $\delta^{2}H$-CH_4 values around -150‰) deriving

from CO_2 reduction. Contributions from a biogenic source cannot be excluded for those samples having $CH_4/(C_2H_6+C_3H_8)$ ratios <1000 (Bernard ratio ranges from 9 to 4810).

Some N_2-rich gases from IH discharge in correspondence of the ophiolitic bodies that crop out in the Hellenic territory (Pe-Piper and Piper, 2002), where hyperalkaline waters (pH from 9.72 to 11.98) were found at Othrys (central Greece - Etiope et al., 2013a; 2013b; D'Alessandro et al., 2014) and at Argolida (D'Alessandro et al., 2017). CH_4collected in these hyperalkaline springs show $\delta^{13}C\text{-}CH_4$ values ranging from -37.4 to -26.6‰ and $\delta^{2}H\text{-}CH_4$from -311 to-250‰, excluding sample 88 that has more positive values (-2.0 and -127‰ respectively) that were attributed by D'Alessandro et al. (2017) to microbial oxidation processes. Such values, on the diagram of Figure 27 b, fall all, except sample 88, within the field of land-based serpentinization systems as defined by Etiope and Schoell (2014) and have been attributed by the previous authors to an abiogenic origin (Etiope et al., 2013; D'Alessandro et al., 2014; 2017).

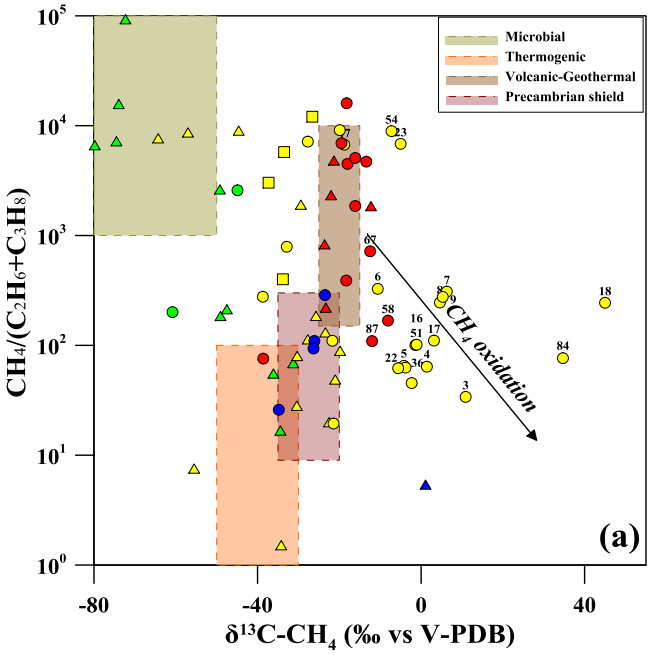

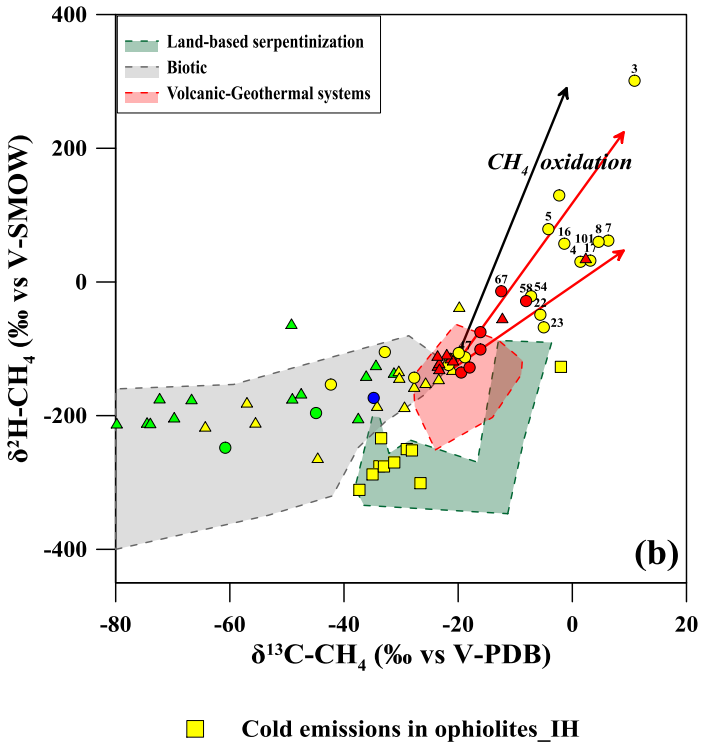

Figure 27: a) Bernard diagram (Bernard et al., 1978) correlating the $CH_4/(C_2H_6+C_3H_8)$ concentration ratios with the $\delta^{13}C$-CH_4isotopic composition of the Hellenic gas discharges. Values for gases of biogenic origin (microbial and thermogenic) and for Precambrian Shield and Geothermal fields are reported (McCollom and Seewald, 2007, and references therein) for comparison, b) modified Schoell binary diagram (Etiope and Schoell, 2014) between δ^2H-CH_4 and $\delta^{13}C$-CH_4ratios for the Hellenic gas discharges. Slopes of biogenic and abiogenic oxidation of $CH_4$are respectively plotted as red- and black- coloured lines. Symbols as in Figure 7.

4.4.3. Secondary post-genetic processes

Many processes can significantly modify the isotopic signature of primary methane. Methanotrophic bacteria, for instance, may oxidize biogenic CH_4, causing a shift toward less negative isotopic values of the residual gas (Coleman et al., 1981).

The majority of the thermal gases of Subpelagonian and Vardar/Axios zones (IH), the cold manifestations of the Rhodope massif (HH) and some of the volcanic-hydrothermal ones show low $CH_4/[C_2H_6+C_3H_8]$ ratios (Figure 27 a, Table 8) and strongly positive isotopic ratios of CH_4 ($\delta^{13}C$ up to +45‰ and $\delta^{2}H$ up to +301‰ – Figure 27, Table 7). Such chemical and isotopic features were likely caused by oxidation of CH_4 (Figure 28). In these environments, microbes obtain energy from aerobic or anaerobic CH_4 oxidation (Murrell and Jetten, 2009), preferentially consuming CH_4 with respect to higher hydrocarbons and preferring light isotopes. Thermophilic and acidophilic methanotrophs oxidize CH_4 also in the harsh environment of thermal waters up to temperatures of more than 80°C (Sharp et al., 2014). The temperatures of the sampling sites in which we found enriched $\delta^{13}C$ and $\delta^{2}H$ values for CH_4 are mostly in the range from 40 to 63 °C but reaching up to 73.7 °C in the case of sample 54. Although until now, no microbiological studies have been made on these waters to definitely support the occurrence of methanotrophs, the measured temperatures are well within the range that allows the presence of methane oxidizing microorganisms.

Inorganic oxidation of CH_4 (Kiyosu and Imaizumi, 1996) in some samples cannot be ruled out. Nevertheless, the isotopic fractionations of organic and inorganic oxidation of CH_4 follow different fractionation paths. The former follows $\Delta H/\Delta C$ slopes ranging from 5.9 to 13 (Cadieux et al., 2016 and references therein), and the latter a slope of 21 (Kiyosu and Imaizumi, 1996). Since in our samples it is not always possible to establish the primary isotopic composition before oxidation, we can only make some hypothesis about it. Looking at Figure 27 b it is evident that most of the samples within the volcanic-geothermal field cluster around the following values: $\delta^{13}C \approx -21$‰ and $\delta^{2}H \approx -130$‰. Taking these values as the isotopic composition of CH_4 before oxidation, we obtain $\Delta H/\Delta C$ values comprised between 3.8 and 13.6 mostly overlapping the typical range of biogenic oxidation processes. Furthermore, the strongly positive values shown by some samples imply low values of the residual fraction of CH_4 (< 0.25).

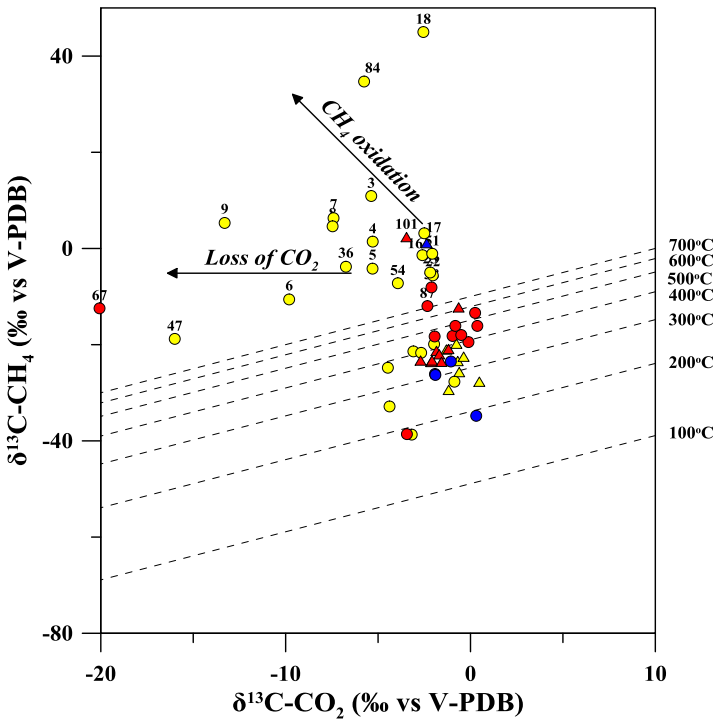

Figure 28: $\delta^{13}C–CO_2$ vs. $\delta^{13}C–CH_4$. Temperature scales are based on the isotope fractionation factors from Bottinga (1969). Symbols as in Figure 7.

The relationship between $\delta^{13}C$ values of CO_2 and CH_4 can be used to obtain useful information about the origin of these gas compounds (Whiticar et al., 1986). Assuming the attainment of an isotopic equilibrium between CH_4 and CO_2, equilibrium temperatures between the two gases can be computed according to Bottinga (1969) and Horita (2001). The estimation of the reservoir temperature through these geothermometers is outside the scope of this work. Nevertheless, most gases from VA and some thermal samples from IH and HH cover an estimated temperature interval between 270 and 500°C indicating the possible achievement of isotopic equilibrium between CH_4 and CO_2. Among these, only for samples collected at Nisyros fumaroles Fiebig et al. (2004, 2009) demonstrated the attainment of equilibrium through the comparison with chemical geothermometers and temperatures measured in exploration wells. For all other samples, though indicating temperatures that are reasonable for geothermal systems, there is no proof for carbon isotope equilibration and the estimations may be likely only fortuitous. Instead all the samples plotting above the 700°C isotherm are likely affected by secondary processes that isotopically fractionate CO_2 and CH_4. Such processes, as evidenced previously, are the CO_2 loss and the microbially-driven CH_4 oxidation. The former affects only the $\delta^{13}C$-CO_2 through either

gas dissolution in water or precipitation as carbonate, whereas the latter tends towards more positive $\delta^{13}C\text{-}CH_4$ values and more negative $\delta^{13}C\text{-}CO_2$ values (Figure 28).

As shown in Figure 29, the CH_4/C_2H_6 concentration ratios of the gas emissions vary by more than four orders of magnitude. On the contrary, the ratios between the main light hydrocarbons, i.e. C_2H_6, C_3H_8 and C_6H_6, vary only within two orders of magnitude. In this respect, the $CO_2(CO)$–CH_4 interaction that likely controls the CH_4 abundance in volcanic fluids does not seem to affect the higher hydrocarbons whose origin could be entirely related to thermal degradation of organic matter (Fiebig et al. 2009, 2015).

CH_4polymerization is accompanied by relatively small carbon isotope fractionations between C_{2+} n-alkanes and residual CH_4 (Sherwood Lollar et al., 2006; McCollom et al., 2013). This hypothesis should be supported by C-isotope data on C_{2+} alkane series' that unfortunately are not available for this study. Likewise, the residual CH_4 retains its primary carbon isotopic composition if the degree of polymerization is low. This, alternatively, might provide an explanation why there occurs no significant correlation between the ^{13}C composition of $CH_4$and the magnitude of the Bernard ratio values for gases from VA (Figure 27 a), with $\delta^{13}C\text{-}CH_4$ being entirely controlled by $\delta^{13}C\text{-}CO_2$ and temperature.

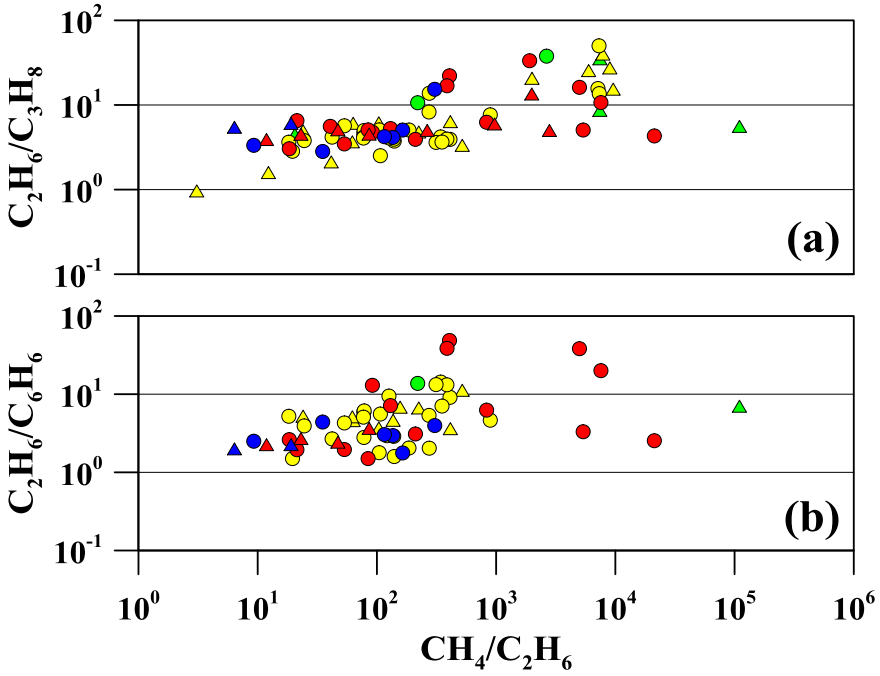

Figure 29: a) CH_4/C_2H_6 vs. C_2H_6/C_3H_8 and b) CH_4/C_2H_6 vs. C_2H_6/C_6H_6 binary diagrams for the Hellenic gas discharges. Symbols as in Figure 7.

4.5. Environmental Hazards

Geogenic sources release huge amounts of gases that can have important influences on the global climate, the environment and a strong impact on human health. Many volcanic and geothermal regions are densely populated and several are close to major cities, threatening local populations (Francis and Oppenheimer, 2004). In large enough quantities or high enough concentrations, almost everything can be bad for human health.

Very high concentrations of atmospheric CO_2 can produce a state of "hypercapnia" or an excessive amount of CO_2 in the blood (Nahas et al., 1968; Brackett et al., 1969; van Ypersele de Strihou, 1974), which typically results in "acidosis", a serious and sometimes fatal condition expressed in the terms of headache, nausea and visual disturbances (Poyart and Nahas, 1968; Turino et al., 1974). However, these phenomena do not have an impact on human health until the atmosphere's CO_2 concentration reaches approximately 15,000 ppm (Luft et al., 1974; Schaefer, 1982), approximately 40 times greater than its current concentration in uncontaminated atmosphere. H_2S is both an irritant and asphyxiant gas. Levels of up to 20 ppm generally have no effect on healthy people, while asthmatics can respond to levels of 2 ppm (WHO, 2003). Concentrations above 20 ppm cause irritations to the eyes and respiratory tract, above 50–100 ppm neurotoxic effects appear and 500–1,000 ppm are considered of immediate danger to life (WHO, 2003). Although the human odour threshold is very low (0.02 ppm), the warning signal is lost above 150 ppm because of olfactory nerve paralysis by H_2S itself. H_2S like CO_2 is heavier than air and tend to accumulate in closed and/or depressed areas.

Some of the fatal incidents with volcanic gases worldwide were attributed to the effects of these gases released by low-temperature fumarolic vents or by gas bubbling through thermal springs. In the 20^{th} century, more than 2000 people died and nearly 3000 were injured by volcanic gases worldwide (Witham, 2005). The most dangerous gas species is CO_2, responsible of more than 90% of the victims and of the worst episodes (Lake Nyos and Lake Monoun - Holloway, 2000; Cameroon and Dieng Plateau - Le Guern, 1982), but lethal episodes are also attributed to SO_2 and H_2S. Gas hazard is often disregarded because it is almost always connected to low or absent volcanic activity when attention is low. In the Hellenic territory, dangerous or even lethal concentrations of H_2S have been previously reported in Greek natural gas manifestations at least at Katakolo in (EH) – Etiope et al., 2006b, at Sousaki - D'Alessandro et al., 2009 and at Nisyros - D'Alessandro et al., 2010 in VA. In the present study H_2S concentrations are not reported in

extend, but it is important to underscore that this gas is often present in natural gas emissions, at hazardous levels.

In the period of 1992 – 2011, at least 2 lethal accidents with a total of 3 victims had occurred in Greece (D'Alessandro and Kyriakopoulos, 2013). The 1st occurred in Neos Kafkasos, a village located close to Florina, in the period of 1995-1997. In the above referred area, a natural CO_2 accumulation in the subsoil takes place. For about 30 years, the company Air Liquide has been exploiting the CO_2 reservoir and it has been one of the study areas for a research program NASCENT financed by the European Community for the study of natural equivalents of geological carbon storage sites (Pearce, 2004; D'Alessandro et al., 2011a). The origin of the CO_2 accumulations in the area were attributed to the nearby Quaternary volcanic activity in the Voras mountains. An exploration well was made in 1993 by IGME (Greek Geological Survey) and CO_2 was found at various depths. The gas pressure at the well bottom was underestimated and a leakage of CO_2 -rich water was observed bubbling from the soil. The leakage of the bubbling water increased and formed a lake with a surface area of about 25 m^2 and 50 m depth in which CO_2 was vigorously bubbling. In order to diminish the bubbling gas pressure of the well, another drilling well was constructed. Also this attempt was unsuccessful and in the end, for the resolution of the problem, the pond was filled with sediments and the gas emission was slightly decreased. Some years later, the local authorities created a circular pond with a cement lining around the gas vent. This pool was used by local people as a health cure, by immersion of their feet sitting at the rim of the pool and thereby keeping their heads about 1 m above the water surface where the CO_2 was concentrated. Unfortunately, a man tried to swim in the pool and died by asphyxiation (Pearce, 2004). In 2011, the flux measurements did not indicate anomalous levels in an area of about 100 m^2 around the pool (Roppolo, 2012) indicating that the reservoir was either exhausted or sealed again.

The 2nd fatal accident occurred in 2009 at the Pausanias' thermal baths on the northern coast of the peninsula of Methana. The volcanic system of Methana is the site of many hydrothermal degassing manifestations (D'Alessandro et al., 2008) and the thermal bath of Pausanias is associated with these. The bath is formed by a spring that emerges very close to the sea and is captured with a small pool (about 2 m^3) inside a small building. The pool is about 90 cm below the threshold of the small entrance of the building. It has no artificial water outflow and the water in the pool is generally found cool. To drive new warm water into the pool, it has to be emptied

manually or with an electric pump. The thermal water flows very slowly but eventually fills the pool. Sometimes in the freshly filled pool, gas starts to bubble. Pausanias is composed of almost pure CO_2 that, being heavier than air, accumulates above the water. The persons that take a bath within this pool will have their heads in an area, where CO_2 will slowly accumulate to lethal levels. This is probably what happened to a pair of elderly people (79 and 76 years) of the city of Patras, who were found dead in the pool on the 2nd of August 2009. Unfortunately, no autopsy of the two victims was made and the report by the police gives only a generic cause of death. Drowning was excluded due to the position of the bodies.

Conclusions

This project presented a new improved catalogue of all the known gas manifestations located in the Hellenic territory. The determination of the chemical and isotope composition of the gases contributed in the identification of the origin of the gases and of the secondary processes that affect them. Furthermore, from this study possible relationships between the geochemical composition of the gases and both the different geological settings and the geodynamic regime were revealed.

Both CO_2 and He present a wide range of chemical concentrations (from 17 to 1,000,000 μmol/mol and from 0.10 to 3370 μmol/mol, respectively) and isotope values (from -29.9 to +6.0 vs. V-PDB for $\delta^{13}C\text{-}CO_2$ and from 0.01 to 7.10 for R/R_A). A schematic description of the results connecting the geological setting, the heat flow values, the crustal thickness and the He and CO_2 concentrations of the gases collected in Greece is proposed in the summary flow chart diagram of Figure 30.

Results of $^4He/^{20}Ne$ showed that the atmospheric contribution was mostly negligible except from gases collected in EH. From the geographical distribution of the gases, it is evident that CO_2 concentrations and R/R_A ratios have a similar behavior, increasing in areas characterised by thin crust, enhanced heat flow values, Plio-Quaternary volcanic activity and deep routed extensional or transtensional regional faults. Geology plays also a fundamental role in their concentrations. The highest CO_2 and R/R_A values are therefore found along VA and the lowest in EH. Furthermore, based on the R/R_A and the $^4He/^{20}Ne$ values, it was determined that He is prevailingly of mantle origin for samples collected in VA, whereas in the other regions it has a mainly radiogenic source with important atmospheric contribution in few samples. On the other hand, $CO_2/^3He$ and $\delta^{13}C\text{-}CO_2$ values highlighted that the majority of the collected samples present a prevailing limestone C component and only few samples have a prevailing mantle C component. However, with the present data, it is not possible to determine if CO_2 derives from subducted carbonate bearing sediments or from assimilated crustal limistones. Due to the complex geodynamic history, the mantle C isotope composition could be affected by subduction-related metasomatism and, similarly to the nearby Italian area (Martelli et al., 2008), the C isotope composition could be more positive. In this case, the mantle contribution is probably underestimated. Some samples display very low $CO_2/^3He$ and $\delta^{13}CO_2$ values due to the CO_2 loss

caused either by dissolution of CO_2 in shallow groundwater or by the calcite precipitation that is taking place in most of the thermal springs.

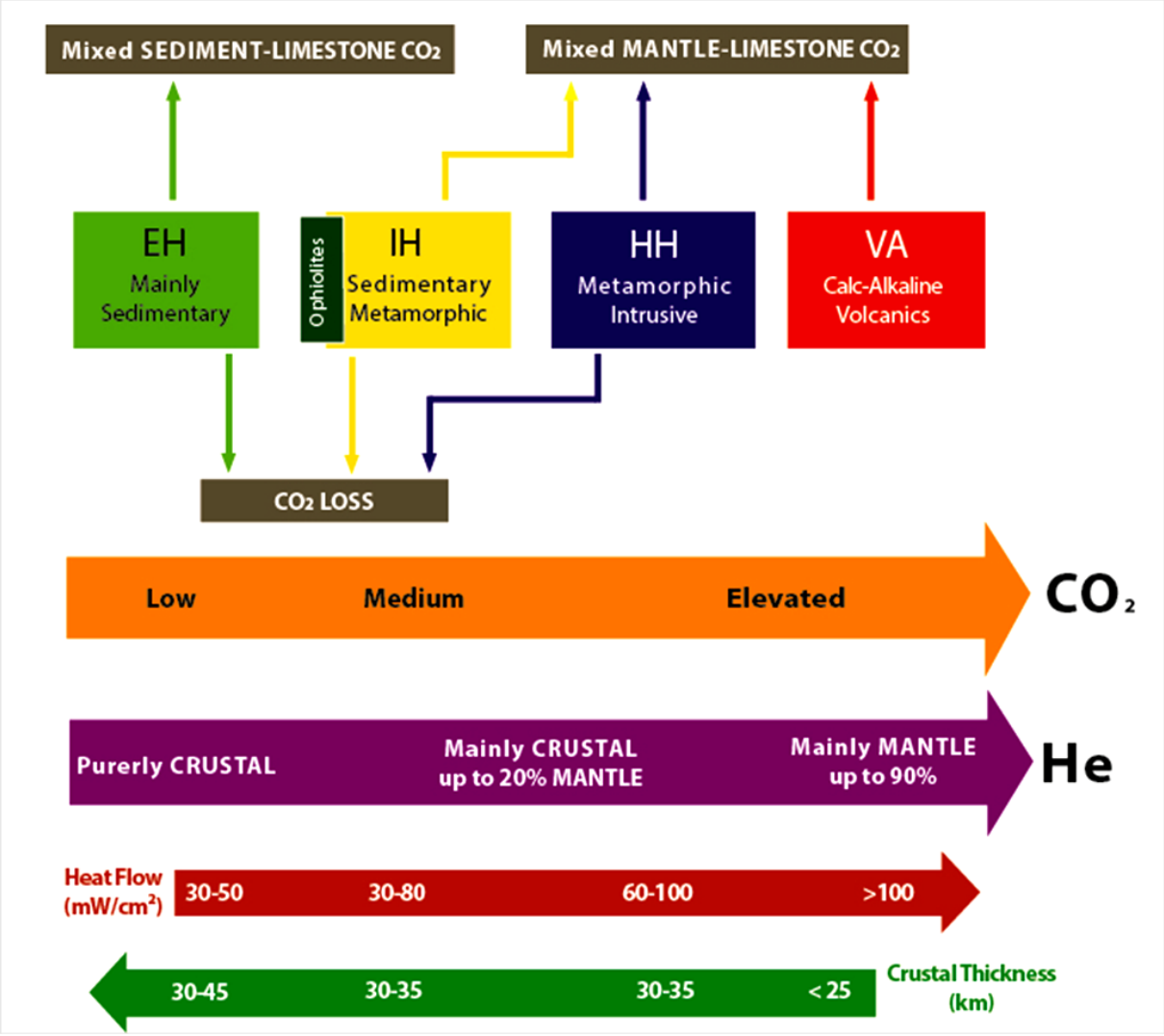

Figure 30: A graphical description of the different possible origins of CO_2 and He, including secondary post-genetic processes. Bottom arrows show the correlation of the gases with the crustal thickness and the heat flow in the areas, whereas connectors emerging from the boxes of the geographical distribution describe possible sources and processes that are affecting the gases. The main boxes provide information about the geological setting of the area in the different geologic regions.

In the case of CH_4, our results show that CH_4 from the Hellenic territory describes a wide range of both concentrations (from <0.5 to 925,200 μmol/mol) and isotope values ($\delta^{13}C$-CH_4 from -79.8 to +45.0‰; $\delta^{2}H$-CH_4 from -311 to +301‰). Furthermore, the $CH_4/(C_2H_6+C_3H_8)$

concentration ratio displays a broad range of values (1.5 – 93,200). Such a large variability in hydrocarbon concentration ratios and methane isotopic compositions is indicative for methane originating from different sources and for the importance of secondary, post genetic processes such as microbial oxidation. A schematic description of the results combined with the variations of the geology, the heat flow values, and CO_2 and CH_4 concentrations along the Hellenic territory is proposed in the summary flow chart diagram (Figure 31).

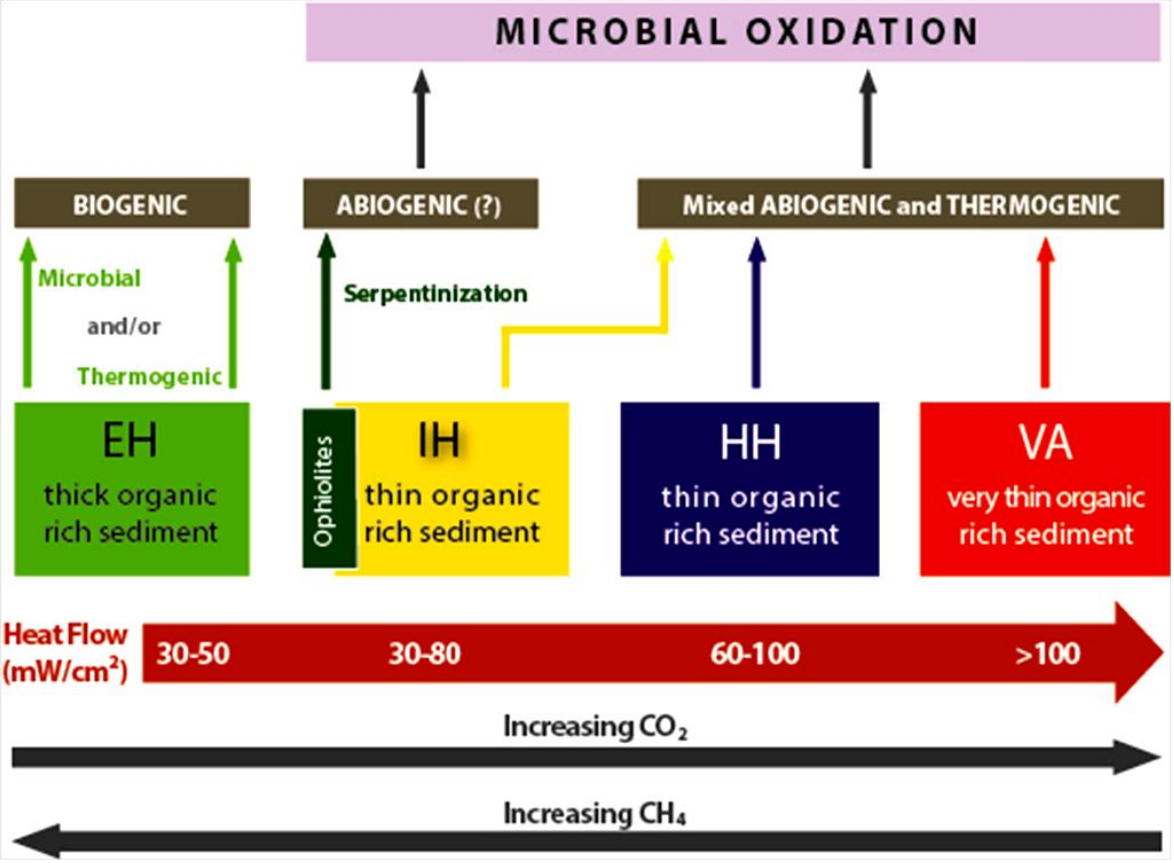

Figure 31: A graphical description of the different possible origins of CH_4 including postgenetic processes. Connectors are emerging from the central boxes to the possible origins and the processes that are affecting its origin. The main boxes provide information about the thickness of the sedimentary sequences in the different geologic regions. Both variations of heat flow values and CO_2 and CH_4 concentrations along the regions are plotted on the lower part of the flow chat (Daskalopoulou et al., 2018).

Taking into account the different lithological facies of the study area and the dominant gas species, it is noticeable that samples found on the western part of Greece (EH) display higher CH_4 and N_2 concentrations with respect to those found in the eastern part (IH, HH), where CO_2

is the prevailing gas. This can be explained by the sedimentary regime that characterises the EH, in which solid organic substances dominate, favouring the occurrence of hydrocarbon deposits. Moreover, the continuous changes in the relief and the mainly intrusive and metamorphic formations of both IH and HH contain few or no amounts of organic matter.

Biogenic methane was mainly found in the N_2-CH_4 and CH_4-dominated gases from EH. More specifically, gases collected in the Gavrovo-Tripolis zone show a dominating microbial origin. Gas samples of the Ionian and Pindos zones are produced by both microbial activity and thermal maturation of sedimentary organic matter. On the contrary pure thermogenic samples are less represented in the sampled manifestations and are connected either to high geothermal gradients (samples 21 and 75) or to very thick sedimentary sequences in the Ionian (EH) and Aegean Sea (IH) (samples 104, 105 and 110 to 113) (Table 7, Table 8).

Hydrocarbons contained in CO_2-rich thermal manifestations from HH (Rhodope massif) and IH (Pelagonian and Subpelagonian zones) are -regarding their isotopic composition- similar to those emitted from the crystalline or metamorphic rocks of the Precambrian shield (Sherwood Lollar et al., 2006). They therefore, may be considered of abiogenic origin. However, for most of these samples, the measured values could also be explained by a biogenic origin modified by methane oxidation processes.

CO_2 dominated thermal gases from VA and N_2-CO_2-dominated thermal gases from IH show a relatively narrow range of $\delta^{13}C$-CH_4 values (-25 to -15‰) and a much larger range of $CH_4/(C_2H_6+C_3H_8)$ concentration ratios (10 to 10,000) that show chemical and isotopic characteristics that are apparently consistent with an abiogenic origin for CH_4 with a minor contribution of a thermogenic source. For the geothermal system of Nisyros, which belongs to the VA, CH_4 is mostly originated from inorganic reactions in the hydrothermal reservoir while the light hydrocarbons have a prevailingly thermogenic origin.

Some of the N_2-rich gas manifestations of the IH collected in Pindos zone, seem to have a possible abiogenic origin for CH_4 as they are associated with serpentinization processes within the ophiolitic sequences of Othrys and Argolida. Finally, microbial oxidation processes have been evidenced for some of the CO_2-dominated gas discharges from the main thermal springs located in the Subpelagonian and Vardar-Axios zones (IH) and in the Rhodope massif (HH). Such processes lead to sometimes very strong isotopic fractionation of CH_4 reaching very positive $\delta^{13}C$ (+45.0‰) and $\delta^{2}H$ (+301‰) values.

Finally, we want to underscore that, although further studies are necessary to answer a number of questions that remained open such as the accurate origin of hydrocarbons, the important contribution of this paper is to show how hydrocarbons from all over Greece distribute in the Schoell and Bernard plots. Considering this, our study may be a starting point for those who want to investigate the geochemistry of fluids from a specific area included in this study and to examine in more detail their origin by applying new scientific approaches, such as those based on clumped isotopes.

As said before, gases collected in the Hellenic territory present a wide range of values. However, their concentrations in some cases reach hazardous levels, which may severely impact on both the environment and the human health. Since deaths due to natural gases are often wrongly attributed, the risk might be higher than assessed in the Hellenic territory. Although very low, this risk should not be neglected, not only because it is possibly underestimated, but also because simple countermeasures could be adopted for risk reduction. Dangerous areas can be easily identified and delimited by geochemical prospecting and their hazards properly highlighted.

References

2014, the Gre.Da.S.S. Working Group, http://eqgeogr.weebly.com/database-of-active-faults.html

Allard, P., Maiorani, A., Tedesco, D., Cortecci, G., Turi, B., 1991. Isotopic study of the origin of sulfur and carbon in Solfatara fumaroles, Campi Flegrei caldera. J. Volcanol. Geotherm. Res. 48, 139-159.

Ambraseys, N.N., 2000. The seismicity of the Marmara Sea area 1800– 1899, J. Earthquake Eng., 4(3), 377–401.

Ambraseys, N.N., 2001. Far-field effects of Eastern Mediterranean earthquakes in Lower Egypt, J. Seismology 5, 263-268.

Anders, B., Reischmann, T., Kostopoulos, D., 2006. The oldest rocks of Greece: first evidence for a Precambrian terrane within Pelagonian Zone, Geol. Mag., 143, 41–58.

Anderson, D.L., 1998b. A model to explain the various paradoxes associated with mantle noble gas geochemistry, Proc. Nat. Acad. Sci., 95, 9087 – 9092.

Andritsos, N., Arvanitis, A., Dalabakis, P., Karytsas, C., Mendrinos, D., Papachristou, M., 2013. Geothermal energy use, country update for Greece. Proceedings of the geothermal congress. Pisa, Italy.

Andritsos, N., Dalambakis, P., Arvanitis, A., Papachristou, M., Fytikas, M., 2015. Geothermal Developments in Greece – Country update 2010-2014. Proceedings World Geothermal Congress 2015. Melbourne, Australia, 19-25.

Armijo, R., Meyer, B., Hubert, A., Barka, A., 1999. Westward propagation of the North Anatolian fault into the northern Aegean: Timing and kinematics. Geology, 27, 267-270.

Arnorsson, S., 1995. "Calcium Carbonate Deposition From Geothermal Fluids: Causes, Operational Problems and Their Solution", in Scaling Problems and Treatment of Separated Water Before Injection, 79-94.

Arvanitis, A., 2003. Geothermal study in the SW part of the Strymon basin, PhD Thesis, Aristotle University of Thessaloniki, Thessaloniki (in Greek).

Arvanitis, A., 2011. Geothermal activities in Greece. International Trade Fair Energy 2011 Renewable EnergyIndustry and Export Forum, 4–8 April 2011, Hannover, Germany.

Athanasoulis, K., Vakalopoulous, P., Xenakis, M., Persiani, D., Taktikos, S., 2009. Periodic monitoring of the Hellenic thermal springs. Book published by IGME (in greek).

Baines, S.J., Worden, R.H., 2004. Geological Storage of Carbon Dioxide (eds Baines, S.J. & Worden, R. H.) 59–85, The Geological Society of London.

Ballentine, C.J., Burgess, R., Marty, B., 2002. Tracing fluid origin, transport andinteraction in the crust, in: Porcelli, D.R., Ballentine, C.J., Weiler, R. (Eds.), Noble Gases in Geochemistry and Cosmochemistry, 539-614.

Ballentine, C.J., Schoell, M., Coleman D., Cain B.A. 2001. 300-Myr-old magmatic CO_2 in natural gas reservoirs of the west Texas Permian basin. Nature, 409, 327-331.

Barnes, I., O'Neil, J.R., 1969. The relationship between fluids in some fresh alpine type ultramafics and possible modern serpentinization, western United States. Geol. Soc. Am. Bull. 80, 1947-1960.

Beaubien, S.E., Lombardi, S., Ciotoli, G., Annunziatellis, A., Hatziyannis, G., Metaxas, A., Pearce, J.M., 2004. Potential Hazards of CO_2 leakage in storage systems – learning from natural systems. Paper presented at GHGT7, Vancouver, Sept. 5-8, 2004.

Bellani, S., Magro, G., Gherardi, F., 2015. Heat Flow and Helium Isotopes in the Geothermal Areas of Tuscany (Central Italy). GRC Transactions, Vol. 39, 399-405.

Bernard, B.B., Brooks, J.M., Sackett, W.M., 1978. A geochemical model for characterization of hydrocarbon gas sources in marine sediments. Offshore Technology Conference, Houston, USA, 435-438.

Berndt, M.E., Allen, D.E., Seyfried, W.E., 1996. Reduction of CO_2 during serpentinization of olivine at 300 °C and 500 bar. Geology 24, 351–354.

Besenecher, H., Pichler, H., 1974. Die jungen Vulkanite der Insel Chios (Ostlich Agais, Griechenland). Geol. Jb.,9, 41–65.

Bornovas, J., Rondogianni, T., 1983. Geological map of Greece, 1:500,000 scale. Inst. Geol. Min. Explor. (IGME), Athens.

Bottinga, Y., 1969. Calculated fractionation factors for carbon and hydrogen isotope exchange in the system calcite-carbon dioxide-graphite-methane-hydrogen-water vapor. Geochim. Cosmochim. Acta 33, 49-64.

Brackett, N.C., Wingo, C.F., Muren, O., Solano, J.T., 1969. Acid-base response to chronic hypercapnia in man. New England Journal of Medicine 280, 124-130.

Bradley, A.S., Summons, R.E., 2010. Multiple origins of methane at the Lost City hydrothermal field. Earth Planet. Sci. Lett. 297, 34-41.

Bradshaw, J., Boreham, C., La Pedalina, F., 2004. Storage retention time of CO_2 in sedimentary basins, examples from petroleum systems. Proc. 7th Internat. Conf. Greenhouse Gas Control Technol., GHGT-7. eds Rubin, E., Keith, D. & Gilboy, C., 541–550. Elsevier Science.

Bräuer, K., Kämpf, H., Niedermann, S., Strauch, G., 2013. Indications for the existence of different magmatic reservoirs beneath the Eifel area (Germany): A multi-isotope (C, N, He, Ar) approach. Chemical Geology 356, 193-208.

Bräuer, K., Kämpf, H., Niedermann, S., Strauch, G., Tesař, J., 2008. Natural laboratory NW Bohemia: Comprehensive fluid studies between 1992 and 2005 used to trace geodynamic processes. Geochemistry Geophysics Geosystem, 9, Q04018, doi:10.1029/2007GC001921.

Bredehoeft, J.D., Ingebritsen, S.E., 1990. Degassing of Carbon Dioxide as a Possible Source of High Pore Pressures in the Crust, the Role of Fluids in Crustal Processes. National Academy Press, Washington, DC, 158–164.

Briole, P., Rigo, A., Lyon-Caen, H., Ruegg, J.C., Papazissi, K., Mitsakaki, C., Balodimou, A., Veis, G., Hatzfeld, D., Deschamps, A., 2000. Active deformation of the Corinth rift, Greece: results from repeated global positioning system surveys between 1990 and 1995. Journal of Geophysical Research B: Solid Earth 105 (B11), 25605–25625.

Bruni, J., Canepa, M., Cipolli, F., Marini, L., Ottonello, G., Vetuschi Zuccolini, M., et al., 2002. Irreversible water-rock mass transfer accompanying the generation of the neutral, Mg-HCO_3 and high-pH, Ca-OH spring waters of the Genova province, Italy. Appl. Geochem. 17, 455-474.

Burke, R.A., Martens, C.S., Sackett, W., 1988a. Seasonal variations of D/H and $^{13}C/^{12}C$ ratios of microbial methane in surface sediments. Nature, 332, 829 – 831.

Burke, R.A., Barber, T., Sackett, W., 1988b. Methane flux and stable H and C isotope composition of the sedimentary methane from the Florida Everglades. Global Biogeochem. Cycles, 2, 329 – 340.

Burnard, P.G., Graham, D.W., Farley, K.A., 2002. Mechanisms of magmatic gas loss along the Southeast Indian Ridge and the Amsterdam -St. Paul Plateau. Earth and Planetary Science Letters 203, 131.

Burton, P., Xu, Y., Qin, C., Tselentis, G., Sokos, E., 2004. A catalogue of seismicity in Greece and the adjacent areas of the twentieth century. Tectonophys.390, 117-127.

Cadieux, S.B., White, J.R., Sauer, P.E., Peng, Y., Goldman, A.E., Pratt, L.M., 2016. Large fractionations of C and H isotopes related to methane oxidation in Arctic lakes. Geochim. Cosmochim. Acta 187, 141–155.

Camerlenghi, A., Cita, M.B., Della Vedova, B., Fusi, N., Mirabile, L., Pellis, G., 1995. Geophysical evidence of mud diapirism on the Mediterranean Ridge accretionary complex. Marine Geophysical Researches, 17/2, 115-141.

Capasso, G., Inguaggiato, S., 1998. A simple method for the determination of dissolved gases in natural waters. An application to thermal waters from Vulcano Island. Appl. Geochem., 13, 631-642.

Caprai, P.I.A., 2005. Volcanic and Geothermal Gases and Low-enthalpy Natural Manifestations Methods of Sampling and Analysis by Gas Chromatography. Journal of Applied Sciences 5 (1): 85-92, ISSN 1607-8926.

Cartigny, P., Pineau, F., Aubaud, C., Javoy, M., 2008. Towards a consistent mantle carbon flux estimate: insights from volatile systematics (H_2O/Ce, δD, CO_2/Nb) in the North Atlantic mantle (14° N and 34° N). Earth Planet. Sci. Lett. 265, 672–685.

Cathles, L.M., Schoell, M., 2007. Modeling CO_2 generation, migration and titration insedimentary basins.Geofluids, 7, 441–450.

Chanton, J.P., Chasar, L.C., Glaser, P., Siegel, D., 2005. Carbon and hydrogen isotopic effects in microbial methane from terrestrial environments, in Stable Isotopes and Biosphere-Atmosphere Interactions, Physiol. Ecol. Ser., edited by L. B. Flanagan, J. R. Ehleringer, and D. E. Pataki, chap. 6, 85 – 105, Elsevier, New York.

Chiodini, G., 1994. Temperature, pressure and redox conditions governing the composition of the cold CO_2 gases discharged in the volcanic area of North Latium (Central Italy). Appl. Geochem. 9, 287-295.

Chiodini, G., Cardellini, C., Amato, A., Boschi, E., Caliro, S., Frondini, F., Ventura, G., 2004. Carbon dioxide Earth degassing and seismogenesis in central and southern Italy. Geophys. Res. Lett., 31, 10.1029/2004GL019480.

Chiotis, E., Fytikas, M., Taktikos, S., 1990. Overview of the geothermal activities in Greece during 1985-1989. Geothermal Resources Council Transactions, Vol. 14(1), 79-85.

Ciais, P., Sabine, C., Bala, G., Bopp, L., Brovkin, V., Canadell, J., Chabra, A,. De Fries, R., Galloway, J., Heimann, M., Jones, C., Le Quéré, C., Myneni, R.B., Piao, S., Thornton, P.,

2013. Carbon and other biogeochemical cycles. In: Stocker, T.F. et al. (eds) Climate change 2013: the physical science basis. Contribution of working group I to the fifth assessment report of IPCC, Cambridge University Press, Cambridge.

Clément, C., Hirn, A., Charvis, P., Sachpazi, M., Marnelis, F., 2000. Seismic structure and the active Hellenic subduction in the Ionian Islands. Tectonophysics, 329, 141-156.

Coleman, D.D., Risatti, J.B., Schoell, M., 1981. Fractionation of carbon and hydrogen isotopes by methane-oxidizing bacteria. Geochim. Cosmochim. Acta 45, 1033-1037.

D'Alessandro, W, Daskalopoulou, K., Calabrese, S., Bellomo, S., 2017. Water chemistry and abiogenic methane content of a hyperalkaline spring related to serpentinization in the Argolida ophiolite (Ermioni, Greece). Mar. Petr. Geol., doi:10.1016/j.marpetgeo.2017.01.028.

D'Alessandro, W, Kyriakopoulos, K, 2013. Preliminary gas hazard evaluation in Greece. Nat. Hazard 69, 1987-2004.

D'Alessandro, W., Bellomo, S., Brusca, L., Karakazanis, S., Kyriakopoulos, K., Liotta, M., 2011a. The impact on water quality of the high carbon dioxide contents of the groundwater in the area of Florina (N. Greece). In: Lambrakis N, Stournaras G, Katsanou K (eds) Advances in the research of aquatic environment, vol 2. Springer, Berlin, 135–143.

D'Alessandro, W., Brusca, L., Kyriakopoulos, K., Michas, G., Papadakis, G., 2008. Methana, the westernmost active volcanic system of the south Aegean arc (Greece): insight from fluids geochemistry. J. Volcanol. Geotherm. Res. 178, 818–828.

D'Alessandro, W., Brusca, L., Kyriakopoulos, K., Michas, G., Papadakis, G., 2009. Hydrogen sulphide as a natural air contaminant in volcanic/geothermal areas: the case of Sousaki, Corinthia (Greece). Environ Geol 57(8), 1723–1728.

D'Alessandro, W., Brusca, L., Martelli, M., Rizzo, A., Kyriakopoulos, K., 2010. Geochemical characterization of natural gas manifestations in Greece. In: Proceedings of 12th international congress of the geological society of Greece, Patras, May, 2010. Bull Geol Soc Greece 43/5, 2327–2337.

D'Alessandro, W., Brusca, L., Kyriakopoulos, K., Bellomo, S., Calabrese, S., 2014. A geochemical traverse along the "Sperchios Basin — Evoikos Gulf" Graben (Central Greece): origin and evolution of the emitted fluids. Mar. Petr. Geol. 55, 295-308, doi:10.1016/j.marpetgeo.2013.12.011.

Darling, W. G., 1998. Hydrothermal hydrocarbons gases: 1. Genesis and geothermometry, Appl. Geochem., 13, 815–824.

Dasgupta, R., Mallik, A., Tsuno, K., Withers, A., Hirth, G., Hirschmann, M., 2013. Carbon-dioxide-rich silicate melt in the Earth's upper mantle. Nature 493, 211–215.

Daskalopoulou, K., Calabrese, S., Grassa, F., Kyriakopoulos, K., Parello, F., Tassi, F., D'Alessandro, W., 2018. Origin of methane and light hydrocarbons in natural fluid emissions: a key study from Greece. Chem. Geol. 479: 286-301 - doi.org/10.1016/j.chemgeo.2018.01.027.

Dewey, J.F., Sengör, M.C., 1979. Aegean and surrounding regions: Complex multiplate and continuum tectonics in a convergent zone. Geol. Soc. Am. Bull,. 90 (1): 84-92.

Dimitrakopoulos, R., Muehlenbachs, K., 1987. Biodegradation of petroleum as a source of ^{13}C enriched carbon dioxide in the formation of carbonate cements. Chem. Geol. 65, 283-291.

Dixon, J.E., Stolper, E.M., 1995. An experimental study of water and carbon dioxide solubilities in mid-oceanic ride basaltic liquids. Part II: applications to degassing. J. Petrol. 36, 1633–1646.

Doglioni, C., Agostini, S., Crespi, M, Innocenti, F., Manetti, P., Riguzzi, F., Savasçin, Y. 2002. On the extension in western Anatolia and the Aegean sea. In: Rosenbaum, G. and Lister, G. S. Reconstruction of the evolution of the Alpine-Himalayan Orogen. Journal of the Virtual Explorer, 8, 161-176.

Dotsika, E., Poutoukis, D., Michelot, J. L. and Raco, B., 2009. Natural tracers for identifying the origin of the thermal fluids emerging along the Aegean volcanic arc (Greece): Evidence of arc-type magmatic water (ATMW) participation, J. Volcanol. Geotherm. Res., 179, 19–32, doi:10.1016/j.jvolgeores.2008.09.024.

Doutsos, T., Piper, D.J.W., 1990. Listric faulting, sedimentation, and morphological evolution of the Quaternary eastern Corinth rift, Greece: first stages of continental rifting. Geol. Soc. Am. Bull. 102, 812–829.I.G.M.E., 1969 Geological Map of Greece, Korinthos Sheet, scale 1: 50.000.

Doutsos, T., Koukouvelas, I.K., Xypolias, P., 2006. Geological Society, London, Special Publications, 260, 507-520, doi.org/10.1144/GSL.SP.2006.260.01.21.

Du, J., 1994. Hellium isotope evidence of mantle degassing in rift valley, Eastern China. Chin. Sci. Bull. 39 (12), 1021-1024.

Du, J., Cheng, W., Zhang, Y., Jian, c., Guan, Z., 2006. Helium and Carbon isotopic compositions of thermal springs in earthquake zone of Sichuan, Southwestern China. J. Asia Earth Sci., 26: 533-539.

Du, J., Xu, Y., Sun, M., 1998. $^{3}He/^{4}He$ and heat flow in oil gas bearing basins, China's mainland. Chinese J. Geophy., 14 (2): 239- 247.

Etiope, G., Caracausi, A., Favara, R., Italiano, F., Baciu, C., 2009. Methane emission from the mud volcanoes of Sicily (Italy), J. Geophys. Res. Lett., 29, 8, 1215.

Etiope, G., 2009. A global dataset of onshore gas and oil seeps: a new tool for hydrocarbon exploration. Oil and Gas Business, http://ogbus.ru/eng/authors/Etiope/Etiope_1.pdf (accessed 07/07/2017).

Etiope, G., 2015. Natural Gas Seepage.The Earth's Hydrocarbon Degassing. Springer International Publishing Switzerland, e- book. 7.1.5, 119 DOI:10.1007/978-3-319-14601-0.

Etiope, G., Christodoulou, D., Kordella, S., Marinaro, G., Papatheodorou, G., 2013a. Offshore and onshore seepage of thermogenic gas at Katakolo Bay (Western Greece). Chem. Geol. 339, 115–126.

Etiope, G., Ionescu, A., 2015. Low-temperature catalytic CO_2 hydrogenation with geological quantities of ruthenium: a possible abiotic CH_4 source in chromite-rich serpentinized rocks. Geofluids 15, 438-452.

Etiope, G., Papatheodorou, G., Christodoulou, D., Ferentinos, G., Sokos, E., Favali, P., 2006b. Methane and hydrogen sulfide seepage in the northwest Peloponnesus petroliferous basin (Greece): Origin and geohazard. AAPG Bull 90, 701–713.

Etiope, G., Schoell, M., 2014. Abiotic gas: atypical but not rare. Elements 10, 291-296.

Etiope, G., Sherwood Lollar, B., 2013. Abiotic methane on Earth. Rev. Geophys., 51, 276–299, doi:10.1002/rog.20011.

Etiope, G., Tsikouras, B., Kordella, S., Ifandi, E., Christodoulou, D., Papatheodorou, G., 2013b. Methane flux and origin in the Othrys ophiolite hyperalkaline springs, Greece Chem. Geol. 347, 161–174.

Fiebig, J., Chiodini, G., Caliro, S., Rizzo, A., Spandenberg, J., Hunziker, J.C., 2004. Chemical and isotopic equilibrium between CO_2 and CH_4 in fumarolic gas discharges: generation of CH_4 in arc magmatic-hydrothermal systems. Geochim. Cosmochim. Acta 68, 2321–2334.

Fiebig, J., Hofmann, S., Tassi, F., D'Alessandro, W., Vaselli, O., Woodland, A.B., 2015. Isotopic patterns of hydrothermal hydrocarbons emitted from Mediterranean volcanoes. Chem. Geol. 396, 152–163, doi: 10.1016/j.chemgeo.2014.12.030.

Fiebig, J., Tassi, F., D'Alessandro, W., Vaselli, O., Woodland, A., 2013.Carbon-bearing gas geothermometers for volcanic-hydrothermal systems. Chem. Geol. 351, 66–75.

Fiebig, J., Woodland, A., D'Alessandro, W., Puttmann, W., 2009. Excess methane in continental hydrothermal emissions is abiogenic. Geology, 37, 495–498.

Fischer, F., Tropsch, H., 1923.The preparation of synthetic oil mixtures (synthol) from carbon monoxide and hydrogen. Brennst. Chem., 4, 276–285.

Fischer, F., Tropsch, H., 1926. Über die direkte Synthese von Eerdöl-kohlenwasserstoffen bei gewöhnlichtem Druck. Berichte der Deutschen Chemischen Gesellschaft 59, 830-831.

Formolo, M., 2010.The microbial production of methane and other volatile hydrocarbons. In: Kenneth N. (ed.) Timmis handbook of hydrocarbon and lipid microbiology, Springer, New York., 113–126.

Foustoukos, D.I., Seyfried, W.E., 2004. Hydrocarbons in hydrothermal vent fluids: the role of chromium-bearing catalysts. Science 304, 1002–1004.

Francis, P., Oppenheimer, C., 2004. Volcanoes. 2nd edn. Oxford: Oxford University Press. Chapter 18.

Fytikas, M., Dalambakis, P., Karkoulias, V., Mendrinos, D., 1995. Geothermal exploration and development activities in Greece during 1990-1994. In Proc. World Geothermal Congress 1995, IGA, Rome, 119-127.

Fytikas, M., 1988. Geothermal situation in Greece. Geothermics, 17 (2/3), 549-556.

Fytikas, M., Innocenti, F., Manetti, P., Mazuoli, R., Peccerilo, A., Villari, L., 1984. Tertiary to Quaternary evolution of the volcanism in Aegean Sea. In: Dixon J.E., Robertson AHF (eds). The geological evolution of the Eastern Mediterranean, vol 17, 687-699. (Geol. Soc. London Spec. Pub.).

Fytikas. M., Kolios, N., 1979. Preliminary heat flow map of Greece. In: Cermak, V., Rybach, L. (eds.) Terrestrial heat flow in Europe. Springer-Verlag, Berlin Heidelberg New York, 197–205.

Giggenbach, W., 1992. The composition of gases in geothermal and volcanic systems as a function of tectonic setting. Water-Rock Interaction, 2: 873-878.

Giggenbach W., 1996. Chemical composition of volcanic gases. Monitoring and mitigation of volcano hazard, 221-56.

Giggenbach, W.F., 1980. Geothermal gas equilibria. Geochim. Cosmochim. Acta 44, 2021-2032.

Giggenbach, W.F., 1987. Redox processes governing the chemistry of fumarolic gas discharges from White Island, New Zealand. Appl. Geochem. 2, 143-161.

Giggenbach, W.F., Gougel, R.L., 1989. Method for the collection and analysis of geothermal and volcanic water and gas samples.NZ-DSIR Report CD 2387, 53.

Giggenbach, W.F., Sano, Y., Schmincke, H.U., 1991. CO_2-rich gases from Lakes Nyos and Monoun, Cameroon, Laacher See, Germany, Dieng, Indonesia, and Mt. Gambier, Australia-variations on common theme. J. Volcanol. Geotherm. Res., 45, 311-323.

Gilfillan, S.M.V., Ballentine, C.J., Holland, G., Blagburn, D., Sherwood Lollar, B., Stevens, S., Schoell, M., Cassidy, M., 2008. The noble gas geochemistry of natural CO_2 gas reservoirs from the Colorado Plateau and Rocky Mountain provinces, USA. Geochim. Cosmochim. Acta 72, 1174–1198.

Goguel, J., 1953. Le regime termique de l'eau souterraine. Ann. Mines 10, 1–29.

Grassa, F., Capasso, G., Oliveri, Y., Sollami, A., Carreira, P., Rosário Carvalho, M. , Marques, J.M., Nunes, J.C., 2010. Nitrogen isotopes determination in natural gas: analytical method and first results on magmatic, hydrothermal and soil gas samples. Isotop. Environ. Health Stud. 46, 141-155.

Grigoriadis, V., Tziavos, I., Tsokas, G., Stampolidis, A., 2016. Gravity data inversion for Moho depth modeling in the Hellenic area. Pure Appl. Geophys. 173, 1223–1241. DOI:10.1007/s00024-015-1174-y

Gulec, N., Hilton, D.R., Mutlu, H., 2002. Helium isotope variations in Turkey: relationship to tectonics, volcanism and recent seismic activities. Chem. Geol., 187, 129-142.

Gulec, N.H., Hilton, D.R., 2006. Helium and heat distribution in western Anatolia, Turkey: Relationship to active extension and volcanism. In: Dilek, Y., Pavlides, S., (Eds). Postcollisional Tectonics and Magmatism in the Mediterranean Region and Asia. In: Geological Society of America Special Papers, Vol. 409, 305–319.

Gunter, B.D., 1978. C1-C4 hydrocarbons in geothermal gases. Geochim. Cosmochim. Acta, 42, 137-139.

Hatziyannis, G., 2011. The geothermal energy of Epirus: fields and and perspectives exploitation. EGEWorkshop"The geological research as a lever of development of Epirus" July, 2011, Ioannina, Greece.

Hinrichs, K.U., Hayes, J.M., Bach, W., Spivack, A.J., Hmelo, L.R., Holm, N.G, Johnson, C.G., Sylva, S.P., 2006. Biological formation of ethane and propane in the deep marine subsurface. Proc. Natl. Acad. Sci. 103(40): 14684-9. DOI: 10.1073/pnas.0606535103

Hoefs, J., 2003. Isotope Geochemistry. 4th, Completely Revised, Updated, and Enlarged Edition with 73 Figures and 22 Tables, Springer

Hoefs, J., 2009. Stable Isotope Geochemistry. Springer, Berlin-Heidelberg, 285.

Holloway, J.R., 1984. Graphite-CH4-H2O-CO2 equilibria at metamorphic conditions, Geology, 12, 455-458.

Holloway, M., 2000. The Killing Lakes: Scientific American, 283, 92-99.

Holocher, J.,Peeters, F.,Aeschbach-Hertig, W., Hofer, M.,Brennwald, M.,Kinzelbach, W., Kipfer, R., 2002. Experimental investigations on the formation of excess air in quasi-saturated porous media Geochim. Cosmochim. Acta, 66, 4103-4117.

Horita, J., 2001. Carbon isotope exchange in the system CO_2-CH_4 at elevated temperatures. Geochim. Cosmochim. Acta 65, 1907-1919.

Horita, J., Berndt, M.E., 1999. Abiogenic formation and isotopic fractionation under hydrothermal conditions. Science 285, 1055–1057.

Hornibrook, E.R.C., Longstaffe, F.J., Fyfe, W.S., 1997. Spatial distribution of microbial methane production pathways in temperate zone wetland soils: Stable carbon and hydrogen isotope evidence, Geochim. Cosmochim. Acta, 61(4), 745 – 753.

Jackson, J. and McKenzie, D., 1988. Rates of active deformation in the Aegean Sea and surrounding regions. Basin Res., 1, 121-128

Jackson, J., Haines, J. & Holt, W., 1994. A comparison of satellite laser ranging and seismicity data in the Aegean region. Geophys. J. Int., (21-25), 2849-2852.

Javoy, M. and Pineau, F., 1991. The volatiles record of a 'popping' rock from the Mid-Atlantic Ridge at 14 °N: chemical and isotopic composition of gas trapped in the vesicles. Earth Planet. Sci. Lett. 107, 598–611.

Jenden, P.D., Hilton, D.R., Kaplan, I.R., Craig, H., 1993. Abiogenic hydrocarbons and mantle helium in oil and gas fields. In: Howell, D.G. (Ed.), The Future of Energy Gases: US Geol. Surv. Profes.Paper, 1570, 31-56.

Kamberis, E., Rigakis, N., Tsaila-Monopolis, S., Ioakim, C., Sotiropoulos, S., 2000. Shallow biogenic gas-accumulations in late Cenozoic sands of Katakolon Peninsula, western Greece. Geol. Soc. Greece, Spec. Publ. 9, 121–138.

Kanellopoulos, C., 2012. Distribution, lithotypes and mineralogical study of newly formed thermogenic travertines in Northern Euboea and Eastern Central Greece. Cent. Eur. J. Geosci. 4(4), 545-560 DOI: 10.2478/s13533-012-0105-z.

Kanellopoulos, C., Mitropoulos, P., Valsami-Jones, E., Voudouris, P., 2017. A new terrestrial active mineralizing hydrothermal system associated with ore-bearing travertines in Greece (northern Euboea Island and Sperchios area). J. Geochem. Explor.179, 9-24.

Karagianni, E.E., Papazachos, C.B., 2007. Shear velocity structure in the Aegean region obtained by joint inversion of Rayleigh and Love waves, in: Taymaz, T.,Yilmaz, Y., Dilek, Y. (Eds.), The Geodynamics of the Aegean and Anatolia. Special Publ. Geol. Soc. 291, London, 159–181.

Karagianni, E.E.,Papazachos, C.B.,Panagiotopoulos, D.G.,Suhadolc, P.,Vuan, A.,Panza, G.F., 2005. Shear velocity structure in the Aegean area obtained byinversion of Rayleigh waves, Geophys. J. Int. 160, 127–143. http://dx.doi.org/10.1111/j.1365-246X.2005.02354.x.

Katsikatsos, G., Kounis, G., Fytikas, M., Mettos, A., Vidakis, M., 1980. Geological map of Greece in 1: 50,000: Limni sheet. Institute of Geological and Mineral Exploration, Athens.

Kennedy, B.M., Kharaka, Y.K., Evans, W.C., Ellwood, A., De Paolo, D.J., Thordsen, J.J., Ambats, G., Mariner, R.H., 1997. Mantle fluids in the San Andreas fault system, California Science, 278, 1278-1281.

Kietäväinen, R., Purmako, L., 2015. The origin, source, and cycling of methane in deep crystalline rock biosphere. Frontiers Microbiol. 6, 725.

Kinnaman, F.S., Valentine, D.L., Tyler, S.C., 2007. Carbon and hydrogen isotope fractionation associated with the aerobic microbial oxidation of methane, ethane, propane and butane. Geochim. Cosmochim. Acta 71, 271–283.

Kipfer, R., Aeschbach-Hertig, W., Peeters, F., Stute, M., 2002. Noble gases in lakes and ground waters. Rev. Mineral. Geochem. 47, 615-700.

Kiyosu, Y., Imaizumi, S., 1996. Carbon and hydrogen isotope fractionation during oxidation of methane by metal oxides at temperatures from 400° to 530 °C. Chem. Geol. 133, 279–287.

Klusman, R.W., Jakel, M.E., 1998. Natural microseepage of methane to the atmosphere from the Denver-Julesburg basin, Colorado, USA, J. Geophys. Res., 103D, 28,042 – 28,045.

Koçyiğit, A., Rojay, B., Cihan, M., Özacar, A., 2001. The June 6, 2000 Orta (Çankırı, Turkey) earthquake: sourced from a new antithetic sinistral strike-slip structure of the North Anatolian Fault system, the Dodurga Fault Zone. Turk. J. Earth Sci. 10, 69–82.

Konn, C., Charlou, J.L., Holm, N. G., Mousis O., 2015. The Production of Methane, Hydrogen, and Organic Compounds in Ultramafic- Hosted Hydrothermal Vents of the Mid-Atlantic Ridge. Astrobiology, 15 (5), 381- 399.

Kvenvolden, K.A., 1993. Gas hydrates—Geological perspective and global change, Rev. Geophys.31, 173 – 187.

Le Guern, F., Tazieff, H., Faivre Pierret, R., 1982. An example of health hazard: People killed by gas during a phreatic eruption: Dieng plateau (Java, Indonesia), February 20th 1979. Bulletin of Volcanology 45(2), 153-156.

Le Pichon, X., Chamot-Rooke, N., Huchon, P., Luxey, P., 1993. Implications des nouvelles mesures de gèodèsie spatiale en Grèce et en Turquie sur l'extrusion latèrale de l'Anatolie et de l'Egèe. C.R. Acad. Sci. Ser. II 316, 983– 90.

Le Pichon, X. and Angelier, J., 1979. The Hellenic Arc and Trench system: A key to the neotectonic evolution of the Eastern Mediterranean area. Tectonophys., 60: 1-42.

Le Pichon, X., Sengor, A. M. C., Demirbag, E., Rangin, C., Imren, C., Armijo, R., Gorur, N., Cagatay, N., Mercier de Lépinay, M., Meyer, B., Saatcilar, B., and Tok, B., 2001. The active Main Marmara fault, Earth Planet. Sci. Lett., 192, 595–616.

Lee H., Yang T.F., Lan T.F., Song S., Tsao S., 2005.Fumarolic gas composition of the Tatun Volcano Group, northern Taiwan. Terr Atmos Ocean Sci.,16(4):843-864.

Luft, U.C., Finkelstein, S., Elliot, J.C. (1974). Respiratory gas exchange, acid-base balance, and electrolytes during and after maximal work breathing 15 mm Hg $PICO_2$. In: Carbon Dioxide and Metabolic Regulations. G. Nahas and K.E. Schaefer (Eds.). Springer-Verlag, New York, NY, 273-281.

Lupton, J.E., 1983. Terrestrial inert gases: isotope tracer studies and clues to primordial components in the mantle. Annu. Rev. Earth Planet. Sci. 11, 371–414.

Machel, H.G., Krouse, H.R., Sassen, R., 1995. Products and distinguishing criteria of bacterial and thermochemical sulphate reduction.Applied Geochemistry 10,373-389.

Mamyrin, B.A., Tolstikhin, I.N., 1984. Fluid Geochemistry of Ambon Island (Indonesia). Geothermics 28 (2, 1): 189-204.

Mango, F. D., 2000.The origin of light hydrocarbons, Geochim.Cosmochim. Acta, 64, 1265–1277.

Mantovani E., Viti M., Cenni N., Albarello D. and Babbucci D., 2001a: Short and long term deformation patterns in the Aegean-Anatolian systems: insights from space geodetic data (GPS). Geophys. Res. Lett., 28, 2325-2328.

Marini, L. and Fiebig, J., 2005. Fluid geochemistry of the magmatic-hydrothermal system of Nisyros (Greece). In: The geology, geochemistry and evolution of Nisyros volcano (Greece). Implications for the volcanic hazards (Hunziker, J.C. and Marini, L. eds.), Memoires de Geologie, 44, 121-163.

Martelli, M., Nuccio, P.M., Stuart, F.M., Di Liberto, V., Ellam, R.M., 2008. Constraints on mantle source and interactions from He-Sr isotope variation in Italian Plio-Quaternary volcanism. G^3, Volume 9, 2.

Marty B, Zimmermann L., 1999. Volatiles (He, C, N, Ar) in mid-ocean ridge basalts:Assessment of shallow-level fractionation and characterization of sourcecomposition. GeochimCosmochimActa 63:3619-3633.

Marty, B., Jambon, A., 1987. $C/^3He$ in volatile fluxes from the solid Earth:Implications for carbon geodynamics. Earth and Planetary Science Letters 83, 16-26.

Marty, B., O'Nions, R.K., Oxburgh, E.R., Martel, D., Lombardi, S., 1992. Helium isotopes in Alpine regions Tectonophysics, 206, 71-78.

McClusky, S., Balassanian, S., Barka, A., Demir, C., Ergintav, S., Georgiev, I., Gurkan, O., Hamburger, M., Hurst, K., Kahle, H., Kastens, K., Kekelidze, G., King, R., Kotzev, V., Lenk, O., Mahmoud, S., Mishin, A., Nadariya, M., Ouzounis, A., Paradissis, D., Peter,, Y., Prilepin,, M., Reilinger, R., Sanli, I., Seeger, H., Tealeb, A., Toksöz, M. N., Veis, G., 2000. Global Positioning System constraints on plate kinematics and dynamics in the eastern Mediterranean and Caucasus. Papers on Geodesy and Gravity Tectonophysics, Volume 105, Issue B3, Pages 5695–5719. DOI: 10.1029/1999JB900351McKenzie, D. (1978). Active tectonics of the

Alpine Himalayan belt: the Aegean Sea and surrounding regions. Geophys. J. R. Astr. Soc., 55: 217-254.

McCollom, T.M., 2013. Laboratory simulations of abiotic hydrocarbon formation in Earth's deep subsurface. Rev. Mineral. Geochem. 75, 467-494.

McCollom, T.M., Seewald, J.S., 2007. Abiotic synthesis of organic compounds in deep- sea hydrothermal environments. Chem. Rev. 107, 382-401.

McKenzie, D., Jackson, J., 1983. The relationship between strain rates, crustal thickening, palaeomagnetism, finite strain and fault moments within a deforming zone. Earth Planet. Sci. Lett. 65:182–202.

McNeill, L.C., Collier, R.E.L., 2004. Uplift and slip rates of the eastern Eliki fault segment, Gulf of Corinth, Greece, inferred from Holocene and Pleistocene terraces. Journal of the Geological Society 161 (1), 81–92.

Milkov, A.V., 2000. Worldwide distribution of submarine mud volcanoes and associated gas hydrates, Mar. Geol. 167, 29 – 42.

Miller, H.M., Mayhew, L.E., Ellison, E.T., Kelemen, P., Kubo, M., Templeton, A.S., 2017. Low temperature hydrogen production during experimental hydration of partially-serpentinized dunite. Geochim. Cosmochim. Acta 209, 161–183.

Miller, S.A., Ben- Zion, Y., Burg, J-P., 1999. A three dimensional fluid controlled earthquake model: behavior and implications. J. Geophy. Res. 104 (B5): 10621- 10638.

Miller, S.A., Collettini, C., Chiaraluce, L., Cocco, M., Barchi, M., Kaus, B.J.P., 2004. Aftershocks driven by a high-pressure CO_2 source at depth. Nature, 427, 724-727.

Minissale, A., 2004.Origin, transport and discharge of CO_2 in central Italy.Earth-Science Reviews 66,89-141.

Minissale, A., Duchi, V., Kolios, N., Nocenti, M., Verrucchi, C., 1997. Chemical patterns of thermal aquifers in the volcanic islands of the Aegean arc, Greece. Geothermics, 26, 501-518.

Minissale, A., Duchi, V., Kolios, N., Totaro, G., 1989. Geochemical characteristics of Greek thermal springs. Journal of Volcanology and Geothermal Research 39, 1-16.

Morgan, P., Blackwell, D.D., Spafford, R.E., Smith, R.B., 1977. Heat flow measurements in Yellowstone Lake and the thermal structure of the Yellowstone Caldera. Journal of Geophysical Research, Solid Earth and Planets, 82, 3719–3732.

Mörner, N.A., Etiope, G., 2002. Carbon degassing from the lithosphere, Global. Planet. Change, 33, 185–203.

Mountrakis, D.M., 1985. Geologia tis Elladas.University Studio Press, Thessaloniki, 207, in Greek.

Mountrakis, D.M., 1986. The Pelagonian Zone in Greece: A Polyphase-Deformed Fragment of the Cimmerian Continent and Its Role in the Geotectonic Evolution of the Eastem Mediterranean. J. Geoph. 94, 335-347.

Mountrakis, D.M., 2010. Geologia kai geotektoniki exelixi tis Elladas.University Studio Press, Thessaloniki, 374, in Greek.

Murrell, C.J., Jetten, M.S.M., 2009. The microbial methane cycle. Environ. Microbiol. Rep. 1, 279–284.

Mutlu, H., Guelec, N., Hilton, D.R., 2008. Helium–carbon relationships in geothermal fluids of western Anatolia, Turkey. Chem. Geol., 247, 305-321.

Nahas, G., Poyart, C., Triner, L., 1968. Acid base equilibrium changes and metabolic alterations. Annals of the New York Academy of Science. 150, 562-576.

O'Nions, R.K., Oxburgh, E.R., 1988. Helium volatile fluxes and the development of continental crust Earth Planet. Sci. Lett., 90, 331-347.

Oppenheimer, C., Fischer, T.P., Scaillet, B., 2014. Volcanic degassing: process and impact. Holland, H.D. et al. (Eds.), Elsevier, Pergamon, Oxford, 111-179.

Özeren, M.S., 2002. Crustal structure and forces in continental deformation. PhD thesis. Univ. Cambridge, Fitzwilliam Coll., 255.

Ozima, M. &Podosek, F. A., 1983. Noble Gas Geochemistry, Cambridge University Press.

Palacas, J.G., Monopolis, D., Nicolaou, C.A., Anders, D.E., 1986.Geochemical correlation of surface and subsurface oils, western Greece. Org. Geochem. 10, 417-423.

Pallasser, R.J., 2000.Recognising biodegradation in gas/oil accumulations through the δ^{13}compositions of gas components. Org. Geochem.31, 1363-1373.

Paonita, A., Caracausi, A., Iacono-Marziano, G., Martelli, M., Rizzo, A., 2012.Geochemical evidence for mixing between fluids exsolved at different depths in the magmatic system of Mt Etna (Italy). Geochim. Cosmochim. Acta 84, 380–394.

Papadakis, G., Vallianatos, F., Sammonds, P., 2016. Non-extensive statistical physics applied to heat flow and theearthquake frequency–magnitude distribution in Greece. Physica A 456, 135–144.

Papadopoulos, G.A., 1991. Seismicity and related phenomena in the Hellenic Arc: their influence on the Eastern Mediterranean region. In: M.J. Salem, A.M. Sbeta, and M.R. Bakbak (eds.), The Geology of Libya, vol. 4, Elsevier, Amsterdam, 2441-2449.

Pearce, J.M., 2004. Natural analogues for the geological storage of CO_2. Final report of the Nascent project. British Geological Survey Technical Report, 122.

Pe-Piper, G., Piper, D.J.W., 2002. The igneous rocks of Greece, The anatomy of an orogen. Beiträge zur regionalen Geologie der Erde, Band 30, Gebrüder Bornträger, Berlin - Stuttgart.

Pe-Piper, G., Piper, D.J.W., 2006. Unique features of the Cenozoic igneous rocks of Greece. Geological Society of America, Special Paper 409, 259- 282.

Pik, R., Marty, B., 2009. Helium isotopic signature of modern and fossil fluids associated with the Corinth rift fault zone (Greece): Implication for fault connectivity in the lower crust, Chem. Geol., 266, 67-75.

Plank, T., Langmuir, C.H., 1993. Tracing trace elements from sediment input to volcanic output at subduction zones. Nature, 362: 739-743.

Polyak, B.G., Tolstikhin, I.N., 1985. Isotopic composition of the Earth's helium and the problem of tectogenesis. Chem. Geol., 52, 9-33.

Poulimenos G., 1993. Tectonics and sedimentation in the Western Corinth graben, N. Jb. Geol. Paleontol. Mh., H10: 607-630.

Poulimenos G., Alberts G., Doutsos T., 1989. Neotectonic evolution of the central section of the Corinth graben. Z. Dtsch. Geol. Ges. 140, 173–182.

Poyart, C.F. and Nahas, G., 1968. Inhibition of activated lipolysis by acidosis. Molecular Pharmacol. 4, pp. 389-401.

Prinzhofer, A.A., Battani, A., 2003. Gas isotopes tracing: an important tool for hydrocarbon exploration. Oil and Gas Sci. Technol. 58, 229-311.

Proskurowski, G., Lilley, M., Seewald, J.S., Fruh-Green, G.I., Olson, E.J., Sylva, S.P., Kelley, D.S., 2008. Abiogenic hydrocarbon production at Lost City hydrothermal field.Science 319, 604-607.

Proskurowski, G., Lilley, M.D., Kelley, D.S., Olson, E.J., 2006. Low temperature volatile production at the Lost City hydrothermal field, evidence from a hydrogen stable isotope geothermometer. Chem. Geol. 229, 331-343.

Quingley, T.M., MacKenzie, A.S., 1988. The temperatures of oil and gas formation in the sub-surface.Nature 333, 549–552.

Reid, R.C., Prausnitz, J.M., Poling, B.E., 1987. The Properties of Gases & Liquids, 4 ed. Boston: McGraw-Hill.

Reischmann, T., Kostopoulos, D., 2007.Terrane accretion in the internal Hellenides.Geophys. Res. Abstracts 9, 05337.

Ricard, Y., Doglioni, C., and Sabadini, R. 1991. Differential rotation between lithosphere and mantle: a consequence of lateral mantle viscosity variations. Journal of Geophysical Reserach, 96, B5, 8407-8415.

Rigakis, N., Roussos, N., Kamberis, E., Proedrou, P., 2001. Hydrocarbon gas accumulations in Greece and their origin. Bull. Geol. Soc. Greece 34/3, 1265-1273.

Rikitake, T., 1982. Earthquake forecasting and Warning. Tokyo: Center for Academic Publications.

Rizzo, A.L., Barberi, F., Carapezza, M.L., Di Piazza, A., Francalanci, L., Sortino, F., D'Alessandro, W., 2015, New mafic magma refilling a quiescent volcano: Evidence from He-Ne-Ar isotopes during the 2011–2012 unrest at Santorini, Greece, Geochem. Geophys. Geosyst., 16, doi:10.1002/2014GC005653.

Rizzo, A.L., Caracausi, A., Chavagnac, V., Nomikou, P., Polymenakou, P.N., Mandralakis, M., Kotoulas, G., Magoulas, A., Castillo, A., Lampridou, D., 2016. Kolumbo submarine volcano (Greece): An active window into the Aegean subduction system. Scientific Reports 6:28013. doi: 10.1038/srep28013

Roppolo L., 2012. Equivalenti naturali dei siti di stoccaggio geolologico della CO_2: il caso di Florina (Grecia), unpublished degree thesis, University of Palermo.

Saal, A.E., Hauri, E.H., Langmuir, C.H., Perfit, M. R., 2002. Vapor undersaturation in primitive mid-ocean-ridge basalts and the volatile content of Earth′s upper mantle. Nature 419, 451–455.

Sachpazi, M.,Galve, A.,Laigle, M.,Hirn, A.,Sokos, E.,Serpetsidaki, A.,Marthelot, J.-M., Pi Alperin, J.M.,Zelt, B., Taylor, B., 2007. Moho topography under centralGreece and its

compensation by Pn time-terms for the accurate location of hypocenters: The example of the Gulf of Corinth 1995 Aigion earthquake, Tectonophysics 440 (2007) 53–65. http://dx.doi.org/10.1016/j.tecto.2007.01.009.

Sano, Y., Marty, B., 1995. Origin of carbon in fumarolic gas from island arcs. Chemical Geology 119,265-274.

Sano, Y., Wakita, H., 1985. Geographical distribution of $^{3}He/^{4}He$ ratios in Japan: Implications for arc tectonics and incipient magmatism. Journal of Geophysical Research 90: 8729–8741. doi: 10.1029/JB080i010p08729. issn: 0148-0227.

Sano, Y., Williams, S.N., 1996. Fluxes of mantle and subducted carbon along convergent plate boundaries. Geophysical Research Letters, 23: 2749–2752.

Şaroğlu, F., 1985. Dogu Anadolu'nun Neotektonik Donemde Jeolojik ve Yapısal Evrimi. PhD thesis. Istanbul Univ., Fen Bilim. Enst., Istanbul. 240.

Schaefer, K.E., 1982. Effects of increased ambient CO_2 levels on human and animal health. Experientia 38, pp. 1163-1168.

Schoell, M., 1980.The hydrogen and carbon isotopic composition of methane from natural gases of various origins. Geochim. Cosmochim. Acta 44, 649-661.

Schoell, M., 1988.Multiple origins of methane in the Earth. Chem. Geol. 71, 1–10.

Seewald, J.S., 2001. Aqueous geochemistry of low molecular weight hydrocarbons at elevated temperatures and pressures. Constraints from mineral buffered laboratory experiments. Geochim. Cosmochim. Acta 65,1641-1664.

Şengör, A.M.C., 1979a. The North Anatolian Transform Fault: its age, offset and tectonic significance. J. Geol. Soc. London 136, 269–82.

Şengör, A.M.C., Özeren, S., Genç, T., Zor, E., 2003. East Anatolian high plateau as a mantle-supported, north-south shortened domal structure. Geophys. Res. Lett. 30, 8045.

Sharp, C.E., Smirnova, A.V., Graham, J.M., Stott, M.B., Khadka, R., Moore, T.R., Grasby, S.E., Strack, M., Dunfield, P.F., 2014. Distribution and diversity of Verruco microbia methanotrophs in geothermal and acidic environments. Environ. Microbiol. 16, 1867-1878.

Sherwood Lollar, B., Ballentine, C.J., O'Nions, R.K., 1997. The fate of mantle derived carbon in a continental sedimentary basin: Integration of C/He relationshipsand stable isotope signatures. Geochimica et Cosmochimica Acta 61, 2295-2308.

Sherwood Lollar, B., Lacrampe-Couloume, G., Slater, G.F., Ward, J.A., Moser, D.P., Gihring, T.M., Lin, L.H., Onstott, T.C., 2006. Unravelling abiogenic and biogenic sources of methane in the Earth's deep subsurface. Chem. Geol. 226, 328-339.

Sherwood Lollar, B., O'Nions, R.K., Ballentine, C.J., 1994. Helium and neon isotope systematics in carbon dioxide-rich and hydrocarbon-rich gas reservoirs. Geochimica et Cosmochimica Acta 58, 5279.

Shimizu, A., Sumino, H., Nagao, K., Notsu, K., Mitropoulos, P., 2005. Variation in noble gas isotopic composition of gas samples from the Aegean arc, Greece. Journal of Volcanology and Geothermal Research 140, 321–339.

Snyder, G., Poreda, R.J., Fehn, U. and Hunt, A., 2003. Sources of nitrogen and methane in Central American geothermal settings: Noble gas and ^{129}I evidence for crustal and magmatic volatile components, Geochem. Geophys. Geosyst., 4, doi: 10.1029/2002GC000363.

Snyder, G., Poreda, R.J., Hunt, A., Fehn, U., 2001. Regional variations in volatile composition: Isotopic evidence for carbonate recycling in the Central American volcanic arc, Geochem. Geophys. Geosyst., 2, doi: 10.1029/2001GC 000163.

Stampolidis, A.,Tsokas, G.N., 2002. Curie point depths of Macedonia and Thrace, N. Greece, Pure Appl. Geophys. 159, 2659–2671.

Stefánsson, A., Lemke. K.H., Bènèzeth, P., Schott, J., 2017. Magnesium bicarbonate and carbonate interactions in aqueous solutions: An infrared spectroscopic and quantum chemical study. Geochim. Cosmochim.Acta 198, 271–284.

Stefánsson, A., Sveinbjörnsdòttir, A.E., Heinemeier, J., Arnòrsson, S., Kjartansdòttir, R., Kristmannsdòttir, H., 2016. Mantle CO_2 degassing through the Icelandic crust: Evidence from carbon isotopes in groundwater. Geochim. Cosmochim. Acta 191, 300–319.

Stephens, J.C., Hering, J.G., 2002. Comparative characterization of volcanic ash soils exposed to decade-long elevated carbon dioxide concentrations at Mammoth Mountain, California Chemical Geology, 186, 301-313.

Stolper, D.A., Lawson, M., Davis, C.L., Ferreira, A.A., Santos Neto, E.V., Ellis, G.S., Lewan, M.D., Martini, A.M., Tang, Y., Schoell, M., Sessions, A.L., Eiler, J.M., 2014. Gas formation. Formation temperatures of thermogenic and biogenic methane.Science, 344, 1500-1503.

Takai, K., Nakamura, K., Toki, T., Tsunogai, U., Miyazaki, M., Miyazaki, J., Hirayama, H., Nakagawa, S., Nunoura, T., Horikoshi, K., 2008. Cell proliferation at 122°C and isotopically

heavy CH_4 production by a hyperthermophilic methanogen under high pressure cultivation. Proc. Nation. Acad. Sci. 105, 10949–10954.

Taran, Y., Giggenbach, W., 2003. Geochemistry of Light Hydrocarbons in Subduction-Related Volcanic and Hydrothermal Fluids.Society of Economic Geologists Special Publication 10, Ch. 6, 61–74.

Tassi, F., Vaselli, O., Papazachos, C.B., Giannini, L., Chiodini, G., Vougioukalakis, G.E., Karagianni, E. Vamvakaris, V., Panagiotopoulos, D., 2013. Geochemical and isotopic changes in the fumarolic and submerged gas discharges during the 2011–2012 unrest at Santorini caldera (Greece), Bull. Volcanol., 75, 1–15, doi:10.1007/s00445-013-0711-8.

Taymaz T, Jackson J, McKenzie D. 1991. Active tectonics of the north and central Aegean Sea. Geophys. J. Int. 106:433–90.

Taymaz, T., Yilmaz, Y., Dilek, Y., 2007. The geodynamics of the Aegean and Anatolia: Introduction. Geological Society, London, Special Publications, 291, 1–16. doi:10.1144/SP291.1

Thomas, R.P., 1986. Heat flow mapping at the Geysers Geothermal Field, Publication No. TR37, Master thesis.

Tilley, B., Muehlenbachs, K., 2013. Isotope reversals and universal stages and trends of gas maturation in sealed, self-contained petroleum systems.Chem. Geol., 339 (2013), 194-204.

Tranos, M.D., Kachev, V.N., Mountrakis, D.M., 2008. Transtensional origin of the NE-SW Simitli basin along the Strouma (Strymon) Lineament, SW Bulgaria. J. Geol. Soc. Lond., 165, 499-510.

Trull, T., Nadeau, S., Pineau, F., Polve, M., Javoy, M., 1993. C-He systematics inhotspot xenoliths: Implications for mantle carbon contents and carbon recycling. Earth and Planetary Science Letters 118, 43.

Tsokas, G.N., Hansen, R.O., 1997. Study of the crustal thickness and the subducting lithosphere in Greece from gravity data. J. Geophys. Res., 102 (B9), 585–597. doi:10.1029/97JB00730.

Tsokas, G.N., Hansen, R.O.,Fytikas, M., 1998. Curie point depth of the island of Crete (Greece), Pure Appl. Geophys. 152. 747–757.

Turino, G.M., Goldring, R.M., Heinemann, H.O., 1974. The extracellular bicarbonate concentration and the regulation of ventilation in chronic hypercapnia in man. In:Carbon

Dioxide and Metabolic Regulations. G. Nahas and K.E. Schaefer (Eds.). Springer-Verlag, New York, NY, 273 -281.

Umeda, K., Ninomiya, A., McCrank, G.F., 2008. High ^{3}He emanations from the source regions of recent large earthquakes, central Japan. Geochem. Geophys. Geosyst., 9.

Van Ypersele de Strihou, C., 1974. Acid-base equilibrium in chronic hypercapnia. In: Carbon Dioxide and Metabolic Regulations. G. Nahas and K.E. Schaefer (Eds.). Springer-Verlag, New York, NY, 266.

Varekamp, J.C., Kreulen, R., Poorter, R.P.E., Van Bergen, M.J., 1992. Carbon sources in arc volcanism, with implications for the carbon cycle. Terra Nova, 4: 363-373.

Vougioukalakis, G., Eleftheriadis, G., Christofides, G., Pavlides, S., Fytikas, M., and Villa, I., 2004, Volcanological study of the Almopias Pliocene volcanic formations (N Greece): Proceedings of the 5th International Symposium on Eastern Mediterranean Geology 3, 1318–1321.

Wang, D.T., Gruen, D.S., Lollar, B.S., Hinrichs, K.U., Stewart, L.C., Holden, J.F., Hristov, A.N., Pohlman, J.W., Morrill, P.L., Könneke, M., Delwiche, K.B., Reeves, E.P., Sutcliffe, C.N., Ritter, D.J., Seewald, J.S., McIntosh, J.C., Hemond, H.F., Kubo, M.D., Cardace, D., Hoehler, T.M., Ono, S., 2015. Methane cycling. Nonequilibrium clumped isotope signals in microbial methane. Science, 348(6233), 428-431.

Wang, S., Jaffe, P.R., 2004. Dissolution of a mineral phase in potable aquifers due to CO_2 releases from deep formations. Effect of dissolution kinetics Energy Conversion and Management, 45, 2833-2848.

Welhan, J.A., 1988. Origins of methane in hydrothermal systems. Chem. Geol. 71, 183-198.

Welhan, J.A., Craig, H., 1983. Methane, hydrogen and helium in hydrothermal fluids of 21 °N on the East Pacific Rise. In: P.A. Rona, P.A., K. Boström, K., L. Laubier, L., and K.L. Smith, Jr, K.L.. (Editors.), Hydrothermal Processes at Seafloor Spreading Centers. Plenum, New York, N.Y., 391-409.

Whiticar, M.J., 1999. Carbon and hydrogen isotope systematics of bacterial formation and oxidation of methane. Chem. Geol. 161, 291 -314.

Whiticar, M.J., 1999. Stable isotope geochemistry of coals, humic kerogen and related natural gases. Int. J. Coal Geol. 32, 191-215.

Whiticar, M.J., Faber, E., Schoell, M., 1986. Biogenic methane formation in marine and freshwater environments: CO_2 reduction vs. acetate fermentation - isotopic evidence. Geochim. Cosmochim. Acta, 50, 693-709.

Whiticar, M.J., Suess, E., 1990. Hydrothermal hydrocarbon gases in the sediments of the King-George Basin, Bransfield Strait, Antarctica. Appl. Geochem.5, 135-147.

WHO, (2003). Hydrogen sulphide: human health aspects. Concise International Chemical Assessment Document 53. World Health Organization, Geneva, p 26.

Winkel, L.H.E., Casentini, B., Bardelli, F., Voegelin, A., Nikolaidis, N.P., Charlet, L., 2013. Speciation of arsenic in Greek travertine: Co-precipitation of arsenate with calcite. Geochimica et Geologica Acta 106, 99-110.

Witham, C S, 2005. Volcanic disasters and incidents: a new database. Journal of Volcanology and Geothermal Research 148, 191–233

Worden, R.H., Smalley, P.C., 1996. H_2S-producing reactions in deep carbonate gas reservoirs: Khuff Formation, Abu Dhabi. Chem. Geol. 133,157-171.

Wüthrich, E.D., 2009. Low temperature thermochronology of the northern Aegean Rhodope Massif. Doctor of Sciences Thesis, Swiss Federal Institute of Technology Zurich, Switcherland.

Xu, Y., Sheng, P., Liu, W., Tao, M., Sun, M., Du, J., 1998. Geochemistry of Noble Gases in Natural Gases. Beijing: Science Press.

Yılmaz Y., Genç, Ş.C, Gürer F, Bozcu M, Yılmaz, K, et al. 2002. When did the western Anatolian grabens begin to develop? In Tectonics and Magmatism in Turkey and Surrounding Area, ed. E Bozkurt, JA Winchester, J.D.A., Piper, 353–84. Geol. Soc. London, Spec. Publ. No. 173

Yolsal, S., Taymaz, T., Yalciner, A.C., 2009. Earthquake source parameters along the Hellenic-Cyprus arcs and simulations of historical tsunamis in the eastern Mediterranean. Tectonophysics.

Zagorcev, I., 1992a. Neotectonic development of the Struma (Kraistid) Lineament, southwest Bulgaria and northern Greece. Geol. Mag., 129, 197-222.

Zagorcev, I., 1992b. Neotectonics of the central parts of the Balkan Peninsula: basic features and concepts. Geol. Rundsch., 81, 635-654

Zelilidis A., Kontopoulos N., 1996. Significance of fan deltas without toe-sets within rift and piggy-back basins: examples from the Corinth graben and the Mesohellenic trough, Central Greece. Sedimentology 43, 253–262.

I.G.M.E., 1970 Geological Map of Greece, Nemeas Sheet, scale 1: 50.000,

I.G.M.E., 1973. Geological Map of Greece, Dervenion Sheet, scale 1: 50.000.

I.G.M.E., 1975 Geological Map of Greece, Kadhila Sheet, scale 1: 50.000.

Appendix

Table 1: Coordinates of the gases (general database)

ID	Sample	Date		Sector	Coordinates		Type of emission
					E	N	
1	Biros	27/9/10	EH	34S	486258	4364745	bubbling gas
2	Preveza	28/8/10	EH	34S	478818	4311376	dissolved gas
3	Nelles	23/6/11	EH	34S	471767	4425929	dissolved gas
4	Katakolo sea	28/5/07	EH	34S	528219	4166444	bubbling gas
5	Katakolo sea		EH	Etiope et al., 2007			
6	Katakolo port		EH	Etiope et al., 2008			
7	Katakolo volcano 1	28/5/07	EH	34S	527702	4166241	soil gas
8	Katakolo volcano 3	28/5/07	EH	34S	527702	4166241	soil gas
9	Katalolo WKA-1A		EH	Rigakis et al 2001			
10	Killini		EH	Etiope et al., 2006			
11	Loutra Killinis	28/5/07	EH	34S	510332	4190219	bubbling gas
12	Loutra Killinis	22/5/10	EH	34S	510332	4190219	bubbling gas
13	Trapeza	23/5/10	EH	34S	608149	4224957	dissolved gas
14	LYS	7/9/13	EH	34S	600613	4315572	dissolved gas
15	PPG-1	23/8/15	EH	34S	560778	4227579	bubbling gas
16	Patra	1/10/14	EH	34S	560839	4227475	bubbling gas
17	Selianitika	18/11/10	EH	34S	589714	4238025	dissolved gas
18	Nerazies	23/5/10	EH	34S	589262	4235877	dissolved gas
19	LP11 Chanopoulo	31/5/10	EH	34S	495013	4338544	dissolved gas
20	LP5 Petra	30/5/10	EH	34S	484632	4333841	dissolved gas
21	KRE	7/9/13	EH	34S	540945	4302734	dissolved gas
22	Kabasilos	2/6/08	EH	34T	475087	4439548	dissolved gas
23	Amarantos	2/6/08	EH	34T	477160	4447217	fumarole
24	Kaiafas		EH	Etiope et al., 2009			
25	Kaiafas	22/5/10	EH	34S	553247	4152690	dissolved gas

ID	Sample	Date		Sector	Coordinates		Type of emission
					E	N	
26	Amplas	7/2/05	IH	34S	591217	4308687	bubbling gas
27	Amplas	28/3/08	IH	34S	591217	4308687	bubbling gas
28	Amplas	12/10/08	IH	34S	591217	4308687	bubbling gas
29	Amplas 2	10/5/17	IH	34S	590949	4308949	bubbling gas
30	Archani	26/6/09	IH	34S	600613	4315572	dissolved gas
31	Archani	6/9/13	IH	34S	600613	4315572	dissolved gas
32	Archani	10/5/17	IH	34S	600613	4315572	dissolved gas
33	Archani 159	10/5/17	IH	34S	600571	4315552	bubbling gas
34	Archani 160	10/5/17	IH	34S	600579	4315550	dissolved gas
35	Archani 161	10/5/17	IH	34S	600581	4315551	bubbling gas
36	Archani drill	7/10/16	IH	34S	601327	4315970	dissolved gas
37	Archani drill	10/5/17	IH	34S	601327	4315970	dissolved gas
38	Kamaroules	10/5/17	IH	34S	601018	4315720	dissolved gas
39	Ekkara	5/10/15	IH	34S	602820	4334018	bubbling gas
40	Ekkara	19/6/14	IH	34S	602820	4334018	dissolved gas
41	Ekkara	9/5/17	IH	34S	602820	4334018	dissolved gas
42	Ekkara Ps	9/5/17	IH	34S	602786	4334990	dissolved gas
43	Ekkara creek	9/5/17	IH	34S	602820	4334018	bubbling gas
44	Ekkara creek	5/10/15	IH	34S	602820	4334018	bubbling gas
45	Kato Pasali	9/5/17	IH	34S	602601	4334825	bubbling gas
46	Kato Pasali	9/5/17	IH	34S	602601	4334825	dissolved gas
47	Psoronera	9/5/17	IH	34S	602618	4334806	dissolved gas
48	Agia Eleni (Chios)	27/7/11	IH	35S	424638	4241828	dissolved gas
49	DLF	8/9/13	IH	34S	631295	4260476	dissolved gas
50	Kaitsa	5/10/15	IH	34S	599542	4330466	dissolved gas
51	Ilion port	4/10/15	IH	34S	684091	4301909	dissolved gas

ID	sample	Date		Sector	Coordinates		Type of emission
					E	N	
52	Epanomi EP-1		IH	Rigakis et al 2001			
53	Epanomi EP-B1		IH	Rigakis et al 2001			
54	Giatsovo	19/6/11	IH	34T	536275	4516533	bubbling gas
55	Giatsovo	4/3/07	IH	34T	536275	4516533	bubbling gas
56	Giatsovo soil	11/10/14	IH	34T	536532	4516507	soil gas
57	Giatsovo soil	22/5/16	IH	34T	536532	4516507	bubbling gas
58	Giatsovo soil	18/3/17	IH	34T	536532	4516507	bubbling gas
59	GS2	18/3/17	IH	34 T	536505	4516483	bubbling gas
60	GS3	18/3/17	IH	34 T	536539	4516507	bubbling gas
61	GS4	18/3/17	IH	34 T	536406	4516434	bubbling gas
62	Kampos	1/6/08	IH	34T	540876	4528545	bubbling gas
63	Marina 2*	4/3/07	IH	34T	541533	4523591	bubbling gas
64	Analypsis	20/6/11	IH	34T	546014	4508588	bubbling gas
65	Analypsis	22/5/16	IH	34T	546046	4508659	bubbling gas
66	Mesochori	3/3/07	IH	34T	545179	4526208	well gas
67	Mesochori 2	1/6/08	IH	34T	545038	4526525	well gas
68	Mesochori 3	28/4/10	IH	34T	536948	4526761	well gas
69	Mesochori 3	20/6/11	IH	34T	536948	4526761	well gas
70	Mesochori 3	11/10/14	IH	34T	536948	4526761	well gas
71	Mesochori gas	18/3/17	IH	34T	544910	4526652	well gas
72	Mesochori gas	22/5/16	IH	34T	544910	4526652	well gas
73	Papagiannis 2	1/6/08	IH	34T	539383	4520850	bubbling gas
74	Sarri	21/9/10	IH	34T	536983	4519729	bubbling gas
75	Sarri	19/6/11	IH	34T	536983	4519729	bubbling gas
76	Sarri	11/10/14	IH	34T	536983	4519729	bubbling gas
77	Chamsas	20/6/11	IH	34T	545443	4513945	dissolved gas
78	Itea	20/6/11	IH	34T	542915	4523793	bubbling gas
79	Itea	4/3/07	IH	34T	542915	4523793	bubbling gas

ID	Sample	Date		Sector	Coordinates		Type of emission
					E	N	
80	Itea	21/5/16	IH	34T	542915	4523793	bubbling gas
81	Tropeouchos	21/9/10	IH	34T	536669	4511216	bubbling gas
82	Tropeouchos	19/6/11	IH	34T	536669	4511216	bubbling gas
83	Tropeouchos	12/10/14	IH	34T	536669	4511216	bubbling gas
84	Profitis Ilias	1/6/08	IH	34T	537545	4521708	bubbling gas
85	Profitis Ilias	21/6/11	IH	34T	537545	4521708	dissolved gas
86	Profitis Ilias 2	21/6/11	IH	34T	537578	4522327	dissolved gas
87	Synergio	21/6/11	IH	34T	536974	4520639	bubbling gas
88	Synergio	11/10/14	IH	34T	536974	4520639	bubbling gas
89	Vassiliadis	21/6/11	IH	34T	539733	4524048	dissolved gas
90	XinoAchladi	20/6/11	IH	34T	545248	4515723	dissolved gas
91	Papadia	13/5/17	IH	34T	559477	4527512	bubbling gas
92	Papadia 2	13/5/17	IH	34T	559477	4527512	bubbling gas
93	Petres	21/5/16	IH	34T	556165	4508558	bubbling gas
94	Petres	19/3/17	IH	34T	556165	4508558	bubbling gas
95	Kilkis	25/9/10	IH	34T	652385	4542260	dissolved gas
96	Kilkis 2	25/9/10	IH	34T	652103	4542157	bubbling gas
97	Xino Nero (Kilkis2)	4/10/14	IH	35T	333979	4579275	bubbling gas
98	Xino Nero 2 (Kilkis2)	4/10/14	IH	34T	652131	4542157	bubbling gas
99	Agia Fotini	16/3/15	IH	35S	458581	4321922	dissolved gas
100	Loutrochori	22/9/10	IH	34T	593851	4508930	dissolved gas
101	Loutrochori 2	11/10/14	IH	34T	593654	4508672	bubbling gas
102	Loutrochori 3	12/10/14	IH	34T	593654	4508683	dissolved gas
103	Souroti	30/5/08	IH	34T	676028	4482364	dissolved gas
104	Pikrolimni	29/5/08	IH	34T	676796	4481724	dissolved gas
105	Platystomo	26/6/09	IH	34S	595056	4314276	dissolved gas
106	Platystomo	6/9/13	IH	34S	595056	4314276	dissolved gas

ID	Sample	Date		Sector	Coordinates		Type of emission
					E	N	
107	Platystomo SPA	10/5/17	IH	34S	595281	4314047	dissolved gas
108	Promachoi	25/9/10	IH	34T	585704	4542558	bubbling gas
109	Promachoi	27/5/08	IH	34T	585704	4542558	bubbling gas
110	Promachoi	28/5/16	IH	34T	585704	4542558	bubbling gas
111	Sani	31/5/08	IH	34T	697102	4441666	well gas
112	Sani	10/10/14	IH	34T	697102	4441666	well gas
113	Sani	27/5/16	IH	34T	697102	4441666	well gas
114	Sykies	31/5/10	IH	34S	492201	4340217	dissolved gas
115	Orea Elenis	2/11/09	IH	34S	675683	4193227	dissolved gas
116	Kokkinonero	26/9/10	IH	34S	652866	4410686	bubbling gas
117	Kokkinonero	9/6/14	IH	34S	652866	4410686	bubbling gas
118	Kokkinonero 2	9/6/14	IH	34S	653229	4409962	bubbling gas
119	Kokkinonero 2	26/9/10	IH	34S	653229	4409962	bubbling gas
120	Xyna	27/5/16	IH	34S	652173	4293691	bubbling gas
121	Ag. Anargyroi	11/4/16	IH	34S	695940	4138819	dissolved gas
122	Ag. Anargyroi 2	11/4/16	IH	34S	695930	4138800	dissolved gas
123	Katakali	17/5/16	IH	34S	557859	4419686	bubbling gas
124	Ag. Anargyroi Kithnos	4/6/16	IH	35S	272100	4146863	bubbling gas
125	Soulanta	19/6/14	IH	34S	584243	4331656	bubbling gas
126	Loutraki	2/11/09	IH	34S	673004	4205720	dissolved gas
127	Agiasmata (Chios)	27/7/11	IH	35S	407142	4271537	dissolved gas
128	Agia Paraskevi	31/5/08	IH	34T	721319	4422619	dissolved gas
129	Agia paraskevi sea	10/10/14	IH	34S	721316	4422572	bubbling gas
130	Agia paraskevi sea	28/5/16	IH	34S	721316	4422572	bubbling gas
131	Agia paraskevi sea 2	28/5/16	IH	34S	721318	4422552	bubbling gas
132	Koniavitis	22/3/15	IH	34S	652173	4293691	bubbling gas
133	Koniavitis	9/4/16	IH	34S	652173	4293691	bubbling gas

ID	Sample	Date		Sector	Coordinates		Type of emission
					E	N	
134	Koniavitis	11/5/17	IH	34S	652173	4293691	bubbling gas
135	Edipsos	27/6/09	IH	34S	677748	4302697	bubbling gas
136	Edipsos 2	29/3/08	IH	34S	677748	4302697	bubbling gas
137	Ilion	27/6/09	IH	34S	684748	4302522	bubbling gas
138	Ilion	9/9/13	IH	34S	684748	4302522	bubbling gas
139	Ilion	4/10/15	IH	34S	684748	4302522	bubbling gas
140	Ilion sea	4/10/15	IH	34S	684779	4302527	bubbling gas
141	Ilion sea	4/10/15	IH	34S	684779	4302527	dissolved gas
142	Edipsos pool	9/11/05	IH	34S	677748	4302697	bubbling gas
143	EdipsosStadium	4/10/15	IH	34S	677818	4302852	bubbling gas
144	Thermopotamos	9/9/13	IH	34S	677804	4303017	bubbling gas
145	Thermopotamos	23/3/15	IH	34S	677804	4303017	bubbling gas
146	Thermopotamos	4/10/15	IH	34S	677804	4303017	bubbling gas
147	Termopotamos 2	23/3/15	IH	34S	677804	4303017	bubbling gas
148	Gialtra	15/9/06	IH	34S	672356	4302010	dissolved gas
149	Gialtra	29/3/08	IH	34S	672356	4302010	bubbling gas
150	Gialtra	27/6/09	IH	34S	672356	4302010	bubbling gas
151	Kallydica	9/4/16	IH	34S	651735	4293616	bubbling gas
152	Kammena Vourla	27/3/08	IH	34S	654801	4293063	bubbling gas
153	Kammena Vourla	25/6/09	IH	34S	654801	4293063	bubbling gas
154	Kammena Vourla 2	8/9/13	IH	34S	654797	4293124	bubbling gas
155	Kammena Vourla 2	3/10/15	IH	34S	654797	4293124	bubbling gas
156	Kammena Vourla 2	22/3/15	IH	34S	654797	4293124	bubbling gas
157	Thermopyles	8/9/13	IH	34S	632503	4294861	bubbling gas
158	Thermopyles	3/10/15	IH	34S	632503	4294861	bubbling gas
159	Thermopyles	9/4/16	IH	34S	632503	4294861	bubbling gas
160	Leonidas	3/10/15	IH	34S	633420	4295533	bubbling gas

ID	Sample	Date		Sector	Coordinates		Type of emission
					E	N	
161	Ikaria (Ag. Kyr.1)	1/10/06	IH	35S	437916	4163309	bubbling gas
162	Kivotos 2	4/10/14	IH	34T	536200	4454843	dissolved gas
163	Eftalou	15/3/15	IH	35S	432247	4359057	bubbling gas
164	Lisvori	16/3/15	IH	35S	430924	4328291	bubbling gas
165	Polychnitos	16/3/15	IH	35S	430754	4325288	bubbling gas
166	Skala Sikaminias	15/3/15	IH	35S	435756	4358931	bubbling gas
167	Kolpos Geras	17/3/15	IH	35S	455577	4330184	bubbling gas
168	Pozar	27/5/08	IH	34T	576793	4536059	bubbling gas
169	Pozar	25/9/10	IH	34T	576793	4536059	bubbling gas
170	Pozar	12/10/14	IH	34T	576793	4536059	bubbling gas
171	Loutra Ypatis	5/10/15	IH	34S	610707	4306179	bubbling gas
172	Loutra Ypatis	14/9/06	IH	34S	610707	4306179	bubbling gas
173	Ypatis	14/9/06	IH	34S	611133	4305762	bubbling gas
174	Ypatis	7/9/13	IH	34S	611133	4305762	bubbling gas
175	Ypatis	19/6/14	IH	34S	611133	4305762	dissolved gas
176	Nea Tenedos	25/9/10	IH	34T	689840	4465429	dissolved gas
177	Smokovo	11/10/08	IH	34S	587401	4331600	bubbling gas
178	Smokovo	19/6/14	IH	34S	587401	4331600	bubbling gas
179	Psoroneria 1	7/9/13	IH	34S	629828	4296107	bubbling gas
180	Psoroneria 1	20/6/14	IH	34S	629828	4296107	bubbling gas
181	Psoroneria 1	10/4/16	IH	34S	629828	4296107	bubbling gas
182	Psoroneria 2	14/9/06	IH	34S	630034	4295988	bubbling gas
183	Psoroneria 2	27/10/07	IH	34S	630034	4295988	bubbling gas
184	Psoroneria 2	27/3/08	IH	34S	630034	4295988	bubbling gas
185	Kolona	5/6/16	IH	35S	272100	4146863	bubbling gas
186	Doumbia	30/5/08	HH	34T	699024	4506939	dissolved gas
187	Nigrita	30/5/08	HH	34T	714872	4530666	bubbling gas

ID	Sample	Date		Sector	Coordinates		Type of emission
					E	N	
188	Nigrita 1	5/10/14	HH	34T	715140	4530549	dissolved gas
189	Sappes	23/9/10	HH	35T	390583	4541724	dissolved gas
190	Therma Limani	8/9/11	HH	35T	381584	4484685	bubbling gas
191	Therma Limani	7/10/14	HH	35T	381584	4484685	bubbling gas
192	Therma Limani	20/3/17	HH	35T	381584	4484685	bubbling gas
193	Kavala PR2		HH	Rigakis et al 2001			
194	Kavala SKA-1		HH	Rigakis et al 2001			
195	Angistro	4/10/14	HH	34T	703045	4582418	dissolved gas
196	Elefteres	30/5/08	HH	34T	715132	4530500	bubbling gas
197	Elefteres	5/10/14	HH	35T	254384	4513563	bubbling gas
198	Elefteres	20/5/16	HH	34T	715132	4530500	bubbling gas
199	Eleftere agia marina	20/5/16	HH	35T	254191	4513674	bubbling gas
200	Krinides	8/10/14	HH	35T	269277	4543551	dissolved gas
201	Langada	25/9/10	HH	34T	676097	4511124	dissolved gas
202	Nea Apollonia	24/9/10	HH	34T	703157	4503711	dissolved gas
203	Nea Apollonia 3	24/9/10	HH	34T	704453	4503375	dissolved gas
204	Nea Kessani	23/9/10	HH	35T	336165	4542498	bubbling gas
205	Nea Kessani	8/10/14	HH	35T	336165	4542498	bubbling gas
206	Nea Kessani	18/5/16	HH	35T	336165	4542498	bubbling gas
207	Nigrita 2	30/5/08	HH	34T	716088	4531100	dissolved gas
208	Ninfopetra	30/5/08	HH	35T	254396	4513566	bubbling gas
209	Ninfopetra	24/9/10	HH	34T	699021	4506948	bubbling gas
210	Paranesti 1	6/10/14	HH	35T	287142	4593629	dissolved gas
211	Paranesti 2	6/10/14	HH	35T	287142	4593629	bubbling gas
212	Paranesti 3	6/10/14	HH	35T	286796	4593869	dissolved gas
213	Giotrisi	7/10/14	HH	35T	381626	4483861	bubbling gas
214	Giotrisi	23/5/16	HH	35T	381626	4483861	bubbling gas

ID	Sample	Date		Sector	Coordinates		Type of emission
					E	N	
215	Giotrisi	20/3/17	HH	35T	381626	4483861	bubbling gas
216	B Pigi	10/9/11	HH	35T	381626	4483861	dissolved gas
217	A Pigi	7/10/14	HH	35T	381626	4483861	dissolved gas
218	Pool	7/10/14	HH	35T	381574	4484049	dissolved gas
219	Thermopigi	5/10/04	HH	34T	697963	4572767	bubbling gas
220	Thermopigi	5/10/14	HH	34T	697963	4572767	bubbling gas
221	Thermopigi	20/5/16	HH	34T	697963	4572767	bubbling gas
222	Traianoupoli drill	23/9/10	HH	35T	418561	4524337	dissolved gas
223	Traianoupoli drill	8/10/14	HH	35T	418557	4524350	dissolved gas
224	Thermes (Xanthi)	6/10/14	HH	35T	333719	4579342	bubbling gas
225	Thermes 1	16/3/15	HH	35S	456582	4337023	dissolved gas
226	Thermes 3 (Xanthi)	6/10/14	HH	35T	333820	4579249	bubbling gas
227	Thermes 3 (Xanthi)	22/3/17	HH	35T	333820	4579249	bubbling gas
228	XNT-1 (Thermes)	26/8/08	HH	35T	333725	4579328	bubbling gas
229	Gyali	2/9/10	VA	35S	511048	4057840	bubbling gas
230	Gyali	1/10/15	VA	35S	511048	4057840	bubbling gas
231	Gyali	3/10/16	VA	35S	511048	4057840	bubbling gas
232	Gyali lake	4/10/16	VA	35S	511222	4058099	bubbling gas
233	Gyali Nord	3/10/16	VA	35S	510958	4058232	bubbling gas
234	Gyali West	3/10/16	VA	35S	510511	4055549	bubbling gas
235	Gyali Nord	1/10/15	VA	35S	510958	4058232	bubbling gas
236	Katsouni	13/9/11	VA	35S	517346	4051911	bubbling gas
237	Katsouni	4/10/16	VA	35S	517346	4051911	bubbling gas
238	Lies	2/10/15	VA	35S	518202	4050287	bubbling gas
239	Lies	2/10/16	VA	35S	518202	4050287	bubbling gas
240	KKN1	19/3/14	VA	35S	521911	4075842	soil gas
241	KKN1	29/9/15	VA	35S	521911	4075842	soil gas

ID	Sample	Date		Sector	Coordinates		Type of emission
					E	N	
242	Kos Kokkinonero	5/9/10	VA	35S	521902	4078954	bubbling gas
243	Kos Kokkinonero	19/3/14	VA	35S	521902	4078954	bubbling gas
244	Kos Kokkinonero 2	29/9/16	VA	35S	522116	4078886	bubbling gas
245	Kos Kokkinonero 2	19/3/14	VA	35S	522116	4078886	bubbling gas
246	Kos Kokkinonero 2	29/9/15	VA	35S	522116	4078886	bubbling gas
247	Kefalos	28/9/15	VA	35S	497339	4065831	bubbling gas
248	Kefalos	29/9/16	VA	35S	497339	4065831	bubbling gas
249	Kos Paradise	3/9/10	VA	35S	500794	4068393	bubbling gas
250	Kos Paradise	27/9/15	VA	35S	500794	4068393	bubbling gas
251	Kos Paradise	29/9/16	VA	35S	500794	4068393	bubbling gas
252	Kos Paradise 2	30/9/16	VA	35S	500836	4068302	bubbling gas
253	Kos Paradise 3	30/9/16	VA	35S	500828	4068313	bubbling gas
254	KAT-1	28/9/15	VA	35S	521910	4075843	bubbling gas
255	Irini2 - KAT	30/9/16	VA	35S	499740	4068795	bubbling gas
256	KAK-1	28/9/15	VA	35S	520916	4075676	bubbling gas
257	Irini - KAK	30/9/16	VA	35S	499740	4068795	bubbling gas
258	Thiafi	11/6/06	VA	34S	712355	4163891	soil gas
259	Pallis	13/9/06	VA	34S	711362	4162310	dissolved gas
260	Thiafi	24/6/06	VA	34S	712355	4163891	soil gas
261	Thiafisea	24/6/06	VA	34S	712366	4163876	bubbling gas
262	Thiafi sea	25/9/15	VA	34S	712366	4163876	bubbling gas
263	Thiafi sea	28/9/16	VA	34S	712366	4163876	bubbling gas
264	Thiafi sea 2	28/9/16	VA	34S	712361	4163870	bubbling gas
265	Thiafi sea3	13/6/17	VA	34S	712357	4163663	bubbling gas
266	Ag. Kyriaki	9/6/17	VA	35S	276233	4060937	bubbling gas
267	Skinopi	17/9/14	VA	35S	270211	4067712	bubbling gas
268	Skinopi	8/6/17	VA	35S	270211	4067712	bubbling gas

ID	Sample	Date		Sector	Coordinates		Type of emission
					E	N	
269	Mandrakia	10/6/17	VA	35S	271841	4070059	bubbling gas
270	Pausanias sea	19/3/15	VA	34S	708237	4168274	bubbling gas
271	Pausanias sea	28/9/16	VA	34S	708237	4168274	bubbling gas
272	KVO1	27/9/15	VA	35S	499601	4068664	soil gas
273	KVO2	20/3/14	VA	35S	499783	4068858	soil gas
274	KVO33	27/9/15	VA	35S	499596	4068661	soil gas
275	KVO52	27/9/15	VA	35S	499740	4068795	soil gas
276	Thermia (Kos)	5/9/10	VA	35S	528211	4077679	bubbling gas
277	Thermia (Kos)	19/3/14	VA	35S	528211	4077679	bubbling gas
278	Thermia (Kos)	29/9/16	VA	35S	528211	4077679	bubbling gas
279	Thermia sea(Kos)	29/9/16	VA	35S	528287	4077666	bubbling gas
280	Methana	1/12/04	VA	34S	710771	4161629	atmosphere in contact with water
281	Methana	24/6/06	VA	34S	710771	4161629	dissolved gas
282	Methana	26/5/07	VA	34S	710771	4161629	atmosphere in contact with water
283	Methana 2	26/5/07	VA	34S	710778	4161543	atmosphere in contact with water
284	Ag. Nicholaos	24/6/06	VA	34S	711755	4162729	dissolved gas
285	Pausanias	4/6/06	VA	34S	708237	4168270	bubbling gas
286	Pausanias	23/6/06	VA	34S	708237	4168270	bubbling gas
287	Pausanias	19/3/15	VA	34S	708237	4168270	bubbling gas
288	Pausanias fracture	4/6/06	VA	34S	708237	4168270	soil gas
289	Pausanias mofette	23/6/06	VA	34S	708258	4168272	soil gas
290	Thiafi	25/9/15	VA	34S	712355	4163891	soil gas
291	Milos 1 (Skinopi)	5/9/08	VA	35S	270211	4067712	bubbling gas
292	Adamas F70	11/6/17	VA	35S	272188	4068108	fumarole
293	Milos 3 (Paleochori)	12/8/08	VA	35S	272157	4068098	bubbling gas
294	Paleochori cave	9/6/17	VA	35S	277789	4061612	bubbling gas
295	Paleochori1	9/6/17	VA	35S	278091	4061589	bubbling gas
296	Paleochori2	9/6/17	VA	35S	277945	4061589	bubbling gas
297	Milos 6 (Paleochori)	5/9/08	VA	35S	277948	4061589	bubbling gas
298	Milos C3 (Fyriplaka)	1/6/07	VA	35S	275902	4061000	fumarolic gas

ID	Sample	Date		Sector	coordinates		Type of emission
					E	N	
299	Milos DEH	24/6/14	VA	35S	274009	4065181	bubbling gas
300	Milos 2 (Adamas DEH)	12/8/08	VA	35S	274009	4065181	bubbling gas
301	Milos Mad 1 (DEH)	12/10/07	VA	35S	274009	4065181	bubbling gas
302	DEH	8/6/17	VA	35S	274009	4065181	bubbling gas
303	Milos MZR-1	13/2/10	VA	35S	274245	4064912	bubbling gas
304	Milos Paleochori	17/9/14	VA	35S	278091	4061589	bubbling gas
305	Milos Paleochori 3	21/6/07	VA	35S	278029	4061589	bubbling gas
306	Milos Paleochori 4	21/6/07	VA	35S	278032	4061591	bubbling gas
307	Spathi bay 1	9/6/17	VA	35S	279277	4061414	bubbling gas
308	Spathi bay 2	9/6/17	VA	35S	279289	4061423	bubbling gas
309	Kalamos 35	11/6/17	VA	35S	275925	4060917	fumarole
310	Voudia	10/6/17	VA	35S	279595	4069246	bubbling gas
311	A13 Nisyros	30/8/10	VA	35S	514702	4048539	fumarole
312	A13 Nisyros	6/6/13	VA	35S	514702	4048539	fumarole
313	A13 Nisyros	4/10/16	VA	35S	514702	4048539	fumarole
314	PP9N Nisyros	2/9/09	VA	35S	514855	4048684	fumarole
315	PP9N Nisyros	30/8/10	VA	35S	514855	4048684	fumarole
316	S15 Nisyros	31/8/09	VA	35S	515023	4048167	fumarole
317	S15 Nisyros	1/9/10	VA	35S	515023	4048167	fumarole
318	S15 Nisyros	5/6/13	VA	35S	515023	4048167	fumarole
319	AM Nisyros	11/10/07	VA	35S	514695	4048520	fumarole
320	AM Nisyros	9/9/08	VA	35S	514695	4048520	fumarole
321	AM Nisyros	4/9/09	VA	35S	514695	4048520	fumarole
322	K6 Nisyros	10/9/08	VA	35S	515525	4048153	fumarole
323	K6 Nisyros	3/9/09	VA	35S	515525	4048153	fumarole
324	K6 Nisyros	1/9/10	VA	35S	515525	4048153	fumarole
325	K7 Nisyros	6/6/13	VA	35S	515491	4047973	fumarole

ID	Sample	Date		Sector	Coordinates		Type of emission
					E	N	
326	K7 Nisyros	30/9/15	VA	35S	515491	4047973	fumarole
327	K7 Nisyros	2/10/16	VA	35S	515491	4047973	fumarole
328	PP9S Nisyros	10/10/07	VA	35S	514853	4048674	fumarole
329	PP9S Nisyros	10/9/08	VA	35S	514853	4048674	fumarole
330	PP9S Nisyros	5/6/13	VA	35S	514853	4048674	fumarole
331	S4 Nisyros	1/9/10	VA	35S	515139	4048107	fumarole
332	S4 Nisyros	5/6/13	VA	35S	515139	4048107	fumarole
333	S4 Nisyros	2/10/16	VA	35S	515139	4048107	fumarole
334	Lefkos	2/10/16	VA	35S	512807	4046707	bubbling gas
335	Erinia	6/4/16	VA	35S	356566	4030709	bubbling gas
336	Santorini Kameni B	6/10/07	VA	35S	356170	4030054	fumarole
337	Nea Kameni	6/4/16	VA	35S	356167	4030015	fumarole
338	Santorini SK3 (N.Kameni)	12/5/10	VA	35S	356212	4030054	bubbling gas
339	SNK1	18/2/15	VA	35S	356170	4030054	fumarole
340	Palea Kameni	6/4/16	VA	35S	354705	4029378	bubbling gas
341	Palea Kameni	7/5/96	VA	35S	354705	4029378	bubbling gas
342	Palea Kameni	14/10/12	VA	35S	354705	4029378	bubbling gas
343	Sousaki well	5/11/05	VA	34S	683447	4200477	well gas
344	Sousaki well	8/9/13	VA	34S	683447	4200477	well gas
345	Sousaki well	18/3/15	VA	34S	683447	4200477	well gas
346	Sousaki big cave	18/5/10	VA	34S	683429	4200665	mofette
347	Sousaki big cave	23/6/14	VA	34S	683429	4200665	mofette
348	Sousaki big cave	18/3/15	VA	34S	683429	4200665	mofette
349	Sousaki small cave	11/12/03	VA	34S	683393	4200696	mofette
350	Sousaki small cave	8/9/13	VA	34S	683393	4200696	mofette
351	Sousaki small cave	11/4/16	VA	34S	683393	4200696	mofette
352	Sousaki cave 3	7/11/05	VA	34S	683393	4200696	mofette

Table 2: Coordinates of the gases (extracted database)

N.	sample	date		Sector	UTM Coordinates (WGS84)	
		dd/mm/yy			E	N
1	Katakali	17/5/2016	IH	34S	557859	4419686
2	Psoroneria	7/9/2013	IH	34S	629828	4296107
3	Psoroneria	10/4/2016	IH	34S	629828	4296107
4	Thermopyles	3/10/2015	IH	34S	632503	4294861
5	Thermopyles	9/4/2016	IH	34S	632503	4294861
6	Koniavitis	22/3/2015	IH	34S	652173	4293691
7	Kammena Vourla	8/9/2013	IH	34S	654797	4293124
8	Kammena Vourla	22/3/2015	IH	34S	654797	4293124
9	Kallydica	9/4/2016	IH	34S	651735	4293616
10	Gialtra	9/9/2013	IH	34S	672356	4302010
11	Thermopotamos	23/3/2015	IH	34S	677804	4303017
12	Thermopotamos	4/10/2015	IH	34S	677804	4303017
13	Patra	1/10/2014	EH	34S	560839	4227475
14	Sousaki well	18/3/2015	VA	34S	683447	4200477
15	Sousaki cave	18/3/2015	VA	34S	683429	4200665
16	Ilion	23/3/2015	IH	34S	684748	4302522
17	Ilion	4/10/2015	IH	34S	684748	4302522
18	Ilion sea	4/10/2015	IH	34S	684779	4302527
19	Pausanias	19/3/2015	VA	34S	708237	4168270
20	Pausanias sea	19/3/2015	VA	34S	708237	4168274
21	Thiafi sea	25/9/2015	VA	34S	712366	4163876
22	Agia paraskevi sea	28/5/2016	IH	34S	721293	4422552
23	Agia paraskevi sea 2	28/5/2016	IH	34S	721278	4422518
24	Xyna	27/5/2016	IH	34S	731638	4423292
25	PPG-1	23/8/2015	EH	34S	560778	4227579

N.	sample	date		Sector	UTM Coordinates (WGS84)	
		dd/mm/yy			E	N
26	Soulanta	19/6/2014	EH	34S	584243	4331656
27	Smokovo	19/6/2014	EH	34S	587401	4331600
28	Ekkara	19/6/2014	IH	34S	602820	4334018
29	Ekkara creek	5/10/2015	IH	34S	602820	4334018
30	Ypati	7/9/2013	IH	34S	611133	4305762
31	Loutra Ypatis	5/10/2015	IH	34S	611133	4305762
32	Leonidas	3/10/2015	IH	34S	633420	4295533
33	Kokkinonero	9/6/2014	IH	34S	652866	4410686
34	Kokkinonero 2	9/6/2014	IH	34S	653229	4409962
35	Edipsos stadium	4/10/2015	IH	34S	677818	4302852
36	Ag. Paraskevi	10/10/2014	IH	34S	721319	4422619
37	Giatsovo soil	22/5/2016	IH	34T	536484	4516474
38	Analipsi	22/5/2016	IH	34T	546046	4508659
39	Tropeouchos	12/10/2014	IH	34T	536669	4511216
40	Mesochori gas	22/5/2016	IH	34T	545080	4526135
41	Mesochori 3	11/10/2014	IH	34T	536948	4526761
42	Synergio	11/10/2014	IH	34T	536974	4520639
43	Sarri	11/10/2014	IH	34T	536983	4519729
44	Itea	21/5/2016	IH	34T	542915	4523793
45	Pozar	12/10/2014	IH	34T	576793	4536059
46	Promachoi	25/9/2010	IH	34T	585704	4542558
47	Loutrochori 2	11/10/2014	IH	34T	593654	4508672
48	Xino Nero (Kilkis)	4/10/2014	HH	35T	333979	4579275
49	Xino Nero 2 (Kilkis)	4/10/2014	HH	34T	652131	4542157
50	Sani	27/5/2016	IH	34T	697105	4441666
51	Thermopigi	5/10/2014	IH	34T	697963	4572767
52	Eleftheres	20/5/2016	HH	34T	715132	4530500

N.	sample	date		Sector	UTM Coordinates (WGS84)	
		dd/mm/yy			E	N
53	Polychnitos	16/3/2015	IH	35S	430754	4325288
54	Lisvori	16/3/2015	IH	35S	430924	4328291
55	Eftalou	15/3/2015	IH	35S	432247	4359057
56	Skala Sikaminias	15/3/2015	IH	35S	435756	4358931
57	Kolpos Geras	17/3/2015	IH	35S	455577	4330184
58	Milos Skinopi	17/9/2014	VA	35S	270211	4067712
59	Milos DEH	24/6/2014	VA	35S	274009	4065181
60	Kefalos	29/9/2016	VA	35S	497339	4065831
61	Kos Paradise	27/9/2015	VA	35S	500794	4068393
62	Kos Kokkinonero	19/3/2014	VA	35S	521902	4078954
63	KKN1	19/3/2014	VA	35S	521911	4075842
64	Kos Kokkinonero 2	19/3/2014	VA	35S	522116	4078886
65	KVO2	20/3/2014	VA	35S	499785	4068850
66	KVO52	27/9/2015	VA	35S	499740	4068795
67	Ag. Irini 2	30/9/2016	VA	35S	521910	4075843
68	Ag. Irini 1	28/9/2015	VA	35S	520916	4075676
69	Gyali nord	1/10/2015	VA	35S	510958	4058232
70	Gyali	1/10/2015	VA	35S	511048	4057840
71	Gyali lake	4/10/2016	VA	35S	511222	4058099
72	Gyali west	3/10/2016	VA	35S	510511	4055549
73	Katsouni	4/10/2016	VA	35S	517346	4051911
74	Lies	2/10/2015	VA	35S	518202	4050287
75	Nea Kessani	18/5/2016	HH	35T	336174	4542511
76	Eleftheres Ag. Marina	20/5/2016	HH	35T	254191	4513674
77	Paranesti 2	6/10/2014	HH	35T	287142	4593629
78	Thermes (Xanthi)	6/10/2014	HH	35T	333719	4579342
79	Thermes 3 (Xanthi)	6/10/2014	HH	35T	333820	4579249

N.	sample	date		Sector	UTM Coordinates (WGS84)	
		dd/mm/yy			E	N
80	Thermia (Kos)	19/3/2014	VA	35S	528211	4077679
81	Thermia sea (Kos)	29/9/2016	VA	35S	528230	4077660
82	Therma Limani	7/10/2014	IH	35T	381584	4484685
83	Geotrisi	7/10/2014	IH	35T	381626	4483861
84	Ag. Anargyroi Kithnos	4/6/2016	IH	35S	272100	4146863
85	Kolona	5/6/2016	IH	35S	267612	4144489
86	Nea Kameni	6/4/2016	VA	35S	356167	4030015
87	Erinia (N. Kameni)	6/4/2016	VA	35S	356566	4030709
88	Ag. Anargyroi	11/4/2016	IH	34S	695940	4138819
89	Ag. Anargyroi 2	11/4/2016	IH	34S	695930	4138800
90	Archani	6/9/2013	IH	34S	600613	4315572
91	Lysimachia	7/9/2013	EH	34S	529376	4269008
92	Kaitsa	5/10/2015	EH	34S	599542	4330466
93	Amplas	6/9/2013	EH	34S	591217	4308687
94	Platystomo	6/9/2013	IH	34S	595056	4314276
95	PP9S Nisyros	4/6/2009	VA	35S	514853	4048674
96	S4 Nisyros	1/10/2012	VA	35S	515139	4048107
97	A13 Nisyros	5/6/2009	VA	35S	514702	4048539
98	S15 Nisyros	4/6/2009	VA	35S	515023	4048167
99	K7 Nisyros	1/10/2012	VA	35S	515491	4047973
100	Thermia (Kos)	28/9/2012	VA	35S	528211	4077679
101	Ag. Irini 2	27/9/2011	VA	35S	521910	4075843

Table 3: Literature data

	Abbreviation or ID number	He	N_2	Ar	CO_2	$\partial^{13}C$-CO_2	R/Ra	$^4He/^{20}Ne$	$CO_2/^3He$
		µmol/mol				‰			
Popping rock	MORB	32.6	1200	24	949500	-3.80	8	1000	2.60E+09
SCLM (Massif Central)	MC	28.3	6500	58	992000	-3.72	6.35	1000	3.94E+09
SCLM (Eifel)	E	22.6	4740	87	993800	-3.35	5.62	387	5.59E+09
SCLM (Eger rift)	ER	17.6	2420	56	996800	-1.99	6.21	10.9	6.51E+09
Air	Air	5.24	780840	9340	400	-8	1	0.318	5.45E+07
Air Saturated Water	ASW	2.7	652000	17670	15300		1	0.267	4.05E+09
Air Saturated Seawater	ASSW	2.4	640300	19170	16100		1	0.267	4.87E+09
Kolumbo	A2	23	11000		980000		7.01	270.3	4.34E+09
	V2	15	85000		883000		6.84	9.1	6.15E+09
	V3	26	9000		984000		7.04	248.3	3.84E+09
	V4	22	50000		915000		6.95	29.1	4.27E+09
	V5	25	31000		954000		7.05	48	3.87E+09
	V6	19	6000		974000		7	234.4	5.23E+09
	V7	41	13000		967000		6.98	139.4	2.41E+09
	NA007-081	24	3000		994000		6.84	990	4.33E+09

Table 4: Chemical composition of the gases (general database)

ID	sample	He	H_2	O_2	N_2	CH_4	CO_2	H_2S	Ne	Ar
		ppm	ppm	ppm	ppm	ppm	ppm	ppm	ppm	ppm
1	Biros	5.00	< 5	168,000	806,000	2.90	3700	n.d.	14.99	n.d.
2	Preveza	5.98	< 10	2180	816,000	98,200	83,400	n.d.	0.00	n.d.
3	Nelles	28.3	< 10	59,700	936,000	189	4290	n.d.	0.00	n.d.
4	Katakolo sea	454	< 5	53,600	190,000	741,000	2300	n.d.	0.61	n.d.
5	Katakolo sea					400,000				
6	Katakolo port					93,000				
7	Katakolo volcano 1	204	392	89,000	406,000	445,000	49,000	n.d.	n.d.	n.d.
8	Katakolo volcano 3	247	466	35,900	317,000	563,000	69,100	n.d.	5.35	n.d.
9	Katalolo WKA-1A					738,000				
10	Killini					172,100				
11	Loutra Killini	212	19	600	167,000	803,000	17,100	n.d.	4.77	n.d.
12	Loutra Killini	327	< 5	333	254,000	712,000	18,300	n.d.	0.39	3320
13	Trapeza	39.9	< 10	10,100	989,000	294	207	n.d.	0.00	n.d.
14	LYS	9.90	< 10	978	602,000	363,000	34,800	n.d.	n.d.	n.d.
15	PPG-1	0.41	< 2	49	40,100	914,000	21,400	< 5	0.54	1180
16	Patra	1.70	50	301	193,000	704,000	11,100	< 5	2.86	3500
17	Selianitika	3.80	< 10	644	866,000	111,000	22,100	n.d.	0.00	n.d.
18	Nerazies	4.70	< 10	4640	995,000	76.7	145	n.d.	0.00	n.d.
19	LP11 Chanopoulo	140	< 10	773	989,000	823	9660	n.d.	0.00	n.d.
20	LP5 Petra	72.1	44	897	990,000	85.8	8580	n.d.	0.00	n.d.
21	KRE	24.3	17.3	2270	981,000	1000	16,000	n.d.	0.00	n.d.
22	Kabasilos	1320	< 10	1420	978,000	2320	16,700	n.d.	0.00	n.d.
23	Amarantos	7.00	< 5	193,000	777,000	10.0	1200	n.d.	n.d.	n.d.

ID	sample	He	H_2	O_2	N_2	CH_4	CO_2	H_2S	Ne	Ar
		ppm	ppm	ppm	ppm	ppm	ppm	ppm	ppm	ppm
24	Kaiafa					85,400				
25	Kaiafa	917	< 10	854	995,000	1730	1400	n.d.	0.00	n.d.
26	Amplas	52.0	< 5	1400	116,000	884,000	7000	n.d.	n.d.	n.d.
27	Amplas	57.0	24.0	600	81,600	915,000	100	n.d.	0.89	n.d.
28	Amplas	114	29.0	< 200	161,000	829,000	3500	n.d.	n.d.	2500
29	Amplas 2	160	16.0	1000	110,000	882,000	129	< 10	n.d.	n.d.
30	Archani	10.0	< 10	16,600	946,000	37,700	17	n.d.	0.00	n.d.
31	Archani	12.9	< 10	7420	948,000	44,700	18	n.d.	0.00	n.d.
32	Archani	< 4	< 3	3530	973,000	23,200	41	< 20	n.d.	n.d.
33	Archani 159	10	122	1400	954,000	35,100	116	< 10	n.d.	n.d.
34	Archani 160	< 4	2480	2630	959,000	35,400	38	< 20	n.d.	n.d.
35	Archani 161	9.0	162	1300	791,000	199,000	932	< 10	n.d.	n.d.
36	Archani drill	5	<2	738	727,000	279,000	222	<5	n.d.	10,200
37	Archani drill	< 4	< 3	2870	937,000	59,700	31	< 20	n.d.	n.d.
38	Kamaroules	< 4	21.1	2030	977,000	21,100	40	< 20	n.d.	n.d.
39	Ekkara	6	37	178,000	775,000	11,500	3700	< 5	n.d.	9670
40	Ekkara	22.8	673	600	918,000	80,100	466	n.d.	0.00	n.d.
41	Ekkara	< 4	< 3	16,300	916,000	67,730	49	< 20	n.d.	n.d.
42	Ekkara Ps	38.8	45.1	3350	875,000	121,000	64	< 20	n.d.	n.d.
43	Ekkara creek	19.0	4.9	1900	907,000	80,000	194	< 10	n.d.	n.d.
44	Ekkara creek	21	11	2500	888,000	77,700	552	< 5	15.53	10,200
45	Kato Pasali	27	2.1	2400	947,000	43,800	143	< 10	n.d.	n.d.
46	Kato Pasali	< 4	< 3	2400	974,000	23,500	150	< 20	n.d.	n.d.
47	Psoronera	25.4	166	1840	858,000	140,000	76	< 20	n.d.	n.d.

ID	sample	He	H_2	O_2	N_2	CH_4	CO_2	H_2S	Ne	Ar
		ppm	ppm	ppm	ppm	ppm	ppm	ppm	ppm	ppm
48	Agia Eleni (Chios)	67.8	< 10	2620	945,000	3.00	52,800	n.d.	0.00	n.d.
49	DLF	11.3	< 10	84,200	880,000	52.8	36,000	n.d.	0.00	n.d.
50	Kaitsa	123	< 10	3070	655,000	316,000	26,200	300	1.76E-04	n.d.
51	Ilion port	< 10	< 10	144,000	855,000	8.7	1080	< 20		n.d.
52	Epanomi EP-1					704,000				
53	Epanomi EP-B1					4000				
54	Giatsovo	29.0	< 5	12,000	51,200	5440	930,000	n.d.	0.40	n.d.
55	Giatsovo	22.0	< 5	24,700	112,000	4120	843,000	n.d.	2.13	n.d.
56	Giatsovo soil	8.0	< 5	932	14,000	2280	972,000	< 5	n.d.	72
57	Giatsovo soil	13	2.0	760	20,800	2690	987,000	n.d.	0.058	28
58	Giatsovo soil	14	< 2	4400	29,000	2620	955,000	< 10		n.d.
59	GS2	13	< 2	4100	31,900	2500	958,000	< 10		n.d.
60	GS3	11	< 2	4000	28,200	2430	967,000	< 10		n.d.
61	GS4	19	2.1	10,100	50,200	4180	936,000	< 10		n.d.
62	Kampos	0.40	< 5	200	600	22.0	993,000	n.d.	0.14	n.d.
63	Marina 2*	25.0	< 5	4600	35,400	1660	949,000	n.d.	0.72	n.d.
64	Analypsis	20.0	< 5	4600	29,300	2710	969,000	n.d.	0.15	n.d.
65	Analypsis	19	< 5	4600	29,600	2350	952,000	< 10	0.547	212
66	Mesochori	3.3	34.0	600	4000	524	990,000	n.d.	1.23	n.d.
67	Mesochori 2	1.7	60.0	130	3100	353	992,000	< 10	0.28	18
68	Mesochori 3	< 5	29.0	2500	5900	85.0	990,000	n.d.	n.d.	n.d.
69	Mesochori 3	1.51	< 5	295	2300	72.0	993,000	n.d.	0.35	n.d.
70	Mesochori 3	1.15	< 5	< 200	2100	214	975,000	< 5	0.02	29
71	Mesochori gas	3.9	< 2	4900	21,000	515	969,000	< 10	0.1	n.d.

ID	sample	He	H_2	O_2	N_2	CH_4	CO_2	H_2S	Ne	Ar
		ppm	ppm	ppm	ppm	ppm	ppm	ppm	ppm	ppm
72	Mesochori gas	4.0	1.5	1005	6500	479	985,000	< 10	0.335	100
73	Papagiannis 2	< 5	< 5	67,100	285,000	106	637,000	n.d.	n.d.	n.d.
74	Sarri	0.30	< 5	143	729	38.0	998,000	n.d.	0.08	n.d.
75	Sarri	0.37	< 5	187	729	41.0	985,000	n.d.	0.03	n.d.
76	Sarri	0.33	< 5	93	1400	95.0	983,000	n.d.	0.21	62
77	Chamsas	547	<10	4520	839,000	1880	154,000	n.d.	n.d.	n.d.
78	Itea	70.0	< 5	3600	49,200	3990	947,000	n.d.	0.30	n.d.
79	Itea	31.0	< 5	1400	41,100	576	949,000	n.d.	0.72	n.d.
80	Itea	36	1.4	5700	38,300	2600	951,000	< 10	1.773	1240
81	Tropeouchos	65.0	< 5	< 100	59,200	13,400	922,000	n.d.	5.40	n.d.
82	Tropeouchos	106	< 5	< 100	86,500	20,800	874,000	n.d.	0.30	n.d.
83	Tropeouchos	29.0	< 5	76	20,000	6200	952,000	n.d.	n.d.	233
84	Profitis Ilias	14.0	14,800	87,400	373,000	16.0	495,000	n.d.	n.d.	n.d.
85	Profitis Ilias	<10	<10	14,000	610,000	137	376,000	n.d.	n.d.	n.d.
86	Profitis Ilias 2	174	<10	27,800	911,000	226	61,300	n.d.	n.d.	n.d.
87	Synergio	0.12	4.00	1100	2800	1.2	973,000	n.d.	0.25	n.d.
88	Synergio	0.43	< 5	187	1100	n.d.	997,000	n.d.	0.32	24
89	Vassiliadis	<10	<10	19,800	963,000	30.0	16,800	n.d.	n.d.	n.d.
90	XinoAchladi	<10	<10	11,100	916,000	35.7	72,700	n.d.	n.d.	n.d.
91	Papadia	0.59	< 3	2900	22,800	19	960,000	< 10	0.44	n.d.
92	Papadia 2	< 4	< 3	1400	13,100	24	977,000	< 10	n.d.	n.d.
93	Petres	73	< 2	131,000	635,000	1	233,000	< 10		n.d.
94	Petres	72	< 2	137,000	644,000	2	227,000	< 10	11.1	n.d.
95	Kilkis	3.20	< 10	27,800	97,600	9.19	875,000	n.d.	n.d.	n.d.
96	Kilkis 2	2.90	< 5	< 100	11,200	56.0	958,000	n.d.	0.24	215

ID	sample	He	H_2	O_2	N_2	CH_4	CO_2	H_2S	Ne	Ar
		ppm	ppm	ppm	ppm	ppm	ppm	ppm	ppm	ppm
97	Xino Nero (Kilkis2)	3.18	< 5	2900	15,200	23.0	965,000	<5	0.21	304
98	Xino Nero 2 (Kilkis2)	6.00	< 5	7300	26,000	82.0	939,000	<5	n.d.	n.d.
99	Agia Fotini	< 20	28.2	115,000	857,000	2	27,500	n.d.	n.d.	n.d.
100	Loutrochori	481	< 10	469	512,000	471,000	16,300	n.d.	0.00	n.d.
101	Loutrochori 2	374	< 5	175	511,000	436,000	32,400	n.d.	0.00	6290
102	Loutrochori 3	294	39.3	1780	820,000	146,000	31,800	n.d.	n.d.	n.d.
103	Souroti	45.2	< 10	3390	283,000	951	713,000	n.d.	0.00	n.d.
104	Pikrolimni	313	< 10	19,300	328,000	21.7	653,000	n.d.	0.00	n.d.
105	Platystomo	103	33.5	425	853,000	135,000	11,400	n.d.	0.00	n.d.
106	Platystomo	345	< 10	907	860,000	128,000	10,700	n.d.	0.00	n.d.
107	Platystomo SPA	228	8.55	1780	291,000	707,000	63	< 20	n.d.	n.d.
108	Promachoi	223	< 5	54,400	827,000	2.00	108,000	n.d.	8.77	9090
109	Promachoi	259	< 5	34,700	820,000	< 0.1	118,000	n.d.	8.77	n.d.
110	Promachoi	215	< 2	52,100	837,000	7	103,000		11.54	10,900
111	Sani	597	8.00	< 100	192,000	814,000	3300	n.d.	0.42	850
112	Sani	778	18.0	206	225,000	682,000	1000	<5	n.d.	733
113	Sani	762	12.0	332	226,000	764,000	1500	< 10	0.485	927
114	Sykies	98.6	< 10	438	951,000	39,500	9350	n.d.	0.00	n.d.
115	Orea Elenis	431	40.1	70,700	856,000	< 2	72,900	n.d.	0.00	n.d.
116	Kokkinonero	21.0	< 5	< 100	32,200	1180	954,000	n.d.	1.71	n.d.
117	Kokkinonero	1.60	< 5	2500	7200	249	955,000	n.d.	0.68	195
118	Kokkinonero 2	209	< 5	4300	382,000	867	581,000	n.d.	n.d.	5040
119	Kokkinonero 2	200	< 5	< 100	351,000	460	628,000	n.d.	3.16	3610
120	Xyna	91	1.6	13,000	49,600	215	943,000	< 10		n.d.
121	Ag. Anargyroi	20.6	47.7	14,700	957,000	27,000	1360	< 20	2.00E-04	7340

ID	sample	He	H_2	O_2	N_2	CH_4	CO_2	H_2S	Ne	Ar
		ppm	ppm	ppm	ppm	ppm	ppm	ppm	ppm	ppm
122	Ag. Anargyroi 2	19.4	16.7	18,200	779,000	203,000	250	< 20	1.69E-04	5420
123	Katakali	< 5	11.0	589	82,500	880,000	25,000	< 10		n.d.
124	Ag. Anargyroi Kithnos	1104	< 5	2800	664,000	833	329,000	< 10	14.20	9710
125	Soulanta	31.0	22.0	125	350,000	649,000	< 50	n.d.	20.31	5860
126	Loutraki	42.5	< 10	165,000	821,000	5.64	13,900	n.d.	0.00	n.d.
127	Agiasmata (Chios)	56.9	< 10	30,700	752,000	2870	215,000	n.d.	0.00	n.d.
128	Agia Paraskevi	6.18	22.2	1777	601,000	915	396,000	n.d.	n.d.	n.d.
129	Agia paraskevi sea	4.32	< 5	158	23,500	521	929,000	n.d.	0.74	502
130	Agia paraskevi sea	3.08	21.0	10,600	27,000	470	964,000	< 10	5.063	3450
131	Agia paraskevi sea2	92	100	3900	40,500	11,000	946,000	3100	0.198	1810
132	Koniavitis	581	< 5	< 100	701,000	2090	281,000	2200		8340
133	Koniavitis	388	< 5	938	703,000	2180	299,000	137		n.d.
134	Koniavitis	802	< 3	1200	725,000	4810	270,000	< 10	n.d.	n.d.
135	Edipsos	4.80	< 5	417	10,100	3460	979,000	140	0.15	n.d.
136	Edipsos 2	1.80	< 5	< 200	2600	861	991,000	300	0.03	69
137	Ilion	103	< 5	1600	68,900	1510	900,000	< 10	0.91	n.d.
138	Ilion	100	8.00	196	77,600	1740	906,000	< 10	0.67	751
139	Ilion	100	3.7	1100	79,400	1800	901,000	< 5	0.33	742
140	Ilion sea	199	< 2	11,300	271,000	1040	694,000	< 5	n.d.	5030
141	Ilion sea	< 10	122	224,000	770,000	15.9	5360	< 20		n.d.
142	Edipsos pool	17.0	< 5	800	17,900	4910	981,000	250	0.05	331
143	EdipsosStadium	< 4	< 2	525	3000	689	967,000	< 5	n.d.	57
144	Thermopotamos	0.12	1.40	512	1600	24.0	980,000	101	0.06	n.d.
145	Thermopotamos	0.38	< 5	1200	2800	27	977,000	48	0.04	40
146	Thermopotamos	1.53	< 2	4700	18,400	1200	958,000	< 5	0.47	275

ID	sample	He	H_2	O_2	N_2	CH_4	CO_2	H_2S	Ne	Ar
		ppm	ppm	ppm	ppm	ppm	ppm	ppm	ppm	ppm
147	Thermopotamos 2	6	<5	< 200	99,600	580	867,000	<5		2250
148	Gialtra	248	< 10	33,100	873,000	262	93,300	n.d.	0.00	n.d.
149	Gialtra	397	< 5	39,000	864,000	954	130,000	n.d.	8.82	n.d.
150	Gialtra	395	< 5	14,600	888,000	1320	100,000	n.d.	13.3	9800
151	Kallydica	325	< 5	161,000	508,000	1090	332,000			n.d.
152	Kammena Vourla	861	< 5	5100	762,000	1783	232,000	n.d.	5.92	n.d.
153	Kammena Vourla	797	< 5	1700	693,000	10,000	299,000	n.d.	8.92	6180
154	Kammena Vourla 2	700	3.50	< 200	644,000	3360	352,000	< 10	7.03	6050
155	Kammena Vourla 2	721	< 2	122	580,000	4000	393,000	< 5	5.66	n.d.
156	Kammena Vourla 2	727	< 5	218	588,000	4070	402,000	<5	6.28	5940
157	Thermopyles	326	<2	< 200	186,000	836	818,000	14.0	1.29	n.d.
158	Thermopyles	322	< 2	59	218,000	1010	760,000	< 5	1.07	1980
159	Thermopyles	240	< 2	709	176,000	859	831,000	< 10	1.15	6890
160	Leonidas	275	< 2	9200	242,000	799	726,000	< 5	n.d.	2600
161	Ikaria (Ag. Kyr.1)	58.0	< 5	86,600	860,000	< 0.5	35,900	n.d.	n.d.	n.d.
162	Kivotos 2	568	2.10	4780	793,000	184,000	17,400	n.d.	0.00	n.d.
163	Eftalou	1370	< 5	14,400	948,000	219	27,200	<5	12.77	10,400
164	Lisvori	471	< 5	52	21,000	20,500	445,000	<5	4.655	295
165	Polychnitos	192	< 5	3200	193,000	32,800	323,000	< 5	2.25	4690
166	Skala Sikaminias	1280	134	1400	657,000	70,500	259,000	<5	6.72	10,800
167	Kolpos Geras	1020	< 5	16,100	922,000	10	41,200	<5	14.30	9780
168	Pozar	475	< 5	61,700	652,000	0.60	289,000	n.d.	6.65	n.d.
169	Pozar	395	< 5	62,000	637,000	2490	269,000	n.d.	8.60	7760
170	Pozar	474	< 5	56,200	617,000	< 1	323,000	n.d.	10.17	7660
171	Loutra Ypatis	105	< 2	14,500	76,300	5810	887,600	385	0.85	848

ID	sample	He	H_2	O_2	N_2	CH_4	CO_2	H_2S	Ne	Ar
		ppm	ppm	ppm	ppm	ppm	ppm	ppm	ppm	ppm
172	Loutra Ypatis	139	< 5	200	25,400	5400	958,000	2500	0.17	n.d.
173	Ypatis	74.0	5.00	8400	52,400	4600	928,000	1400	n.d.	n.d.
174	Ypatis	14.0	0.60	104	42,400	4457	934,000	1260	2.31	742
175	Ypatis	112	< 10	1270	93,700	4570	900,000	n.d.	0.00	n.d.
176	Nea Tenedos	682	< 10	16,600	569,000	18.6	414,000	n.d.	0.00	n.d.
177	Smokovo	103	28.0	139	136,000	850,000	100	n.d.	1.89	1980
178	Smokovo	100	27.0	272	124,000	850,000	< 50	n.d.	7.49	n.d.
179	Psoroneria 1	887	< 0.5	< 200	427,000	1120	573,000	< 10	3.27	3940
180	Psoroneria 1	711	< 5	2100	342,000	707	657,000	n.d.	7.52	3490
181	Psoroneria 1	487	< 5	1700	336,000	631	658,000	< 10	4.72	4870
182	Psoroneria 2	526	< 5	< 200	311,000	742	674,000	n.d.	3.69	n.d.
183	Psoroneria 2	835	< 5	1900	422,000	1090	563,000	n.d.	11.4	n.d.
184	Psoroneria 2	890	< 5	< 200	367,000	643	624,000	n.d.	1.94	n.d.
185	Kolona	726		26,800	836,000	0.9	136,000	< 10	6.94	8680
186	Doumbia	537	< 10	9890	536,000	789	453,000	n.d.	0.00	n.d.
187	Nigrita	1.20	< 5	144	1300	26.0	988,000	n.d.	0.06	n.d.
188	Nigrita 1	40.0	<1	1610	647,000	95.3	351,000	n.d.	n.d.	n.d.
189	Sappes	214	< 10	613	994,000	1220	3680	n.d.	0.00	n.d.
190	Therma Limani	0.28	< 5	435	10,000	796,000	178,000	n.d.	0.25	n.d.
191	Therma Limani	0.10	15.0	53	7900	576,000	363,000	<5	0.14	150
192	Therma Limani	0.1	37.0	4300	19,000	717,000	264,000	< 10	0.2	n.d.
193	Kavala PR2					214,700				
194	Kavala SKA-1					861,000				
195	Angistro	< 20	< 1	166,000	824,000	202	6120	n.d.	0.00	n.d.
196	Elefteres	27.0	< 5	800	51,700	526	920,000	n.d.	0.71	626

ID	sample	He	H_2	O_2	N_2	CH_4	CO_2	H_2S	Ne	Ar
		ppm	ppm	ppm	ppm	ppm	ppm	ppm	ppm	ppm
197	Elefteres	32.0	< 5	211	105,000	598	895,000	<5	1.43	1720
198	Elefteres	31	< 5	689	72,600	703	921,000	< 5	0.68	1120
199	Eleftere agia marina	51	< 5	3400	180,000	756	809,000	< 5		n.d.
200	Krinides	< 20	1.12	90,800	899,000	333	9560	n.d.	0.00	n.d.
201	Langada	897	< 10	32,700	932,000	12.8	34,200	n.d.	0.00	n.d.
202	Nea Apollonia	1400	< 10	376	955,000	27,200	15,500	n.d.	0.00	n.d.
203	Nea Apollonia 3	1940	< 10	7490	981,000	3640	5870	n.d.	0.00	n.d.
204	Nea Kessani	28.0	< 5	9600	41,400	234	919,000	n.d.	2.70	n.d.
205	Nea Kessani	44.0	38.0	1170	9200	309	963,000	<5	0.14	196
206	Nea Kessani	26	< 5	5900	14,700	386	987,000	< 5		n.d.
207	Nigrita 2	14.2	< 10	15,300	188,000	134	797,000	n.d.	0.00	n.d.
208	Ninfopetra	2530	15.0	2700	968,000	1680	5400	n.d.	10.8	10,200
209	Ninfopetra	2630	< 5	3400	956,000	2910	5900	n.d.	39.9	n.d.
210	Paranesti 1	< 20	6.02	129,000	664,000	106	207,000	n.d.	0.00	n.d.
211	Paranesti 2	< 5	< 5	1700	8700	102	963,000	<5	n.d.	n.d.
212	Paranesti 3	< 20	42.2	26,900	416,000	29.9	553,000	n.d.	n.d.	n.d.
213	Giotrisi	128	97.0	1200	30,200	94,900	857,000	< 5	0.14	624
214	Giotrisi	260	803	3000	66,800	178,000	747,000	< 5	0.286	806
215	Giotrisi	325	648	23,700	141,000	155,000	662,000	< 10	0.54	n.d.
216	B Pigi	226	< 10	1920	651,000	128,000	218,000	n.d.	0.00	n.d.
217	A Pigi	125	6.87	6480	707,000	54,600	232,000	n.d.	n.d.	n.d.
218	Pool	< 20	80.3	103,000	734,000	104	163,000	n.d.	n.d.	n.d.
219	Thermopigi	33.0	< 5	800	13,600	622	978,000	< 10	0.23	n.d.
220	Thermopigi	15.0	< 5	639	13,300	669	967,000	<5	0.20	218
221	Thermopigi	19	< 5	1000	15,800	718	990,000	< 5		n.d.

ID	sample	He	H_2	O_2	N_2	CH_4	CO_2	H_2S	Ne	Ar
		ppm	ppm	ppm	ppm	ppm	ppm	ppm	ppm	ppm
222	Traianoupoli drill	3370	106	697	948,000	2970	4500	n.d.	0.00	n.d.
223	Traianoupoli drill	2730	216	2411	661,000	282,000	52,400	n.d.	0.00	n.d.
224	Thermes (Xanthi)	2242	< 5	9700	537,000	844	467,000	<5	6.93	8090
225	Thermes 1	154	66.5	19,700	884,000	1250	94,400	n.d.	0.00	n.d.
226	Thermes 3 (Xanthi)	1560	< 5	588	417,000	879	574,000	<5	n.d.	7350
227	Therma Xanthi 3	1630	< 2	2900	420,000	1190	575,000	< 10	5.11	n.d.
228	XNT-1 (Thermes)	2940	< 5	< 100	631,000	1010	346,000	n.d.	12.99	8270
229	Gyali	2.08	< 5	2800	9000	8.00	963,000	n.d.	0.50	217
230	Gyali	9	< 2	2200	23,300	68	955,600	< 5	0.32	354
231	Gyali	5	<2	3260	20,500	68	979,000	<5	1.0	330
232	Gyali lake	21	<2	716	139,000	525	870,000	3800	n.d.	n.d.
233	Gyali Nord	<4	<2	6110	11,800	2	983,000	<5	n.d.	186
234	Gyali West	5	31.0	1570	8300	21,000	970,000	<5	0.0	71
235	Gyali Nord	0.46	3.7	2600	9600	5	966,000	< 5	0.29	266
236	Katsouni	106	< 5	3800	478,000	115	490,000	n.d.	n.d.	n.d.
237	Katsouni	120	<2	11,500	855,000	134	155,000	<5	12.8	11,500
238	Lies	145	< 2	10,500	686,000	162	269,000	< 5	7.60	9790
239	Lies	197	<2	43,400	932,000	205	20,800	<5	n.d.	13,700
240	KKN1	3.30	295	3500	24,400	2400	980,000	673	n.d.	184
241	KKN1	4	2.3	535	4000	2700	972,000	2700	n.d.	n.d.
242	Kos Kokkinonero	< 5	< 5	46	12,300	515	966,000	n.d.	n.d.	191
243	Kos Kokkinonero	5.00	3.10	3200	13,600	2970	978,000	< 5	0.37	171
244	Kos Kokkinonero 2	6	<2	154	10,500	3620	994,000	<5	n.d.	105
245	Kos Kokkinonero 2	4.30	30.0	2700	8300	3140	991,000	< 5	n.d.	n.d.
246	Kos Kokkinonero 2	5	< 2	129	7200	3200	974,000	36	n.d.	109

ID	sample	He	H_2	O_2	N_2	CH_4	CO_2	H_2S	Ne	Ar
		ppm	ppm	ppm	ppm	ppm	ppm	ppm	ppm	ppm
247	Kefalos	24	15	3700	33,000	25,700	906,000	< 5	0.24	284
248	Kefalos	18	27.0	3290	25,100	23,900	946,000	<5	0.2	198
249	Kos Paradise	12.0	< 5	788	3600	9350	966,000	n.d.	0.30	n.d.
250	Kos Paradise	14	< 2	3100	8600	12,100	959,000	< 5	0.05	170
251	Kos Paradise	12	<2	1660	5800	10,000	980,000	<5	0.1	n.d.
252	Kos Paradise 2	16	<2	2216	7300	11,000	977,000	<5	n.d.	59
253	Kos Paradise 3	12	<2	798	4100	9650	987,000	<5	n.d.	26
254	KAT-1	412	< 2	2000	613,000	117,000	256,000	< 5	4.88	n.d.
255	Irini2 - KAT	446	<2	2210	989,000	6240	900	<5	10.6	7520
256	KAK-1	0.94	< 2	2600	6600	40	970,000	15	0.16	142
257	Irini - KAK	0.3	<2	6220	14,600	42	968,000	<5	0.2	194
258	Thiafi	0.54	106	200	4900	42.0	966,000	n.d.	0.16	117
259	Pallis	4.85	< 10	40,900	481,000	2.15	479,000	n.d.	0.00	n.d.
260	Thiafi	11.0	143	14,400	87,600	456	881,000	n.d.	n.d.	n.d.
261	Thiafisea	20.0	29.0	6700	42,200	717	942,000	n.d.	0.87	n.d.
262	Thiafi sea	22	< 2	34,100	103,000	916	832,000	< 5	n.d.	n.d.
263	Thiafi sea	<4	2.0	1840	9100	132	974,000	8200	n.d.	63
264	Thiafi sea2	<4	19.0	5740	20,000	95	968,000	<5	n.d.	283
265	Thiafi sea3	< 4	84	3700	16,900	155	979,000	4700	n.d.	n.d.
266	Ag. Kyriaki	26	5.0	19,700	67,600	3670	908,000		n.d.	n.d.
267	Skinopi	63.0	< 5	16,700	73,700	4630	829,000	n.d.	n.d.	n.d.
268	Skinopi	44	3.0	5500	30,300	2370	939,000		n.d.	n.d.
269	Mandrakia	12.0	< 3	5000	19,400	2284	973,000		n.d.	n.d.
270	Pausanias sea	< 5	< 5	6100	14,500	32	984,000	< 5	n.d.	214
271	Pausanias sea	20	3.0	44,000	498,000	219	456,000	<5	n.d.	9780

ID	sample	He	H_2	O_2	N_2	CH_4	CO_2	H_2S	Ne	Ar
		ppm	ppm	ppm	ppm	ppm	ppm	ppm	ppm	ppm
272	KVO1	36	65	814	30,500	20,600	926,000	62	n.d.	n.d.
273	KVO2	34	1980	10,100	75,400	21,000	877,000	54	n.d.	659
274	KVO33	44	49	340	12,400	23,500	943,000	1200	n.d.	n.d.
275	KVO52	44	2.9	317	4000	23,100	947,000	851	0.04	31
276	Thermia (Kos)	27.0	< 5	655	44,700	285	930,000	n.d.	0.13	769
277	Thermia (Kos)	2.43	< 5	1100	8900	51.0	995,000	< 5	0.83	211
278	Thermia (Kos)	2.5	<2	535	9300	64	989,000	<5	0.1	98
279	Thermia sea (Kos)	16	<2	2500	42,400	278	955,000	<5	0.4	701
280	Methana	12.0	< 5	54,300	313,000	4.50	642,000	n.d.	n.d.	n.d.
281	Methana	14.3	< 10	1660	442,000	632	555,000	n.d.	0.00	n.d.
282	Methana	10.0	< 5	67,300	382,000	5.00	548,000	n.d.	n.d.	n.d.
283	Methana 2	10.0	< 5	64,400	385,000	8.00	551,000	n.d.	n.d.	n.d.
284	Ag. Nicholaos	5.24	221	66,900	451,000	4.54	482,000	n.d.	0.00	n.d.
285	Pausanias	< 5	< 5	< 400	10,700	26.0	991,000	n.d.	n.d.	n.d.
286	Pausanias	0.50	< 5	5600	30,900	17.0	970,000	n.d.	0.21	n.d.
287	Pausanias	3.89	< 5	2300	12,900	53	983,000	< 5	6.24	222
288	Pausanias fracture	13.0	7.00	88,100	383,000	3.50	519,000	n.d.	n.d.	n.d.
289	Pausanias mofette	27.0	< 5	61,300	261,000	1.20	671,000	n.d.	n.d.	n.d.
290	Thiafi	6	< 2	80,300	348,000	152	560,000	72	n.d.	n.d.
291	Milos 1 (Skinopi)	50.0	< 5	9200	39,100	2640	944,000	n.d.	3.07	n.d.
292	Adamas F70	12	1610	2300	11,200	2130	979,000	1800	n.d.	n.d.
293	Milos 3 (Paleochori)	14.0	29.0	3800	12,500	7450	957,000	n.d.	n.d.	n.d.
294	Paleochori cave	10	2644	4800	26,800	1660	930,000	18,500	n.d.	n.d.
295	Paleochori1	10	22200	3700	15,900	1670	901,000	35,300	n.d.	n.d.
296	Paleochori2	15.0	31700	4100	18,500	2430	887,000	21,100	0.3	n.d.

ID	sample	He	H_2	O_2	N_2	CH_4	CO_2	H_2S	Ne	Ar
		ppm	ppm	ppm	ppm	ppm	ppm	ppm	ppm	ppm
297	Milos 6 (Paleochori)	80.0	149,000	52,100	144,000	11,000	657,000	n.d.	n.d.	n.d.
298	Milos C3 (Fyriplaka)	8.00	1870	145,000	581,000	471	264,000	n.d.	n.d.	n.d.
299	Milos DEH	8.00	< 5	2200	9600	818	978,000	n.d.	n.d.	257
300	Milos 2 (Adamas DEH)	15.0	13.0	425	20,700	1400	966,000	n.d.	2.22	n.d.
301	Milos Mad 1 (DEH)	69.0	< 5	2800	73,000	4880	896,000	n.d.	1.89	1950
302	DEH	15	< 3	14,800	65,700	1420	924,000	n.d.	n.d.	n.d.
303	Milos MZR-1	27.0	< 5	331	31,200	2640	961,000	n.d.	n.d.	n.d.
304	Milos Paleochori	14.0	30,600	3000	14,800	2300	906,000	n.d.	0.20	n.d.
305	Milos Paleochori 3	49.0	< 5	12,000	62,900	7930	901,000	n.d.	2.59	n.d.
306	Milos Paleochori 4	37.0	< 5	13,800	52,700	6610	905,000	n.d.	1.77	n.d.
307	Spathi bay 1	18	6.0	2700	11,900	3160	936,000	8400	n.d.	n.d.
308	Spathi bay 2	12	4700	200	5100	2560	921,000	27,400	n.d.	n.d.
309	Kalamos 35	8	3170	108,000	483,000	650	392,000	400	n.d.	n.d.
310	Voudia	5	4.0	6100	24,600	850	966,000	3100	n.d.	n.d.
311	A13 Nisyros	27.0	11,900	67	1500	536	764,000	255,000	0.30	16
312	A13 Nisyros	21.0	9540	100	1390	1460	813,000	175,000	0.09	n.d.
313	A13 Nisyros	20	8560	1200	7500	1560	814,000	149,000	0.4	n.d.
314	PP9N Nisyros	19.0	14,100	570	3300	1890	761,000	n.d.	0.99	n.d.
315	PP9N Nisyros	17.0	15,100	1200	5200	1670	743,000	255,000	0.14	65
316	S15 Nisyros	29.0	6590	1200	5200	2700	768,000	n.d.	0.37	n.d.
317	S15 Nisyros	23.0	7880	471	2500	3170	777,000	228,000	n.d.	27
318	S15 Nisyros	19.0	8050	700	21,900	4350	769,000	192,000	2.87	n.d.
319	AM Nisyros	33.0	9230	500	6200	805	809,000	n.d.	3.58	n.d.
320	AM Nisyros	33.0	12,100	509	3900	562	762,000	n.d.	0.75	n.d.
321	AM Nisyros	25.0	11,400	50	3800	833	772,000	n.d.	0.17	n.d.

ID	sample	He	H_2	O_2	N_2	CH_4	CO_2	H_2S	Ne	Ar
		ppm	ppm	ppm	ppm	ppm	ppm	ppm	ppm	ppm
322	K6 Nisyros	19.0	5850	505	24,200	23,600	880,000	n.d.	2.82	n.d.
323	K6 Nisyros	18.0	12,600	668	4100	12,300	876,000	n.d.	0.25	n.d.
324	K6 Nisyros	13.0	12,000	517	18,900	13,600	864,000	87,600	0.27	203
325	K7 Nisyros	11.0	7030	n.d.	3600	31,400	884,000	61,100	0.49	n.d.
326	K7 Nisyros	10	7130	1900	8400	33,900	882,000	45,400	0.277	n.d.
327	K7 Nisyros	10	6670	695	6300	32,400	891,000	47,600	0.4	n.d.
328	PP9S Nisyros	30.0	16,000	1600	8100	1760	743,000	n.d.	9.37	n.d.
329	PP9S Nisyros	30.0	18,600	2500	11,700	1790	734,000	n.d.	1.28	n.d.
330	PP9S Nisyros	16.0	14,800	n.d.	2500	2520	779,000	173,000	0.04	n.d.
331	S4 Nisyros	25.0	6520	185	2100	3570	779,000	236,000	0.30	20
332	S4 Nisyros	19.0	5960	8200	63,000	5060	717,000	170,000	0.07	n.d.
333	S4 Nisyros	20	8240	581	6500	7510	822,000	151,000	0.7	n.d.
334	Lefkos	18	51.0	459,000	415,000	575	142,000	<5	n.d.	n.d.
335	Erinia	245	< 5	42,800	651,000	1300	301,000	< 5	7.54	7220
336	Santorini Kameni B	7.00	11,700	40,800	178,000	119	758,000	n.d.	3.37	n.d.
337	Nea Kameni	6	8100	83,600	367,000	264	526,000	n.d.	6.543	5150
338	Santorini SK3 (N.Kameni)	< 5	< 5	20,100	48,800	3.20	941,000	n.d.	n.d.	n.d.
339	SNK1	6.00	10,100	60,300	278,000	300	643,000	< 5	6.39	n.d.
340	Palea Kameni	4.83	< 5	23,300	42,000	2.4	945,000	n.d.	0.955	1520
341	Palea Kameni	1.10	0.03	750	6400	4.10	980,000	n.d.	0.28	n.d.
342	Palea Kameni	1.77	< 5	3000	6200	6.00	979,000	n.d.	0.16	n.d.
343	Sousaki well	0.94	56.0	2100	11,500	40.0	972,000	5500	0.13	n.d.
344	Sousaki well	1.22	11.0	397	2400	32.0	1,000,000	3270	0.06	n.d.
345	Sousaki well	1.29	10.0		7500	33.0	975,000	2500	0.15	95

ID	sample	He	H_2	O_2	N_2	CH_4	CO_2	H_2S	Ne	Ar
		ppm	ppm	ppm	ppm	ppm	ppm	ppm	ppm	ppm
346	Sousaki big cave	36.0	< 5	362	24,100	10,600	947,000	1200	0.09	n.d.
347	Sousaki big cave	34.0	< 5	2100	32,100	11,000	945,000	n.d.	0.33	n.d.
348	Sousaki big cave	33	< 5	4100	37,400	10,100	938,000	511	0.42	279
349	Sousaki small cave	31.7	< 3	2200	30,200	8100	963,000	1500	n.d.	n.d.
350	Sousaki small cave	33.0	1.80	2500	33,500	11,500	959,000	425	0.47	n.d.
351	Sousaki small cave	31	< 3	6600	46,800	9730	921,000	512	0.559	258
352	Sousaki cave 3	26.0	< 5	4400	59,700	6250	926,000	< 10	0.73	n.d.

Table 5: Chemical composition of the gases (extracted database)

N.	sample	He	H_2	O_2	N_2	CH_4	CO_2	H_2S	Ar
		µmol/mol	µmol/mol	µmol/mol	µmol/mol	µmol/mol	µmol/mol	µmol/mol	µmol/mol
1	Katakali	4.0	11	589	82,500	880,000	25,000	< 5	1640
2	Psoroneria	887	< 0.5	100	427,000	1120	573,000	< 10	3940
3	Psoroneria	487	< 2	1700	336,000	631	658,000	< 5	3900
4	Thermopyles	322	< 2	59	218,000	1010	760,000	< 5	1980
5	Thermopyles	240	< 2	709	176,000	859	831,000	< 5	1910
6	Koniavitis	581	< 5	50	701,000	2090	281,000	2200	8340
7	Kammena Vourla	700	3.5	100	644,000	3360	352,000	< 10	6050
8	Kammena Vourla	727	< 5	218	588,000	4070	402,000	< 5	5940
9	Kallydica	325	< 2	161,000	508,000	1090	332,000	< 5	n.d.
10	Gialtra	112	< 5	137,000	765,000	302	44,000	n.d.	n.d.
11	Thermopotamos	0.4	< 5	1200	2800	27	977,000	48	40
12	Thermopotamos	1.5	< 2	4700	18,400	1200	958,500	< 5	275
13	Patra	1.7	50	301	192,000	704,000	11,100	< 5	3500
14	Sousaki well	1.3	10	1700	7500	33	975,000	2500	95
15	Sousaki cave	33.0	< 5	4100	37,400	10,100	937,000	511	279
16	Ilion	100	< 5	940	78,900	1820	899,000	< 5	733
17	Ilion	100	3.7	1100	79,400	1800	901,000	< 5	742
18	Ilion sea	199	< 2	11,300	271,000	1040	694,000	< 5	5030
19	Pausanias	< 5	< 5	2300	12,900	53	983,000	< 5	222
20	Pausanias sea	< 5	< 5	6100	14,500	32	984,000	< 5	214
21	Thiafi sea	22.0	< 2	34,100	103,000	916	832,000	< 5	n.d.
22	Agia paraskevi sea	3.1	21.0	10,600	27,000	470	964,000	< 5	458
23	Agia paraskevi sea 2	92.0	100	3900	40,500	11,000	946,000	3100	555
24	Xyna	91.0	1.6	13,000	49,600	215	943,000	< 5	815
25	PPG-1	0.4	< 2	50	40,100	913,000	21,400	< 5	1180
26	Soulanta	31.0	22	125	350,000	649,000	25	n.d.	n.d.
27	Smokovo	100	27	272	124,000	850,000	25	n.d.	n.d.
28	Ekkara	4.0	16	177,000	750,000	5720	25	n.d.	n.d.
29	Ekkara creek	21.0	11	2500	888,000	77,700	552	< 5	10,200
30	Ypati	14.0	0.6	104	42,400	4460	934,000	1260	742
31	Loutra Ypatis	105	< 2	14,500	76,300	5810	888,000	385	848
32	Leonidas	275	< 2	9200	242,000	799	726,000	< 5	2600
33	Kokkinonero	1.6	< 5	2500	7200	249	955,000	n.d.	195
34	Kokkinonero 2	209	< 5	4300	382,000	867	581,000	n.d.	5040

N.	sample	He	H_2	O_2	N_2	CH_4	CO_2	H_2S	Ar
		µmol/mol	µmol/mol	µmol/mol	µmol/mol	µmol/mol	µmol/mol	µmol/mol	µmol/mol
35	Edipsos stadium	< 4	< 2	525	3000	689	967,000	< 5	57
36	Ag. Paraskevi	4.3	< 5	158	23,500	521	929,000	17,400	502
37	Giatsovo soil	12.5	2.0	760	20,800	2690	987,000	< 5	622
38	Analipsi	19.2	< 2	4600	29,600	2350	952,000	< 5	128
39	Tropeouchos	29.0	< 5	76	20,000	6200	952,000	n.d.	233
40	Mesochori gas	4.0	1.5	1000	6500	479	985,000	< 5	42
41	Mesochori 3	1.1	< 5	50	2100	214	975,000	< 5	29
42	Synergio	0.4	< 5	187	1100	<0.5	997,000	< 5	24
43	Sarri	0.3	< 5	93	1400	95	983,000	n.d.	62
44	Itea	36.0	1.4	5700	38,300	2600	951,000	< 5	223
45	Pozar	474	< 5	56,200	617,000	< 1	323,000	< 5	7660
46	Promachoi	223	< 5	54,400	827,000	2.0	108,000	n.d.	9090
47	Loutrochori 2	374	< 5	175	510,000	436,000	32,400	< 5	6290
48	Xino Nero (Kilkis)	< 5	< 5	2900	15,200	23	965,000	< 5	304
49	Xino Nero 2 (Kilkis)	6.0	< 5	7300	26,000	82	939,000	< 5	n.d.
50	Sani	762	12	330	226,000	764,000	1500	< 5	870
51	Thermopigi	15.0	< 5	639	13,300	669	967,000	< 5	218
52	Eleftheres	31.0	< 2	690	72,600	703	921,000	< 5	1180
53	Polychnitos	192	< 5	3200	193,000	32,800	766,000	< 5	4690
54	Lisvori	471	< 5	5200	519,000	20,500	444,000	< 5	7300
55	Eftalou	1370	< 5	14,400	948,000	219	27,200	< 5	10,400
56	Skala Sikaminias	1280	134	1400	657,000	70,500	259,000	< 5	10,800
57	Kolpos Geras	1020	< 5	16,100	922,000	10	41,200	< 5	9780
58	Milos Skinopi	63.0	< 5	16,700	73,700	4630	829,000	n.d.	n.d.
59	Milos DEH	8.0	< 5	2200	9600	818	978,000	n.d.	n.d.
60	Kefalos	18.0	27	3290	25,100	23,900	946,000	< 5	105
61	Kos Paradise	14.0	< 2	3100	8600	12,100	959,000	< 5	170
62	Kos Kokkinonero	5.0	3.1	3200	13,600	2970	978,000	< 5	171
63	KKN1	3.3	295	3500	24,400	2400	980,000	673	n.d.
64	Kos Kokkinonero 2	4.3	30	2700	8300	3140	991,000	< 5	n.d.
65	KVO2	34.0	1980	10,100	75,400	21,000	877,000	54	n.d.
66	KVO52	44.0	2.9	317	4000	23,100	947,000	851	31
67	Ag. Irini 2	446	< 2	2210	989,000	6240	900	< 5	7520
68	Ag. Irini 1	0.9	< 2	3900	9200	24	963,000	15	200

N.	sample	He	H_2	O_2	N_2	CH_4	CO_2	H_2S	Ar
69	Gyali nord	0.5	3.7	2600	9600	5.0	966,000	< 5	266
70	Gyali	9.0	< 2	2200	23,300	68	956,000	< 5	354
71	Gyali lake	21.0	< 2	716	139,000	525	869,000	3800	n.d.
72	Gyali west	5.0	31	1570	8300	21,000	970,000	< 5	71
73	Katsouni	120	< 2	11,500	855,000	134	155,400	< 5	11,500
74	Lies	135	< 2	18,800	643,000	140	315,200	< 5	9790
75	Nea Kessani	26.0	< 2	5900	14,700	386	987,000	< 5	208
76	Eleftheres Ag. Marina	51.0	< 2	3400	180,000	756	809,300	< 5	2760
77	Paranesti 2	< 5	< 5	1700	8700	102	963,200	< 5	n.d.
78	Thermes (Xanthi)	2240	< 5	9700	537,000	844	467,000	< 5	8090
79	Thermes 3 (Xanthi)	1570	< 5	588	417,000	879	573,900	< 5	7350
80	Thermia (Kos)	2.4	< 5	1100	8900	51	994,600	< 5	211
81	Thermia sea (Kos)	16.0	< 2	2500	42,400	278	955,000	< 5	98
82	Therma Limani	0.10	15	53	7900	576,000	363,000	< 5	150
83	Geotrisi	128	97	1200	30,200	94,900	857,000	< 5	624
84	Ag. Anargyroi Kithnos	1100	< 2	2800	664,000	833	329,000	< 5	8420
85	Kolona	726	< 2	26,800	836,000	0.90	136,000	< 5	8400
86	Nea Kameni	6.0	8100	83,600	367,000	264	526,000	< 5	4740
87	Erinia (N. Kameni)	245	< 2	42,800	651,000	1300	301,000	< 5	9510
88	Ag. Anargyroi	< 5	48	14,700	957,000	27,000	1360	n.d.	n.d.
89	Ag. Anargyroi 2	< 5	17	18,200	779,000	203,000	250	n.d.	n.d.
90	Archani	12.9	< 10	7420	948,000	44,700	18	n.d.	n.d.
91	Lysimachia	9.9	< 10	978	602,000	363,000	34,800	n.d.	n.d.
92	Kaitsa	123	< 10	3070	655,000	316,000	26,200	300	n.d.
93	Amplas	83.4	27	1780	199,000	800,000	29	n.d.	n.d.
94	Platystomo	345	< 10	907	860,000	128,000	10,700	n.d.	n.d.
95	PP9S Nisyros	16.0	14,800	100	2500	2520	779,000	173,000	n.d.
96	S4 Nisyros	20.0	8240	581	6500	7510	822,000	151,000	n.d.
97	A13 Nisyros	21.0	9540	100	1390	1460	813,000	175,000	n.d.
98	S15 Nisyros	19.0	8050	700	21,900	4350	769,000	192,000	n.d.
99	K7 Nisyros	10.0	6670	695	6300	32,400	891,000	47,600	n.d.
100	Thermia (Kos)	2.5	<2	535	9300	64	989,000	<5	98
101	Ag. Irini 2	412	< 2	2000	613,000	117,000	256,000	< 5	n.d.

n.d. = not determined

Table 6: Isotope values of the gases (general database)

ID	$\delta^{13}C\text{-}CO_2$	$\delta^{13}C\text{-}CH_4$	$\delta^{2}H\text{-}CH_4$	R/R_A	R/R_Acor	$^4He/^{20}Ne$
	‰	‰	‰			
1	n.d.	n.d.	n.d.	1.19	-	0.34
2	-10.5	-61.2	n.d.	1.02	-	0.34
3	-13.5	n.d.	n.d.	0.66	0.32	0.57
4	n.d.	n.d.	n.d.	0.08	0.08	119
5	n.d.	-36.1	-140	n.d.	n.d.	n.d.
6	n.d.	-31.2	-135	n.d.	n.d.	n.d.
7	n.d.	n.d.	n.d.	n.d.	n.d.	n.d.
8	-5.1	-33.3	n.d.	0.04	0.04	43.1
9	n.d.	-34.4	-124	n.d.	n.d.	n.d.
10	n.d.	-49.0	-174	n.d.	n.d.	n.d.
11	-15.4	-51.6	n.d.	0.05	0.03	12.5
12	n.d.	n.d.	n.d.	0.04	0.04	810
13	-13.5	n.d.	n.d.	0.22	0.08	1.81
14	-29.5	-72.3	-174	n.d.	n.d.	n.d.
15	-7.0	-74.5	-210	0.41	0.00	0.77
16	-14.1	-79.8	-211	0.39	-	0.59
17	n.d.	n.d.	n.d.	1.03	-	0.33
18	-12.6	n.d.	n.d.	0.59	0.32	0.72
19	-21.2	n.d.	n.d.	0.10	0.05	5.45
20	-17.5	n.d.	n.d.	0.43	0.23	1.07
21	-11.1	n.d.	n.d.	0.46	0.07	0.75
22	-10.3	n.d.	n.d.	0.14	0.14	307
23	n.d.	n.d.	n.d.	n.d.	n.d.	n.d.
24	n.d.	-47.5	-166	n.d.	n.d.	n.d.
25	-6.1	n.d.	n.d.	0.08	0.07	35.9
26	-7.3	-37.5	-203	n.d.	n.d.	n.d.
27	n.d.	-50.2	n.d.	0.05	0.04	55.9

ID	$\partial^{13}C$-CO_2	$\partial^{13}C$-CH_4	$\delta^{2}H$-CH_4	R/R_A	R/R_Acor	$^{4}He/^{20}Ne$
	‰	‰	‰			
28	n.d.	n.d.	n.d.	n.d.	n.d.	n.d.
29	n.d.	-50.5	-200	n.d.	n.d.	n.d.
30	n.d.	-44.7	n.d.	0.37	-	0.75
31	n.d.	-35.0	-288	0.38	0.01	0.84
32	n.d.	-37.9	-247	n.d.	n.d.	n.d.
33	n.d.	n.d.	n.d.	n.d.	n.d.	n.d.
34	n.d.	-18.0	-188	n.d.	n.d.	n.d.
35	n.d.	-54.5	-343	n.d.	n.d.	n.d.
36	n.d.	-74.5	-275	n.d.	n.d.	n.d.
37	n.d.	-72.0	-250	n.d.	n.d.	n.d.
38	n.d.	-32.2	-110	n.d.	n.d.	n.d.
39	n.d.	-33.9	-273	n.d.	n.d.	n.d.
40	n.d.	n.d.	n.d.	0.34	0.24	2.05
41	n.d.	-30.1	-223	n.d.	n.d.	n.d.
42	n.d.	-24.7	-205	n.d.	n.d.	n.d.
43	n.d.	-37.0	-215	n.d.	n.d.	n.d.
44	n.d.	-33.5	-234	0.30	-	0.99
45	n.d.	-43.4	-159	n.d.	n.d.	n.d.
46	n.d.	-14.5	-101	n.d.	n.d.	n.d.
47	n.d.	-28.6	-242	n.d.	n.d.	n.d.
48	-16.3	n.d.	n.d.	0.93	0.92	3.35
49	-20.1	n.d.	n.d.	0.84	0.50	0.41
50	n.d.	-49.2	-62	0.08	0.04	8.73
51	n.d.	n.d.	n.d.	n.d.	n.d.	n.d.
52	n.d.	-30.4	-133	n.d.	n.d.	n.d.
53	n.d.	-30.3	-143	n.d.	n.d.	n.d.
54	0.01	n.d.	n.d.	0.50	0.50	77.2
55	0.25	n.d.	n.d.	0.27	0.24	9.78

ID	$\partial^{13}C$-CO_2	$\partial^{13}C$-CH_4	$\delta^{2}H$-CH_4	R/R_A	R/R_Acor	$^{4}He/^{20}Ne$
	‰	‰	‰			
56	-0.4	-23.0	n.d.	n.d.	n.d.	n.d.
57	n.d.	n.d.	n.d.	0.47	0.47	189
58	-0.5	n.d.	n.d.	n.d.	n.d.	n.d.
59	-0.6	-21.0	-79	n.d.	n.d.	n.d.
60	-0.3	-21.3	n.d.	n.d.	n.d.	n.d.
61	-0.6	-14.7	-62	n.d.	n.d.	n.d.
62	-1.7	n.d.	n.d.	0.46	0.40	3.15
63	-0.3	n.d.	n.d.	0.24	0.24	31.1
64	-1.3	n.d.	n.d.	0.21	0.20	186
65	n.d.	n.d.	n.d.	0.23	0.22	29.7
66	-1.6	n.d.	n.d.	0.61	0.55	2.70
67	-1.5	n.d.	n.d.	0.66	0.64	5.95
68	-1.6	n.d.	n.d.	n.d.	n.d.	n.d.
69	-2.1	n.d.	n.d.	0.78	0.76	4.10
70	-0.4	-22.5	n.d.	0.66	0.66	50.7
71	-1.7	n.d.	n.d.	0.64	0.63	23.0
72	n.d.	n.d.	n.d.	0.62	0.60	5.11
73	-1.7	n.d.	n.d.	n.d.	n.d.	n.d.
74	-1.6	n.d.	n.d.	0.82	0.80	3.35
75	-1.1	n.d.	n.d.	0.28	0.26	11.3
76	n.d.	n.d.	n.d.	0.56	0.45	1.57
77	-1.4	n.d.	n.d.	n.d.	n.d.	n.d.
78	-0.9	n.d.	n.d.	0.30	0.30	227
79	-0.3	n.d.	n.d.	0.28	0.28	41.2
80	n.d.	n.d.	n.d.	0.30	0.29	15.3
81	0.1	-27.3	-151	0.32	0.30	11.7
82	0.3	n.d.	n.d.	0.30	0.30	309

ID	$\partial^{13}C$-CO_2	$\partial^{13}C$-CH_4	$\delta^{2}H$-CH_4	R/R_A	R/R_Acor	$^{4}He/^{20}Ne$
	‰	‰	‰			
83	-1.2	-29.4	-187	n.d.	n.d.	n.d.
84	-2.0	n.d.	n.d.	n.d.	n.d.	n.d.
85	-2.1	n.d.	n.d.	n.d.	n.d.	n.d.
86	-3.7	n.d.	n.d.	n.d.	n.d.	n.d.
87	-1.6	n.d.	n.d.	1.11	-	0.42
88	-0.8	n.d.	n.d.	0.57	0.43	1.36
89	-9.3	n.d.	n.d.	n.d.	n.d.	n.d.
90	-2.8	n.d.	n.d.	n.d.	n.d.	n.d.
91	-1.6	n.d.	n.d.	1.20	1.26	1.34
92	-1.8	n.d.	n.d.	n.d.	n.d.	n.d.
93	n.d.	n.d.	n.d.	n.d.	n.d.	n.d.
94	-7.6	n.d.	n.d.	0.20	0.16	6.67
95	-3.5	n.d.	n.d.	n.d.	n.d.	n.d.
96	-2.6	n.d.	n.d.	0.33	0.31	12.0
97	-2.4	1.1	n.d.	0.26	0.24	14.8
98	n.d.	n.d.	n.d.	n.d.	n.d.	n.d.
99	-22.5	n.d.	n.d.	n.d.	n.d.	n.d.
100	-16.0	-16.2	n.d.	0.14	0.14	113
101	-16.0	-18.8	-113	0.15	0.15	54.9
102	-18.7	n.d.	n.d.	n.d.	n.d.	n.d.
103	-3.0	n.d.	n.d.	0.35	0.33	5.20
104	-6.4	n.d.	n.d.	0.33	0.31	4.56
105	-24.3	-25.4	n.d.	0.10	0.09	15.7
106	-24.5	-42.3	-154	0.06	0.05	17.1
107	n.d.	-42.2	-175	n.d.	n.d.	n.d.
108	-7.2	n.d.	n.d.	1.27	1.27	30.3
109	-7.4	n.d.	n.d.	1.27	1.27	30.3

ID	$\partial^{13}C$-CO_2	$\partial^{13}C$-CH_4	$\delta^{2}H$-CH_4	R/R_A	R/R_Acor	$^{4}He/^{20}Ne$
	‰	‰	‰			
110	n.d.	n.d.	n.d.	1.36	1.37	17.9
111	n.d.	-58.4	n.d.	0.63	0.63	1000
112	-9.7	-57.0	-178	n.d.	n.d.	n.d.
113	n.d.	n.d.	n.d.	0.68	0.68	1000
114	-29.9	-79.7	n.d.	0.14	0.08	4.07
115	-9.4	n.d.	n.d.	0.28	0.26	12.7
116	-1.0	-15.5	n.d.	0.35	0.33	12.7
117	-0.8	-19.8	-37	0.23	0.11	2.35
118	n.d.	n.d.	n.d.	n.d.	n.d.	n.d.
119	-2.2	5.9	n.d.	0.28	0.27	69.8
120	n.d.	n.d.	n.d.	n.d.	n.d.	n.d.
121	n.d.	-2.0	-127	0.97	0.96	0.82
122	n.d.	-26.6	-301	0.87	0.81	0.93
123	n.d.	n.d.	n.d.	n.d.	n.d.	n.d.
124	n.d.	n.d.	n.d.	0.81	-	0.44
125	n.d.	-60.8	-248	0.07	0.03	7.82
126	-14.1	n.d.	n.d.	0.41	0.30	1.09
127	-5.6	n.d.	n.d.	1.32	1.35	3.05
128	-1.4	n.d.	n.d.	n.d.	n.d.	n.d.
129	-6.7	-3.8	n.d.	0.74	0.72	5.86
130	n.d.	n.d.	n.d.	0.79	-	0.61
131	n.d.	n.d.	n.d.	0.74	0.74	308
132	-9.8	-10.6	n.d.	n.d.	n.d.	n.d.
133	-9.3	-12.7	nd	n.d.	n.d.	n.d.
134	-9.7	-21.7	-74	n.d.	n.d.	n.d.
135	-2.5	-24.1	n.d.	0.35	0.34	32.7
136	-3.0	n.d.	n.d.	0.42	0.42	54.9

ID	$\partial^{13}C$-CO_2	$\partial^{13}C$-CH_4	$\delta^{2}H$-CH_4	R/R_A	R/R_Acor	$^{4}He/^{20}Ne$
	‰	‰	‰			
137	n.d.	2.50	n.d.	0.28	0.28	107
138	n.d.	2.00	74	0.27	0.27	193
139	-2.5	3.15	32	0.25	0.25	252
140	-2.5	45.0	n.d.	n.d.	n.d.	n.d.
141	n.d.	n.d.	n.d.	n.d.	n.d.	n.d.
142	-2.6	n.d.	n.d.	0.39	0.38	195
143	-3.0	n.d.	n.d.	n.d.	n.d.	n.d.
144	-2.9	n.d.	n.d.	1.03	1.04	2.05
145	-3.1	-21.4	-115	0.43	0.40	8.50
146	-2.7	-21.7	-124	0.44	0.38	3.2
147	-4.7	-21.7	n.d.	n.d.	n.d.	n.d.
148	-8.3	n.d.	n.d.	0.40	0.39	16.1
149	-10.7	n.d.	n.d.	0.44	0.44	80.6
150	-8.1	-9.8	n.d.	0.42	0.42	41.3
151	-13.3	5.3	n.d.	n.d.	n.d.	n.d.
152	-9.4	n.d.	n.d.	0.48	0.48	222
153	-7.2	-64.8	n.d.	0.52	0.51	96.4
154	n.d.	n.d.	n.d.	0.53	0.53	159
155	-7.3	10.3	50	0.52	0.52	128
156	-7.5	4.6	60	0.51	0.51	106
157	n.d.	0.9	29	0.22	0.22	258
158	-5.3	1.4	30	0.20	0.20	228
159	-5.3	-4.2	79	0.20	0.20	208
160	-6.0	n.d.	n.d.	n.d.	n.d.	n.d.
161	-19.6	n.d.	n.d.	n.d.	n.d.	n.d.
162	-23.9	n.d.	n.d.	0.02	0.00	14.3
163	-11.8	n.d.	n.d.	0.83	0.83	103

ID	$\partial^{13}C$-CO_2	$\partial^{13}C$-CH_4	$\delta^{2}H$-CH_4	R/R_A	R/R_Acor	$^{4}He/^{20}Ne$
	‰	‰	‰			
164	-3.9	-7.2	-21	0.85	0.85	97.0
165	-2.0	-19.9	-106	0.82	0.82	82.2
166	-5.5	-24.8	n.d.	0.92	0.92	183
167	-9.0	n.d.	n.d.	0.43	0.43	67.1
168	-5.1	n.d.	n.d.	0.72	0.72	68.2
169	-6.6	n.d.	n.d.	0.71	0.71	50.4
170	-5.4	n.d.	n.d.	0.82	0.82	44.5
171	-4.4	-32.8	-104	0.05	0.05	122
172	n.d.	n.d.	n.d.	0.06	0.06	974
173	-5.2	n.d.	n.d.	n.d.	n.d.	n.d.
174	-3.2	-38.7	n.d.	0.13	0.08	6.30
175	n.d.	-35.0	-104	0.09	0.08	38.3
176	-5.8	n.d.	n.d.	0.49	0.49	55.8
177	n.d.	-47.9	n.d.	0.05	0.04	55.1
178	n.d.	-44.9	-196	0.04	0.03	44.0
179	n.d.	-2.3	129	0.07	0.07	281
180	n.d.	16.9	264	0.06	0.06	273
181	-5.4	10.9	301	0.07	0.07	95.1
182	-6.1	n.d.	n.d.	0.08	0.07	136
183	-5.8	n.d.	n.d.	0.07	0.06	42.3
184	-5.3	n.d.	n.d.	0.08	0.08	660
185	n.d.	n.d.	n.d.	0.51	0.50	96.4
186	-5.1	n.d.	n.d.	0.40	0.39	12.1
187	-1.7	n.d.	n.d.	0.33	0.32	20.1
188	-3.4	n.d.	n.d.	n.d.	n.d.	n.d.
189	-13.8	n.d.	n.d.	0.30	0.25	4.05
190	-16.3	-45.9	-270	1.69	1.97	1.11

ID	$\partial^{13}C$-CO_2	$\partial^{13}C$-CH_4	$\delta^{2}H$-CH_4	R/R_A	R/R_Acor	$^{4}He/^{20}Ne$
	‰	‰	‰			
191	6.0	-44.6	-263	0.72	-	0.74
192	4.3	-45.7	-252	1.21	1.40	0.67
193	n.d.	-34.2	-185	n.d.	n.d.	n.d.
194	n.d.	-55.5	-210	n.d.	n.d.	n.d.
195	-15.6	n.d.	n.d.	0.59	0.56	3.60
196	-0.8	n.d.	n.d.	0.48	0.47	19.0
197	-1.5	-21.3	n.d.	0.41	0.40	24.6
198	n.d.	n.d.	n.d.	0.41	0.41	36.5
199	n.d.	n.d.	n.d.	n.d.	n.d.	n.d.
200	-13.6	n.d.	n.d.	0.38	0.20	1.27
201	-9.9	n.d.	n.d.	0.06	0.06	119
202	-10.0	-39.3	n.d.	0.06	0.06	77.0
203	-11.2	n.d.	n.d.	0.06	0.06	120
204	n.d.	-26.8	n.d.	0.53	0.52	8.51
205	-0.3	-30.5	n.d.	0.48	0.48	243
206	n.d.	n.d.	n.d.	n.d.	n.d.	n.d.
207	-1.0	n.d.	n.d.	0.32	0.28	2.84
208	n.d.	n.d.	n.d.	0.05	0.05	304
209	n.d.	n.d.	n.d.	0.03	0.03	106
210	0.8	n.d.	n.d.	0.27	0.25	9.99
211	n.d.	n.d.	n.d.	n.d.	n.d.	n.d.
212	-1.3	n.d.	n.d.	n.d.	n.d.	n.d.
213	-0.9	-27.7	-143	1.15	1.15	185
214	n.d.	n.d.	n.d.	1.14	1.14	380
215	-1.0	-29.0	-134	1.09	1.09	499
216	-5.4	n.d.	n.d.	1.18	1.19	16.1
217	-4.7	n.d.	n.d.	n.d.	n.d.	n.d.

ID	$\partial^{13}C$-CO_2	$\partial^{13}C$-CH_4	$\delta^{2}H$-CH_4	R/R_A	R/R_Acor	$^{4}He/^{20}Ne$
	‰	‰	‰			
218	-4.0	n.d.	n.d.	n.d.	n.d.	n.d.
219	-2.1	n.d.	n.d.	0.60	0.60	110
220	-2.1	-1.1	n.d.	0.65	0.64	107
221	n.d.	n.d.	n.d.	n.d.	n.d.	n.d.
222	-9.8	n.d.	n.d.	0.48	0.47	200
223	-9.7	n.d.	n.d.	0.43	0.43	141
224	-1.9	-26.1	n.d.	0.40	0.40	335
225	-6.4	n.d.	n.d.	0.43	0.40	5.55
226	-1.9	-26.3	n.d.	n.d.	n.d.	n.d.
227	-1.1	-40.8	n.d.	0.44	0.44	313
228	-2.5	n.d.	n.d.	0.43	0.43	218
229	-0.8	n.d.	n.d.	4.65	4.88	5.34
230	-1.2	n.d.	n.d.	4.98	5.03	25.8
231	-0.8	n.d.	n.d.	5.18	5.43	5.59
232	-2.1	n.d.	n.d.	n.d.	n.d.	n.d.
233	-0.7	n.d.	n.d.	n.d.	n.d.	n.d.
234	0.4	-16.1	-101	4.62	4.63	139
235	-0.7	n.d.	n.d.	4.22	5.02	1.6
236	-2.2	n.d.	n.d.	n.d.	n.d.	n.d.
237	-2.7	n.d.	n.d.	3.22	3.30	8.65
238	-2.1	n.d.	n.d.	3.35	3.39	19.5
239	-0.1	n.d.	n.d.	n.d.	n.d.	n.d.
240	-1.0	-18.2	n.d.	n.d.	n.d.	n.d.
241	-2.1	n.d.	n.d.	n.d.	n.d.	n.d.
242	-3.1	-21.5	n.d.	2.12	2.14	17.2
243	-1.9	-18.3	n.d.	2.39	2.42	12.8
244	-1.4	-20.0	-104	n.d.	n.d.	n.d.

ID	$\partial^{13}C$-CO_2	$\partial^{13}C$-CH_4	$\delta^{2}H$-CH_4	R/R_A	R/R_Acor	$^{4}He/^{20}Ne$
	‰	‰	‰			
245	n.d.	n.d.	n.d.	n.d.	n.d.	n.d.
246	-1.5	-19.5	-143	n.d.	n.d.	n.d.
247	-0.6	-10.0	-71	5.60	5.62	92.9
248	0.6	-12.3	-54	6.21	6.22	92.8
249	-0.6	-19.8	n.d.	6.59	6.63	43.9
250	-0.1	-19.5	-135	6.49	6.50	224
251	-0.9	-20.1	-122	6.27	6.28	270
252	-0.9	-20.6	-133	n.d.	n.d.	n.d.
253	-1.8	-35.9	-124	n.d.	n.d.	n.d.
254	-0.8	-16.1	-75	3.67	3.68	81.5
255	-20.1	-12.5	-14	3.88	3.90	48.2
256	-2.5	n.d.	n.d.	0.85	0.84	5.9
257	-2.2	n.d.	n.d.	2.19	2.56	1.35
258	-1.0	n.d.	n.d.	2.34	2.48	3.42
259	-0.1	n.d.	n.d.	1.31	1.70	0.72
260	n.d.	n.d.	n.d.	n.d.	n.d.	n.d.
261	-1.4	n.d.	n.d.	2.55	2.57	21.7
262	-3.4	-38.6	n.d.	n.d.	n.d.	n.d.
263	-1.0	n.d.	n.d.	n.d.	n.d.	n.d.
264	n.d.	n.d.	n.d.	n.d.	n.d.	n.d.
265	-0.5	n.d.	n.d.	n.d.	n.d.	n.d.
266	1.3	-12.2	-105	n.d.	n.d.	n.d.
267	-2.1	-8.1	-29	n.d.	n.d.	n.d.
268	-1.0	-5.0	7	n.d.	n.d.	n.d.
269	0.1	-18.4	-295	n.d.	n.d.	n.d.
270	n.d.	n.d.	n.d.	n.d.	n.d.	n.d.
271	-1.7	n.d.	n.d.	n.d.	n.d.	n.d.

ID	$\partial^{13}C$-CO_2	$\partial^{13}C$-CH_4	$\delta^{2}H$-CH_4	R/R_A	R/R_Acor	$^{4}He/^{20}Ne$
	‰	‰	‰			
272	-0.4	-14	-115	n.d.	n.d.	n.d.
273	0.3	n.d.	n.d.	n.d.	n.d.	n.d.
274	-0.6	-19.0	-132	n.d.	n.d.	n.d.
275	-0.5	-18.0	-128	6.71	6.71	1066
276	-3.3	2.8	n.d.	1.42	1.42	57.0
277	-3.1	n.d.	n.d.	1.04	1.05	2.92
278	-3.5	2.4	36	1.44	1.45	40.6
279	-3.0	n.d.	n.d.	1.55	1.56	44.1
280	-0.9	n.d.	n.d.	n.d.	n.d.	n.d.
281	-1.3	n.d.	n.d.	1.90	2.12	1.77
282	n.d.	n.d.	n.d.	n.d.	n.d.	n.d.
283	-1.8	n.d.	n.d.	n.d.	n.d.	n.d.
284	0.8	n.d.	n.d.	1.24	1.58	0.73
285	n.d.	n.d.	n.d.	n.d.	n.d.	n.d.
286	-2.0	n.d.	n.d.	2.06	2.22	2.43
287	-2.9	n.d.	n.d.	0.73	0.46	0.62
288	-3.5	n.d.	n.d.	n.d.	n.d.	n.d.
289	-2.0	n.d.	n.d.	n.d.	n.d.	n.d.
290	-0.1	n.d.	n.d.	n.d.	n.d.	n.d.
291	n.d.	n.d.	n.d.	2.97	3.02	12.6
292	-0.1	-16.5	-125	n.d.	n.d.	n.d.
293	-0.4	n.d.	n.d.	n.d.	n.d.	n.d.
294	-0.4	n.d.	n.d.	n.d.	n.d.	n.d.
295	-0.4	n.d.	n.d.	n.d.	n.d.	n.d.
296	-0.1	-13.9	-120	2.72	2.73	46.7
297	n.d.	n.d.	n.d.	n.d.	n.d.	n.d.
298	-1.5	n.d.	n.d.	n.d.	n.d.	n.d.

ID	$\partial^{13}C$-CO_2	$\partial^{13}C$-CH_4	$\delta^{2}H$-CH_4	R/R_A	R/R_Acor	$^{4}He/^{20}Ne$
	‰	‰	‰			
299	n.d.	n.d.	n.d.	n.d.	n.d.	n.d.
300	-1.3	n.d.	n.d.	3.04	3.15	6.14
301	-0.9	n.d.	n.d.	3.37	3.39	37.8
302	0.0	n.d.	n.d.	n.d.	n.d.	n.d.
303	-1.9	n.d.	n.d.	n.d.	n.d.	n.d.
304	-1.5	-12.7	n.d.	2.73	2.74	70.0
305	-0.3	n.d.	n.d.	2.57	2.62	12.5
306	n.d.	n.d.	n.d.	2.52	2.55	20.2
307	n.d.	n.d.	n.d.	n.d.	n.d.	n.d.
308	n.d.	n.d.	n.d.	n.d.	n.d.	n.d.
309	-0.5	n.d.	n.d.	n.d.	n.d.	n.d.
310	0.1	n.d.	n.d.	n.d.	n.d.	n.d.
311	-0.8	-22.9	n.d.	5.77	5.77	200
312	-2.7	-23.3	-121	5.78	5.78	242
313	-0.8	n.d.	n.d.	5.87	5.89	58.3
314	-0.9	n.d.	n.d.	5.75	5.85	14.3
315	-0.6	-21.2	n.d.	5.75	5.79	38.0
316	-1.2	n.d.	n.d.	5.57	5.59	63.7
317	-1.3	-22.5	n.d.	n.d.	n.d.	n.d.
318	-2.1	-23.6	-110	5.53	5.75	6.78
319	-0.4	n.d.	n.d.	5.72	5.72	752
320	-0.4	n.d.	n.d.	5.78	5.82	40.3
321	-0.8	n.d.	n.d.	5.60	5.61	118
322	-1.1	n.d.	n.d.	5.25	5.49	5.97
323	n.d.	n.d.	n.d.	5.77	5.79	59.4
324	-0.6	-22.2	n.d.	5.89	5.93	45.0
325	-1.8	-23.4	-109	5.39	5.44	27.8

ID	$\partial^{13}C$-CO_2	$\partial^{13}C$-CH_4	$\delta^{2}H$-CH_4	R/R_A	R/R_Acor	$^{4}He/^{20}Ne$
	‰	‰	‰			
326	-2.0	n.d.	n.d.	5.62	5.67	34.5
327	-2.1	-23.3	-130	5.91	5.97	29.1
328	-0.6	n.d.	n.d.	4.21	4.22	95.2
329	-0.8	n.d.	n.d.	5.69	5.76	22.2
330	-1.7	-22.0	-108	5.66	5.66	536
331	-1.1	-23.3	n.d.	6.01	6.03	79.4
332	-1.5	-23.3	-108	5.80	5.80	313
333	-1.6	-23.6	-125	6.08	6.13	30.1
334	-4.0	n.d.	n.d.	n.d.	n.d.	n.d.
335	-2.3	-12.0	n.d.	4.12	4.15	30.3
336	0.5	n.d.	n.d.	3.35	3.81	1.94
337	0.3	n.d.	n.d.	2.65	3.52	0.92
338	n.d.	n.d.	n.d.	n.d.	n.d.	n.d.
339	n.d.	n.d.	n.d.	2.96	3.76	1.09
340	0.0	n.d.	n.d.	3.28	3.43	5.1
341	-1.1	n.d.	n.d.	3.34	3.52	4.00
342	-0.7	n.d.	n.d.	3.76	3.85	10.8
343	-1.5	n.d.	n.d.	0.78	0.77	7.38
344	-1.3	-20.2	-111	0.59	0.58	19.4
345	-1.2	-20.9	-117	0.46	0.44	8.62
346	n.d.	n.d.	n.d.	0.18	0.18	445
347	n.d.	n.d.	n.d.	0.19	0.19	75.6
348	-1.8	-21.3	-114	0.21	0.21	76.7
349	-1.7	n.d.	n.d.	n.d.	n.d.	n.d.
350	n.d.	-19.6	-108	0.22	0.21	68.9
351	n.d.	n.d.	n.d.	0.22	0.21	54.1
352	-1.1	n.d.	n.d.	0.31	0.30	29.3

Table 7: Isotope composition of the gases (extracted database)

N.	$\delta^{13}C(CO_2)$	$\delta^{13}C(CH_4)$	$\delta^{2}H(CH_4)$	R/R_A	$^{4}He/^{20}Ne$
	‰	‰	‰		
1	8.5	-64.3	-216	n.d.	n.d.
2	n.d.	-2.3	129	0.07	281
3	-5.4	10.9	301	0.07	95.1
4	-5.3	1.4	30	0.20	228
5	-5.3	-4.2	79	0.20	208
6	-9.8	-10.6	n.d.	n.d.	n.d.
7	-7.4	6.3	62	0.53	159
8	-7.5	4.6	60	0.51	106
9	-13.3	5.3	n.d.	n.d.	n.d.
10	n.d.	n.d.	n.d.	0.46	23.8
11	-3.1	-21.4	-115	0.43	8.5
12	-2.7	-21.7	-124	0.44	3.2
13	-14.1	-79.8	-211	0.39	0.59
14	-1.2	-20.9	-117	0.46	8.6
15	-1.8	-21.3	-114	0.21	76.7
16	-2.6	-1.4	57	0.26	5.4
17	-2.5	3.2	32	0.25	252
18	-2.6	45.0	n.d.	n.d.	n.d.
19	-2.9	n.d.	n.d.	n.d.	n.d.
20	n.d.	n.d.	n.d.	n.d.	n.d.
21	-3.4	-38.6	n.d.	n.d.	n.d.
22	-2.0	-5.6	-49	0.79	0.61
23	-2.2	-5.0	-68	0.74	308
24	-2.5	n.d.	n.d.	n.d.	n.d.
25	-7.0	-74.5	-210	0.41	0.77

N.	$\delta^{13}C(CO_2)$	$\delta^{13}C(CH_4)$	$\delta^{2}H(CH_4)$	R/R_A	$^{4}He/^{20}Ne$
	‰	‰	‰		
26	n.d.	-60.8	-248	0.07	7.8
27	n.d.	-44.9	-196	0.04	44.0
28	n.d.	-33.8	-276	0.34	2.0
29	n.d.	-33.5	-234	0.30	1.0
30	-3.2	-38.7	n.d.	0.13	6.3
31	-4.4	-32.9	-105	0.05	122
32	-6.0	n.d.	n.d.	n.d.	n.d.
33	-0.8	-19.8	-37	0.23	2.3
34	n.d.	n.d.	n.d.	n.d.	n.d.
35	-3.0	n.d.	n.d.	n.d.	n.d.
36	-6.7	-3.8	n.d.	0.74	5.9
37	-0.6	-25.7	-151	0.47	189
38	-0.7	-23.4	-145	0.23	29.8
39	-1.2	-29.4	-187	n.d.	n.d.
40	-1.3	-21.0	-131	0.62	5.1
41	-0.4	-22.5	n.d.	0.66	50.7
42	-0.8	n.d.	n.d.	0.57	1.4
43	n.d.	n.d.	n.d.	0.56	1.6
44	0.5	-27.7	-157	0.30	15.3
45	-5.4	n.d.	n.d.	0.82	44.5
46	-7.2	n.d.	n.d.	1.27	30.3
47	-16.0	-18.8	-113	n.d.	n.d.
48	-2.4	1.1	n.d.	0.26	14.8
49	n.d.	n.d.	n.d.	n.d.	n.d.
50	-9.4	-57.0	-180	0.68	1490
51	-2.1	-1.1	n.d.	0.65	107
52	-1.1	-23.5	n.d.	0.41	36.5

N.	$\delta^{13}C(CO_2)$	$\delta^{13}C(CH_4)$	$\delta^{2}H(CH_4)$	R/R_A	$^{4}He/^{20}Ne$
	‰	‰	‰		
53	-2.0	-19.9	-106	0.82	82.2
54	-3.9	-7.2	-21	0.85	97.0
55	-11.8	n.d.	n.d.	0.83	103
56	-4.5	-24.8	n.d.	0.92	183
57	-9.0	n.d.	n.d.	0.43	67.1
58	-2.1	-8.1	-29	n.d.	n.d.
59	n.d.	n.d.	n.d.	n.d.	n.d.
60	-0.6	-12.3	-54	6.21	92.8
61	-0.1	-19.5	-136	6.49	224
62	-1.9	-18.3	n.d.	2.38	12.8
63	-1.0	-18.2	n.d.	n.d.	n.d.
64	n.d.	n.d.	n.d.	n.d.	n.d.
65	0.3	-13.4	n.d.	n.d.	n.d.
66	-0.5	-18.0	-128	6.71	1070
67	-20.1	-12.5	-14	3.88	48.3
68	-2.5	n.d.	n.d.	0.85	5.9
69	-0.7	n.d.	n.d.	4.22	1.6
70	-1.2	n.d.	n.d.	4.98	25.8
71	-2.1	n.d.	n.d.	n.d.	n.d.
72	0.4	-16.1	-101	4.62	139
73	-2.7	n.d.	n.d.	3.22	8.7
74	-2.1	n.d.	n.d.	3.35	19.5
75	0.3	-34.8	-174	n.d.	n.d.
76	-1.0	n.d.	n.d.	n.d.	n.d.
77	n.d.	n.d.	n.d.	n.d.	n.d.
78	-1.9	-26.1	n.d.	0.40	335

N.	$\delta^{13}C(CO_2)$	$\delta^{13}C(CH_4)$	$\delta^{2}H(CH_4)$	R/R_A	$^{4}He/^{20}Ne$
	‰	‰	‰		
79	-1.9	-26.3	n.d.	n.d.	n.d.
80	-3.1	n.d.	n.d.	1.04	2.9
81	-3.0	n.d.	n.d.	1.55	44.1
82	6.0	-44.6	-263	0.72	0.74
83	-0.9	-27.7	-143	1.15	185
84	-5.8	34.7	n.d.	0.44	18.1
85	-12.3	n.d.	n.d.	0.51	96.4
86	0.3	n.d.	n.d.	2.65	0.92
87	-2.3	-12.0	n.d.	n.d.	n.d.
88	n.d.	-2.0	-127	0.97	0.82
89	n.d.	-26.6	-301	0.87	0.93
90	n.d.	-35.0	-288	0.38	0.84
91	n.d.	-72.3	-174	n.d.	n.d.
92	n.d.	-49.2	-62	0.08	8.7
93	n.d.	-37.5	-204	0.07	16.4
94	n.d.	-42.3	-154	0.06	17.1
95	-1.7	-22.0	-108	5.66	536
96	-1.6	-23.6	-125	6.08	30.1
97	-2.7	-23.3	-121	5.78	242
98	-2.1	-23.6	-110	5.53	6.8
99	-2.1	-23.3	-130	5.91	29.1
100	-3.5	2.4	36	1.44	40.6
101	-0.8	-16.1	-75	3.67	81.5

n.d. = notdetermined

`

Table 8: Concentrations of C2-C6 hydrocarbons (extracted database)

N.	C_2H_6	C_3H_8	C_3H_6	i-C_4H_{10}	n-C_4H_{10}	i-C_4H_8	i-C_5H_{12}	n-C_5H_{12}	C_6H_6	$CH_4/(C_2H_6+ C_3H_8)$
	µmol/mol	µmol/mol	µmol/mol	µmol/mol	µmol/mol	µmol/mol	µmol/mol	µmol/mol	µmol/mol	
1	112	2.8	b.d.l.	0.12	b.d.l.	b.d.l.	b.d.l.	b.d.l.	b.d.l.	7667
2	21	3.7	0.018	2.3	2.1	3.7	0.45	0.45	4.9	45
3	15	3.6	0.02	1.8	2.1	2.6	0.42	0.51	5.6	34
4	13	2.8	0.03	2.6	1.2	1.5	0.55	0.33	2.2	64
5	11	2.2	0.04	2.1	1.5	1.4	0.48	0.25	1.8	65
6	5.1	1.3	b.d.l.	0.45	1.1	0.68	0.33	0.21	0.56	327
7	8.7	2.2	b.d.l.	0.85	0.71	1.3	0.36	0.31	0.66	308
8	13	3.6	0.01	1.4	1.7	1.5	0.62	0.33	0.98	245
9	3.1	0.85	b.d.l.	0.33	0.75	0.55	0.69	0.25	0.44	276
10	1.1	0.08	b.d.l.	b.d.l.	b.d.l.	0.51	b.d.l.	b.d.l.	0.54	256
11	1.1	0.29	b.d.l.	0.12	0.17	0.22	0.09	0.05	0.28	19
12	8.6	2.3	0.03	0.62	1.3	0.95	0.26	0.39	5.4	110
13	95	11	b.d.l.	b.d.l.	b.d.l.	b.d.l.	b.d.l.	b.d.l.	b.d.l.	6645
14	n.d.	n.d.	n.d.	n.d.	n.d.	n.d.	n.d.	n.d.	n.d.	n.c.
15	2.1	b.d.l.	b.d.l.	b.d.l.	b.d.l.	b.d.l.	b.d.l.	b.d.l.	b.d.l.	4810
16	15	3.1	0.06	2.5	3.1	5.5	1.3	0.66	5.1	101
17	13	3.3	0.08	2.3	2.6	4.4	1.5	0.71	4.5	110
18	3.8	0.46	b.d.l.	0.15	0.16	0.11	0.08	0.06	0.71	244
19	2.3	0.51	b.d.l.	0.15	0.26	0.75	0.08	0.11	0.85	19
20	1.5	0.23	b.d.l.	0.11	0.22	0.54	0.05	0.08	0.77	18
21	10	2.1	0.02	1.1	0.65	0.85	0.44	0.26	0.77	76

`

N.	C_2H_6	C_3H_8	C_3H_6	i-C_4H_{10}	n-C_4H_{10}	i-C_4H_8	i-C_5H_{12}	n-C_5H_{12}	C_6H_6	$CH_4/(C_2H_6+ C_3H_8)$
	µmol/mol	µmol/mol	µmol/mol	µmol/mol	µmol/mol	µmol/mol	µmol/mol	µmol/mol	µmol/mol	
22	6.1	1.5	0.02	1.1	0.66	0.74	0.21	0.22	1.2	62
23	1.5	0.11	b.d.l.	b.d.l.	0.06	b.d.l.	b.d.l.	b.d.l.	b.d.l.	6832
24	3.4	0.56	0.02	0.41	0.36	0.41	0.56	0.15	0.74	54
25	123	3.5	b.d.l.	0.15	b.d.l.	b.d.l.	b.d.l.	b.d.l.	b.d.l.	7221
26	2960	278	0.21	126	178	155	26	35	215	201
27	321	8.5	b.d.l.	b.d.l.	b.d.l.	b.d.l.	b.d.l.	b.d.l.	b.d.l.	2579
28	11	3.3	b.d.l.	1.2	1.3	1.6	0.56	0.61	0.98	400
29	13	0.51	b.d.l.	b.d.l.	b.d.l.	b.d.l.	b.d.l.	b.d.l.	b.d.l.	5751
30	13	3.1	b.d.l.	2.5	1.4	1.5	0.39	0.33	0.91	277
31	6.5	0.85	b.d.l.	0.41	0.85	0.76	0.05	0.13	1.4	790
32	4.3	0.85	0.02	0.41	0.69	0.64	0.15	0.22	2.1	155
33	2.4	0.39	b.d.l.	0.15	0.21	0.26	0.05	0.06	0.65	89
34	2.1	0.33	b.d.l.	0.11	0.25	0.29	0.11	0.12	0.58	357
35	6.6	1.3	0.04	0.55	1.1	0.88	0.12	0.26	3.7	87
36	6.7	1.6	b.d.l.	0.55	0.69	1.3	0.25	0.36	2.4	63
37	12	2.5	0.04	1.5	2.1	3.6	1.1	0.66	1.8	186
38	15	2.9	0.03	1.1	2.6	3.1	0.74	0.51	2.2	131
39	3.1	0.15	b.d.l.	b.d.l.	b.d.l.	b.d.l.	b.d.l.	b.d.l.	b.d.l.	1908
40	7.7	2.1	0.03	1.2	0.77	1.1	0.25	0.26	1.5	49
41	8.9	1.8	0.006	1.1	0.85	1.3	0.21	0.21	1.7	20

`

N.	C_2H_6	C_3H_8	C_3H_6	i-C_4H_{10}	n-C_4H_{10}	i-C_4H_8	i-C_5H_{12}	n-C_5H_{12}	C_6H_6	$CH_4/(C_2H_6+ C_3H_8)$
	µmol/mol	µmol/mol	µmol/mol	µmol/mol	µmol/mol	µmol/mol	µmol/mol	µmol/mol	µmol/mol	
42	b.d.l.	b.d.l.	b.d.l.	b.d.l.	b.d.l.	b.d.l.	b.d.l.	b.d.l.	b.d.l.	n.c.
43	b.d.l.	b.d.l.	b.d.l.	b.d.l.	b.d.l.	b.d.l.	b.d.l.	b.d.l.	b.d.l.	n.c.
44	19	3.9	0.11	2.4	2.8	4.9	1.8	0.75	4.1	114
45	b.d.l.	b.d.l.	b.d.l.	b.d.l.	b.d.l.	b.d.l.	b.d.l.	b.d.l.	b.d.l.	n.c.
46	0.08	b.d.l.	b.d.l.	b.d.l.	b.d.l.	b.d.l.	b.d.l.	b.d.l.	b.d.l.	25
47	61	3.9	b.d.l.	b.d.l.	b.d.l.	b.d.l.	b.d.l.	b.d.l.	b.d.l.	6712
48	3.6	0.66	b.d.l.	0.65	0.78	1.2	0.15	0.24	1.8	5.4
49	4.3	0.71	b.d.l.	0.78	0.85	1.6	0.21	0.26	1.9	16
51	5.3	1.3	0.008	0.31	0.39	0.75	0.08	0.07	0.56	101
52	2.3	0.15	0.02	0.11	0.14	0.25	0.08	0.06	0.58	287
53	3.6	b.d.l.	b.d.l.	b.d.l.	b.d.l.	b.d.l.	b.d.l.	b.d.l.	b.d.l.	9111
54	2.3	b.d.l.	b.d.l.	b.d.l.	b.d.l.	b.d.l.	b.d.l.	b.d.l.	b.d.l.	8913
55	12	3.3	0.02	1.4	2.1	3.3	0.55	1.2	2.3	14
56	b.d.l.	b.d.l.	b.d.l.	b.d.l.	b.d.l.	b.d.l.	b.d.l.	b.d.l.	b.d.l.	n.c.
57	0.51	0.18	b.d.l.	0.05	b.d.l.	0.11	b.d.l.	b.d.l.	0.34	14
58	22	5.6	0.008	2.2	2.9	3.7	1.1	1.2	7.1	168
59	9.5	2.1	0.007	1.3	1.1	1.9	0.26	0.31	2.6	71
60	12	0.89	b.d.l.	b.d.l.	b.d.l.	b.d.l.	b.d.l.	b.d.l.	b.d.l.	1853
61	1.6	0.15	b.d.l.	b.d.l.	0.12	b.d.l.	b.d.l.	b.d.l.	0.08	6914
62	7.3	0.33	b.d.l.	0.11	0.21	0.25	0.08	0.05	0.15	389

`

N.	C_2H_6	C_3H_8	C_3H_6	i-C_4H_{10}	n-C_4H_{10}	i-C_4H_8	i-C_5H_{12}	n-C_5H_{12}	C_6H_6	$CH_4/(C_2H_6+ C_3H_8)$
	µmol/mol	µmol/mol	µmol/mol	µmol/mol	µmol/mol	µmol/mol	µmol/mol	µmol/mol	µmol/mol	
63	0.15	b.d.l.	b.d.l.	b.d.l.	b.d.l.	b.d.l.	b.d.l.	b.d.l.	b.d.l.	16,000
64	8.1	0.48	b.d.l.	0.16	0.25	0.33	0.12	0.11	0.21	366
65	4.2	0.26	b.d.l.	0.13	0.21	0.25	0.05	b.d.l.	0.11	4709
66	4.3	0.85	b.d.l.	0.54	0.15	0.65	0.15	0.22	1.3	4485
67	7.5	1.2	0.04	0.58	0.74	0.65	0.06	0.11	1.2	718
68	0.45	0.13	b.d.l.	b.d.l.	b.d.l.	0.15	b.d.l.	b.d.l.	0.23	41
69	b.d.l.	b.d.l.	b.d.l.	b.d.l.	b.d.l.	b.d.l.	b.d.l.	b.d.l.	b.d.l.	n.c.
70	0.99	0.23	b.d.l.	0.08	0.11	0.05	b.d.l.	b.d.l.	0.39	56
71	5.1	1.8	0.02	1.7	0.56	0.75	0.35	0.15	1.4	76
72	11	0.33	b.d.l.	b.d.l.	b.d.l.	b.d.l.	b.d.l.	b.d.l.	b.d.l.	1854
73	3.3	0.59	0.02	0.24	0.25	0.33	0.21	0.15	0.47	34
74	7.6	2.5	0.08	1.1	0.95	1.6	0.78	1.1	2.9	14
75	11	3.9	0.03	1.3	1.5	2.8	0.43	1.1	2.5	26
76	4.6	0.91	0.08	0.45	0.45	0.69	0.11	0.25	2.6	137
77	11	3.3	0.009	1.6	1.9	2.2	0.58	0.91	4.4	7.1
78	6.2	1.5	0.008	1.6	1.8	2.3	0.66	0.91	2.1	110
79	7.6	1.8	0.009	1.5	2	2.6	1.2	1.1	2.5	94
80	4.3	1.1	0.006	0.23	0.36	0.81	0.11	0.13	1.9	9.4
81	3.3	0.65	0.01	0.15	0.33	0.77	0.15	0.19	2.2	70
82	60	3.9	b.d.l.	b.d.l.	b.d.l.	b.d.l.	b.d.l.	b.d.l.	b.d.l.	9013

`

N.	C_2H_6	C_3H_8	C_3H_6	i-C_4H_{10}	n-C_4H_{10}	i-C_4H_8	i-C_5H_{12}	n-C_5H_{12}	C_6H_6	$CH_4/(C_2H_6+ C_3H_8)$
	µmol/mol	µmol/mol	µmol/mol	µmol/mol	µmol/mol	µmol/mol	µmol/mol	µmol/mol	µmol/mol	
83	13	0.26	b.d.l.	b.d.l.	b.d.l.	b.d.l.	b.d.l.	b.d.l.	b.d.l.	7157
84	7.8	3.1	0.05	0.56	0.71	0.56	0.54	0.23	1.4	76
85	b.d.l.	b.d.l.	b.d.l.	b.d.l.	b.d.l.	b.d.l.	b.d.l.	b.d.l.	b.d.l.	n.c.
86	5.6	1.1	0.15	0.26	0.54	0.78	0.31	0.11	2.3	39
87	10	1.9	0.06	1.6	1.3	1.1	0.36	0.25	1.4	109
88	n.d.	n.d.	n.d.	n.d.	n.d.	n.d.	n.d.	n.d.	n.d.	n.c.
89	16.8	b.d.l.	b.d.l.	b.d.l.	b.d.l.	b.d.l.	b.d.l.	b.d.l.	b.d.l.	12,072
90	n.d.	n.d.	n.d.	n.d.	n.d.	n.d.	n.d.	n.d.	n.d.	n.c.
91	3.3	0.59	0.02	0.24	0.25	0.33	0.21	0.15	0.47	93,213
92	120	b.d.l.	b.d.l.	b.d.l.	b.d.l.	b.d.l.	b.d.l.	b.d.l.	b.d.l.	2630
93	n.d.	n.d.	n.d.	n.d.	n.d.	n.d.	n.d.	n.d.	n.d.	n.c.
94	n.d.	n.d.	n.d.	n.d.	n.d.	n.d.	n.d.	n.d.	n.d.	n.c.
95	0.9	0.18	b.d.l.	b.d.l.	b.d.l.	b.d.l.	b.d.l.	b.d.l.	b.d.l.	2331
96	n.d.	n.d.	n.d.	n.d.	n.d.	n.d.	n.d.	n.d.	n.d.	n.c.
97	5.51	1.1	b.d.l.	b.d.l.	b.d.l.	b.d.l.	b.d.l.	b.d.l.	b.d.l.	220
98	4.48	0.75	b.d.l.	b.d.l.	b.d.l.	b.d.l.	b.d.l.	b.d.l.	b.d.l.	831
99	n.d.	n.d.	n.d.	n.d.	n.d.	n.d.	n.d.	n.d.	n.d.	n.c.
100	n.d.	n.d.	n.d.	n.d.	n.d.	n.d.	n.d.	n.d.	n.d.	n.c.
101	23	b.d.l.	b.d.l.	b.d.l.	b.d.l.	b.d.l.	b.d.l.	b.d.l.	b.d.l.	5078

b.d.l. = below detection limit; n.d. = not determined; n.c. = not calculated